University of Sheffield

EX-VIVO HIGH-THROUGHPUT DRUG SCREENING IN BLADDER CANCER

AN OPPORTUNITY TO INCREASE TREATMENT PERSONALISATION, IMPROVE PATIENT SELECTION, AND EXPEDITE NOVEL DRUG DISCOVERY

Written by Miss Samantha Conroy

PhD candidate number: 159716906

Department of Oncology & Metabolism

Supervised by Prof James Catto
&
Dr Greg Wells

Submitted September 2023

Acknowledgements

Prof James Catto, my primary supervisor, I am deeply grateful for his unwavering guidance, support, and invaluable mentorship throughout this journey. Aside from his expertise, he has provided me with multiple opportunities to develop many key academic attributes. His continued faith in my ability and regular positive feedback have supported my personal, professional, and academic growth, for which I am extremely grateful.

Dr Greg Wells, my co-supervisor, I will be forever grateful for his hands-on support. His day-to-day supervision has fostered my confidence, diversified my skillset, and provided regular reassurance of the project direction. He has been patient, approachable, and available when I've needed him. Most of all, thank you for tolerating me through the highs and the lows.

Miss Hannah Gagg, my friend and fellow PhD student. Thank you for going through this journey with me and providing technical support every time I have needed it. Your patience and willingness to help has been unparalleled.

Prof Sarah Danson and the wider EVIDENT consortium. Thank you for providing the opportunity to present my work on a regular basis, for providing navigation towards bringing this work to the clinic, and helping me to always keep patients at the heart of this process.

Thank you to The Urology Foundation and the Royal College of Surgeons of England for seeing value and credibility in my research. Your personal, professional, and financial support have allowed my research to progress across my PhD tenure. Thank you for enabling equitable and welcoming application and interview processes.

Importantly, thank you to all the patients who participated in the study and donated their tissue for research. Your generosity, selflessness, and bravery to contribute towards this research, whilst receiving no personal benefit, will always be remembered.

And finally, thank you to Chelsea – my wife – and the rest of my incredible family for supporting (and tolerating) me through this challenging process. You have always been by my side and there for me when I needed you most. I couldn't have done it without you.

Successful Grants Acquired Throughout PhD Tenure

PI, The Urology Foundation Research Scholarship Award 2020: *Ex-vivo* high-throughput drug screening for bladder cancer: Personalised treatment selection. Amount: **£60,000**

PI, The Urology Foundation Research Scholarship Award 2022: *Ex-vivo* high-throughput drug screening in bladder and Kidney cancer. Amount: **£60,000**

PI, Royal College of Surgeons Honorary One-Year Research Fellowship 2022 **(£5,000).**

Co-PI, Weston Park Cancer Charity Programme Grant (174873), 2022: Expanding early phase trial capabilities with *ex-vivo* drug screening as an exemplar project. Amount: **£295,224.05**

Publications Throughout PhD Tenure

Conroy S, Catto JWF, Bex A, Brown J, Cartledge J, Fielding A, Jones RJ, Khoo V, Nicol D, Stewart GD, Sullivan M, Tran MGB, Woodward R, and Cumberbatch MG. Diagnosis, treatment, and survival from kidney cancer: real-world NHS England data between 2013-2019. *BJUI*. 2023; In press.

Conroy S, Griffin J, Cumberbatch M, et al Acute haemorrhage from a large renal epithelioid angiomyolipoma: diagnostic and management considerations in a teenage patient with a rare cancer. *BMJ Case Reports*. 2023;16:e252351.

Conroy S, Pang K, Jubber I, Hussain SA, Rosario DJ, Cumberbatch MG, Catto JWF, and Noon AP. Hyperthermic intravesical chemotherapy with mitomycin-C for the treatment of high-risk non-muscle-invasive bladder cancer patients. *BJUI Compass*. 2023; 4(3): 314-21.

Conroy S, Hubbard R, Noon AP, Hussain SA, Griffin J, Kennish S, Catto JWF. Case of the month from the University of Sheffield, UK: Expediting definitive treatment in patients with invasive bladder cancer: an MRI-guided pathway. *BJUI.* 2022; 129(6): 691-694.

Conroy S and Nguyen AHT. Compound to Clinic? A Preclinical High-throughput Screening Pathway To Expedite Drug Discovery in Bladder Cancer. *Eur Urol.* 2022; 83(3):271-72.

Conroy S. Editorial: Undergraduate Urology Education: A Fundamental Pillar in Building the Next Generation of Urologists. *Eur Urol*. 2020; 78(3):385-386.

Gagg H, Williams ST, **Conroy S** et al. *Ex-vivo* drug screening of surgically resected glioma stem cells to replace murine avatars and provide personalise cancer therapy for glioblastoma patients [version 1; peer review: awaiting peer review]. F1000Research 2023, 12:954. doi.org/10.12688/f1000research.135809.1

MacLennan S, Azevedo N Duncan E, Dunsmore J, Fullwood L, Lumen N, Plass K, Ribal MJ, Roobol MJ, Nieboer S, Schouten N, Skolarusi TA, Smith EJ, N'Dow J, Mottet N, Briganti A, on behalf of the Pan-European National Urological Society IMAGINE Collaborative **(…S**

Conroy et al.). Mapping European Association of Urology Guideline Practice Across Europe: An Audit of Androgen Deprivation Therapy Use Before Prostate Cancer Surgery in 6598 Cases in 187 Hospitals Across 31 European Countries. *Eur Urol*. 2023; 83(5): 393-401.

Tessel E. Galesloot, Anne J. Grotenhuis, Dimitar Kolev, Katja K. Aben, Richard T. Bryan, James W.F. Catto, Kar K. Cheng, **Samantha Conroy**, Lars Dyrskjøt, Neil E. Fleshner, Nicholas D. James, Philippe Lamy, Sia Viborg Lindskrog, Núria Malats, Lourdes Mengual, Gerald Verhaegh, Maurice P. Zeegers, Lambertus A.L.M. Kiemeney, Sita H. Vermeulen**.** Genome-wide meta-analysis identifies novel genes associated with recurrence and progression in non-muscle invasive bladder cancer. European Urology Oncology. *Eur Urol.* 2022; 5(1): 70-83.

Williams, S., Wells, G., **Conroy, S**., Gagg, H., Allen, R., Rominiyi, O., Helleday, T., Hullock, K., Pennington, C.E.W., Rantala, J., Collis, S., and Danson, S. Precision oncology using ex vivo technology: A step towards individualised cancer care? *Expert Reviews in Molecular Medicine*, 24, E39. doi:10.1017/erm.2022.32

James W.F. Catto, Kathryn Gordon, Michelle Collinson, Heather Poad, Maureen Twiddy, Mark Johnson, Sunjay Jain, Rohit Chahal, Matt Simms, Mohantha Dooldeniya, Richard Bell, Phillip Koenig, **Samantha Conroy**, Louise Goodwin, Aidan P Noon, Julie Croft, and Julia M. Brown on behalf of the BRAVO study group*. Radical Cystectomy against intra-vesical BCG immunotherapy for high risk non-muscle invasive bladder cancer: Results from the randomised controlled BRAVO-feasibility study. J. Clin. Oncol. 2021; 39(3):202-214

Jubber I, Shariat SF, **Conroy S**, Tan WS, Gordon PC, Lotan Y, Messing EM, Stenzl A, Rhijn BV, Kelly JD, Catto JWF, Cumberbatch MG. Non-visible haematuria for the detection of Bladder, Upper tract and Kidney cancer: An updated systematic review and meta-analysis. *Eur Urol.* 2020; 77(5):583-598

Khetrapal P, **Conroy S**, Kelly JD, Catto JWF. Comparing Open Radical Cystectomy and Robot-assisted Radical cystectomy: Current status and analysis of the evidence. *Curr Opin Urol.* 2020; 30(3):400-406

Conroy S, Salawu A, Hussain SY, Catto JWF. Oxford Textbook of Oncology. Genuitourinary Cancers (*accepted, in press*).

Pang K and Catto JWF, eds. *Challenging Cases in Urological Surgery*. Oxford, 2023. Oxford Academic. **Conroy S** and Catto JWF. Chapter 5: Muscle-invasive bladder cancer.

Pang K and Catto JWF, eds. *Challenging Cases in Urological Surgery*. Oxford, 2023. Oxford Academic. **Conroy S** and Noon AP. Chapter 5: Non-muscle-invasive bladder cancer.

Cumberbatch MG , **Conroy S,** Lawrentschuk N. Managing the primary - upper tract TCC. BJUI Knowledge: Oncology – Upper tract cancer. DOI: 10.18591/BJUIK.

[ABSTRACT] **Conroy S,** Wells G, Allen R, Rantala J, Helleday T, and Catto, JWF. P10-16 Preliminary experience of *ex-vivo* high- throughput drug screening in muscle invasive bladder cancer: moving towards improved patient selection and treatment personalisation. *Journal of Clinical Urology*. 2021; 14(1S), pp. 4–95. doi: 10.1177/20514158211013240.

[ABSTRACT] **Conroy S**, Wells G, Gagg H, Hansford S, Helleday T, Cumberbatch MG, Danson S, and Catto, JWF. P4-8 Exploring the feasibility of an *ex-vivo* high throughput screening platform in Kidney Cancer to improve treatment selection and novel drug discovery. *Journal of Clinical Urology*, 2023. 14(1S), pp. 4–95. doi: 10.1177/20514158211013240.

Prizes and Achievements

British Association of Urological Surgeons Oncology Annual Meeting 2023: Invited Session Chair, Nov 2023 (National Meeting)

The University of Sheffield Medical School Research Day: Third place oral presentation, July 2023

National Institute of Health Research: Associate PI Scheme completion (FINESSE trial), May 2023

Royal Society of Medicine Urology Section: Invited Session Chair, Dec 2022 (National Meeting) and Jan 2023 (International Winter Meeting)

European Urology: Reviewer of the Month (IF: 24.3), Nov 2022

Yorkshire Urology Audit Group Regional Meeting: Second place oral presentation, Nov 2022

Cancer Research UK Eureka Virtual School Graduate: A Translational Approach to Oncology Course, May 2022

Experimental Cancer Medicine Centres Junior Investigator Networking Group: Training the Next Generation Course, 2021

Royal Society of Medicine Urology Section: Sir Geoffrey Chisholm Communication Prize, Dec 2020

Commendation for Contribution to Undergraduate Urology Education 2018-2023

Table of Contents

Table of Contents

Table of Contents

Table of Contents

LIST OF FIGURES

LIST OF FIGURES

LIST OF TABLES

LIST OF ABBREVIATIONS

AC	adjuvant chemotherapy
AML	acute myeloid leukaemia
ATCC	America Type Culture Collection
AUC	area under dose-response curve
BB1	bladder batch 1
BB2	bladder batch 2
BBN	N-butyl-N-(4-hydroxybutyl)-nitrosamine
BC	bladder cancer
BCG	bacille Calmette-Guerin
BSA	bovine serum albumin
ccRCC	clear cell renal cell carcinoma
CIMM	chemically induced mouse model
CIS	carcinoma-in-situ
CK19	Cytokeratin-19
CLA	cell line allograft
CLX	cell line xenograft
COSMIC	Catalogue of Somatic Mutations in Cancer
COV	coefficient of variation
CTG	CellTiter-Glo®
DAPI	4', 6-diamidino-2-phenylindole
DIN	DNA Integrity Number
DMSO	dimethylsulfoxide
DP	depth of coverage
EAU	European Association of Urology
EMT	epithelial to mesenchymal transition
EV	enfortumab vedotin
EVIDENT	Ex-VIvo DetErmiNed cancer Therapy study

LIST OF ABBREVIATIONS

EVP	*ex-vivo* phenotype
FBS	foetal bovine serum
FDA	food and drug administration
FGFR	fibroblast growth factor receptor
GC	gemcitabine-cisplatin
GEMM	genetically engineered mouse model
HG	high grade
HIVEC	heated intravesical chemotherapy
HR NMIBC	high-risk non-muscle invasive bladder cancer
ICGC	International Cancer Genome Consortium
ICL	immortal cell line
IMF	immunofluorescence microscopy
IR NMIBC	intermediate-risk non-muscle invasive bladder cancer
ITS	insulin-transferrin selenium
KC	kidney cancer
LG	low grade
LR NMIBC	low-risk non-muscle invasive bladder cancer
LY:V	live cell yield to tumour sample volume ratio
MAD	median absolute deviation
mBC	metastatic bladder cancer
MIBC	muscle invasive bladder cancer
MMC	Mitomycin C
MVAC	methotrexate, vinblastine, doxorubicin, cisplatin
NAC	neoadjuvant chemotherapy
NGS	next generation sequencing
NMIBC	non-muscle invasive bladder cancer
PanCK	pan-cytokeratin

LIST OF ABBREVIATIONS

PBS	phosphate buffered saline
PDC	patient-derived *ex-vivo* cultures
PDCL	patient-derived cell line
PDE	patient-derived explant
PDX	patient-derived xenograft
PFA	paraformaldehyde
QD	quality divided by the unfiltered depth of coverage
QUAL	quality scores
RC	radical cystectomy
RCC	renal cell carcinoma
RNA-seq	whole transcriptome sequencing
RTK	receptor tyrosine kinase
rZauc	modified Z-score
SC	stromal cell
SCC	squamous cell carcinoma
TC	tumour cell
TCGA	The Cancer Genome Atlas
TP53	tumour protein 53
TSG	tumour suppressor gene
TURBT	transurethral resection of bladder tumour
WES	whole exome sequencing
WGS	whole genome sequencing

ABSTRACT

Introduction: Ex-vivo high-throughput drug screening has the potential to improve risk-stratification, treatment personalisation, and novel drug development within clinically relevant timeframes. Bladder cancer (BC) is particularly challenging cancer to treat, with high morbidity and mortality rates, stagnant clinical outcomes, and poor patient reported experiences. The primary aim of this thesis was to explore the feasibility of *ex-vivo* drug screening using fresh patient BCs, its ability to identify differential standard and novel treatment responses, and whether whole exome sequencing (WES) could provide further molecular insight into response phenotypes.

Patients and methods: Bladder tumours were collected fresh from surgery and dissociated into BC patient-derived *ex-vivo* cultures (PDCs) (ethical approval STH15574/STH20854). Cells were incubated on bespoke, pre-loaded drug plates for four days. Endpoint metabolic (CellTiterGlo) assessment generated area dose-response curves (AUC). Tumours with vehicle-control (n=28) coefficient of variation >0.25 were excluded as methodological failures. AUC scores were normalised (modified-Z) across the tumour cohort and positive drug hits explored to determine differential *ex-vivo* phenotypic signatures. Whole exome sequencing (WES) was performed by MacrogenEurope and data used to identify candidate response biomarkers.

Results: There was high methodological success using the optimised *ex-vivo* methodological protocol, where 75.9% (41/54) of tumours screened passed quality control. In total, 39 (39/54, 72.2%) were malignant BCs. Diverging drug and tumour clusters and *ex-vivo* response phenotypes (EVP) were identified. Resistant-EVP was significantly associated with more aggressive clinical features (grade 3, p=0.0002, stage ≥T1, p=0.025, and carcinoma-in-situ, p=0.041. Resistant-EVP tumours had a higher median number of mutations per tumour (11.4 versus 7.5, p=0.036) and differential genotype to sensitive-EVP tumours. *Ex-vivo* determined cisplatin-resistant tumours dichotomised into those with alternative sensitivities and multi-drug resistant phenotypes, with differential genetic enrichment (Figure.1B&C).

Conclusions: *Ex-vivo* screening of BCs is feasible and can identify differential phenotypic behaviours. Resistant-EVP tumours displayed more aggressive clinical, drug phenotypic, and genotypic features. Identification of specific drug resistant cohorts may aid in clinical triage to more effective therapies or radical surgery.

CHAPTER 1

INTRODUCTION

1.1 BLADDER CANCER

1.1.1 EPIDEMIOLOGY

Bladder cancer (BC) is a common urological malignancy. It is the tenth most common cancer worldwide, and accounts for 3% of all cancer diagnoses (1). Annually, over 500,000 people are diagnosed with BC and over 200,000 die of the disease (1). BC has an estimated world-wide five-year prevalence of 1.7 million (2). Over three-quarters of all new BC diagnoses occur in men, making it the sixth most common cancer in men (2). BC is typically a disease of older people, where age-adjusted incidence climbs dramatically over 50 years of age (3). Geographically, the highest incidence rates are seen in Europe and North America, as well as, countries with high levels of schistosomiasis infection, such as North Africa and Western Asia (2).

1.1.2 AETIOLOGY

Risk factors for BC can be divided into acquired and hereditary. The most common acquired risk factor is smoking. Approximately 50% of all BCs arise following exposure to cigarette smoke, where risk is proportional smoking intensity and is higher risk in current versus ex-smokers; the risk slowly reduces after smoking cessation (2). It is estimated that 5.7% of BCs arise following exposure to occupational carcinogens, such as: Benzidine, 2-naphthylamine, 4-chloro-ortho-toluidine, ortho-toluidine, 4-aminobiphenyl, and 2-Mercaptobenzothiazole, tetrachloroethylene, and soot or coal tar (2). Hence, the risk of BC is higher in those who have worked in industries such as, tobacco, dye, hairdressing, printing, textile, rubber and metal production; in those who have been exposed to high levels of passive smoking, for example, cooks, stewards, and waiters; and in those who have been exposed to soot and carbon, for example, chimney sweeps and firefighters (2–4).

Other acquired risk factors include: past history of radiotherapy to the bladder or surrounding organs; schistosomiasis exposure; drug treatment with pioglitazones or cyclophosphamides and opium consumption; lifestyle factors, such as, lack of exercise, high body mass index, Western diet and low fibre intake (2,5); and socio-economic factors, such as, living in heavily industrialised areas or areas of socio-economic deprivation (3), which is likely related to lifestyle factors such as smoking (5).

Non-modifiable risk factors for the development of BC include: increasing age, male sex, and a positive family history of bladder cancer (in up to 5% of patients) or any other cancer (in up to 50% of patients) (2). In addition, studies have shown that specific germline mutations may increase susceptibility to BC, for example, *MLH1*, *MSH2*, and *BRCA1/2* (6,7), although germline genetic testing is not currently recommended (8,9).

1.1.3 CLINICAL AND HISTOLOGICAL SUBTYPES

1.1.3.1 CLINICAL SUBTYPES

BC is broadly divided into two distinct disease states with differing clinicopathological behaviour. Non-muscle invasive BC (NMIBC) is the less aggressive, superficial form of the disease, and accounts for 75% of cases. Muscle invasive BCs (MIBC) or metastatic BCs (mBC) are much more aggressive, and account for the remaining 25% of cases. The two disease states are histologically divided by tumour invasion into the muscularis propria of the detrusor muscle (histologically), or radiologically by evidence of detrusor muscle invasion or metastases.

1.1.3.2 HISTOLOGICAL SUBTYPES

Most (90-95%) BCs are urothelial carcinomas. Some urothelial carcinomas have variant growth patterns (for example, micropapillary) or mixed histological differentiation (for example, squamous differentiation) that are more aggressive than pure urothelial carcinoma (10). Only a minority (5-7%) of BCs in Europe and North America are non-urothelial BCs (11). Pure squamous cell carcinoma (SCC) of the bladder is the most common form of non-urothelial BCs and is usually caused by chronic urothelial inflammation (infection, foreign body, catheterisation) (11,12). Other non-urothelial BCs have been documented but are rarely encountered in clinical practice; these include small cell carcinomas, adenocarcinomas, sarcomas, lymphomas, and melanomas of the bladder.

1.1.4 DIAGNOSIS

Cystoscopy, which allows for direct visualisation with or without tissue sampling of the urothelium, is the gold standard for diagnosis of BC. Typically, this is coupled with imaging of

the upper urinary tract to exclude synchronous upper tract urothelial carcinomas. Cytological evaluation of the urine may provide a useful adjunct in patients with NMIBC, but has variable sensitivity and specificity (13). Histological analysis of tissue is required for a definitive diagnosis to be made, which can be achieved through cystoscopy or trans-urethral resection of bladder tumours (TURBT). The critical diagnostic step is differentiation between NMIBC and MIBC (as described in section 1.1.3.1). Advances in imaging techniques may provide better delineation of muscle invasion, allowing for adapted triage of patients with more advanced disease states; for example, through a combination of flexible cystoscopic (outpatient) biopsy and multiparametric magnetic resonance imaging (14,15). Completion staging is performed using computed tomography. In recent years, there has been an expanding number of urinary biomarkers (DNA, RNA, epigenetic modifiers, exosomes, proteins, and microbiome components) explored for the detection of BC (16). Six of these have been Food and Drug Administration (FDA) approved for the diagnosis and surveillance of BC patients (17), however, none of them are currently accepted as part of routine clinical practice (9).

1.1.5 GRADING AND STAGING

Grading of exophytic BCs uses two systems (10): the 1973 WHO criteria grade from grade 1 (low grade) to grade 3 (high grade) (18) and the 2004 ISUP classification which uses low grade (LG) and high grade (HG) (19). Carcinoma-in-situ (CIS) is a sessile, HG, non-invasive form of BC that may arise in conjunction with, or after treatment of, a HG exophytic tumour. BCs are staged using traditional tumour, node, metastasis systems (20). In the context of NMIBC, tumours are staged as pTa (non-invasive), pT1 (invades the lamina propria), and pTis (CIS only) disease. For patients with MIBC, staging classification defines the depth and extent of local tumour invasion, presence of locoregional nodal involvement, and presence distant metastases. Conventional staging aims to assist with risk-stratifying patients, selecting patients for appropriate treatment options, and in providing prognostic information.

1.1.6 CLINICAL RISK-STRATIFICATION

1.1.6.1 NMIBC

NMIBC is a heterogenous disease, with huge variations in recurrence (15-78%) and progression (1-75%) at five years follow-up (21). Tumours are classified as low, intermediate, high, and very high-risk using clinical parameters, such as: patient age, tumour grade, size, multiplicity, depth of invasion (tumour stage), concurrent CIS, evidence of lymphovascular invasion, prior recurrence rate, and histological subtype (13). The risk-stratification provides prognostic information about recurrence and progression. The risk of progression is of particular importance, as patients who progress from NMIBC to MIBC have a poorer prognosis than those presenting with *de novo* MIBC (22,23). The one to ten-year risk of progression, as per European Association of Urology risk classes, are 0.06-3.7% for low risk, 1.0-4.9% for intermediate risk, 3.5-14.0% for high risk, and 16.0-53.0% in very high risk patients (24). Hence, risk class plays an important role in dictating subsequent clinical management.

1.1.6.2 MIBC

Pre-operative risk stratification in MIBC is predominantly focussed around the TNM classification. Local staging is best performed using mpMRI, as it has superior soft tissue resolution than computed tomography, and high diagnostic accuracy of muscle invasion (25). computed tomography imaging, however, is more accessible, provides information regarding synchronous upper tract tumours, and provides concurrent thorax staging. Computed tomography and magnetic resonance imaging may also provide information regarding suspected lymph node (LN) involvement; however, both are limited by size-guided criteria (>8mm pelvic LNs, >10mm abdominal lymph nodes) with low sensitivity (<50%) and high specificity (>90%). 2-Deoxy-2-(18F)fluoro-d-glucose positron emission tomography-computed tomography in lymph node staging remains controversial, as it has not shown benefit over standard computed tomography (26).

1.1.7 GENOMIC RISK-STRATIFICATION

Advances in next generation sequencing, collaborative research efforts, knowledge of tumour sampling, and enhanced biobanking techniques have led to a better understanding of BC disease biology. A number of multi-omic approaches have highlighted molecular subtypes of both NMIBC (27–31) and MIBC (27,32–35), which are rapidly evolving. A recent meta-analysis, conducted by Tan et. al (36) collated gene expression data from 2,411 individual BCs using publicly available datasets. They identified clusters within the 10,596 commonly expressed signatures and defined six molecular subtypes (neural, luminal-like, papillary-like,

human epidermal growth factor receptor 2 (HER2)-like, mesenchymal-like, and SCC-like). The subtypes had distinct molecular features, variable overall survival, and were differentially spread across the disease landscape; for example, neural, mesenchymal and SCC-like were predominantly found in MIBCs, papillary and luminal-like were predominantly found in NMIBCs, whereas HER2-like was distributed across both disease states.

In NMIBC, the most recent study from the UROMOL discovery cohort (31) of 862 NMIBCs used transcriptomic, genomic, and proteomic analysis to establish four molecular classes of NMIBC (Class 1, 2a, 2b, and 3) (Table 1). This expanded on the previous three subclasses (37), by expanding class 2 (highest risk) into 2a and 2b. Patients with class 2a tumours had the worst progression-free survival, were associated with high-risk clinical features, and had a higher proportions of p53 alterations. In addition, the transcriptomic and proteomic analysis revealed class-based immunoresponse phenotypes. In immune-poor classes (class 1 & 3), there were high rates of fibroblast growth factor receptors (FGFR) 3 mutations, highlighting potential alternative therapeutic avenues.

In MIBC, Kamoun et al. (35) created a consensus of molecular subtypes using transcriptomic profiles from 1,750 MIBCs across 18 publicly available datasets. This yielded six distinct molecular subtypes with differential mutational and transcriptomic profiles, infiltrating micro-environment components, treatment responses, and outcomes (Table 2). The six classes were defined as luminal unspecified, luminal-papillary, luminal-unstable, stroma-rich, basal-squamous, and neuro-endocrine like. These subtypes displayed differences in treatment response and survival outcomes.

Examples of current molecular subtypes are shown in Tables 1 and 2. However, currently in the clinic, molecular profiling of BCs is not commonplace and does not influence clinical decision-making. To explore predictive utility of these subtypes in MIBC and NMIBC, in terms of treatment response and outcome, they must be prospectively evaluated. Some of the most promising clinical biomarker-driven trials are exploring FGFR inhibition, as the majority of NMIBCs (38), and a smaller number of MIBCs (35), harbour *FGFR* mutations. There are two ongoing phase III clinical trials exploring the pan-FGFR inhibitor Erdafitinib; one in advanced urothelial cancer (NCT03390504) and one in BCG-failed high-risk NMIBC (NCT04172675). As for exploring predictive molecular subtypes, the Genotype in Urothelial cancer: Stratified Treatment and Oncological outcomes (GUSTO) trial (ISRCTN17378733), aims to explore whether molecular stratification of MIBCs is feasible within an NHS infrastructure and its utility in directing neoadjuvant therapy.

Table 1: Molecular classification of NMIBCs – adapted from Lindskrog et al. (31)

Class	Grade/ stage	RR	Gene expression	Regulation activity	Mutations	Immune/ stromal signatures	Class hetero-geneity	Rx
1	Lower grade/ stage	Low	Early cell cycle Uroplakins	HIF1A, KAT5, HDAC3	FGFR3, RAS	-	-	AS, Chemotherapy, FGFRi
2a	Higher grade/ stage	High	Late cell cycle DNA replication Uroplakins	FOXM1, ESR2, ERBB2/3	TP53, RB1, APOBEC+	-	High	BCG, CPI, RC
2b	Mixed	Mid	Cancer stem cell markers EMT	ESR1, PGR, FGFR1	-	High	-	BCG, CPI
3	Lower grade/ stage	Mid	Early cell cycle FGFR3	AR, KMT2E, KAT2A, HDAC10	FGFR3, PIK3CA	Low	Low	AS, Chemotherapy, FGFRi

RR – recurrence risk; EMT – epithelial-mesenchymal transition; RX – proposed treatment; AS – active surveillance; FGFRi – FGFR inhibition; CPI – checkpoint inhibition.

Table 2: Consensus molecular classification of MIBCs – adapted from Kamoun et al. and Robertson et al. (34,35)

Class	%	Mechanisms	Mutations	Stomal/immune infiltrates	Histology	Clinical	Proposed Treatment	Median OS (years)
Lum-P	24	FGFR3+, PPARG+, CDKN2A-	FGFR3, KMD6A	-	Papillary	T2+ stage	NAC, FGFRi	4
Lum-NS	8	PPARG+		Stromal+	Micro-papillary variant	Older pts (80+)	-	1.8
Lum-U	15	PPARG+, E2F3+, ERBB2+, Cell cycle+	TP53, ERCC2, TMB/APOBEC+	-	-	-	NAC*	2.9
Stroma-rich	15	-	-	Stromal+++ Immune+	-	-	-	3.8
Ba/Sq	35	EGFR+	TP53, RB1	Stromal++ Immune+++	Squamous differentiation	Women T3/4 stage	CPI, NAC	1.2
NE-like	3	TP53-, RB1-, Cell cycle+	TP53, RB1	-	Neuro-endocrine differentiation	-	Etop/cis NAC	1

**low response rate. LumP – luminal papillary; LumNS – luminal non-specified; LumU – luminal unstable; Ba/Sq – basal squamous; NE-like – neuroendocrine-like; SM – smooth muscle; NAC – neoadjuvant chemotherapy; CPI – checkpoint inhibitors; Etop/cis – etoposide and cisplatin; OS – overall survival.*

1.1.8 CLINICAL MANAGEMENT

1.1.8.1 NMIBC

The management of NMIBC requires a risk-adapted patient-centred approach. The key aim is to achieve local disease control, minimise recurrence and progression, whilst optimising quality of life during treatment. In general, patients should be offered support with lifestyle modifications (for example, smoking cessation and weight loss) and optimisation of competing comorbidities.

LOW RISK NMIBC (LR NMIBC)

This group have a low risk of progression, which means that treatment focuses on local disease control (39). Complete surgical resection through TURBT, with or without a single instillation of peri-operative chemotherapy (typically, Mitomycin C (MMC)), is the mainstay of treatment (40). After resection, an active cystoscopic surveillance is required for a minimum of 12 months (41).

INTERMEDIATE RISK NMIBC (IR NMIBC)

The intermediate risk group is particularly heterogenous with many overlapping features of low and high risk groups (13). IR NMIBCs are also heterogeneously defined across international guidelines (42). Similar to the LR NMIBCs, IR NMIBC patients require local resection (TURBT) and a single dose of peri-operative intravesical chemotherapy (40). Following this, it is recommended that patients receive adjuvant intravesical MMC (13,41). In some circumstances intravesical BCG (43,44) may be considered, for example, in recurrent chemo-refractory disease. More recently, advances in chemotherapy delivery systems had led to the introduction of chemohyperthermia treatment in IR NMIBC, which has shown superior disease-free survival to ambient instillations and similar outcomes to BCG (45). After treatment for IR NMIBC, patients should then be placed on an individualised active surveillance strategy, with 3 to 6-month cystoscopic reviews. In the UK, the recommendation is to continue active surveillance for a period of five years (41).

HIGH RISK NMIBC (HR NMIBC)

As we move towards the high-risk group, recurrence and progression risk sharply increases Hence, after initial TURBT, patients should be offered adjuvant therapy – either in the form of

intravesical BCG or radical surgical removal of the bladder (radical cystectomy, RC). The BCG vaccination was first administered in the 1920s in humans, but it was only in the 1960s and 1970s where the use of antibiotic and vaccine treatments became a popular research endevour for cancer treatment (46). Research underpinning its efficacy in BCs soon followed, where its mechanism of action is delivered through engagement with the urothelium and a granulomatous reaction that facilitates T cell infiltration – mediating an immunotherapy action again BCs (46). Currently, intravesical BCG is recommended as an induction and maintenance immunotherapy (13,47,48) for up to 3 years (44). Unfortunately, adjuvant BCG fails in up to one-third of patients at one year (49) and BCG manufacturing shortages have led to rationing of BCG schedules in the clinic (50). A number of alternative bladder-sparing therapies are currently under investigation, including systemic and intravesical immunotherapies, targeted therapies, combination chemotherapies, and device assisted therapies, but randomised phase 3 clinical trial evidence are lacking.

Alternative to bladder sparing approaches, primary RC may be offered to selected patients who are appropriately counselled. Primary RC offers superior oncological control (51), but also the risk of surgical complications, impaired quality of life during recovery, and impaired sexual function (52–55). Recent attempts to randomise patients with HR NMIBC to intravesical BCG versus primary RC have proven challenging (56).

VERY HIGH RISK NMIBC (VHR NMIBC)

VHR NMIBC have a high rate of progression and thus need to be managed more aggressively. As described previously, those who progress from NMIBC to MIBC have poorer outcomes (22,23). Hence, in this group, it is reasonable to recommend primary RC as the first treatment to achieve oncological control. If unfit or unwilling to undergo primary RC, then treatment would follow the guidelines as described for HR NMIBC.

1.1.8.2 MIBC

To achieve cure in patients with MIBC, radical therapy is required. This can be delivered either via radical surgery or radiotherapy, with or without systemic anti-cancer therapy. Treatment choice depends on a combination of patient factors (fitness, comorbidities, and prior treatment to the pelvis or abdomen), disease factors (histopathological staging, associated obstructive uropathy, and metastases), and of course, patient choice.

NEOADJUVANT CHEMOTHERAPY

Neoadjuvant chemotherapy (NAC) prior to RC for patients is the gold standard of care for patients with MIBC. It should be offered to all eligible patients with pT2-T4a cN0M0 urothelial carcinoma. NAC offers potential advantages, including: improved compliance, identification of in-vivo sensitivity, and treatment of occult or overt metastatic disease at its lowest volume, without compromising surgical outcomes (57,58). Cisplatin-based combination NAC is most frequently used, conferring an 8% 5-year survival advantage (59). Gemcitabine-Cisplatin (GC) or MVAC regimen (Methotrexate, Vinblastine, Doxorubicin, Cisplatin) may be used depending on patient factors and relative toxicities (60,61), where a dose-dense MVAC regime provides a marginal 3-year progression-free survival advantage (61). Complete response to NAC, defined as no residual tumour at time of RC (pT0 pN0), occurs in 23 – 30% of patients and is strongly associated with improved overall survival (62,63).

Patients with histological variant MIBC have less predictable responses to NAC (64), however, the current literature still supports its use in most patients (65). Alternative strategies, such as molecular risk-stratification of MIBCs may provide scope to better select and triage patients for the most appropriate neoadjuvant therapy. Neoadjuvant immunotherapy has emerged as a promising treatment through the inhibition of PD-1/PD-L1 or CTLA-4. Results from phase 2 trials evaluating Atezolizumab (PD-L1 inhibitor) and Pembrolizumab (PD-1 inhibitor) have been promising with complete response rates of 29% and 42%, respectively, and durable clinical responses up to 3 years (66,67).

RADICAL SURGERY

RC with or without lymphadenectomy has been shown to achieve the greatest survival benefit (68). It is recommended as the standard of care for patients with T2-4a, N0-Nx, M0 disease (69) and is typically performed open or robotically (70). RC should be performed in a high volume centre, within three months of initial TURBT (22,71). Standard RC in men involves removal of the bladder, prostate, seminal vesicles, and distal ureters; and in women, the bladder, entire urethra, uterus, fallopian tubes and part of the vagina. Although not to be offered as the standard therapy for all, sexual preserving techniques in both men and women have been implemented; tumour location, stage, and patient factors must be considered, and patients appropriately counselled (69). Lymphadenectomy is an integral part of the RC process for patients with MIBC, as it provides pathological staging information that may influence subsequent management. In addition, it confers a potential therapeutic benefit should there be active lymph node involvement, as these regional metastatic sites are retrieved during surgery (72,73). The optimal extent of lymphadenectomy remains controversial (74).

Once the pelvic organs are removed, there are several options for reconstruction of the urinary tract, which again are influenced by patient and disease factors (69). Some patients with lower-stage, organ confined disease, are offered continent diversion of urine. This includes surgical construction of a neobladder using bowel, which is anastomosed to the native urethra. Incontinent diversions are typically in the form of an ileal conduit, where the ureters are anastomosed within the abdomen to segment of ileum brought out to the skin. In a minority of cases, this may be delivered as cutaneous ureterostomies, where the ureters are brought directly through the abdominal wall to the skin.

RC has a high associated morbidity, with major complications (Clavien Dindo grade 3 or above) occurring in one-third of patients (71). Aside from complications, RC also has significant implications on quality of life. Patients face major changes in self-reported body-image, sexual intimacy, sexual enjoyment, and male sexual problems (54). Despite this, global quality of life scores return to baseline at around 6 months after surgery (52). Patients, therefore, must be carefully counselled about all available treatment options when embarking upon RC.

RADICAL RADIOTHERAPY AND CHEMORADIOTHERAPY

Some patients are ineligible or unwilling to undergo RC. Organ preservation may be achieved using radical radiotherapy with or without chemotherapy. Radiotherapy may be delivered in conventional (60-64Gy in 30-32 fractions) or hypofractionated (52.5-55Gy in 20 fractions) forms (75)). Due how radiotherapy affects bladder capacity and storage, the most favourable patients for this treatment are those with good baseline bladder capacity, minimal storage symptoms, and no prior incontinence (76). However, modern techniques have helped to make radiotherapy much more tolerable, with reasonable acute and late toxicity rates (77,78). Quality of life initially declines after radiotherapy, but subsequently return to baseline at around 6 months (79).

More recent strategies have highlighted the benefit of adding chemo-sensitising agents. The most commonly used chemo-sensitising agents are MMC/5Fluorouracil (80), but alternatives have also been utilised (81). Chemoradiation therapy has shown significantly enhanced locoregional control and lower salvage cystectomy rates (over radiotherapy alone) (82). The addition of chemotherapy to radiotherapy does not significantly impact on quality of life scores (79); thus, radiotherapy in isolation is not recommended as the sole organ preserving approach in eligible patients.

TRIMODAL THERAPY

Trimodal therapy described the combination of maximal TURBT with chemo-radiotherapy. Trimodal therapy is the optimal bladder-preserving strategy in selected patients who are unwilling to undergo RC (69). The approach is usually reserved for patients with smaller, solitary tumours (<5cm, stage T2) tumours, minimal CIS, no hydronephrosis, no radiographic lymph node disease, and good pre-therapy bladder function (76,83). Trimodal therapy has been shown to have equivalent oncological outcomes (84) and survival (<10 years) (85) to RC in carefully selected patients, but prospective randomised trial data are lacking. Trimodal therapy must be provided using a rigorous multi-disciplinary approach with close surveillance and high levels of patient compliance.

ADJUVANT THERAPY FOR MIBC

Cisplatin-based adjuvant chemotherapy (AC) (in patients who did not receive NAC) may provide a survival benefit in selected patients (86). Unlike, NAC, AC reduces overtreatment in patients who do not harbour micro-metastatic disease and does not delay definitive surgery. However, the morbidity of surgery may deem patients ineligible for AC or make adjuvant treatment intolerable. The evidence supporting AC is in high risk patients, for example, those with pT3/4 or node positive disease at RC. A recent meta-analysis suggests that cisplatin-based AC delivers a 6% survival advantage at five years (Burdett *et al.*, 2022). Adjuvant Nivolumab has also recently been approved for use in the adjuvant setting in PD-L1 positive (>1%) tumours [NICE:TA817], as it showed a significant disease-free survival benefit over placebo (88). Interestingly, atezolizumab, which has a similar mechanism of action, did not show an improved disease-free survival benefit (89).

1.1.8.3 METASTATIC BLADDER CANCER

Approximately 50% of patients with MIBC will relapse following radical treatment and subsequently develop mBC during clinical follow-up (90), although some patients present with *de novo* mBC. The mainstay of treatment is systemic platinum-based combination chemotherapy. Poor performance status, inadequate renal function, and unacceptability of systemic therapy are the main barriers to treatment.

FIRST-LINE THERAPY – PLATINUM ELIGIBLE

Platinum chemotherapy has been standard of care since the 1980s with well-defined eligibility criteria, toxicity profiles, and outcomes. The most frequently used is cisplatin. Eligibility for cisplatin is based around performance status, renal function, baseline hearing loss, peripheral neuropathy, and evidence of heart failure. In those eligible to receive cisplatin, combination therapy with either gemcitabine or dose-dense MVAC, is the current standard of care (60,91).

Unfortunately, only 50% of patients are eligible for cisplatin-based therapy in this setting (92), where the alternative is carboplatin-combination therapy (93). Currently, there is no evidence to suggest a survival advantage with the addition of immunotherapy to cisplatin-based chemotherapy (94,95) nor dual combined immunotherapy (96). However, in patients who have a good response to GC therapy, maintenance with avelumab (versus best supportive care) has been shown to provide a significant overall survival advantage (97).

FIRST-LINE THERAPY – PLATINUM INELIGIBLE

Patients who are ineligible for platinum-based therapy represent a patient group with poor performance status or renal function. Both of these characteristics often exclude patients from enrolment in clinical trials and are therefore underrepresented. The FDA has approved first-line pembrolizumab or atezolizumab in these patients (8), however, due to lack of supporting evidence it has not been approved by NICE [NICE: TA674] for use in England.

SECOND-LINE THERAPY

There are limited treatment options for patients who progress despite platinum-based chemotherapy. Some patients may benefit from re-challenging with the same chemotherapy if there was an initial response (98); some may benefit from trial of an alternative second-line chemotherapy (for example, paclitaxel, docetaxel, vinflunine, and oxaliplatin) but response rates are often poor (0-28%) (99,100). Immunotherapies have shown promise in these patients. Atezolizumab was the first approved in this setting by the FDA, although it has not shown an overall survival advantage compared to chemotherapy (101). Pembrolizumab is the most promising, which has shown a significant overall survival advantage over mono-chemotherapy regardless of PD-L1 expression (102), hence is considered the standard of care in the second-line setting.

THIRD-LINE THERAPY

Once patients have failed first and second-line therapy, options are extremely limited outside of exploratory clinical trials. Enfortumab vedotin (EV), an antibody-drug conjugate of nectin-4, is the only FDA approved novel agent in the third-line setting. Used as a monotherapy in patients who have progressed despite platinum and immunotherapy, it delivers a significant overall survival advantage (versus chemotherapy alone) (103). However, EV has not yet been approved for use in England by NICE [NICE: TA797].

NOVEL THERAPIES

Molecular profiling of urothelial carcinomas has highlighted several actionable genetic targets, the most promising of which is *FGFR*. In patients with actionable *FGFR2/3* alterations, systemic Erdafitinib (pan-FGFR inhibitor) treatment after prior chemotherapy delivers a response rate of 40% (104). Data from the ongoing phase III THOR trial of systemic Erdafitinib versus chemotherapy in advanced urothelial carcinoma with selected FGFR aberrations (NCT03390504) is awaited.

PALLIATIVE TREATMENT

Patients who fail or who are unsuitable for the above treatments, may require alternative therapies for local or systemic side-effects of their disease. Most frequently, this includes persistent haematuria, which may be treated using palliative surgery, palliative radiotherapy, or supportive approaches (blood and/or iron transfusions). Complications of malignant urinary tract obstruction may be treated with urinary diversion in the form of urethral or suprapubic catheterisation, palliative ureteric stenting, or nephrostomy tube insertion. In very few and highly selected cases (high-volume bladder disease and low-volume metastatic disease), palliative cystectomy may be considered; this procedure carries a very high morbidity and mortality, which must be weighed up against pre-surgical quality of life and prognosis.

1.1.8.4 REAL WORLD DATA ON THE TREATMENT OF BLADDER CANCER

Although the above chapter describes recommended treatment algorithms across the disease spectrum, real-world data on treatment patterns paint a different perspective. Real-world data may differ from guideline recommendations due to a range of factors that are physician-related (physician experience, perceptions, and values), patient-related (comorbidity/frailty, patient values, healthcare experiences, and decisional control), and healthcare system-related (clinical environments, treatment networks, healthcare economics).

Catto et al. have recently reported real-world data regarding the delivery of treatments to different patient cohorts with urothelial carcinoma between 2013-2019 in England (105). Almost all patients with T1 NMIBC (HR) received surgery, or surgery and adjuvant therapy; although therapy completion and tolerability data were lacking. Over 38% of patients with MIBC received systemic anticancer therapy, with a trend towards increasing use over time. A total of 41% of patients with MIBC received radiotherapy (radical or palliative), and 40% of these patients received concurrent chemotherapy (chemoradiotherapy). Radical surgery was delivered in 24% of cases, with half of these patients receiving systemic anticancer therapy.

However, 27-29% of MIBC patients did not receive radical or palliative surgery, radiotherapy, or chemotherapy, suggesting that just under one-third of patients receive no active treatment.

1.1.9 OUTCOMES AND SURVIVAL

As described in the body of this introduction, outcomes remain difficult to predict and vary with patient and tumour characteristics. Patient suitability (fitness, prior treatment, comorbidity, histology) for necessary treatment also plays an important role. Even within distinct cohorts, for example, NMIBC or MIBC, outcomes are extremely heterogenous. For example, patients with NMIBC have extremely variable recurrence (15-78%) and progression (1-75%) rates at 5 years (106); and patients with MIBC have variable responses to NAC (20-30%) (107,108). Survival trends vary between different BC cohorts. Typically, BC is a disease of the older patient, and many of these patients are current or ex-smokers with competing co-morbidities that may contribute to poor outcomes (5,109). In addition, survival outcomes in BC have not improved over time (105,110,111).

Patients with NMIBC have the best cancer-specific outcomes, with low cancer-specific mortality (1-29% (112,113)). However, overall survival falls in the region of 70-80% at five years (105), due to competing comorbidity. On the other hand, cancer-specific mortality is high in MIBC and mBC patients. Approximately, 50% of patients with MIBC die from their disease within 3-5 years of radical treatment (107,109,114,115). In patients with mBC, this reduces to only 45% of patients surviving 12 months (116).

1.1.10 CONCLUSIONS

1.1.10.1 RATIONALE FOR IMPROVING MODELS OF PATIENT SELECTION AND TREATMENT PERSONALISATION IN BLADDER CANCER

INCIDENCE, PREVALENCE, AND MORTALITY

BC is the second most common urological malignancy and almost half of patients die of the disease. BC also has a particularly high prevalence, affecting millions of people at any one time worldwide (Section 1.1.1: Epidemiology).

HEALTHCARE BURDEN

BC is one of the most expensive cancers to treat and has the highest per-patient lifetime cost of all cancers (117). In the UK alone, BC costs over £66 million per year (118), and is thought cost Europe €5 billion per year (119). The high cost of diagnosing and managing patients with BC is primarily due to the high recurrence rates, expensive and repeated treatments, and intense and lengthy surveillance strategies.

TREATMENT STRATEGIES

The gold standard intravesical and systemic therapies to treat patients with BC have not changed in the last 20-40 years. In addition, just under one-third of patients diagnosed with MIBC do not receive surgery (local or radical), chemotherapy, or radiotherapy, but receive 'other' treatments, which likely reflect palliative strategies (105). Recent advances in treatments such as systemic immunotherapy have provided promise, but have not displaced cisplatin-based combination therapy as standard of care.

SURVIVAL TRENDS

Survival outcomes in BC have not dramatically improved in 30 years (110,111). More recent analysis of NHS England data from 2013-2019 suggests no recent improvement in outcomes (105). Patients with the most aggressive forms of disease have the worst outcomes. For example, only half of patients diagnosed with MIBC will survive five years despite radical treatment (107,114,115), and less than half of patients with mBC survive for 12 months (116).

PATIENT EXPERIENCES

The diagnosis and treatment of BC significantly impacts on the physical, psychological, and social wellbeing of patients. For example, patients with NMIBC, often they undergo years of cystoscopic surveillance and may require repeated surgical resection or adjuvant therapies, which may result in high financial toxicity (particularly for younger patients)(54); and in patients with MIBC, radical treatment strategies carry a high physical and psychological morbidity. Hence, patients diagnosed with BC have some of the poorest reported experiences of all cancers (53,120,121).

SUMMARY

Hence, there is an urgent clinical need to develop predictive BC models that can improve patient selection for treatment and the number of treatments available in the clinic to optimise patient outcomes and experiences.

1.2 PRE-CLINICAL MODELS IN BLADDER CANCER

1.2.1 INTRODUCTION

Despite advances in our understanding of complex cancer biology and knowledge of therapeutic targets, the disease remains fatal for many patients. Next generation sequencing (NGS) of cancers has provided promise for the delivery of precision oncology. However, to date, the utility of genomic-driven treatments has not proven successful in many cancers (122). NGS may, of course, provide valuable information about gene expression, translation, epigenetic, and post-transcriptional changes in cancer; but currently, genomics in isolation struggle to define phenotypic characteristics of cancer cells and patient tumours. Pre-clinical models may assist in filling this void, where phenotypic responses to drug treatment can be assessed; this data forms the foundation of many early phase clinical trials. Sadly, the translational success from pre-clinical model to the clinic (bench to bedside) is poor, where 90-95% of novel drugs never reach the clinic (123,124).

1.2.2 CLASSES OF PRE-CLINICAL MODELS

Pre-clinical cancer models can be broadly divided into *in vitro* and *in vivo* approaches. *In vitro* studies commonly use immortal cancer cell lines or patient-derived cell lines (grown at low passage number from patient tumour tissue), which can be further subclassified by their growth format (for example, 2D versus 3D). *In vivo* work is predominantly classified by the host organism (for example, mouse or rat), which can be further subdivided by how the cancer is developed (for example, xenograft or genetically modified models) and, if a xenograft or allograft, where the cells or tissue have been implanted (for example, heterotopic versus orthotopic). A final class of pre-clinical model to consider are *ex-vivo* models of cancer. *Ex-vivo* techniques use patient-derived tissue to explore disease biology and treatment responses, without grafting the tissue into a host organism. All of the different models described have advantages and disadvantages that must be considered, which are summarised in Figure 1. In the remainder of this chapter, I will describe the contemporary landscape of pre-clinical BC models that have been used to improve patient or treatment selection.

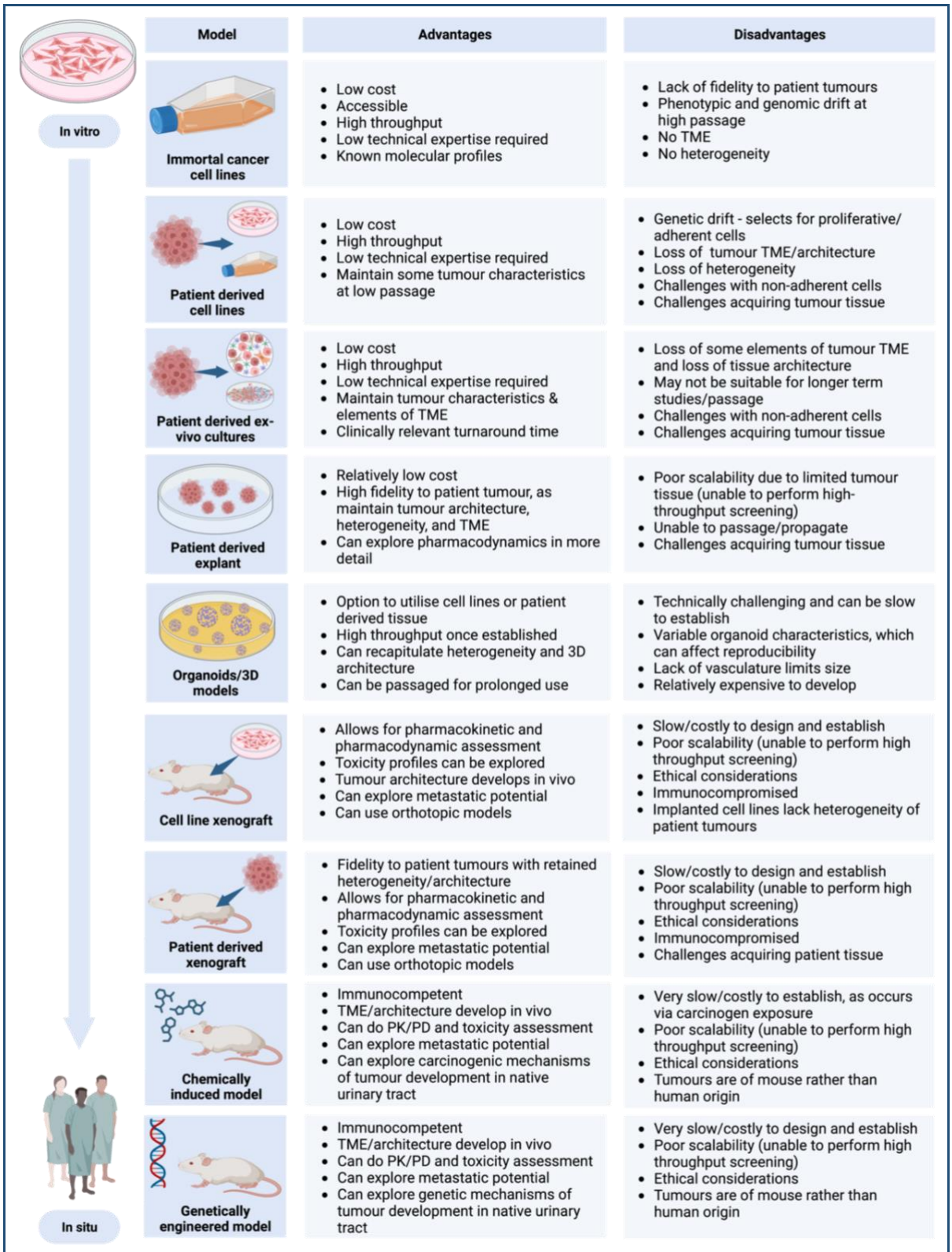

Figure 1: Summary of advantages and disadvantages of pre-clinical models used in BC. TME – tumour microenvironment; 3D – three dimensional, PK – pharmacokinetics; PD – pharmacodynamics.

1.2.2.1 IMMORTAL CANCER CELL LINES

Cell line research using immortal cell lines (ICLs) has historically been instrumental in our understanding of cancer processes and drug discovery. ICLs are established from patient tumours, grown in 2D monolayers, and repeatedly passaged. ICLs are accessible, cheap, and require minimal training or resources to maintain; however, they lack the complexity of solid tumours (125). To date, 127 human, and 30 murine or canine BC cell lines have been established for use (126). Access to multi-omic technologies and NGS has led to a better understanding of genetic aberrations harboured by BC cell lines, and therefore, their suitability and limitations in translational research. At least 69 cell lines have now been profiled by one omic technology (126), which has facilitated the development of a BC cell line atlas. This compares cell lines characteristics to clinical patient outcomes and genomic data, allowing for mapping of BC cell lines to contemporary molecular subtypes (127,128). Similarly, rodent BC cell lines have been genomically stratified into those with characteristics of muscle-invasive or non-muscle invasive disease (129). Thus, although cell lines cannot replicate tumour heterogeneity or the complex tumour microenvironment (TME), they can now be more appropriately selected to answer specific biological questions.

1.2.2.2 PATIENT DERIVED CELL LINES

Patient-derived cell lines (PDCLs) are cell lines generated from primary tumour tissue; this requires tumour dissociation into a single cell suspension before subsequent passaging or conditional reprogramming (125). Manipulation of media conditions facilitates the propagation of desired cell types of different lineages. PDCLs are closer to patient tumour characteristics than ICLs, can grow over extended incubation periods, and are less technically challenging to assay than more complex models. PDCLs are therefore useful in exploring phenotypic drug responses to novel and conventional drugs, as they can be easily exploited in a high-throughput manner. High-throughput screening of PDCLs has been described in a range of cancers types, including: head and neck SCC (130), glioblastoma (131), non-small cell lung cancer (132), BC (133), and pancreatic ductal adenocarcinoma (134) to identify effective treatments. For example, a study by Kettunen et al. (133) highlighted the utility of *ex-vivo* PDCL drug screening in BC. They generated four PDCLs using conditional reprogramming from six patient BCs (66.7% success). High-throughput screening of these PDCLs identified a range of effective standard of care, novel, and repurposed therapies. Unfortunately, one of the drawbacks of using PDCLs is their cellular plasticity with increasing passage and manipulation. In this study, only two out of four (50%) PDCLs retained similar genomic and proteomic profiles to their parent tumours.

1.2.2.3 PATIENT DERIVED *EX-VIVO* CULTURES

Patient-derived *ex-vivo* cultures (PDCs) are cell suspensions generated from the dissociation of patient tumour tissue. Unlike PDCLs, they are not passaged or maintained over long periods, thus, may retain multiple differential cell populations from the dissociated parental tumour or malignant cellular fluid (for example, ascitic or pleural effusions). High-throughput screening of PDCs has been described in several rare cancer case reports (135–138). Individual PDC phenotypic drug responses were ranked in efficacy and used to deliver personalised treatment to patients with no standard of care treatment options available, with impressive responses. It is also possible to model *ex-vivo* PDCs using 3D platforms, for example, by using a scaffold or matrix, providing a more complex reconstruction of the TME. One of the benefits of *ex-vivo* PDC drug screening is that drug sensitivity profiles can be rapidly returned to the clinic to inform treatment decisions within a clinically relevant window (14, 15, 17). Limitations of this model include: the loss of spatial TME and architecture, which may affect drug sensitivity analysis (in particular for anti-angiogenic or immunotherapies), and the lack of adherence of some solid cancers cells using this platform.

1.2.2.4 CELL LINE XENOGRAFTS AND ALLOGRAFTS

In vivo models also have a long history in cancer research and drug discovery. Traditionally, cell-line xenograft models (CLX), where ICLs are injected into immunodeficient or immunocompromised mice, have been used due to their accessibility, ease of maintenance, and relatively low cost (139). Cells can be injected into a number of sites in the host to replicate different disease pathologies; for example, injection of cells into the flank allows for the development of a localised solid tumours (heterotopic), injection into the bladder to develop local bladder tumours (orthotopic), or injection into the tail vein may allow for the cells to travel and develop distant metastases (metastatic). Cell line allografts (syngeneic model) (CLA), however, use cell lines derived from the host, allowing for a degree of immunocompetence. The benefit of CLXs and CLAs over *in vitro* models is the ability explore drug pharmacodynamics and pharmacokinetics (for dose escalation and toxicity), as well as, solid tumour treatment responses.

The expansion of a cell line atlas has allowed for more appropriate selection of cell lines to answer specific questions. For example, heterotopic CLXs using BC cell lines that harbour specific mutations can be generated to explore novel drug responses (140–144). In addition, mice have a relatively homologous urinary tract to humans (139) and ease of access to the bladder trans-urethrally or transabdominally makes orthotopic engraftment an attractive (but more challenging to develop) pre-clinical model. Advantages of orthotopic models include:

presence of a native bladder microenvironment, biological mechanisms and natural history of metastases, and ability to explore intravesical treatments (145). Furthermore, orthotopic allografts may allow for evaluation of immune-modulatory therapies (146,147) and the biological basis of those responses (148).

1.2.2.5 PATIENT DERIVED XENOGRAFTS

To establish a patient-derived xenograft (PDX) model, human tumour tissue, cell suspensions, or even circulating tumour cells are implanted into an immunodeficient host (149). PDXs have become increasingly popular in contemporary translational research, primarily due to their ability to recapitulate the complex biology of human cancers, with maintenance of tissue architecture, tumour microenvironment (TME), tumour heterogeneity, and ability to explore complex biological processes (for example, epithelial to mesenchymal transition (149)).

One key advantage of such a complex model, is being able to explore the intricate biology of drug-resistance. In BC, cisplatin-resistance dominates, where several PDX studies have looked to explore biological mechanisms, biomarkers of resistance, and potential novel drug targets (150–153). PDXs have become more important in the drug discovery landscape (150–152,154–160), owing to the failure of translatability from CLX to patient clinical trials (124). In some cases, PDXs can be combined with other high-throughput screening models to confirm activity of novel compounds, explore mechanisms of resistance, and attain pharmacodynamic and pharmacokinetic data (154). Given their complexity, PDX models are extremely time consuming and costly to develop with variable tumour take rates (11-80%)(161); thus, limiting their applicability in a clinically relevant timeframe. Like most models, PDXs may suffer from genetic drift from parental primary tumour tissue and between PDXs with increasing passage; and although genetic fidelity at early passage is typically good (80-97%) (156,158), infiltration of murine stromal cells and lack of host immune microenvironment may impact on tumour signalling and drug response (125).

1.2.2.6 GENETICALLY ENGINEERED MODELS

Genetically engineered mouse models (GEMMs) have played a critical role in our understanding of a range of genetic alterations that contribute to BC development, differential disease states, and treatment responses. Through the manipulation of cancer-specific genes (gain-of-function oncogenes or loss-of-function tumour suppressor genes) GEMMs develop *de novo* tumours, at disease-specific kinetics, in an immune-proficient environment. In addition, GEMM tumours recapitulate tumour structure and vasculature, as such, if

metastases do develop, then these mimic natural disease progression mechanisms. Nevertheless, GEMMs are not without limitation; they are costly and time consuming to develop, with slow tumours development and unpredictable disease characteristics. BC is particularly heterogenous and lacks a clear pathway for disease progression, unlike other cancers, making the model more challenging. GEMMs also usually only focus on one or two contributing genes, which may not replicate the complex genetic makeup of human cancers; this is supported by several BC GEMM studies that required synergistic mutations, with or without carcinogen exposure, to develop invasive urothelial cancers (162–165).

1.2.2.7 CHEMICALLY INDUCED MOUSE MODELS

Chemical carcinogens may be excreted in the urinary tract and contribute to the development of BC in humans (Section 1.1.2: Aetiology). Therefore, replication of this process in chemically induced mouse models (CIMMs) provides a unique opportunity to evaluate the association between carcinogen exposure and BC development. The common carcinogen used to develop BCs is N-butyl-N-(4-hydroxybutyl)-nitrosamine (BBN). BBN exposure in mice often produces MIBCs, and in rats produces NMIBCs (145,166). Profiling of the muscle-invasive mouse tumours has shown that they express basal-like molecular phenotypes (160,167,168). Basal-squamous tumours typically harbour higher levels of epidermal growth factor receptor (*EGFR*) mutations and infiltrating immune complement than other subtypes (35) (168). CIMMs have similar advantages and disadvantages to GEMMs; their hosts develop *de novo* tumours under manipulated conditions, at the natural kinetics of the disease, and they have the advantage of an in-tact host TME. However, once again, they are slow and costly to develop, and similar to GEMMs, are of host cell origin, rather than being derived from human tumours.

1.2.2.8 ORGANOID AND 3D MODELS

Organoids or spheroids are 3-dimensional (3D) cultures that have the potential to propagate indefinitely. In practical terms, organoids are cells that are allowed to self-aggregate in culture by suspension in a low-attachment vessel. They can be derived from established cell lines (169–175) or patient-derived tumour tissue (154,176,177); therefore, the contents of organoids can be as uniform as a single cell line or as heterogeneous as their parental patient tumors. They offer potential in high-throughput screening, as they are quicker to establish than PDXs and when generated from patient bladder tumours show comparative genetic profiles (178). However, these models are certainly slower, most costly, more technically challenging, and less reproducible than PDCs, due to their varied growth metrics and characteristics.

1.2.2.9 PATIENT-DERIVED TUMOUR EXPLANTS

Patient-derived tumour explants (PDEs) and precision tumour tissue slice systems are generated from solid pieces of tumors taken directly from a patient, either through surgical resection or tumour biopsy. PDEs undergo minimal mechanical dissociation and are either left whole or dissociated into smaller 1-2mm^3 fragments, whereas, precision tissue slice systems slice the tumour. Both allows for retention of tissue architecture, host tumour heterogeneity, and a platform to examine the TME in a low-throughput, high-complexity manner; this makes them a particularly attractive model for exploring complex drug responses and hence their uptake across a range of cancer types (125). More recently, there has also been exploration of precision tumour tissue slice systems Although they have not been used to direct patient treatment, their *ex-vivo* treatment responses have been shown to map to patient clinical responses (179). Similarly in BC, Kelly et al. showed good correlation between PDEs (n=14) responses and patient clinical responses to MMC treatment (180).

Across BC explants and tissue slicing systems, the methodology for culture is inconsistent, spanning a range of growth matrices, tumour-culture interfaces, and media conditions (180–189). BC explants/tissue slices have been seen to last up to 20 days in culture (181), but they become more apoptotic the longer they are in culture (particularly after 12 days) (182). BC PDEs and precision-cut tissues slices, therefore, represent a temporary model for rapid drug testing upon tumour retrieval, which could be delivered in a clinically relevant timeframe. Maintenance of tissue architecture and TME also lends itself to exploring complex tumour responses to treatment. For example, Muthuswamy et al. used BC PDEs to show differential release of chemokines in response to BCG, IFN-alpha, and poly-I:C (TLR3 ligand) treatment (183). However, one of the major limitations of PDEs is their lack of scalability. PDEs are not dissociated, expanded, or maintained for long periods of time; this limits the number of technical replicates performed and the number of drugs that can be tested (which in itself will be predetermined by the size and quality of tumour sample acquired). Hence, there limited scope for high-throughput screening using these models.

1.2.3 CONSIDERATIONS AND CONCLUSIONS

As described throughout this chapter, there are a range of different pre-clinical cancer models that can be utilised to explore cancer biology and treatment responses, all of which have advantages and disadvantages. None of these models perfectly recapitulate the complexities of human BC, nor the dynamic drug-tumour interplay. The choice of pre-clinical model should be tailored to the biological question at hand; although, undoubtedly, time constraints, financial

burden, technical expertise, and equipment availability impact on this decision. Two other factors that should be considered by all undertaking cancer research are the burden of animal use and the environmental impact.

When using animals in research, it is essential to employ the 3Rs principles, to replace, refine, or reduce the number of animals required to meet the study needs. In addition, animal welfare should be optimised at all stages of the experimental design. Abiding to these common principles is not only ethically sound, but paramount in delivering high quality scientific research (190). At the University of Sheffield, we provide a responsible and accountable approach to animal research. We employ strict animal research policies and procedures, recommend the use of animals with the lowest neurophysiological sensitivity, and publish annual audit data on the number of animals used (191).

Academics must also be accountable for the environmental impact of their research. As the global scientific research community moves forward, we must recognise the need to be more resource-efficient and climate-change aware. Laboratories consume up to 10 to 100-fold more energy than an office building of the same size (192). In addition, in 2014 it was estimated that the worldwide burden of plastic waste produced by biological, medical, and agricultural research equated to 5.5 million tonnes (193). Several steps can be taken towards combatting these issues, including: optimising greener lab protocols and set-up; improved sharing of equipment, resources, and reducing research waste; reviewing procurement processed to reduce carbon footprints; and embedding sustainability and climate change into funding requirements (194). Here, at the University of Sheffield, we have taken steps towards greener working since 2009 by embedding behavioural changes to reduce carbon emissions. Since 2009, there has been a saving of 3 million kg of carbon dioxide (195).

1.3 *EX-VIVO* HIGH-THROUGHPUT DRUG SCREENING IN CANCER RESEARCH

1.3.1 INTRODUCTION

As described in the previous section (Section 1.2: Pre-clinical models in bladder cancer), there are an array of pre-clinical models available to cancer researchers, including a number of different *ex-vivo* approaches (Figure 2). The term '*ex-vivo'* describes a variety of techniques, such as 2-dimensional or 3D patient-derived cultures, patient-derived explants (PDEs), or even patient-derived xenograft (PDX) models. However, only a few of these *ex-vivo* approaches have so far been used to direct patient therapy. The remainder of this chapter will be used to describe the evidence supporting *ex-vivo* screening in the field of cancer research, and the rationale for using this as a patient selection and drug discovery platform in this PhD.

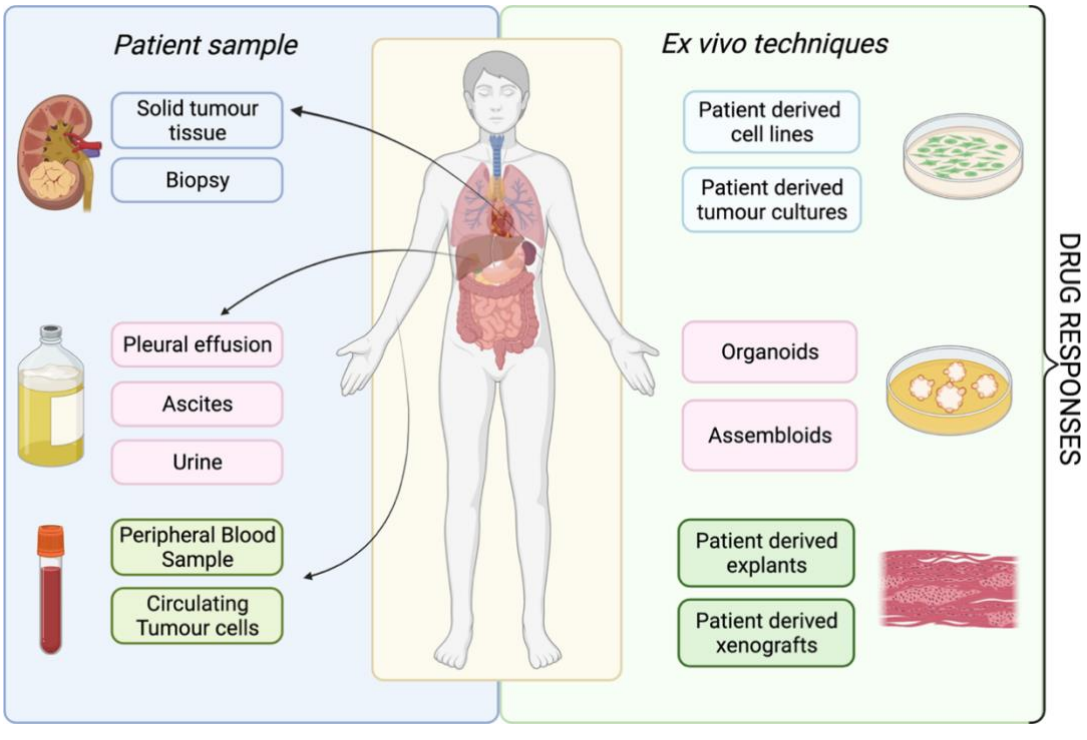

Figure 2: Summary of potential patient samples available to use for ex-vivo research and the differential ex-vivo methodological approaches. Adapted from Williams et al. (126) with permission from the authors.

1.3.2 CHALLENGES INTEGRATING *EX-VIVO* PRE-CLINICAL MODELS INTO CLINICAL PRACTICE

Ex-vivo drug screening is not a new concept and has been used in clinical practice for almost a century. The most obvious example is the use of *ex-vivo* drug testing of patient fluid or tissue to optimise antibiotic treatment selection. Thus, *ex-vivo* drug screening to direct patient therapy in clinical practice is feasible; however, there are several barriers to implementing such methodology in oncological care (Figure 3).

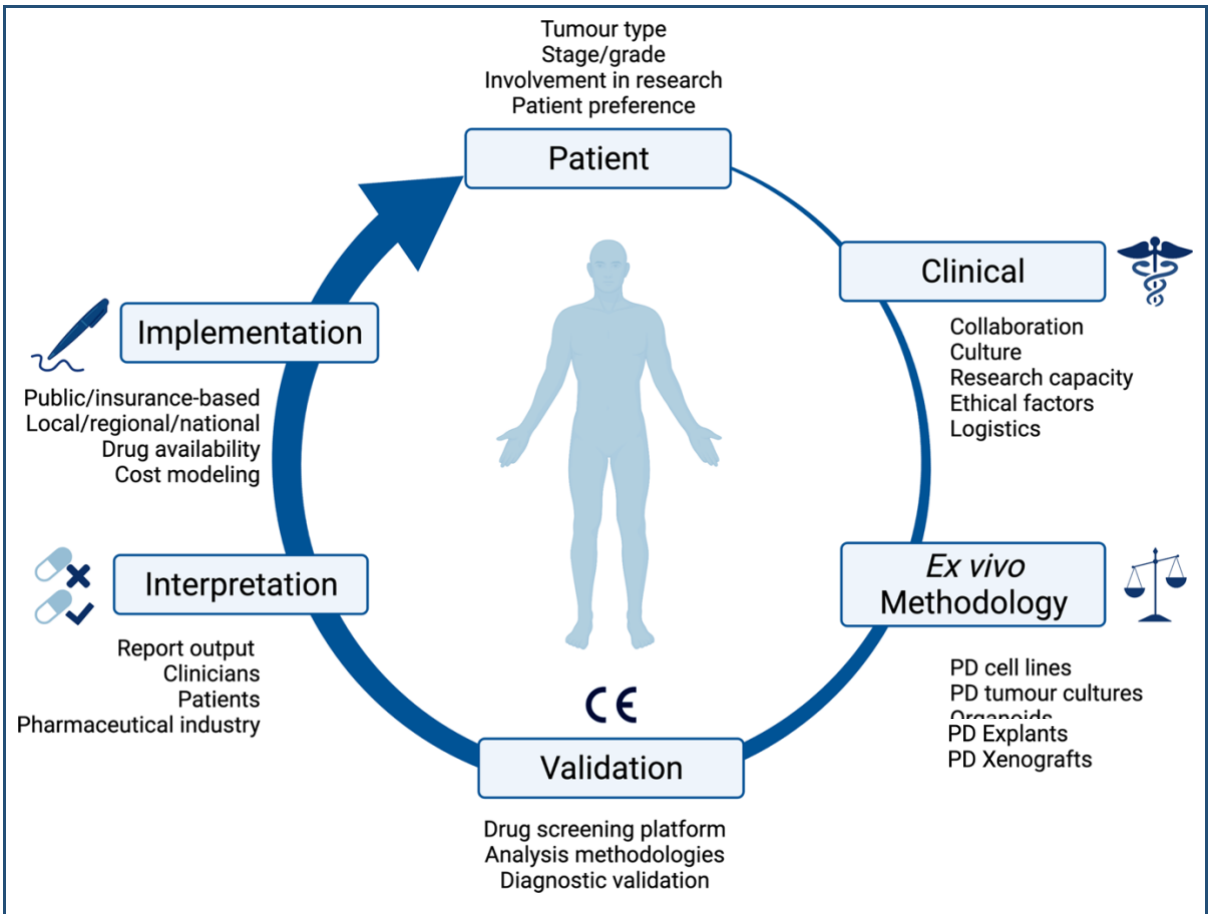

Figure 3: Considerations when implementing ex vivo approaches in clinical practice. PD, patient-derived; CE, Conformité Européenne. Adapted from Williams et al. (125) *with permission from the authors.*

Firstly, there is the issue of patient tumour tissue acquisition. Bespoke models of tissue acquisition will be required per cancer type, tumour stage, and the diagnostic or prognostic relevance of the sample tissue. For example, in haematological malignancies, cancerous 'tissue' can be easily, and repeatedly, sampled at clinically relevant intervals by peripheral venepuncture (a simple, low-cost, acceptable, and non-invasive procedure). The process is much more complex for sampling of solid tumours, where the site and stage of tumour, type

of acquisition (biopsy or surgical resection), technical expertise required, and associated patient morbidity, must all be considered. In addition, any tissue retrieved for research purposes must not compromise clinical care; this means that *ex-vivo* research tumour samples are prone to sampling bias, particularly in spatially heterogenous tumours. For example, in some cancers, the invasive front of the tumour holds the greatest diagnostic and prognostic information; this area of tumour tissue is also one of the most academically sought after, but ethically, often cannot be sampled.

Secondly, the implementation of *ex-vivo* research requires a coordinated effort. A multi-disciplinary approach is paramount, with input from oncologists, surgeons, histopathology, radiologists, research staff, patient, and often industry collaborators. Individual cancer and stage-specific clinical pathways must be meticulously studied and screened, by appropriate delegated team members, to identify eligible patients. Prior to recruitment, logistical pipelines for tumour sample retrieval must be agreed between all stakeholders, which then need to be navigated if the patient consents to participate. Institutional research culture and willingness to collaborate often underpin the success of such pipelines.

Finally, once an *ex-vivo* tumour tissue acquisition pipeline and drug-screening method have been chosen, there are the issues of validation and implementation. These can fall under the categories of translational validation, clinical validation, or interventional trials. To date, relatively few *ex-vivo* translational studies have bridged the gap towards a clinical trial (125). Many factors contribute to this, including patient, tumour, clinician, and institution factors, variability in model platform and end-point analysis choice, and lack of clinical information to support the transition to a larger, more complex, and expensive clinical trial.

1.3.3 *EX-VIVO* HIGH-THROUGHPUT SCREENING EFFICACY IN HAEMATOLOGICAL CANCERS

Ex-vivo high-throughput drug screening has been most successful in haematological malignancies, where it has been used to direct patient treatment. *Ex-vivo* directed treatment was initially trialled in a small pilot study of 12 acute myeloid leukaemia patients (AML) with limited but promising results (196). A recent study expanded on this, including 187 AML patients, where 37 patients who had relapsed or refractory disease were treated with *ex-vivo* directed therapy (197). *Ex-vivo* drug screening results were delivered in a clinically relevant window (median of four days), with a 59% objective response rate, and 45% complete response rate in those who received *ex-vivo* directed therapy. Advances in microscopy quality and computation technology have allowed for more sophisticated methods of imaging

individual cancer cell populations within *ex-vivo* suspensions. Image-based *ex-vivo* drug screening in advanced haematological malignancies – described as 'pharmacoscopy' – has been equally promising (198,199). In 56 patients treated with pharmacoscopy-directed therapy, 54% yielded a 1.3-fold increase in their progression-free survival, compared to their previous standard of care treatment.

These clinical trials highlight that *ex-vivo* directed therapy, based on phenotypic response profiles, can deliver promising clinical responses, even in patients with advanced disease. Results were returned in clinically meaningful timeframe and did not delay treatment decision making. Unlike genomically-stratified treatment, *ex-vivo* drug screening (when high-throughput) can provide an expanded library of therapeutic options for patients. These results highlight that functional drug screening can deliver clinically meaningful impact in haematological cancers and warrants further investigation with a randomised controlled trial.

1.3.4 *EX-VIVO* HIGH-THROUGHPUT DRUG SCREENING EFFICACY IN SOLID CANCERS

Implementation of *ex-vivo* phenotypic drug screening in solid tumours is slightly more complex, as described in section 1.3.2 (Challenges integrating *ex-vivo* pre-clinical models into clinical practice). Bespoke and meticulous ethical planning for each cancer type and by tissue acquisition method, are required. Once an individual has consented to participate, there is then the logistical challenge of harvesting the tumour tissue, which requires collaboration between surgical, medical, histopathological, and research teams. Any sample retrieved for research must not alter diagnostic or prognostic information; thus, research specimens may also be influenced by sampling bias.

A range of *ex-vivo* drug screening methodologies have been implemented across a number of solid tumour types (200), including: lung cancer (134), colorectal cancer (201,202), melanoma (203,204), and glioblastoma (205). However, very few studies have used PDCs for *ex-vivo* screening (135–138). This may reflect that PDCs require deconstruction of tissue architecture, which may not be an appropriate model for all solid tumour types. *Ex-vivo* PDCs have been used to explore novel drug responses in several case reports of rare cancers (epithelial-myoepithelial cancer salivary gland cancer (136), recurrent thymoma (137), urachal carcinoma (138), and Krukenberg tumours (135)) in whom treatment options remain largely under-researched. *Ex-vivo* high-throughput screening results were used to direct patient treatment in three of these studies (135–137), with promising durable responses lasting 5-13 months. In these cases, *ex-vivo* screening successfully identified novel targeted therapies for

patients with rare and difficult to treat cancers, whilst simultaneously developing insight into the implicated molecular biology of these diseases. Given the paucity of clinical trials for patients with rare cancers, *ex-vivo* directed therapy tested with a bespoke clinical trial design may provide scope to personalise treatment and improve treatment options in the clinic.

1.3.5 *EX-VIVO* HIGH-THROUGHPUT DRUG SCREENING IN BLADDER CANCER

As described in the previous chapter, *ex-vivo* screening of any kind in BC is rarely reported. Only nine studies have used non-xenograft, *ex-vivo* methodology to study treatment effects in BC since 1990 (133,147,181–185,206,207); furthermore, only one of these has explored high-throughput drug screening (133). The clinical landscape and timelines in BC care provide several opportunities for *ex-vivo* tumour tissue sampling (Figure 4). Firstly, patients with visualised bladder tumours almost all require diagnostic resection of their tumour (TURBT), providing an opportunity for research sampling.

In addition, there are several unique windows of opportunity to validate *ex-vivo* drug screening or even implement it as a predictive tool within the care pathway (Figure 4). These fall into three categories:

- Patients with IR or HR NMIBC who are due to receive adjuvant intravesical therapy; clinical endpoints: recurrence and progression; (Figure 4, yellow shaded pathway)
- Patients with MIBC who are fit to receive NAC and RC; clinical endpoints: overall response rate, pathological complete response at RC, and subsequent progression, metastases or death; (Figure 4, green shaded pathway)
- Patients with mBC who undergo biopsy (or limited resection of their tumour) who are due to receive systemic therapy; clinical endpoints: overall response rate, progression, and death; (Figure 4, blue shaded pathway)

Hence, not only is there a clinical unmet need for patients with BC (as described in the introductory chapter) that could potentially be alleviated by improved models of patient and treatment selection; but the BC cancer clinical pathway seems an optimal setting to explore the feasibility and utility of *ex-vivo* high throughput drug screening.

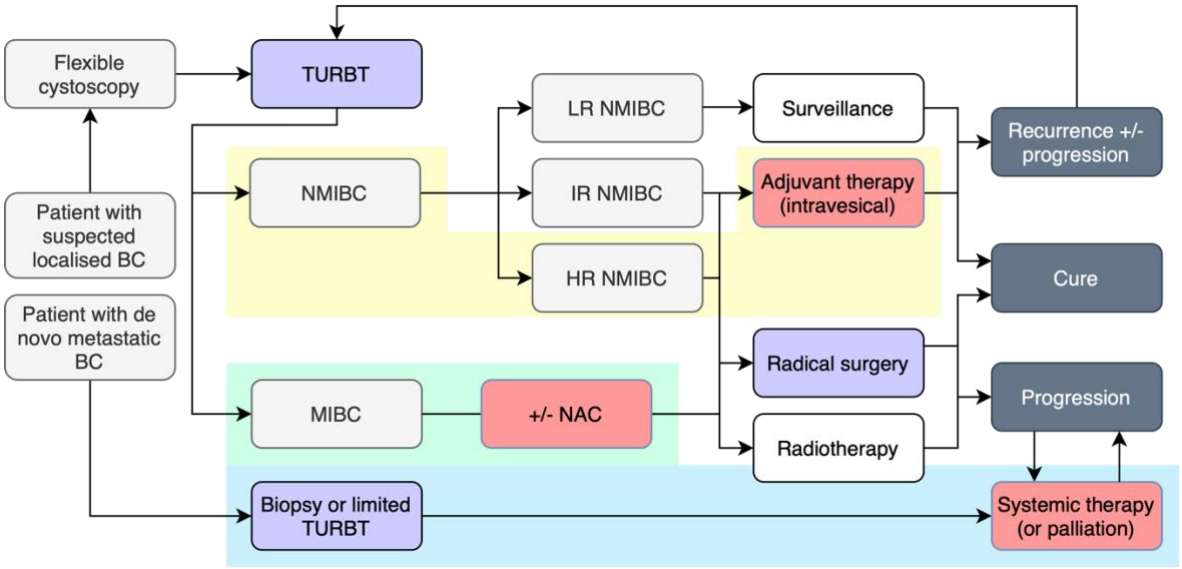

Figure 4: Flow diagram showing the potential for ex-vivo tissue sampling in BC NHS patient timelines. The procedures where ex-vivo samples can potentially be accrued are in purple; the intravesical or systemic treatments that patients receive are in red; the endpoints are in grey. Three key potential opportunities for implementation of ex-vivo drug screening are highlighted in yellow (high-risk NMIBC pathway in those who recur), in green (MIBC pathway in those due to receive NAC and radical surgery), and in blue (in those fit for systemic therapy who are due to undergo biopsy or limited tumour resection). BC – bladder cancer; TURBT – transurethral resection of bladder tumour; NMIBC – non-muscle invasive bladder cancer; MIBC – muscle invasive bladder cancer; LR NMIBC – low risk non-muscle invasive bladder cancer; IR NMIBC – intermediate risk non-muscle invasive bladder cancer; HR NMIBC – high risk non-muscle invasive bladder cancer; NAC – neoadjuvant chemotherapy.

1.4 CONCLUSIONS

In summary, BC is common, with a high prevalence and poor outcomes. Outcomes are particularly poor for those with advanced disease, where in the real world, almost one third receive no active treatment. In those who do receive treatment, the therapy we deliver has seen little advance in 30 years. Compounding this, our current patient risk stratification for treatment in the clinic is stagnant, based predominantly on traditional clinical staging parameters, and does not account for molecular or phenotypic properties. All of this contributes to BC being one of the most expensive cancers to treat, with high recurrence rates due to treatment failure, toxicity in patients who do not benefit from treatment, and high morbidity and mortality in those undergoing radical therapy. Hence, there is a need to first and foremost increase the number of anti-cancer agents available to our patients in the clinic; and secondly, enhance our current treatment selection strategies for those treatments to better incorporate the complex molecular make-up of individual BCs.

One suggested method to deliver this is to use molecularly-guided therapy (genetic, transcriptomic, or proteomic biomarkers) to direct patient treatment. Many cancers have been found to have actionable mutations (208–210), however, there are barriers to delivering these therapies in the clinic, including: off-label drug use restrictions, patient ineligibility, and lack of accessible clinical trials. In addition, the utility of genomic-driven treatments has not proven successful in many cancers. Another method of drug development and exploring risk stratification in cancer is through the use of pre-clinical models, where phenotypic responses of tumour cells or tissues can be assessed in a multitude of formats. Sadly, the translational success from pre-clinical model to the clinic (bench to bedside) is time consuming and often ineffective, where most drugs evaluated never reach the patient.

Ex-vivo high-throughput drug screening using PDCs is a relatively novel approach. There is a growing body of evidence in haematological cancers to suggest that *ex-vivo* high throughput drug screening can be used to direct patient treatment, and in well selected patients, may improve clinical outcomes compared to standard of care therapy. *Ex-vivo* high throughput drug screening in BC seems feasible, with several ways to access invaluable patient tumour tissue that have defined clinical endpoints and would otherwise not alter the patient journey. There are also several unique windows of opportunity to validate this model in BC. In addition, high-throughput drug screening may assist in identifying novel compounds, tested for efficacy directly on BC PDCs, which may expand the number of treatments available to patients with BC, which have not really changed since the 1980s.

Currently, there is no standardised methodology for *ex-vivo* tissue processing of BCs to develop PDCs. The purpose of this PhD is to evaluate the feasibility of adapting published *ex-vivo* methodology on patient BCs to develop viable BC PDCs. To explore whether *ex-vivo* high throughput drug screening of *ex-vivo* PDCs can be used to identify differential treatment responses in patient BC PDCs. And finally, to correlate these results with whole-exome sequencing data to explore the underlying mechanisms of response, or non-response, to identify novel biomarkers for treatment stratification.

CHAPTER 2

AIMS AND OBJECTIVES

2.1 HYPOTHESIS

Ex-vivo high throughput drug screening in bladder cancer (BC) is logistically and methodologically feasible and can be used to explore differential responses to standard of care and novel therapies to personalise patient treatment selection.

2.2 AIMS

1. To explore the feasibility of *ex-vivo* high-throughput drug screening by generating patient-derived *ex-vivo* cultures (PDCs) from fresh patient BC tumour samples;

2. To generate proof of concept data which demonstrate that *ex-vivo* high throughput drug screening of BC PDCs can identify differential responses to standard of care therapy;

3. To explore whether *ex-vivo* high throughput drug screening using BC PDCs, combined with whole exome sequencing (WES) of tumour tissue, can inform about effective novel therapies.

2.3 OBJECTIVES

1. Explore the logistical feasibility of study patient identification, patient recruitment, and fresh bladder tumour tissue acquisition from surgery; develop an adapted methodological protocol for the development of BC PDCs *de novo* throughout this PhD; generate cancer-specific drug plates containing standard-of-care, repurposed, and novel therapeutic agents; evaluate success of the *ex-vivo* methodological protocol.

2. Evaluate endpoint drug sensitivity results of individual, *ex-vivo* processed PDCs to generate patient and tumour-specific drug sensitivity profiles; explore differential *ex-vivo* drug sensitivity phenotypes and correlate with patient, tumour, and clinical outcome parameters; explore its utility as a pre-clinical predictive model of response.

3. Explore the feasibility of *ex-vivo* high throughput drug screening of fresh patient BCs as a novel drug discovery tool; use paired whole-exome sequencing of stored tumour tissue to explore implicated molecular biomarkers of clinical outcomes and *ex-vivo* phenotypic responses.

CHAPTER 3

PATIENTS, MATERIALS AND METHODS

3.1 ETHICAL STATEMENT

3.1.1 ETHICAL APPROVAL AND ELIGIBILITY CRITERIA

Ethical approval was granted for the processing of fresh patient bladder tumour tissue (STH15574); this was subsequently updated during the study period to ensure that it would cover the longevity of the project and also was expanded to include other tumour types as part of the Ex-VIvo DetErmiNed cancer Therapy (EVIDENT) study consortium objectives (STH20854; IRAS number 262315). Patient eligibility criteria are described in Table 3.

Table 3: Patient inclusion and exclusion criteria for this *ex-vivo* high throughput drug screening study

Inclusion criteria:	Exclusion criteria:
- Patients with a bladder tumour identified at outpatient flexible cystoscopy who are due to undergo surgical resection of their tumour; - Patients with radiological evidence of a bladder tumour who are due to undergo surgical resection of their tumour; - Patients undergoing radical cystectomy for confirmed high-risk non-muscle invasive bladder cancer (HR NMIBC) or muscle invasive bladder cancer.	- Patients undergoing transurethral resection of bladder tumour (TURBT) or biopsy of a bladder lesion, where the pathology is not anticipated to be malignant; - Patients undergoing benign cystectomy; - Patients undergoing primary radical cystectomy for HR NMIBC, where it is anticipated there will be minimal residual bladder tumour; - Patients who are unable to provide informed consent; - Patients who have tested positive for COVID-19 infection.

3.1.2 RECRUITMENT AND CONSENT

As an NHS professional and Honorary Clinical Fellow in Urology, I performed screening of urological operating lists. Review of patient letters, case notes, as well as blood, imaging, and histopathology results, determined eligibility. I am clinically and academically (as per NIHR Good Clinical Practice guidelines) trained in the process of gaining informed consent. Patients were recruited prior to their surgical procedure. Written informed consent was obtained from all participants. It was made clear to all patients that they may decline to participate or withdraw at any stage without affecting their care. Patients were given time to read and discuss the patient information sheet prior to consent. A copy of the signed consent form, contact details for members of the research team, and information about withdrawal from the study were provided for every participant. After initial recruitment, there was no further physical, verbal, or virtual interaction between the research team and participant. No additional study visits were required.

3.1.3 HANDLING OF PATIENT TUMOUR TISSUE

After providing written informed consent, participants underwent their surgical procedure. Participation in the study did not alter their surgical procedure. For TURBT specimens, a visibly resected fresh tumour sample, identified by the operating surgeon, was transported directly to the *ex-vivo* tissue culture laboratory for processing. For radical cystectomy (RC) specimens, the organ was transferred immediately to histopathology for specimen sampling. On receipt, the sample was processed as described in (section 3.3.2). A proportion of tissue was frozen and stored at -80°C for DNA/RNA extraction. All incubators and freezers were located in locked rooms, in a card-access only area of the research department. All tumour tissue was collected and stored according to the principles of the Declaration of Helsinki and use of tumour tissue was compliant with the Human Tissue Act, 2004.

3.1.4 PARTICIPANT DATA MANAGEMENT

Information about data capture and storage can be found in the Data Management Plan for the study (Section 9.1: Appendix 1: Data management protocol).

3.2 MATERIALS

3.2.1 *EX-VIVO* TUMOUR TISSUE PROCESSING

The general laboratory equipment used in this study are described in Section 9.2: Appendix 2: General laboratory consumables.

Non-supplemented Lonza RPMI 1640 Media (Scientific Laboratory Supplies Ltd) was used for specimen receipt and transport. Tumour cell suspensions were cultured in "*ex-vivo* media", which consisted of Lonza RPMI 1640 Media (Scientific Laboratory Supplies Ltd) with 1% L-glutamine (200mM, Scientific Laboratory Supplies Ltd), 1% penicillin/streptomycin solution (100IU/mL penicillin, 100ug/mL streptomycin), 1% Insulin-Transferrin-Selenium (1.0mg/ml, 0.55mg/ml, 0.5ug/ml, respectively, ThermoFisher Scientific), and 5% Fetal Bovine Serum (ThermoFisher Scientific). Media was stored at 4^{o}C and heated to 37^{o}C prior to use.

Sterile phosphate-buffered saline (Dulbecco's Phosphate Buffered Saline) (Lonza) containing 0.0095M PO4 without Ca2+ or Mg2+, was autoclaved locally and stored at room temperature.

TrypLE™ Select Enzyme (ThermoFisher Scientific) was stored at room temperature.

Accutase® solution (Sigma) prepared in PBS containing 0.5 mM EDTA•4Na and 3 mg/L Phenol Red was stored in 5ml aliquots at -20^{o}C. For use, an aliquot was thawed gently to room temperature before heating to 37^{o}C.

Collagenase/Dispase® lyophilized, non-sterile (Sigma) was reconstituted to 100mg/ml and stored in 50uL aliquots at -20^{o}C. For use, an aliquot was thawed gently to room temperature, before mixing with PBS to a working concentration of 1mg/ml. Following this, the working Collagenase/Dispase® solution was passed through a sterile 0.2µm membrane filter and heated to 37^{o}C.

The remainder of *ex-vivo* tumour tissue processing-specific materials and equipment are described in Table 4.

Table 4: *Ex-vivo* tumour tissue processing equipment and reagents		
Item name	Supplier	Storage
Sterile sample pot 100ml Container - metal cap, printed label	Greiner Bio-One International	N/A
Cell Culture Dishes, 60 and 100mm	Eppendorf	N/A
Instrapac Disposable Scalpel No11 (sterile)	Swann-Morton	N/A
AE31E Trinocular inverted microscope	Motic	N/A
ThermoMixer F2.0 with variable thermoblocks	Eppendorf	N/A
Easystrainer 70µM Sterile Filters	Greiner Bio-One International	N/A
Trypan Blue Solution (0.4%)	ThermoFisher Scientific	RT
Cellometer Mini Disposable Counting Chambers	Nexcelom Bioscience	N/A
Cellometer Mini Automated Cell Counter	Nexcelom Bioscience	N/A
E1-ClipTip Electronic Multichannel Pipette	ThermoFisher Scientific	N/A
Dimethyl Sulfoxide (DMSO)	Fisher Bioreagents	RT

RT – room temperature

3.2.2 CELLTITER-GLO® ATP ASSAY

CellTiter-Glo® (CTG) was purchased from Promega and divided into 4-5ml aliquots, before storing at -20^{o}C. Prior to use, CellTiter-Glo® aliquots were either thawed at 4^{o}C overnight, or allowed to thaw to room temperature, not exceeding 25^{o}C.

3.2.3 BLADDER CANCER-SPECIFIC DRUG PLATES

BC-specific drug plates were designed in a 384-well format, with a pseudo-randomised well allocation to minimise plate variation effects. Oncological compounds were purchased from Stratech Scientific Ltd (unless otherwise stated) at pre-defined concentrations of 10mM diluted in dimethylsulfoxide (DMSO) or water (as platinum compounds are deactivated by DMSO). Agents included standard-of-care compounds, repurposed chemotherapeutics, and novel oncological agents that targeted actionable mutations in bladder cancer (BC) (Table 5). All drugs were stored at 4^{o}C prior to batch plate printing, and subsequently frozen to -80^{o}C once the plates were printed ready for use.

Table 5: Summary of purchased drug plate oncological compounds

Compound	Drug Category	Mechanism of Action	Order Ref	Solvent	Conc (mM)
Fulvestrant	Anti-oestrogen	Oestrogen receptor inhibitor	A1428-APE	DMSO	10
Mitomycin C	Antibiotic and alkylating agent	Inhibit DNA replication and transcription	A4452-APE	DMSO	10
Gemcitabine	Anti-metabolite	Deoxycytidine analog	A8437-APE	DMSO	10
Paclitaxel	Microtubule inhibitor	Disruption of replication	A4393-APE	DMSO	10
Vinblastine	Microtubule inhibitor	Disruption of replication	N2256-APE	DMSO	10
AZD8931 (Sapitinib)	Dual tyrosine kinase inhibitor of EGFR	Inhibits HER2 and HER3 signalling	A8375-APE	DMSO	10
AZD6244 (Selumetinib)	MEK or MAPK/ERK inhibitor	Inhibits MEK1 and 2 signalling	A8207-APE	DMSO	10
AZD1152 (Barasertib)	Aurora Kinase B inhibitor	Disrupts spindle checkpoints/ chromosome alignment	A3214-APE	DMSO	10
Erdafitinib	Pan-FGFR inhibitor	Inhibits FGFR-signalling	B8387-APE	DMSO	10
AZD4547	Pan-FGFR inhibitor	Inhibits FGFR-signalling	A8350-APE	DMSO	10
AZD2014 (Vistusertib)	Inhibits mTOR	Induces apoptosis/ reduces proliferation	A8373-APE	DMSO	10
AZD8186	PI3K(Beta) inhibitor	Inhibits PI3K/AKT/ mTOR signalling	B5950-APE	DMSO	10
AZD5363 (Capivasertib)	AKT inhibitor	Inhibits AKT signalling	A1387-APE	DMSO	10
Lenvatinib	Multi-kinase inhibitor	Inhibits VEGF and FGFR signalling	A2174-APE	DMSO	10
Nutlin-3a	Binds to p53 site on MDM2	Induces p53 dependent cell death	A3671-APE	DMSO	10
Etoposide (VP-16)	Topoisomerase II inhibitor	Inhibit RNA and DNA synthesis, and inhibits DNA repair	A1971-APE	DMSO	10
Docetaxel (Taxotere)	Microtubule inhibitor	Disruption of replication	A4394-APE	DMSO	10
Doxorubicin (Adriamycin)	Topoisomerase II inhibitor	Inhibit RNA and DNA synthesis, and inhibits DNA repair	A3966-APE	DMSO	10
TH1579	MTH1 inhibitor	Inhibits MTH1 to obstruct DDR	HL, KI*	DMSO	10
Cisplatin	Alkylating agent	Inhibit DNA replication and transcription	A8321-APE	H20	5
Carboplatin	Alkylating agent	Inhibit DNA replication and transcription	A2171-APE	H20	10
Pembrolizumab	PD-1 binding antibdy	Helps to restore T cell response	A2005-SEL	DMSO	5mg/ml
Olaparib	Inhibits poly (ADP-ribose) polymerase	Inhibits DNA damage repair	A4154-APE	DMSO	10
Thiotepa	Alkylating agent	Inhibit DNA replication and transcription	S1775-SEL	DMSO	10
Pemetrexed	Folate antagonist	Inhibit purine synthesis	A4390-APE	DMSO	10
Methotrexate	Folate antagonist	Inhibit purine synthesis	A4347-APE	DMSO	10
Cabazitaxel	Microtubule inhibitor	Disruption of replication	B2157-APE	DMSO	10
Aphidicolin	Inhibits DNA polymeras	Inhibits DNA synthesis	B7832-APE	DMSO	10
Staurosporine	Inhibits ATP binding to protein kinases	Induces apopotosis	A8192-APE	DMSO	10

**HL, KI – Supplied by the Helleday Laboratory, Karolinska Institutet*

3.2.4 DNA EXTRACTION FROM STORED TUMOUR TISSUE

DNA extraction from stored tumour tissue was performed using the Qiagen DNeasy® Blood and Tissue Kit, which included the following reagents: Proteinase K; Buffer ATL; Buffer AL; Buffer AW1; Buffer AW2; Buffer AE; and included DNeasy® mini spin columns and collection tubes. 98% ethanol required for DNA extraction was stored at room temperature. Quantification and quality assessment of DNA was performed using the NanoDrop® ND-1000 (ThermoScientific).

3.2.5 ANALYSIS OF END POINT DATA

Endpoint CTG data was converted from raw .xml file to .xls or.csv using Microsoft Excel (Version 16.69.1; Microsoft Corp., Redmond, WA, USA). Prism 9.5.1 (GraphPad Software Inc., San Diego, CA, USA) was used to perform basic statistical analyses and to generate graphical data. R studio version 4.2.2 was used to analyse endpoint CTG data and whole exome sequencing data. The command “session_info()” was used to extract information about the R packages used throughout the study, which are summarised in section Appendix 3: List of R packages used for data analysis. More specifically, for analysis of endpoint CTG data, the GRmetrics package was used to generate drug sensitivity data (211); pheatmap was used to generate annotated heatmaps (212); and Maftools package was the main package used to analyse and summarise whole exome sequencing data (213).

3.3 METHODS

3.3.1 DEVELOPMENT OF CANCER-SPECIFIC 384-WELL DRUG PLATES

3.3.1.1 PREPARATON

Methods for drug plate development were completed as described by Gagg et al. for *ex-vivo* tissue processing of glioblastoma tumours (214). In brief, cancer-specific compounds (Table 5) were purchased as pre-diluted liquids (in DMSO), or as solids and reconstituted (in water for platinum-based compounds). Upon acquisition, drugs were aliquoted and stored at -80^{o}C to manufacturer's instructions. The final 384-well plate design was curated in advance, where drug dilutions and controls are dispersed across the plate to minimise the impact of plate effects. Four drug concentrations were used for each compound (Table 6). Highest drug concentrations were based on previous *ex-vivo* tumour tissue high-throughput screening work performed by Dr Rantala (135,136,215). Three technical replicates were performed for each drug concentration. Twenty-eight vehicle (negative) controls were allocated.

3.3.1.2 CURATION

For drug dispensing, a 96-well master plate was created containing drugs at 10x the top concentration required; this was serially diluted using a 1:2 series to create 3 further 96-well master plates at 5x, 2.5x, and 1.25x. Vehicle (DMSO), positive (Staurosporine), and cytostatic (Aphidicolin) controls were then added, completing the master plate layout. Thermo Platemate Liquid Handling automated technology at the Sheffield Institute for Translational Neuroscience was used to accurately transfer and dispense 5µL of drug or vehicle solution from the master plates onto their final allocation on the 384-well plate. Once all drugs were printed onto the 384-well plate, plates were centrifuged briefly for 30s at 800rcf and sealed with a non-permeable cover before immediate storage at -80^{o}C. Final drug concentrations are shown in Table 6. Up to 80 drug plates were created per batch. The 384-well layout organised drugs into pseudo-randomised positions to minimise plate effects (Section 9.1: Appendix 4: Pseudo-randomised 384-well drug plate layout)

Table 6: Table of final working drug concentrations for oncological compounds used in bladder-cancer specific drug plates

Drug name	Batch	P1 (µM)	P2 (µM)	P3 (µM)	P4 (µM)
Doxorubicin	1 & 2	1	0.5	0.25	0.125
Etoposide	1 & 2	2	1	0.5	0.25
Docetaxel	1 & 2	2	1	0.5	0.25
AZD6244	2	2	1	0.5	0.25
TH1579*****	1 & 2	5	2.5	1.25	0.625
Mitomycin C	1 & 2	5	2.5	1.25	0.625
Gemcitabine	1 & 2	5	2.5	1.25	0.625
Paclitaxel	1 & 2	5	2.5	1.25	0.625
Vinblastine	1 & 2	5	2.5	1.25	0.625
AZD8931	2	5	2.5	1.25	0.625
AZD1152	2	5	2.5	1.25	0.625
Erdafitinib	1 & 2	5	2.5	1.25	0.625
AZD4547	1 & 2	5	2.5	1.25	0.625
AZD2014 (Vistusertib)*****	1 & 2	5	2.5	1.25	0.625
AZD8186	1 & 2	5	2.5	1.25	0.625
AZD5363 (Capivasertib)	1 & 2	5	2.5	1.25	0.625
Lenvatinib	1 & 2	5	2.5	1.25	0.625
Nutlin-3a	1 & 2	5	2.5	1.25	0.625
Fulvestrant	2	10	5	2.5	1.25
Carboplatin	2	20	10	5	2.5
Cisplatin	1 & 2	20	10	5	2.5
Pembrolizumab	2	25	12.5	6.25	3.125
Olaparib	1	10	5	2.5	1.25
Thiotepa	1	5	2.5	1.25	0.625
Pemetrexed	1	5	2.5	1.25	0.625
Methotrexate	1	5	2.5	1.25	0.625
Cabazitaxel	1	5	2.5	1.25	0.625

**drug dose changed after first batch*
P1 – highest drug concentration; P4 – lowest drug concentration.

3.3.2 OPTIMISED PROTOCOL FOR *EX-VIVO* TUMOUR TISSUE PROCESSING

All *ex-vivo* tumour tissue processing was performed in a class II biological safety cabinet and waste disposed of in accordance with the University of Sheffield's internal waste management policies. The following section describes the optimised *ex-vivo* high throughput drug screening methodology, defined after performing validation work described in results section 4.3.

3.3.2.1 LOGISTICAL HANDLING OF FRESH TUMOUR TISSUE

Tumour tissue samples were transported immediately from surgery or histopathology to the *ex-vivo* designated tissue culture laboratory (Department of Oncology and Metabolism, University of Sheffield) in sterile sample collection pots containing 10ml of non-supplemented Lonza RPMI 1640 Culture Medium (room temperature). Tumour tissues were processed within 24 hours of receipt.

3.3.2.2 INITIAL SAMPLE PREPARATION

Bladder tumour tissues were transferred from the sample pot to a sterile Eppendorf 60-100mm petri dish relative to the volume of tumour sample received. All transport media was retrieved and centrifuged (200-400rcf, 3 minutes) to salvage dispersed tumour cells. If a visible tissue or cellular pellet was identified through centrifugation, this was retained for processing. Areas of macroscopic tissue char (due to electrocautery) were removed using a sterile scalpel. Tumour sample volumes were calculated prior to dissociation. If excessive macroscopic red blood cells or debris were identified, samples were rinsed with 5-10ml of sterile Phosphate Buffered Saline (PBS).

3.3.2.3 MANUAL DISSOCIATION OF TUMOUR TISSUE

Ex-vivo media (Section 3.2.1) was added to tumour specimens (3-10ml reflecting the size of the sample). Tumour specimens were manually dissociated using sterilised tissue forceps and a 1000µL pipette tip (softer tissues) or sterile scalpel (solid tissues). Mechanical dissociated continued until the tumour was divided into <1mm pieces. Brightfield microscopy assessment of tumour dissociation was performed by sampling 10µL of *ex-vivo* tumour-media suspension prior to enzymatic dissociation. For brightfield assessment, 10µL of tumour cell suspension was added to a glass cover slip and reviewed at 10 and 20x under a Motic AE31E Trinocular inverted brightfield microscope. Tumour pieces and *ex-vivo* media were then transferred into 15ml universal centrifuge tube(s) (1-6 depending on the volume of tumour sample) and centrifuged (200-400rcf, 3 minutes) to generate a tissue pellet for enzymatic dissociation.

3.3.2.4 OPTIONAL STEP: REMOVE OF EXCESS RED BLOOD CELLS

Some samples, after the preceding step, had a clear red blood cell layer that developed on top of the tumour pellet, which could impact on downstream analysis. The optional removal of excess red blood cells included the following steps:

- Gentle aspiration of supernatant, which was then discarded;
- Re-suspension of pellet (including red blood cell layer) in 10ml sterile PBS and allow to stand vertical for 5-10 minutes for tumour cells to move inferiorly;
- Brightfield check (as described in section 3.3.2.3) of PBS suspension to ensure no/minimal tumour cells; if tumour cells were visible, then the contents were centrifuged at 200-400rcf for 30s;
- Gentle aspiration of remaining PBS, which was discarded.

This would leave a tumour tissue pellet ready for enzymatic dissociation.

3.3.2.5 ENZYMATIC DISSOCIATION OF SOFT TUMOUR TISSUE

Depending on the size of tissue pellet(s), 1-3ml of TrypLE™ Select Enzyme was added and gently agitated before incubating (37°C/5%CO_2) with constant mixing using the ThermoMixer device set at 37°C, 500-750rpm. Brightfield examination of tumour-enzyme cell suspension was performed at 5-10 minutes intervals to assess for the presence of micro-aggregates (Figure *5*: A). Once a single cell suspension was reached (Figure *5*: B), dissociation was complete. 10ml of FBS-containing *ex-vivo* media was added to the cell suspension to deactivate enzymatic dissociation and centrifuged (200-400rcf, 3 minutes). Enzyme-containing supernatant was discarded and the single-cell pellet retained.

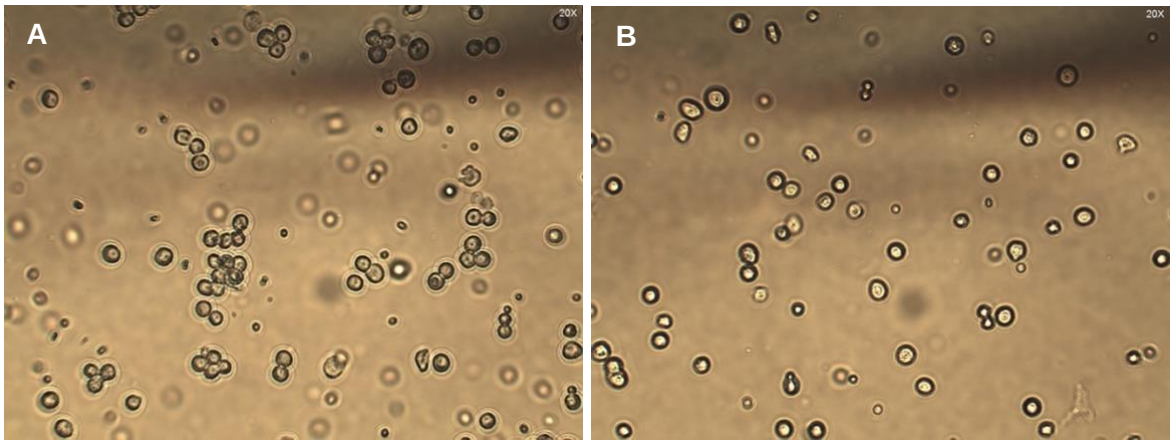

Figure 5: 20x Brightfield microscopy images of 10uL samples of cell suspension. A – pre-dissociation bladder tumour cell suspension showing microaggregates; B - post-enzymatic dissociation showing that a single cell suspension had been achieved.

3.3.2.6 ENZYMATIC DISSOCIATION OF SOLID TUMOUR TISSUE

For tumours with more solid tissue characteristics, CTS™ TrypLE™ Select Enzyme often did not allow for adequate dissociation. Accutase or sterile filtered Collagenase-Dispase solution (1-3ml) were used as alternatives. Dissociation was continued until a single cell suspension was reached, up to a period of 4 hours. All other processes remained as described in section 3.3.2.5.

3.3.2.7 TUMOUR CELL SUSPENSION VIABILITY ASSESSMENT AND CELL COUNT

Tumour tissue pellet(s) were re-suspended in *ex-vivo* media, the volume of which was reflective of pellet size. The reconstituted cellular suspensions were passed through a 70µM sterile filter. Nexcelom Bioscience Cellometer Mini Automated Cell Counter device was used to generate cell counts (live (including estimated percentage viability and histogram of cell size) and total counts performed). 10µL of the single cell suspension solution was added to 10µL of Trypan Blue and mixed. Of this, 10µL was then transferred to the Cellometer Mini Disposable Counting Chamber and counted using manufacturer's instructions.

3.3.2.8 TUMOUR CELL SUSPENSION PLATE SEEDING

Seeding density calculations were generated using the live cell count. Drug plates were thawed at 37°C for 30 minutes prior to cell seeding. 45µL of the resulting cell suspension was

dispensed into the 384-well plates using a Thermoscientific E1-ClipTip Electronic Multichannel Pipette. This resulted in each well containing 50µL in total, including 5µL of drug and 45 µL of cell suspension. Seeding densities varied and were dependent on several factors, most notably the percentage viability (which impacted on live cell count), the volume of tumour cell suspension available, and the number of plates to be seeded per tumour (for example, to complete additional validation experiments). Once drug wells were seeded, outermost wells were filled with 100µL of non-supplemented RPMI to insulate inner wells from evaporative plate effects. In addition, a breathable membrane was applied to the drug plates before incubation for four days, again, to reduce evaporation effects over the assay duration.

3.3.2.9 REMAINING TUMOUR TISSUE

Wherever possible, a proportion of tumour tissue was retained and stored for genetic analysis. Tumour tissues were transferred to cryovials and added to foetal bovine serum (FBS) supplemented with 10% DMSO. Cryovials were placed in cryocontainers (controlled temperature reduction) and frozen to -80ºC for storage.

3.3.3 ENDPOINT METABOLIC ATP-BASED VIABILITY ASSAY

Endpoint metabolic analysis was performed using the adenosine triphosphate based CTG assay. This assay uses ATP as a co-factor in the luciferase reaction to produce oxyluciferin and release luminescence (216). The luminescence readouts correspond to the amount of ATP present within each well, which is a crude marker of cellular metabolic activity and thus number of viable cells per well. Comparisons can then be made with cytotoxic (Staurosporine), cytostatic (Aphidicolin), and vehicle controls. Unlike MTT, MTS, or resazurin assays, CTG has a pre-defined, timely endpoint that is less prone to artifact than the other assays (216). In addition, CTG evaluation may be sensitive even at very low cell counts (as low as 10 cells per well according to manufacturer data) and can be used for non-adherent cell types (216). Both of these factors were important when choosing an endpoint assay for unpredictable primary tumour material.

In brief, at four days, *ex-vivo* drug plates were retrieved from the incubator and left to equilibrate to room temperature for 30 minutes. 10µL of CTG solution was added to each well and shaken at 200rpm for 2 minutes. Plates were left to stand for 10 minutes (to allow for stabilisation of the luminescence signal) before acquiring a luminescence reading (as per

manufacturer guidance). Readings were taken using the SpectraMax iD3 Multi-mode Microplate Reader.

3.3.4 TUMOUR DNA EXTRACTION AND QUANTIFICATION

DNA was extracted using Qiagen DNeasy® Blood and Tissue Kit. The extraction kit uses alkaline lysis, binding, washing and elution to facilitate extraction and purification of DNA. Firstly, tissues or cells are lysed at high temperatures, before loading onto a silica-gel membrane, which selectively adsorbs DNA during the process of centrifugation with chaotropic salts. Two subsequent wash steps assisted in the removal of contaminants, before elution to generate concentrated DNA.

3.3.4.1 PREPARATION OF TISSUES/CELLS

TUMOUR TISSUE

Frozen tumour tissue was thawed to room temperature and weighed (20mg). The tissue was washed with PBS to remove residual storage liquid, before transfer to a clean 1.5ml microfuge tube. Proteinase K (20µl) and Tissue Lysis Buffer ATL (180µl) were added and vortexed. The tube was then incubated on a heat block at 56°C overnight (for up to 24 hours), with gentle mixing at 300rpm throughout. Buffer AL (200µl) and absolute ethanol (200µl) were then added to each sample tube, thoroughly vortexed, and transferred to individually labelled DNeasy® QIAmp MiniElute spin columns.

CELL SUSPENSIONS

Frozen *ex-vivo* cell suspensions were thawed to room temperature and centrifuged (300g, 5 minutes) to generate a pellet that was resuspended in PBS (200uL). The cell suspension was transferred to a 1.5ml microfuge tube. Proteinase K (20µl) and Buffer AL (200µl) were added, the mixture vortexed, and incubated at 56°C for 10 minutes, with gentle mixing at 300rpm throughout. Absolute ethanol (200µl) was added to each sample tube, thoroughly vortexed, and transferred to individually labelled DNeasy® QIAmp MiniElute spin columns.

3.3.4.2 EXTRACTION PROTOCOL

DNA extraction was performed through the sequential process of binding, washing, and elution. In brief, DNeasy® QIAmp MiniElute spin columns were loaded with lysate (fresh tissue or cells), with an adjoined 2ml collection tube and centrifuged (6,000rcf, 1 minute). The collection tube and contents were discarded, and the spin column placed in a fresh 2ml collection tube. Buffer AW1 (500µl) was added to each column, making sure to avoid the rim, and centrifuged (6,000rcf, 1 minute). The flow-through and collection tube were discarded, and the column transferred to a fresh 2ml collection tube. AW2 (500µl) was then added to each column, avoiding the rim, and centrifuged (20,000rcf, 3 minutes). The collection tube and contents were discarded, and the spin column placed into a labelled 1.5ml microfuge tube. DNA was eluted in Buffer AE. The volume of eluent used impacts on DNA yield and concentration, where (in general) smaller eluent volumes give higher DNA concentrations, but lower overall DNA yield. In this study, 100µl of Buffer AE was used. Buffer AE was placed centrally on the column membrane and incubated at room temperature for 1 minute, followed by centrifugation (6,000rcf, 1 minute). The QIAmp MiniElute spin column was then discarded and the microfuge tube containing eluted DNA stored at 4°C.

3.3.4.3 QUANTIFICATION AND PURITY ASSESSMENT

Quantification and quality assessment of DNA was performed using UV-VIS Spectrophotometry through the NanoDrop® ND-1000 (ThermoScientific). The instrument allows for automatic calculation of DNA concentration through a modified Beer-Lambert calculation: absorbance at 260nm, wavelength-dependent absorbance coefficient (50ng·cm/µl for double-stranded DNA), and the path length in cm. Absorbance ratios at 260nm and 280nm (A260/A280), and 260nm and 230nm (A260/A230) were used to determine purity. Briefly, the Nanodrop® instrument was cleaned. 2µl nuclease-free water was loaded to set up the instrument. 2µL of Buffer AE eluting agent was then loaded as a blank measurement. After cleaning, 2µL per DNA sample was loaded and quantified (with the optical surfaces cleaned between individual measurements).

3.3.5 WHOLE EXOME SEQUENCING OF TUMOUR DNA

Whole exome sequencing (WES) was performed by Macrogen Europe BV. Individual tumour DNA samples were labelled and shipped on icepacks to Macrogen Europe BV, Amsterdam,

who performed WES DNA quality checks, library construction, and sequencing. Raw WES data was generated using the following protocol. The subsequent four paragraphs are extracted from the methodology statement provided by Macrogen Europe BV on delivery of the raw WES data.

“Double-stranded DNA quantity was assessed using fluorescence-based PicoGreen Victor 3 fluorometry, as this technique is less likely to overestimate of DNA concentration, even in the presence of contaminants. The condition of the DNA was then evaluated using agarose gel electrophoresis.

A DNA library was prepared from 50ng of input DNA using the Twist Library Preparation Kit with full-length combinatorial dual index TruSeq-compatible Y-adapters (Illumina) according to the Twist Bioscience Library Protocol. Using PicoGreen and agarose gel electrophoresis, an assessment of DNA quantity and quality was performed. 50ng of DNA was diluted with EB Buffer and sheared to a target peak size of 200bp using fragmentation enzyme. Fragmentation was followed by end-repair and the addition of ‘A’ tail. Then Twist CD index adapters were ligated to the fragments. After evaluating the efficiency of ligation, the adapter-ligated product was PCR amplified. The final purified product was quantified by TapeStation DNA screentape D1000 (Agilent) and PicoGreen. For exome capture, each hybridization reaction requires a total of 1500 ng of indexed libraries, made by pooling equal amounts from 8 individual libraries. We mixed Fast hybridization mix, Twist exome probe, Blocker solution, and Universal Blocker, according to the Twist library preparation protocol. The captured DNA was washed and amplified. The final purified product was quantified by qPCR according to the qPCR Quantification Protocol Guide (KAPA Library Quantification kits for Illumina Sequencing platforms) and qualified by the TapeStation DNA screentape D1000 (Agilent).

Illumina utilizes a unique amplification reaction that occurs on the surface of the flow cell. A flow cell containing millions of unique clusters is loaded into the Illumina platform for automated cycles of extension and imaging. Sequencing-by-Synthesis utilizes four proprietary nucleotides possessing reversible fluorophore and termination properties. Each sequencing cycle occurs in the presence of all four nucleotides leading to higher accuracy than methods where only one nucleotide is present in the reaction mix at a time. This cycle is repeated, one base at a time, generating a series of images each representing a single base extension at a specific cluster.

The Illumina platform generates raw images and base calling through integrated primary analysis software called RTA(Real Time Analysis). The base calling files which are expressed

in binary are converted into FASTQ by Illumina package bcl2fastq v2.20.0. The demultiplexing option (--barcode-mismatches) is set to as value: 0”

3.3.6 ANALYSIS OF RAW WHOLE EXOME SEQUENCING DATA

Raw WES data analysis was performed by Dr Lewis Quayle (University of Sheffield) using the following methodological protocol. The subsequent paragraph was provided by Dr Lewis Quayle documenting the methodology he used to analyse the raw WES data for this study.

“The FASTQ files resulting from whole exome sequencing (WES) were analysed using the nf-core Sarek (v3.0) pipeline configured to run in somatic tumour-only WES mode (217). Sequencing quality control was undertaken with FastQC and reads mapped to the human reference genome (GRCh38) using BWA-MEM before GATK was used to mark duplicates (MarkDuplicates) and perform base quality score recalibration (BaseRecalibrator, ApplyBQSR). Samtools and mosdepth were used to provide final pre-processing quality control measures before calling of single-nucleotide polymorphism and insertion/deletion mutation variants using GATK HaplotypeCaller. The resultant VCF files were annotated with genomic variant annotation and functional effect information using dbSNP, VEP, ANNOVAR, and ClinVar. Hard filtration using variant quality control metrics was undertaken using bcftools (v1.16) according to GATK recommendations. Single nucleotide variants (SNVs) were removed when QualByDepth (QD) was less than 2, the Phred-scaled probability of site strand bias (FS) was greater than 60, root mean square mapping quality over all the reads at the site (MQ) was less than 40, the u-based z-approximation from the Rank Sum Test for mapping qualities (MQRankSum) was less than -12.5, and finally the u-based z-approximation from the Rank Sum Test for site position within reads (ReadPosRankSum) was less than -8.0. Similarly, insertion deletion mutations (INDELs) were removed when QD was less than 2, FS was greater than 200, and ReadPosRankSum score was less than -20. All variants that passed these cut-off criteria were then removed according to whether their respective population allele frequency in the 1000 Genomes project exceeded 1% (218). Filtered VCFs were then converted to the MAF format using vcf2maf (v 1.6.21).”

3.3.7 STATISTICAL METHODS

3.3.7.1 GENERAL STATISTICS

Statistical analyses were performed using Prism 9.5.1 (GraphPad Software Inc., San Diego, CA, USA). Mean and standard deviation (parametric data) or median and interquartile range (non-parametric data) were used to describe the data. The choice of statistical method was guided by the research objectives and the underlying data distribution. For example, t-tests or analysis of variance were used for parametric data and Mann-Whitney U test or Kruskal-Wallis used for non-parametric data. Chi-squared or Fisher's exact tests were used to explore differences between categorical variables. Simple linear or logistic regression were used to compare relationships between data or to assess goodness of fit. A p-value of <0.05 was defined as statistically significant. Sample size calculations for this observational study were not relevant, as it was not an interventional study.

3.3.7.2 STATISTICS FOR CTG DATA

With any primary tissue assay, it is anticipated that despite best technical and scientific principles, there will be a degree of accepted variation. Coefficient of variance (COV) (standard deviation divided by the population mean) was calculated for vehicle control wells (n=28) for each drug plate. Plates with vehicle control COV >0.25 were excluded as methodological failures for quality assurance purposes. Z scores were calculated for technical replicates (three for each concentration of drug); replicates with a Z score >2 or <-2 were excluded from analysis.

3.3.7.3 STATISTICS USED FOR DRUG RESPONSE ANALYSIS

Area-under dose-response curve (AUC) was chosen as the single dose-response metric, as it is more robust to experimental noise than other metrics (211,219,220). AUC values were normalised using robust-Z scoring, which uses the median and each values' deviation from the median to normalise data around 0; this was performed to normalise drug response scores across the BC cohort. Robust-Z scoring was chosen as it more robust to outliers than standard Z scoring, where many of the drug responses across the cohort were not normally distributed. K means and Euclidean distance were calculated before applying the elbow method to explore the optimal number of drug and tumour clusters.

CHAPTER 4

OPTIMISING *EX-VIVO* HIGH THROUGHPUT DRUG SCREENING IN BLADDER CANCER

4.1 INTRODUCTION

Bladder cancer is common, and when presenting at more advanced stages, is often lethal despite our best treatments. As described in section 1.1.10.1 (Rationale for improving models of patient selection and treatment personalisation in bladder cancer), there is an urgent unmet need to develop new treatments and implement more personalised approaches for many bladder cancer (BC) patients.

Ex-vivo tumour tissue processing has been described using numerous different methodologies ranging from 2D patient derived tumour cell lines, to explanted tumour tissue, as described in Section 1.2 (Pre-clinical models in bladder cancer), where each approach has different benefits, drawbacks, and challenges (125). In this study, a single cell two-dimensional assay using patient derived *ex-vivo* cultures (PDCs) from bladder tumours was chosen as an optimal platform to deliver a tumour cell high-throughput screening approach. The methodology used was adapted from work by Dr Rantala (135–138), who has experience in *ex-vivo* tumour tissue processing in over 50 different cancer types (Misvik Biology, Finland). The tumour PDCs are not grown for extended periods, nor are they passaged, meaning that they maintain fidelity to the primary tumour sample retrieved from the patient. PDCs are less technically challenging to generate than more complex models such as organoids or xenografts, requiring less technical expertise, less time, and are less costly to generate. All of these factors complement a high-throughput approach (125).

Using *ex-vivo* BC PDCs to evaluate high-throughput drug responses has not yet been described in the literature, highlighting its novelty in this setting. As described in section 1.3.5, the natural history and treatment pathways for BC patients in the NHS provides a unique opportunity for tumour sampling at several different time points. Some of these windows of opportunity may enable for the validation of the *ex-vivo* model through direct correlation with patient *in vivo* responses to therapy.

The remainder of this chapter will describe how the *ex-vivo* high-throughput drug screening methodology using patient BC tumour samples was optimised *de novo* throughout this PhD.

4.2 RESULTS

4.2.1 QUALITY CONTROL EVALUATION OF BESPOKE DRUG PLATES

The design and preparation of bespoke BC drug plates, described in section 3.3.1, were adapted from methods by Gagg et al. (214). Drug plate curation was quality assured by two independent team members, who double-checked all processes. To minimise technical errors in dispending small volumes (5µL), the ThermoScientific Matrix Plate Mate Plus was used. This automated liquid dispensing platform can reproducibly dispense 0.1-300µL and is routinely calibrated and serviced.

The remainder of this section describes the further assessment of intra and inter-batch reproducibility using the SW620 colorectal cancer cell line. SW620, and adenocarcinoma cell line, is well characterised in the literature. It harbours several mutations of interest in BC, providing valuable information regarding activity of some small molecule inhibitors on the BC drug plates. For example, the SW620 cell line is platinum-sensitive (221,222), which is particularly important in validating cisplatin activity in BCs. It also harbours positive *KRAS* (G12V) and *TP53* mutations (R273H;P309S), and is wild-type for *BRAF* and *PIK3CA* (223). For each subsequent experiment described, 1000 SW620 cells were seeded per well onto the BC drug plates and incubated for four days, before performing endpoint CellTiter-Glo® (CTG) analysis (where the area under curve (AUC) value was calculated for each drug response). Simple linear regression was used to assess correlation of responses.

4.2.1.1 INTRA-BATCH REPRODUCIBILITY

To investigate intra-batch reproducibility, simple linear regression of SW620 AUC responses was performed between three plates produced in the same batch (Bladder Batch 1) (three biological replicates). Intra-batch drug responses showed excellent correlation, with an R^2 value of 0.97 (**Error! Reference source not found.**: A). Whilst that provided information about consistency between drug plates produced using in the same batch, it does not necessarily confirm that the drugs were seeded in the correct position on the plate.

4.2.1.2 INTER-BATCH REPRODUCIBILITY

Following this, the inter-batch reproducibility was explored using drug plates from different batches printed using the same methodology at 6-month intervals (Bladder Batch 1, Bladder Batch 2). Only drugs present at the same concentrations in both batches were compared. Inter-batch drug responses showed excellent correlation, with an R^2 value of 0.97 (**Error! Reference source not found.**: B).

4.2.1.3 IMPACT OF ADDITIONAL FREEZE-THAW CYCLE ON DRUG RESPONSES

The final quality control check sought to evaluate the impact of a freeze-thaw cycle on drug activity. Two plates from the same batch (Bladder Batch 2) were compared. One plate was kept refrigerated overnight after printing (no freeze-thaw cycle), and the other underwent one freeze-thaw cycle. Both drug plates showed excellent correlation of AUC drug responses, with an R^2 value of 0.99 (**Error! Reference source not found.**: C), suggesting that the freeze-thaw cycle had minimal impact on drug effect.

4.2.1.4 DRUG RESPONSE VALIDITY

As described, the SW620 cell line harbours *KRAS* (G12V) and *TP53* mutations (R273H;P309S), and is wild-type for *PIK3CA* (223). The cell line is also platinum-sensitive (221,222). Hence, it would be anticipated that SW620 cells would respond to cisplatin, but not nutilin-3a, nor the PI3K inhibitor AZD8186. **Error! Reference source not found.**: B&C highlight these drug responses, which confirm the anticipated results: that the SW620 cell lines responded to cisplatin (AUC value 0.15-0.40, green circle), had a moderate response to AZD6244 (the MEK inhibitor) (AUC <0.6, purple circle), and did not respond to nutlin-3a (MDM2 inhibitor) (AUC value >1.0, red circle) and AZD8186 (PIK inhibitor) (AUC value >1.0, blue circle).

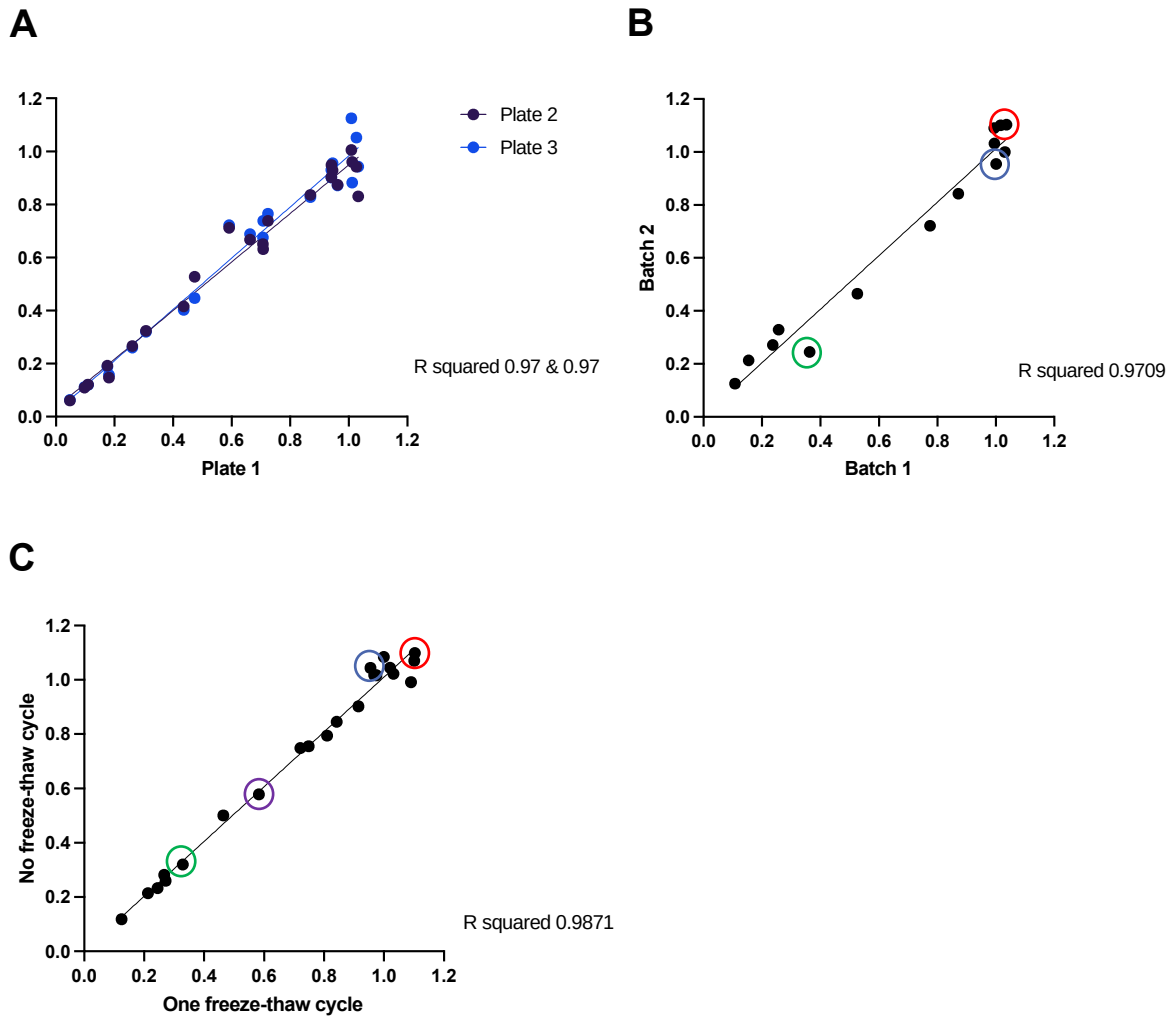

Figure 6: CTG AUC linear regression analysis. A - Intra-batch (Batch 1) reproducibility of drug responses on SW620 cells between three drug plates; B - Inter-batch (Batch 1 and Batch 2) consistency of SW620 drug response results; the red circle highlights the AUC value for nutilin-3a, the blue circle is the AUC for AZD8186 (PI3K inhibitor), and the green circle shows the AUC value for cisplatin, all showing expected responses for this cell line; C – drug response results for SW620 between two Batch 2 drug plates that had undergone either one or no freeze-thaw cycles; additional purple circle shows the AUC value for MEK inhibitor (AZD6244).

4.2.2 PRELIMINARY OPTIMISATION OF *EX-VIVO* TUMOUR PROCESSING METHODOLOGY

The main goal of this work was to create a reproducible *ex-vivo* tissue processing protocol that could deliver meaningful endpoint results. As described in the review by Williams et al.

(125), developing an *ex-vivo* protocol when using primary patient tumour tissue is particularly challenging (challenging factors are summarised in Table 7). Translational tissue processing methods must therefore adapt between and within cancer types (based on patient, tumour, and tissue characteristics). Refining the methodology in BC was particularly difficult due to the variability in size, quality, use of electrocautery, and consistency of the tumour tissue acquired.

Table 7: Challenges faced when using human tumour tissue for *ex-vivo* tissue processing	
Patient and tumour logistics	
Patient selection	Researchers must identify patients where the diagnosis of cancer is clinically confirmed, where tumour tissue is surgically or radiologically accessible, readily available, and where the risk of bacterial colonisation is low (for example, anatomically resectable, large tumours, in patients without an indwelling catheter at the time of surgery); patients must be able to provide informed consent
Patient recruitment	Researchers must be able to access patients within the clinical timeline, before the resection or biopsy procedure, with the necessary skills to acquire written informed consent
Tumour tissue acquisition	Researchers must be able to collect or retrieve the tumour tissue sample, which often requires co-ordination with both the clinical team and/or the histopathology team
Tumour tissue characteristics and tumour sampling	
Necrotic/non-viable tissue	Researchers may be provided with a tissue sample that is non-viable or necrotic in nature rendering it unsuitable for tissue culture assays; this may be due to tumour biology or the method of tumour acquisition, for example, excessive electrocautery during TURBT
Ischaemic tissue	For samples taken from whole organs after surgical retrieval, for example, radical cystectomy specimens, warm ischaemia to the tumour tissue prior to sampling may impact on subsequent viability
Infected tissue	Researchers may receive tumour tissue from a patient that has concurrent asymptomatic or symptomatic infection; again, this may render it unsuitable for tissue culture experiments
Tumour sampling and heterogeneity	Many tumours have elements of intra-tumoural heterogeneity, which may lead to bias when processing tumour tissue samples, and potentially may not reflect the biology of the patient's disease

4.2.2.1 CHOICE OF MEDIA AND SUPPLEMENTATION

Choice of basal media and then media supplementation are important considerations for any tissue culture work, including *ex-vivo* tissue culture. Although drug type, dose, and concentration seem to be the most influential factors on viability assessment, media type and supplementation may have subtle effects on endpoint viability assessment (224).

CHOICE OF BASAL MEDIA

RPMI 1640 was initially developed for culturing human leukocytes and has been widely utilised for suspension or monolayer mammalian cell culture (RPMI 1640 TechSheet, Lonza). The RPMI 1640 formulation, described in section Appendix 5: Description of Lonza RPMI 1640) has been widely adopted for BC cell line and 3D model cultivation (169,170,172,174,175). It has been used to effectively culture at least 32 different BC cell lines, as well as propagating primary patient-derived cell lines (PDCLs) using bladder tumour tissue (225). Hence, this was chosen as the basal media for this study.

FETAL BOVINE SERUM SUPPLEMENTATION

Animal-derived serum, most commonly fetal bovine serum (FBS), is considered a universal component of cell culture media, and was first introduced in the 1950s (226). It contains essential components for attachment, proliferation, and maintenance of cells within a culture system, for example, albumin, hormones, trace elements, and growth factors (227,228). However, there are several issues with using higher concentrations of FBS that include altering proliferation, migration, attachment, and plasticity (229). Higher concentrations of FBS may also impact on concentrations of unbound drug within media (230). When considering the percentage concentration of FBS to supplement for *ex-vivo* purposes, it was imperative to review the literature surrounding the culture conditions of *ex-vivo* PDCs (136,138,215,231). In these studies, primary tumour cells were dissociated and grown successfully in RPMI-1640 supplemented with 5% FBS. In addition, 5% FBS has been advocated in an array of different pre-clinical BC models, including primary patient 2D bladder tumour tissue (232), 2.5D bladder cancer organoids (233), and explanted tissue (234). Thus, given the drawbacks of higher concentrations of FBS in culture media, 5% supplementation was chosen.

INSULIN-TRANSFERRIN-SELENIUM SUPPLEMENTATION

Insulin-Transferrin-Selenium (ITS) is a basal media supplement, which has been used in serum-free media as an FBS replacement, or in FBS-containing media to reduce the concentration of FBS required. The Sigma suspension contains 1.0 mg/ml bovine insulin, 0.55 mg/ml human transferrin (substantially iron-free), 0.5 µg/ml sodium selenite, 50 mg/ml bovine

serum albumin and 470 µg/ml linoleic acid when added at 100x to basal media. ITS supplementation has been shown to help maintain growth and proliferation (235–237). More recently, it has been shown to help maintain the morphological, proliferative, and metabolic characteristics of both urothelial cells and fibroblast cell populations over time and passage (237). Thus, considering the lower concentration of FBS used in the *ex-vivo* media, 1% ITS supplementation was added for the aforementioned reasons.

PENICILLIN-STREPTOMYCIN SUPPLEMENTATION

Standard cell culture protocols produced by the America Type Culture Collection (ATCC) recommend the addition of antibiotics to reduce bacterial infection during cell culture processing. 100IU/mL of penicillin and 100ug/mL of streptomycin were added to the *ex-vivo* media.

L-GLUTAMINE SUPPLEMENTATION

Dr Warburg described the metabolic differences between malignant cancer cells and normal tissues, whereby cancer cells mainly depend on glycolysis for glucose metabolism even in oxygenated conditions (238). Glutamine is a non-essential amino acid that provides a carbon source for lipid and metabolite synthesis, and a nitrogen source for nucleotide synthesis, which is essential for cancer cell growth and proliferation. Glutamine is one of the most rapidly consumed nutrients by cancer cells after glucose, and both are essential for cancer cell growth (239). Hence, 2mM/ml of L-glutamine were added to each batch of media, using aseptic techniques, as per ATCC guidelines.

4.2.2.2 IMPACT OF DMSO CONCENTRATION ON *EX-VIVO* CELL GROWTH

It was important to evaluate whether DMSO used for drug reconstitution had an impact on *ex-vivo* cell growth. Initially, a DMSO titration experiment was performed using three difference cell lines: two BC cell lines (T24 from a non-muscle invasive BC (NMIBC) and HT1376 from a muscle invasive BC (MIBC)) and one ovarian cancer cell line (OVCAR). The titration spanned DMSO concentrations from 1% to 0.008%, with 9 technical replicates for each cell line at each concentration. At a concentration of 0.2% DMSO or lower, there was no significant difference in cell growth over the four-day assay (Figure 7). However, a significant decrease was observed at 1% DMSO. To explore this further in *ex-vivo* processed BC PDCs, the number of DMSO concentrations were expanded between 1% to 0.016%. Three primary tumour *ex-vivo* PDCs were seeded with a minimum of three technical replicates; growth was compared between DMSO concentrations and media only controls using endpoint CTG luminescence. Figure 8 highlights that there was no significant difference in endpoint CTG values between

media controls and all concentrations below 0.125% across the 3 patients derived samples, justifying the use of 0.05% working concentration of DMSO that is used in the *ex-vivo* screen. Hence, providing reassurance that drug effects observed in the *ex-vivo* screen are unlikely related to DMSO concentration and are reflective of drug activity.

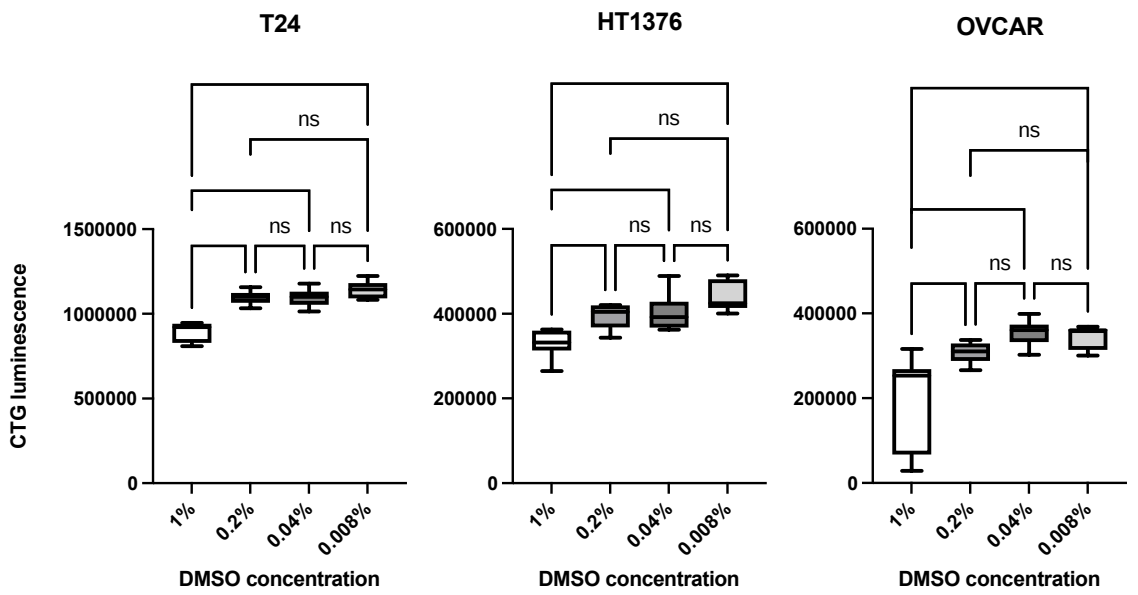

*Figure 7: ANOVA (with multiple comparisons statistic) comparison of DMSO titration experiments showing that there was no significant difference in cell line growth below a concentration of 0.2% DMSO (NS – non-significant; * - p<0.05; ** - p<0.01; *** - p<0.001; **** - p<0.0001).*

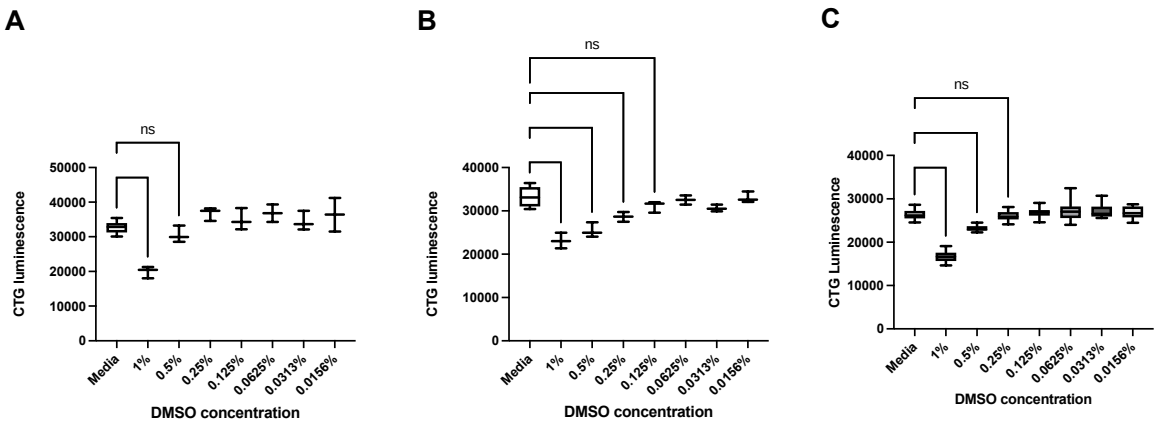

*Figure 8: ANOVA (with multiple comparisons statistic) comparison of DMSO titration experiments confirming that there was no significant difference in ex-vivo tumour cell suspension growth between media controls and media containing the top working concentration of DMSO (0.05%) in the high-throughput assay. A – DMSO titration experiment with ex-vivo processed tumour BT9.2; B – DMSO titration experiment with ex-vivo processed tumour EVD0001; C – DMSO titration experiment with ex-vivo processed tumour EVD0031. (NS – non-significant; * - p<0.05; ** - p<0.01; *** - p<0.001; **** - p<0.0001).*

4.2.2.3 MANAGING TUMOUR TISSUE VOLUMES AND CONSISTENCIES

Bladder tumours were acquired fresh from surgery either through transurethral resection of bladder tumour (TURBT) (47/51, 92%) or retrieval from radical cystectomy (RC) specimens (4/51, 8%). It was noted that there was a huge amount of heterogeneity in tumour sample volume and consistency (Table 8). The majority (28/51, 55%) of BC samples acquired were papillary, whilst 12 (12/51, 24%) were solid, 9 (9/51, 17%) had mixed papillary and solid features, and 2 (2/51, 4%) were lymph nodes only. Three tumours (3/51, 6%) were noted to have necrotic features. The median (interquartile range (IQR)) bladder tumour sample volume aquired was 305 (150-534)mm^3. Hence, even prior to *ex-vivo* tumour dissociation, this data highlights the heterogeneity of tissues received and thus how the methodology had to be continuously adapted.

One example of this was the time required to achieve a single cell suspension from tumour tissue using mechanical and enzymatic dissociation (Table 8). TrypLE™, a trypsin-like protease, was selected as the enzyme of choice for primary tumour tissue dissociation due to its lower toxicity and minimal impact on cell surface antigen expression (240). To prevent over-exposure and inadvertant cellular damage, or under-exposure with poor dissociation,

Brightfield microscopy of cell suspension samples at different stages of enzymatic dissociation were performed. By doing this, the duration of enzymatic dissociation could be adapted on a sample-by-sample basis. TrypLE™ was successful in generating a single cell suspension in 46 (46/51, 90.2%) of tumours, with a median (IQR) dissociation time of 30 (24-35) minutes. For more solid tumours, scalpel mechanical dissociation was used and if TrypLE™ dissociation failed (minimal dissociation on Brightfield inspection), more aggressive enzymes were added. Typically, accutase (proteolytic and collagenolytic) or a combination of collagenase/dispase (collagenolytic and cleaves cells from extracellular matrix) (240) were used and occasionally required longer incubation periods (up to 2.5 hours) before a single cell suspension was achieved.

Table 8: Bladder tumour tissue sample pre and post-processing characteristics

Tumour ID	Tumour description	TURBT/ RC	Diathermy damage	Volume (mm3)	Enzyme	Time	Viability (%)	Total live cells	LY:V ratio
EVD0018	Papillary	TURBT	No	278	TrypLE	24	40	7,416,000	26,676
EVD0016	Papillary	TURBT	Yes	144	TrypLE	17	70	10,400,000	72,222
EVD0015	Papillary	RC	No	440	TrypLE	30	74	30,500,000	69,318
EVD0014	Papillary	TURBT	No	90	TrypLE	15	44	2,230,000	24,778
EVD0013	Papillary, necrotic	TURBT	Yes	967	TrypLE	50	54	10,250,000	10,600
EVD0010	Solid	TURBT	No	165	Accutase	105	23	791,000	4,794
EVD0009	Papillary + Solid	TURBT	Yes	240	TrypLE	30	16	2,892,000	12,050
EVD0007	Solid	RC	No	432	TrypLE + collag/disp	150	28	3,192,000	7,389
EVD0005	Papillary	TURBT	No	232	TrypLE	30	75	22,100,000	95,259
9.4	Papillary	TURBT	No	165	TrypLE	20	40	3,312,000	20,073
9.3	Papillary	TURBT	Yes	590	TrypLE	33	32	4,096,000	6,942
9.2	Papillary	TURBT	No	155	TrypLE	30	80	8,856,000	57,135
9.1	Papillary	TURBT	No	48	TrypLE	30	39	1,467,960	30,583
9	Papillary + Solid	TURBT	Yes	486	TrypLE	35	53	8,904,000	18,321
8.9	Papillary + Solid	TURBT	Yes	929	TrypLE	35	60	24,480,000	26,351
8.8	Papillary	TURBT	No	305	TrypLE	30	27	5,490,000	18,000
8.7	Papillary	TURBT	No	16	TrypLE	20	93	6,990,000	436,875
8.6	Papillary	TURBT	No	48	TrypLE	35	76	6,596,800	137,433
8.5	Papillary	TURBT	Yes	738	TrypLE	40	60	9,840,000	13,333
8.4	Solid	TURBT	No	220	TrypLE	25	47	2,151,660	9,780
8.3	LN	RC	No	4500	Accutase	60	41	71,200,000	15,822
8.2	Papillary	TURBT	No	248	TrypLE	40	42	2,250,000	9,073
8.1	Papillary	TURBT	No	2000	TrypLE	35	55	13,310,000	6,655
7.9	Papillary	TURBT	No	8	TrypLE	35	50	244,500	30,563
7.8	Solid, necrotic	TURBT	No	870	TrypLE	35	37	2,397,600	2,756
7.6	Solid	TURBT	No	429	TrypLE	50	52	7,072,000	16,485
7.4	Papillary	TURBT	No	48	TrypLE	40	42	2,992,500	62,344
7.3	Papillary	TURBT	No	343	TrypLE	35	45	4,590,000	13,382
7.2	Papillary	TURBT	No	8	TrypLE	45	59	5,664,000	708,000
7.1	LN	RC	No	1800	Accutase	60	58	26,030,400	14,461
7	Papillary + Solid	TURBT	No	1750	TrypLE	55	59	26,550,000	15,171
6.9	Papillary	TURBT	No	140	TrypLE	35	76	3,758,200	26,844
6.8	Papillary	TURBT	No	168	TrypLE	30	84	11,239,200	66,900
6.7	Solid	TURBT	No	534	TrypLE	30	19	2,280,000	4,270
6.6	Papillary	TURBT	No	66	TrypLE	30	60	5,616,000	85,091
6.5	Solid	TURBT	No	2000	TrypLE + collag/disp	90	27	1,101,600	551

Tumour ID	Tumour description	TURBT/ RC	Diathermy damage	Volume (mm3)	Enzyme	Time	Viability (%)	Total live cells	LY:V ratio
6.4	Papillary + Solid	TURBT	No	368	TrypLE	35	46	6,697,600	18,200
6.3	Solid	TURBT	No	163	TrypLE	10	57	3,106,500	19,058
6.2	Solid	TURBT	No	1032	TrypLE	25	26	4,732,000	4,585
6.1	Solid	TURBT	No	48	TrypLE	5	51	1,441,260	30,026
6	Solid, necrotic	TURBT	No	535	TrypLE	30	24	2,318,400	4,333
5.9	Papillary + Solid	TURBT	No	320	TrypLE	30	46	4,609,200	14,404
5.8	Papillary	TURBT	No	232	TrypLE	40	51	2,274,600	9,804
5.7	Papillary	TURBT	Yes	346	TrypLE	25	14	607,620	1,756
5.6	Solid	TURBT	No	484	TrypLE	30	49	6,213,200	12,837
5.5	Papillary	TURBT	No	461	TrypLE	15	50	2,920,000	6,334
5.3	Papillary + Solid	TURBT	No	510	TrypLE	30	44	5,346,000	10,482
5.2	Papillary + Solid	TURBT	No	168	TrypLE	25	78	5,121,480	30,485
5.1	Papillary + Solid	TURBT	No	404	TrypLE	20	67	26,197,000	64,844
4.9	Papillary	TURBT	No	150	TrypLE	10	82	7,913,000	52,753
4.5	Papillary	TURBT	No	27	TrypLE	5	55	3,355,000	124,259

TURBT – transurethral resection of bladder tumour; RC – radical cystectomy; LN – lymph node; collag/disp – collagenase/dispase; LY:V – live cell yield:volume.

4.2.2.4 EVALUATION OF TUMOUR SAMPLE VIABILITY

Typically, studies which evaluate the utility of *ex-vivo* primary tumour tissue culture in translational research assess changes in viability across assay duration. However, assessment of pre-seeding viability is rarely documented. In this study, pre-seeding viability assessment was important due to the mechanism by which the tumours were acquired (mainly through TURBT). TURBT involves endoscopic resection of the bladder tumour, often using electrocautery (diathermy). Surgeons use ‘cut’ or ‘blend’ settings which employ a constant or intermittent electrical waveform to generate intense heat at the targeted tissues; this facilitates dissection of tumour away from the bladder muscle, or can allow for the shaving of larger tumours into smaller pieces to facilitate retrieval (241). Through this process, neighbouring cells are desiccated, and the thermal artifact may disperse into the tissues (242); the degree of dispersion is influenced by the electrocautery settings, duration of time taken to cut through the tissues, and tissue contact.

To avoid inclusion of non-viable tissue, visible diathermy artifact on tumour samples were removed prior to processing. Given that it is not possible to predict deeper, non-visible,

electrocautery tissue damage, a pre-seed viability assessment was added. Trypan blue, the first documented cytoplasmic dye to selectively stain dead cells in suspension, is the most widely used assay and is considered a standard measurement (243). It is thought to selectively penetrate the cytoplasm of dead or dying cells that have become porous due to loss of cytoplasmic membrane selectivity (244). By combining a sample of end cell suspension with trypan blue, it was possible to calculate the proportion and number of live cells using the Cellometer Mini Automated Cell Counter. Post-dissociation trypan blue viability assessment of tumour samples showed, again, that there was degree of variability (Table 8). The median (IQR) percentage viability was 50% (40-60%), which did not correlate to tumour sample volume (Figure 9: A, R squared=0.028) and there was only moderate correlation (Figure 9: B, R squared 0.56) between the tumour sample volume and total live cell yield.

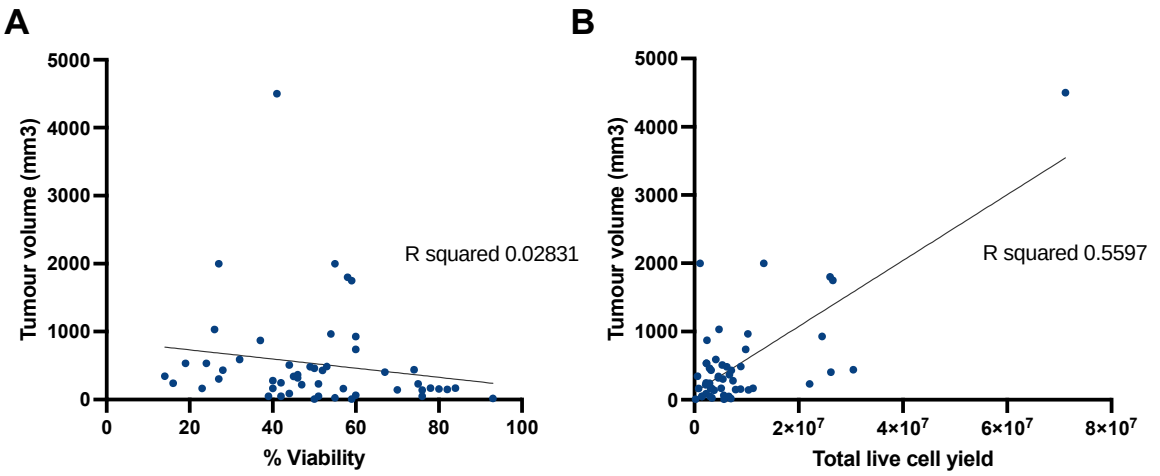

Figure 9: A – Simple linear regression analysis of tumour sample volume versus percentage viability showing poor correlation (R squared 0.028); B – Simple linear regression analysis of tumour sample volume versus live total cell yield showing modest correlation (R squared 0.56).

When comparing tumour tissue consistencies, percentage viability and live cell yield: tumour sample volume (LY:V) ratios differed significantly between groups (Kruskal-Wallis p=0.017 and p=0.0017, respectively). There was a significant difference in percentage viability between papillary tumours (54.5%, n=28) and solid tumours (32.5%, n=12) (p=0.015), but no difference between mixed papillary/solid tumours (53%, n=9) and any other group (Figure 10: A). Papillary tumours had a significantly higher LY:V than solid tumours (LY:V=28,704 compared to 6,092, p=0.0011), but again, no differences were seen between mixed solid/papillary tumours (LY:V=18,200) and any other group (Figure 10: B). There was no significant difference between these groups in terms of the length of time spent in enzyme (Kruskal-Wallis p>0.05). Percentage viability and LY:V ratio did not differ between the method of surgical acquisition (RC versus TURBT) (Mann-Whitney p>0.05) (Figure 10: C&D). This data suggests

that although the volume of tumour tissue received did not correlate with percentage viability, papillary tumours had a significantly higher percentage viability than solid tumours.

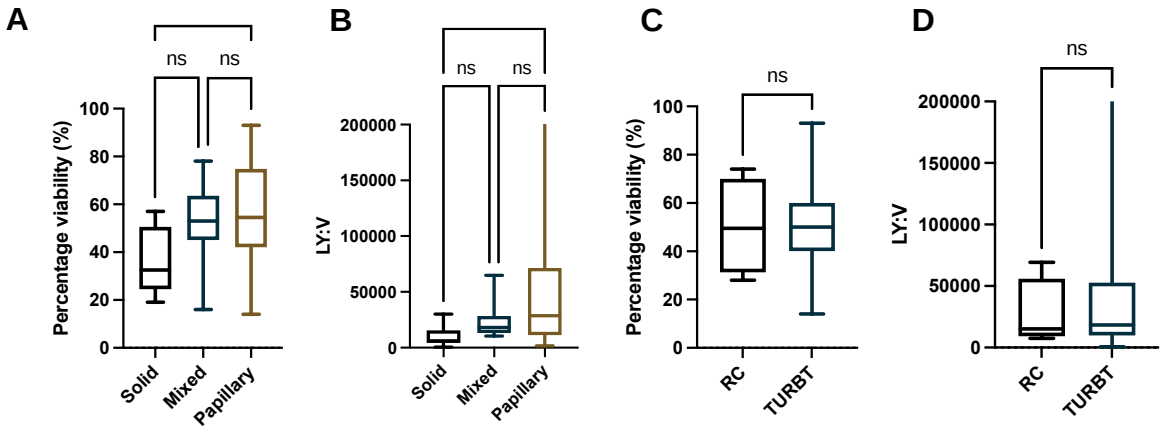

Figure 10: A – Kruskal-Wallis (with multiple comparisons statistic) comparison of median percentage viability between different tumour tissue compositions, showing significant differences; B – Kruskal-Wallis comparison of median live cell yield:volume ratio (LY:V) between tumour tissue compositions, showing significant differences between groups; C – Mann-Whitney comparison of median percentage viability between mode of surgical acquisition, showing no significant difference; D – Mann-Whitney comparison of median LY:V between mode of surgical acquisition, showing no significant difference.

4.2.2.5 OPTIMISING PLATE INCUBATION CONDITIONS

When performing high-throughput screening using 384-well plates, particularly for longer incubation periods, several positional or “plate effects” should be considered. One of the most common of these are “edge effects”, where wells along the perimeter of the plate are subject to different conditions to the innermost wells (245). This is because perimeter wells are not completely surrounded by other media-containing wells, thus, may be subject to different temperatures. These effects can be minimised using by optimising incubator humidity, minimising disruption to incubator environment (opening and closing of incubator doors), and by using dummy perimeter wells.

4.2.2.6 ADDITIONAL STRATEGIES TO MINIMISE “PLATE EFFECTS”

Despite the above standard measures, when performing initial validation experiments, it was noted that there was a degree of media evaporation (up to 15µL) occurring in outer wells (not including dummy perimeter wells). To combat this, the perimeter dummy wells were filled with

100µL of non-supplemented media (to minimise temperature effects), and a permeable membrane was applied (245). The Breathe-Easy® membrane is sterile, 30µM thick, and made from polyurethane, hence, permits gaseous exchange whilst sealing plates. These membranes were chosen because they have been shown to mitigate plate effects over much longer assay durations (246–250), and have been advocated in several high-throughput screening studies to minimise well-to-well variation (248,251–253). To evaluate the impact of the above additional measures, endpoint CTG values between outer (perimeter two wells) and inner DMSO wells for three *ex-vivo* processed bladder tumours were compared (Figure *11*). Day four DMSO CTG values were compared between outer (n=12) and inner wells (n=16) using unpaired t-test with no significant difference detected (P>0.05) across the three tumours. Hence, suggesting that plate effects had been mitigated.

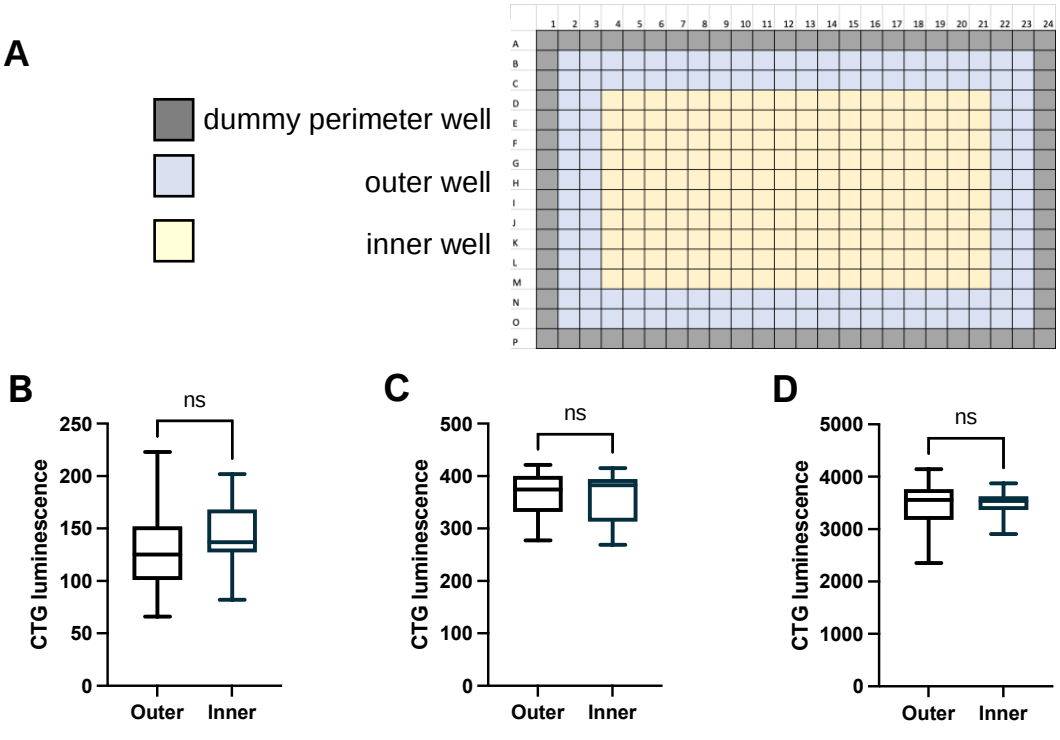

Figure 11: A – Plate layout showing the dummy perimeter wells, outer, and inner wells; B:D – comparison of CTG values for outer (n=12) and inner (n=16) located DMSO vehicle control wells for three ex-vivo processed bladder tumours (B – EVD0009; C – EVD0015; D – EVD0007) showing no significant differences (t-test) (p>0.05).

4.2.2.7 ASSESSING LENGTH OF SCREENING ASSAY DURATION

As with any drug screening assay, a balance must be reached between the duration at which cells can survive and proliferate and the duration required to observe drug responses. *Ex-vivo* bladder tumour tissues can be maintained for up to five days without compromise (187), but

increasing the duration in culture often leads to rising markers of apoptosis, even when maintained as an explant (182). Studies evaluating *ex-vivo* high-throughput drug screening in other solid tumours, using similar methodology, have adopted a 3-4 day assay duration (131,133,134, 200, 201).

To explore whether the *ex-vivo* PDCs were growing across the four-day assay, the number of cell cycles for each individual tumour suspension was calculated using the GRMetrics tool in R (211) through comparison of vehicle to cytostatic controls. The mean [95% CI] number of growth cycles for the forty tumours was 0.20 [0.11-0.28], suggesting that the cells were maintained and, albeit slowly, growing across the assay duration. The low number of cell cycles may be due to stress induced during surgical resection (TURBT) and suggests that the *ex-vivo* high-throughput screen in BC tissues may not be suitable for evaluating certain compounds that require cellular replication to exhibit a cytostatic or cytotoxic effect.

Next, the impact of assay duration on drug response was evaluated. For one *ex-vivo* processed tumour sample (BT 9.0), there was enough end cell suspension to seed four parallel drug plates, which underwent CTG analysis on sequential days of incubation (day 1-4). Figure 12 displayed the differential CTG drug responses per day of incubation. Further analysis of longer assay durations was not possible due to tissue limitations. Of note, Staurosporine, the cytotoxic (positive) control, reached almost complete effect by day four. Similarly, other key drugs of interest in BC treatment that are used in the clinic, for example, cisplatin and mitomycin C, followed a similar pattern with maximal cytotoxicity reached at day four. As these compounds are essential for clinical comparison, a four-day assay duration was chosen.

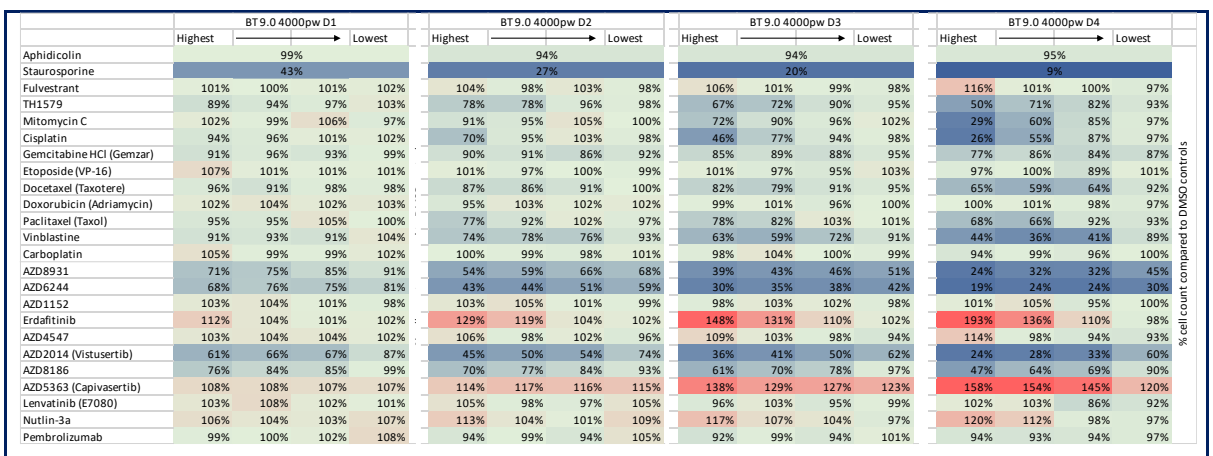

	BT 9.0 4000pw D1				BT 9.0 4000pw D2				BT 9.0 4000pw D3				BT 9.0 4000pw D4			
	Highest →			Lowest	Highest →			Lowest	Highest →			Lowest	Highest →			Lowest
Aphidicolin	99%				94%				94%				95%			
Staurosporine	43%				27%				20%				9%			
Fulvestrant	101%	100%	101%	102%	104%	98%	103%	98%	106%	101%	99%	98%	116%	101%	100%	97%
TH1579	89%	94%	97%	103%	78%	78%	96%	98%	67%	72%	90%	95%	50%	71%	82%	93%
Mitomycin C	102%	99%	106%	97%	91%	95%	105%	100%	72%	90%	96%	102%	29%	60%	85%	97%
Cisplatin	94%	96%	101%	102%	70%	95%	103%	98%	46%	77%	94%	98%	26%	55%	87%	97%
Gemcitabine HCl (Gemzar)	91%	96%	93%	99%	90%	91%	86%	92%	85%	89%	88%	95%	77%	86%	84%	87%
Etoposide (VP-16)	107%	101%	101%	101%	101%	97%	100%	99%	101%	97%	95%	103%	97%	100%	89%	101%
Docetaxel (Taxotere)	96%	91%	98%	98%	87%	86%	91%	100%	82%	79%	91%	95%	65%	59%	64%	92%
Doxorubicin (Adriamycin)	102%	104%	102%	103%	95%	103%	102%	102%	99%	101%	96%	100%	100%	101%	98%	97%
Paclitaxel (Taxol)	95%	95%	105%	100%	77%	92%	102%	97%	78%	82%	103%	101%	68%	66%	92%	93%
Vinblastine	91%	93%	91%	104%	74%	78%	76%	93%	63%	59%	72%	91%	44%	36%	41%	89%
Carboplatin	105%	99%	99%	102%	100%	99%	98%	101%	98%	104%	100%	99%	94%	99%	96%	100%
AZD8931	71%	75%	85%	91%	54%	59%	66%	68%	39%	43%	46%	51%	24%	32%	32%	45%
AZD6244	68%	76%	75%	81%	43%	44%	51%	59%	30%	35%	38%	42%	19%	24%	24%	30%
AZD1152	103%	104%	101%	98%	103%	105%	101%	99%	98%	103%	102%	98%	101%	105%	95%	100%
Erdafitinib	112%	104%	101%	102%	129%	119%	104%	102%	148%	131%	110%	102%	193%	136%	110%	98%
AZD4547	103%	104%	104%	102%	106%	98%	102%	96%	109%	103%	98%	94%	114%	98%	94%	93%
AZD2014 (Vistusertib)	61%	66%	67%	87%	45%	50%	54%	74%	36%	41%	50%	62%	24%	28%	33%	60%
AZD8186	76%	84%	85%	99%	70%	77%	84%	93%	61%	70%	78%	97%	47%	64%	69%	90%
AZD5363 (Capivasertib)	108%	108%	107%	107%	114%	117%	116%	115%	138%	129%	127%	123%	158%	154%	145%	120%
Lenvatinib (E7080)	103%	108%	102%	101%	105%	98%	97%	105%	96%	103%	95%	99%	102%	103%	86%	92%
Nutlin-3a	106%	104%	103%	107%	113%	104%	101%	109%	117%	107%	104%	97%	120%	112%	98%	97%
Pembrolizumab	99%	100%	102%	108%	94%	99%	94%	105%	92%	99%	94%	101%	94%	93%	94%	97%

% cell count compared to DMSO controls

Figure 12: Sequential daily CTG drug response analysis of a primary ex-vivo processed bladder tumour across the four-day incubation period. The heatmaps show percentage response compared to DMSO. Drug concentrations are displayed as highest on the left to lowest on the right. D1 – Day 1; D2 – Day 2; D3 – Day 3; D4 – Day 4.

4.2.2.8 OPTIMISING CELL SEEDING CONDITIONS

The next factor to consider was the impact of cell seeding methodologies. Two different methods were assessed for this study: handheld automated seeding using the E1-ClipTip™ automated dispenser and multi-well automated seeding using the MultiDrop dispenser. Their well-to-well reproducibility was evaluated by seeding 56 DMSO replicates on a 384-well plate and exploring their variance in CTG values.

MULTIDROP AUTOMATED CELL SEEDER REPRODUCIBILITY

The MultiDrop dispenser was examined first, as it is a quick and automated method for cell seeding. *Ex-vivo* PDCs were seeded using the MultiDrop dispensing platform as per recommended protocols (ThermoFisher). Analysis of the replicates showed a snaking pattern (Figure *13*: A), which was in congruence with the route of the MultiDrop dispenser cassette tips (Figure *13*: B). Despite adequate priming with tumour cell suspension, this “snaking” or “striping” effect is recognised as a potential problem with multi-well dispensing platforms (245,254). In this experiment, there was a significant difference between CTG means in alternate rows ($p<0.0001$) and between the first two and end two columns ($p<0.01$) (unpaired t-test). In addition, the CTG values across these replicates had a very high COV 30.6%, and a mean difference between first and last wells of 137% (Table 9), suggesting very poor reproducibility. As the CTG readings were significantly lower at the start of the dispensing cycle, it was thought that this could be due to tip dispensing errors, gravitation effects on cellular weight across the cycle (albeit short), or priming effects.

AUTOMATED HANDHELD MULTICHANNEL CELL SEEDING

To mitigate against these effects, the E1-ClipTip™ multi-channel pipette was evaluated. The E1-ClipTip™ is a hybrid of automated and handheld dispensing technology. It has up to 16 channels where each tip may hold 125µL and required less “dead volume” than the MultiDrop (due to lack of priming). The co-efficient of variance (COV) and mean difference between first and last wells were much improved with the E1-ClipTip™ than when using the Multidrop (Table 9). Although this data only compares variance between the two methods using one different BC PDC for each, it was felt that huge difference in cell seeding reproducibility using primary *ex-vivo* PDCs supported the use of the E1-ClipTip™ over the Multidrop.

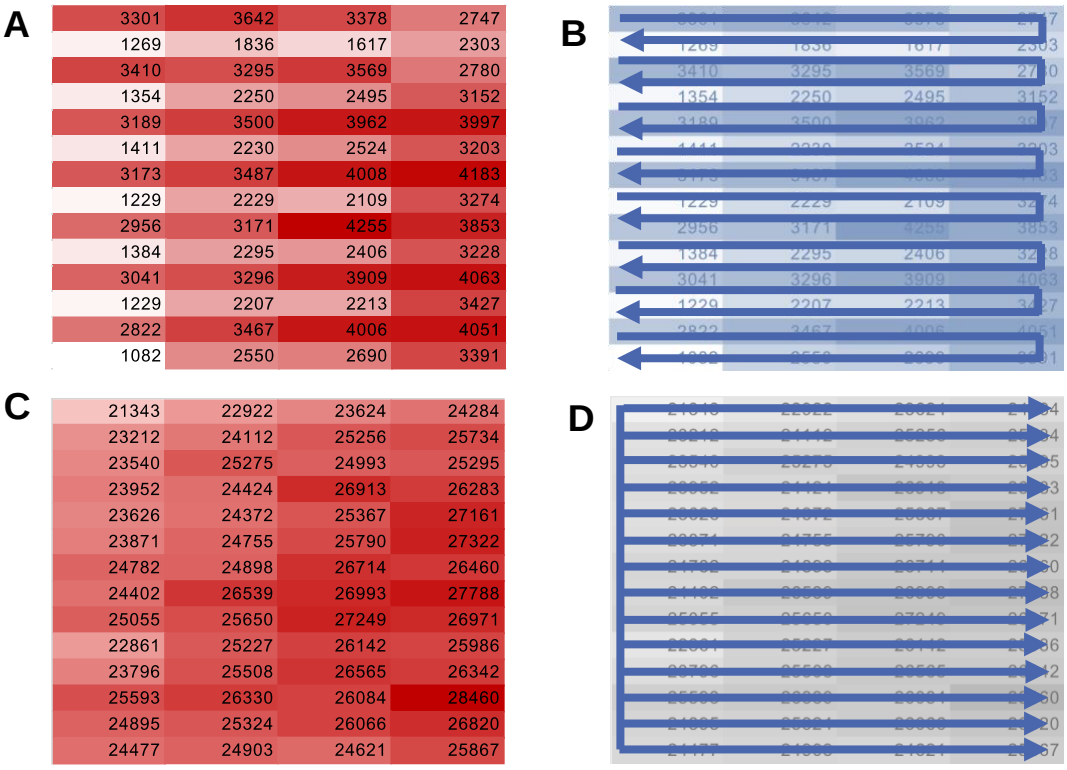

Figure 13: A – Snaking effect seen in CTG results when using the MultiDrop dispenser; B – map of cell seeding route for the MultiDrop dispenser; C – CTG results when seeding from left to right with the E1-ClipTip™ dispenser. D – map of cell seeding route using the handheld E1-ClipTip™ dispenser from left to right across a plate.

Table 9: Comparative reproducibility using Multidrop or E1-ClipTip™ dispensing platforms

Method	Seeding direction	Mean [SD] CTG replicates	COV	Mean difference (%) from first to last well
Multidrop	Snaking pattern	2,877 [880]	30.6%	137 [17]
E1-ClipTip™	Left to right	25,335 [1,380]	5.4%	11 [3]

4.2.2.9 EVALUATION OF OPTIMAL *EX-VIVO* SEEDING DENSITY

Next, it was important to explore the impact of cell seeding density on endpoint CTG results, as the number of cells seeded within a well at any one time may have implications on growth and drug responses of *ex-vivo* cell suspensions. Linearity of growth between differential seeding densities over the assay duration, and impact on drug responses, was explored using *ex-vivo* BC PDCs onto DMSO control plates and bespoke BC drug plates, respectively.

IMPACT OF EX-VIVO PDC SEEDING DENSITY ON GROWTH AND REPRODUCIBILITY METRICS

Cell seeding density experiments were performed on DMSO only plates. Of note, when working with patient samples, experiments were limited by tumour sample characteristics, percentage viability, and final live cell counts; hence, why the maximum seeding density per well in these experiments varied. Figure 14 shows that across three *ex-vivo* BC PDCs, at four days, there was a relatively linear increasing relationship between CTG values and seeding density per well (indicated by the straight line of fit). The linear relationship between seeding density and CTG output metrics suggests that the necessary CTG substrates were not detrimentally consumed at higher seeding densities. It also could highlight that BC PDC growth was not grossly inhibited at high or low seeding densities; although earlier data suggests that the number of cell cycles observed throughout the assay was low (Section 4.2.2.7). The co-efficient of variance between replicates improved with higher seeding densities (Figure 14: D-F).

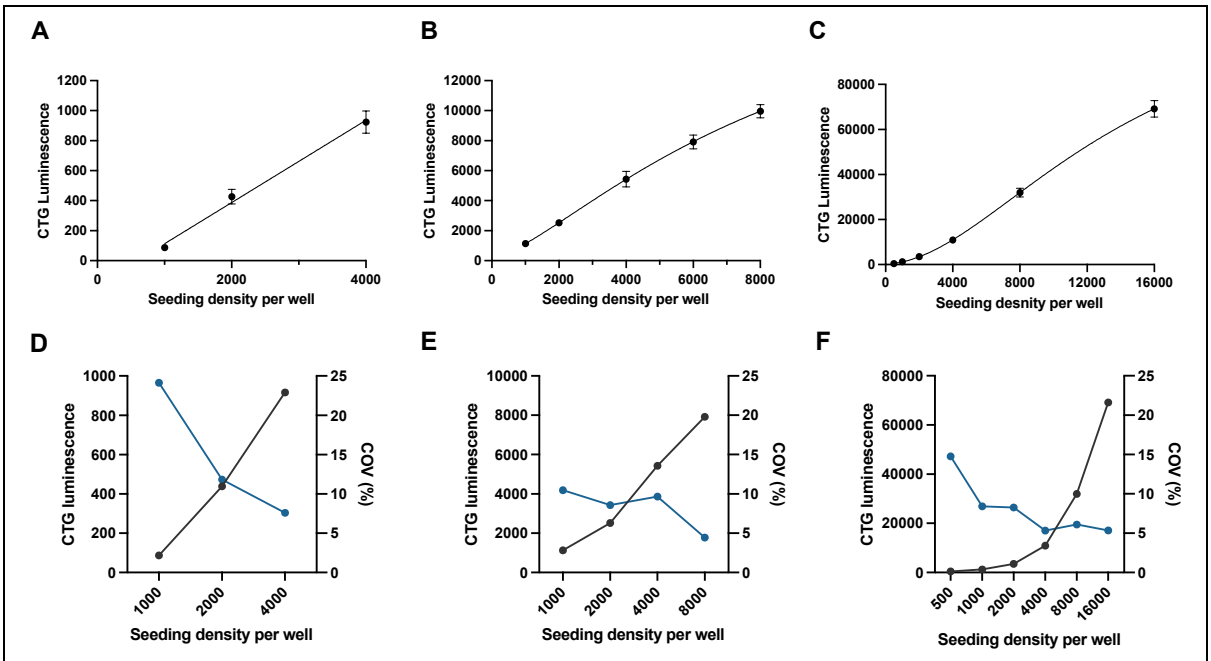

Figure 14: Trends in endpoint CTG analysis of ex-vivo BC PDCs at different seeding densities in 0.05% DMSO control vehicle media. A – BT 4.2, 16 replicates per seeding density (1000-4000 cells per well); B – BT 7.0, 28 replicates per seeding density (1000-8000 cells per well); C – EVD0031, 14 replicates per seeding density (500-16000 cells per well); D-F – comparison of mean CTG luminescence readings (black) and COV between replicates (blue) per seeding density for BT 4.2, BT7.0, and EVD0031, respectively.

IMPACT OF EX-VIVO SEEDING DENSITY ON DRUG RESPONSES

As well as growth metrics and reproducibility, it was important to explore the impact of seeding density on drug responses. For a tumour where there was surplus excess tumour tissue (BT 7.0), *ex-vivo* PDCs were seeded on BC-specific drug plates at different cell densities (1000 to 8000 cells per well). CTG area under dose-response curve (AUC) values were calculated at four days for each drug and compared using simple linear regression between seeding densities. Excellent correlation in drug responses were observed at all seeding densities (all R squared >0.9) (Figure *15*); this suggests that higher and lower seeding densities did not alter drug responses.

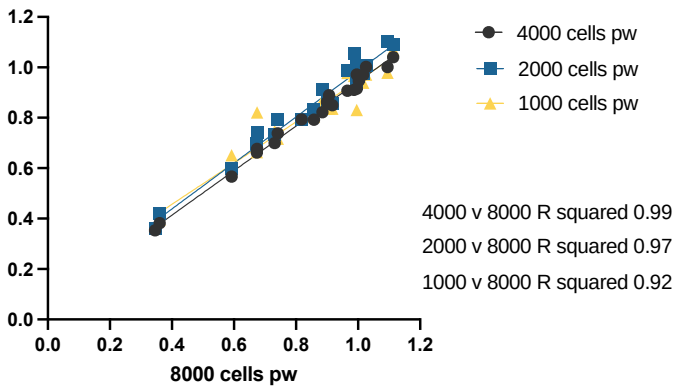

Figure 15: Simple linear regression analysis of endpoint CTG AUC drug responses for different cell seeding densities (1000-8000 cells per well) in an ex-vivo processed bladder tumour (BT 7.0) showing excellent R^2 values.

These data highlight that when considering seeding density of BC PDCs for endpoint CTG analysis, there is linearity in CTG output metrics between 1000 and 8000 cell per well. Higher seeding densities improve the reproducibility of the assay without compromising observed drug responses.

4.3 DISCUSSION

Ex-vivo high-throughput drug screening using BC PDCs has not been described, hence, the methodology for producing BC PDCs from patient tissue had to be developed *de novo* throughout this PhD. The methodology was adapted from others who have generated primary *ex-vivo* PDCs from solid tumours (135–138) through the evaluation of different experimental variables. The final optimised protocol is described in section 3.3.2.

First and foremost, working with BC patient tissue was extremely challenging. The breadth of tumour tissue acquired and the method by which they are surgically resected, meant that tumour sample tissue characteristics were hugely variable. For example, tumour sample volume alone ranged from 8-4500mm^3. Most tumours (47/51, 92.2%) were acquired through TURBT, which uses electrocautery (diathermy) to resect the tumour from adjacent tissues using electrical currents (241). The degree of damage to the tumour specimen is influenced predominantly by surgical technique, including the electrocautery settings, cutting time, and tissue contact; all of which are not under the control of the research team. Aside from macroscopic char that was removed on receipt, the degree of microscopic damage was not quantifiable (242). This may be one of the reasons why tumour sample volume (mm^3) did not correlate with percentage viability.

Another challenge was differential tumour tissue compositions, which required adapted methodology; for example, using different enzymes and incubation times to achieve dissociation into a single cell suspension (Table 8). Papillary tumours had significantly higher median percentage viability and LV:Y than solid tumours, but not mixed consistency tumours, despite there being no difference in the length of enzymatic incubation, nor by the method of acquisition (RC v TURBT) between the groups. Hence, percentage viability and LY:V values may be influenced by the biological composition of the tissues themselves. This highlights the challenges in using standardised methodology and applying it to different samples.

When working with unpredictable primary tumour material, as described above, CTG was chosen as the endpoint assay due to its definitive, uniform, timely luminescence readouts, sensitivity at very low cell counts, and flexibility to include non-adherent cell types (216). Hence, this was also used for optimisation and validation experiments. First, it was essential to ensure that the bespoke drug plates could deliver reproducible and valid results. Both of these were confirmed using cell line experiments that showed excellent intra and inter-batch reproducibility, as well as reproducibility after one freeze-thaw cycle. Drug validity was inferred through appropriate SW620 cell line responses, based on its known chemo-responsiveness

(216, 217) and genomic aberrations (223). The cell lines showed a good response to cisplatin across all experiments (AUC 0.15-0.40), with an IC50 value ranging from 1.5-3.5uM, which is similar to that reported in the literature (255); there was a moderate response to the MEK1/2 inhibitor AZD6244, which SW620 has been shown to be sensitive to given its *KRAS* status (256); finally, there was no response to nutlin-3a or the PI3K inhibitor (AZD8186), which corresponded to the expected responses based on mutational profile (223).

Next, the methodology was adapted to minimise the impact of plate effects across the assay duration by using high-volume dummy perimeter wells and breathable membrane coverage. Subsequent, CTG analysis of outer versus inner DMSO vehicle controls, for three different *ex-vivo* BC PDCs, showed no significant difference, suggesting that plate effects had been mitigated against.

Finally, due to the variability (size and viability) observed between samples it was essential to explore how *ex-vivo* PDC cell-seeding density impacted on growth and drug responses. It is well established in the literature that cell-to-cell contact and paracrine signalling (release of growth factors and cytokines by neighbouring cells) impact on cellular growth and proliferation (257,258). In this study, using a 2D PDC model, cellular interaction may be determined by the cell seeding density within a given area, as well as, potentially impacting on drug response (259). The “inoculum effect” describes the relationship whereby increasing the number of cells per given area increases the minimal concentration of drug for effective killing, a relationship which has been described between cancer cells and chemotherapeutic compounds for many decades (260). As cells approach higher seeding densities, there is a risk of resource and/or space exhaustion, as well as, waste accumulation that may lead to deceleration or saturation of growth (261). However, complex, heterogenous *ex-vivo* cancer PDCs may not always deliver such homogenous growth kinetics. Interestingly, *ex-vivo* PDC seeding density did not seem to impact on growth of *ex-vivo* BC PDCs, with relatively linear CTG values extending up to seeding densities of 16,000 cells per well. Several reasons for this include: the low number of growth cycles observed by the BC PDCs (median of 0.2), suggesting low consumption of available resources and thus limited saturation of growth even at high initial seeding densities; as well as the short assay duration (four days).

Conversely, cells seeded at low densities may suffer from reduced fitness *in vitro* due to impaired co-operative growth (262). Lower seeding densities (<1000 cells per well) showed a slower growth pattern, which could reflect the changes or impaired paracrine signalling. Reassuringly, seeding density seemed to have minimal impact on drug response, with excellent CTG AUC correlation between differential densities (1000-8000 cells per well). In

addition, there were no gross outlier drug responses to suggest impact on individual compounds.

Nonetheless, these results need to be approached with a degree of caution, as individual BC PDCs will inevitably display differing growth kinetics and behaviours, based on their biological invasiveness, post-resection viability, and tumour characteristics. However, the aforementioned results are promising and provide some reassurance that seeding densities above 1000 cells per well, using CTG end-point analysis, had minimal impact on growth kinetics and drug responses.

CHAPTER 5

DRUG SCREENING RESULTS USING *EX-VIVO* APPROACHES IN BLADDER CANCER

5.1 Introduction

Ex-vivo high-throughput drug screening reflects a technique by which human tissue is acquired and tested to explore efficacy of drug responses. In the clinic, this has been used for many years to deliver personalised therapy to patients, for example, in delivering patient and bacteria-specific antibiotic therapy. However, implementing this process to dictate personalised cancer treatment has not yet been achieved, due to barriers in tumour tissue acquisition, methodological throughput, and logistical implementation in clinical cancer pathways. To date, the most advanced development of *ex-vivo* drug screening has been observed in haematological malignancies, where liquid tumour cells are easily accessible and easy to handle. For example, in advanced haematological cancers *ex-vivo* drug screening has been used within clinical trials to direct patient treatment with promising results (196–199). Snijder et al. (198) and Kornath et al. (199) used image-based *ex-vivo* drug screening to direct treatment in patients with advanced haematological cancers who had refractory disease, or no treatment options available; whereas Swords et al. (196) and Malani et al. (197) used *ex-vivo* screening to direct treatment in patients with advanced relapsed or refractory acute myeloid leukaemia. Phase III randomised trial data are still lacking, but these early phase trials have shown the potential of tumour-specific phenotypic drug screening in the clinic within relevant timeframes.

Ex-vivo high throughput screening in solid tumours is more complex. For example, it is harder to retrieve a solution of relevant cancer cells than for blood and retrieved cells are potentially prone to sampling bias. The processing methodology must be matched to the scientific purpose, tissue characteristics, and clinical timeline per cancer type. When considering the clinical pipeline for bladder cancer (BC) patients, there is a unique opportunity for early tumour tissue sampling (section 1.3.5), whereby a diagnostic surgical resection is performed prior to definitive treatment. *Ex-vivo* high throughput drug screening of BC tumour tissue between diagnostic resection and subsequent treatment provides a rare ‘window of opportunity’ to explore the impact of novel, repurposed, or combined therapies in treatment naïve patients before definitive surgical resection. In addition, patients with non-muscle invasive BC (NMIBC) often suffer from recurrence despite best adjuvant therapy; recurrent tumours may be repeatedly sampled during subsequent surgical resections to explore mechanisms of treatment resistance and alternative therapies. Hence, the BC pipeline has several clinically relevant windows whereby *ex-vivo* drug screening of individual patient tumour tissue could provide valuable drug response data to augment treatment decisions in the clinic.

In this study, *ex-vivo* drug screening was performed on BC pateitnt-derived *ex-vivo* cultures (PDCs) generated from fresh surgically resected patient tumour tissue. The methods for generating BC PDCs was adapted from methods used in other solid tumour types, where PDC drug response data assisted in directing patient treatment or had been correlated with sequencing data to validate novel drug responses (135–138). Generation of BC PDCs has not yet been described in the literature, likely owing to the challenging tumour characteristics described in Chapter 4 and that these short-term cultures are often unsuitable for longer term propagation. In this chapter, endpoint *ex-vivo* high throughput drug screening results are discussed in relation to patient characteristics, tumour biology, and clinical outcomes, with particular reference to drug-resistant phenotypes and novel effective agents.

5.2 RESULTS

5.2.1 LOGISTICAL AND METHODOLOGICAL SUCCESS

It is important to detail recruitment, experimental, and methodological success. Figure *16* shows the success of patient recruitment, bladder tumour tissue retrieval, experimental, and methodological success in the 18-month collection period. In general, patients undergoing surgery for resection of their bladder tumours (either transurethral resection of bladder tumour (TURBT) or radical cystectomy (RC)) were willing to participate in the study. The patient recruitment period fell during an extremely challenging time due to the COVID-19 pandemic; nonetheless, 78 patients with suspected BC consented to participate in the study (four to five patients per month; one patient per week). Only two approached patients declined participation in the study. From participants, 59 bladder tumours were acquired. The drop-off (59 tumours from 78 consented) was mostly due to surgical cancellations, reflecting COVID-19 surgical and ward restrictions, or the patient being unfit on the day of surgery; inadequate tissue availability; and difficult cases where the tumour could not be localised or adequately resected, for example, within a bladder diverticulum.

Of the 59 acquired tumours, five were used for methodological optimisation. Leaving 54 tumours that were used for the purpose of *ex-vivo* high-throughput drug screening. Six (6/54, 11.1%) of these were classified as tissue failures. Two harboured fungal or bacterial contamination in the tumour material (one had a long-term catheter prior to TURBT and another suffered from recurrent urinary tract infections); one patient's tumour was inadvertently placed in formalin during theatre before being retrieved; tissue processing was

attempted after multiple phosphate buffered saline (PBS) washes, but the cells were non-viable; the remaining three were either too small or too charred from the diathermy resection for processing.

Quality control measures were defined to improve the reproducibility of the assay. Firstly, the coefficient of variance (COV) (standard deviation divided by the population mean) for each tumour was calculated using the CellTiter-Glo® (CTG) values from the 28 dimethylsulfoxide (DMSO) vehicle control wells, to ensure uniform cell distribution across the plate. If the COV in the control wells exceeded 0.25, it would be classed as a methodological failure due to high variance. Of the 48 tumours which reached end-point results, 7 (7/48, 14.6%) were removed based on high COV. Secondly, in those that passed the COV quality assurance, Z scores of the technical replicates were explored. Any replicates with a Z score greater than 2 would have been removed, however none exceeded this threshold (0/41, 0%). The remaining 41 tumours therefore passed quality control checks, leaving a tumour acquisition to success rate of 75.9% (41/54).

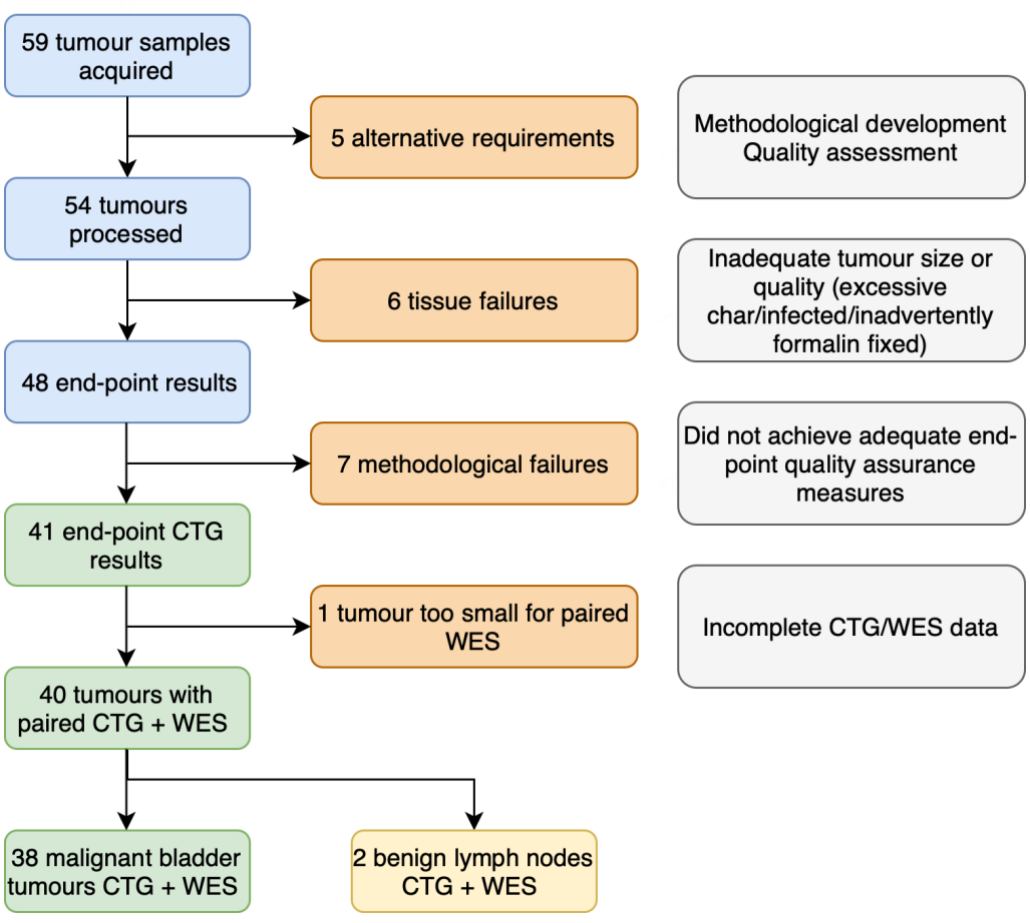

Figure 16: Flow chart depicting logistical and methodological success of ex-vivo high throughput drug screening using CTG in Bladder Cancer. CTG - CellTiter-Glo®; WES – whole exome sequencing.

5.2.2 PATIENT AND TUMOUR CHARACTERISTICS

In total, 41 patients had CTG endpoint data suitable for analysis. Patient and tumour characteristics are summarised in

Table 10: Patient and tumour characteristics for *ex-vivo* processed bladder tumours with endpoint CTG results

. The age, sex, and smoking characteristics of the cohort are in keeping with the demographics expected in BC. Almost one-third (12/41, 29.3%) of participants had previously been diagnosed with another non-bladder cancer. Most (38/41, 92.7%) participants had new bladder tumours. Ten (10/41, 24.4%) tumours expressed variant pathology, suggesting aggressive phenotypes. When classified by the European Association of Urology (EAU) Guidelines (69), most patients had high-risk non-muscle invasive BC (HR NMIBC) (17/41, 41.4%), followed by low-risk non-muscle invasive BC (LR NMIBC) or intermediate-risk non-muscle invasive BC (IR NMIBC) (12/41, 29.3%), and then muscle invasive BC (MIBC) (10/41, 24.4%). Two patients (2/41, 4.9%) had lymph node tissue acquired at the time of RC for MIBC, but both were deemed histologically benign. *For the remainder of this chapter, the two benign lymph nodes will not be included in the drug response analysis.*

5.2.3 PATIENT MANAGEMENT AND CLINICAL OUTCOMES

The clinical outcomes for the whole cohort are described in Table **11**. Median (interquartile range (IQR)) follow-up was 18 (12-26) months. The number of recurrence and progression events in the given follow-up period were relatively low at 30.8% and 15.4%, respectively, likely reflecting the short follow-up and the biology of tumours acquired. The most common management of this predominantly non-muscle invaive BC (NMIBC) cohort was intravesical therapy followed by surveillance. More than one-quarter of patients (11/39, 28.2%) underwent RC for their BC, including 4 (23.5%) HR NMIBC patients and 7 (70.0%) MIBC patients. Only one patient had neoadjuvant chemotherapy (NAC) prior to RC for MIBC (1/7, 14.3%). Of those who recurred, half experienced multiple recurrences, and half required subsequent treatment. Cancer-specific and overall deaths were limited to HR NMIBC and MIBC groups. Of note, all deaths in the HR NMIBC were cancer-specific deaths, as were, two-thirds of the MIBC deaths.

Table 10: Patient and tumour characteristics for *ex-vivo* processed bladder tumours with endpoint CTG results		
Characteristic	n = 41	%
Demographics & history		
Age – years (IQR)	75 (68-80)	
Male sex	32	78.0
Smoking status		
- Current smoker	4	9.8
- Ex-smoker	21	51.2
- Never smoked	16	39.0
Other significant cancer	12	29.3
Tumour characteristics		
New bladder tumour	38	92.7
Pre-treated	4*	9.8
Histology		
- UCC	39	95.1
- Variant pathology	10	24.4
Grade		
- High grade	27	65.9
- Associated CIS	12	29.3
Stage		
- Ta	18	43.9
- T1	11	26.8
- ≥T2	10	24.4
- LN only	2	4.9
EAU 2022 Risk Classification		
LR NMIBC	7	17.1
IR NMIBC	5	12.2
HR NMIBC	17	41.5
MIBC	10	24.4
LN only (benign)	2	4.9

*CTG – CellTiterGlo; IQR – interquartile range; UCC – urothelial cell cancer; CIS – carcinoma in situ; LN – lymph node; EAU – European Association of Urology; LR NMIBC – low-risk non-muscle invasive bladder cancer; IR NMIBC – intemediate-risk non-muscle invasive bladder cancer; HR NMIBC – high-risk non-muscle invasive bladder cancer; MIBC – muscle-invasive bladder cancer; *one patient with metastatic breast cancer to the bladder had received denusomab*

Table 11: Treatment and clinical outcome data sub-stratified by risk class										
EAU 2022 Risk Class	All n = 39		LR NMI n = 7		IR NMI n = 5		HR NMI n = 17		MIBC n = 10	
	n	%	n	%	n	%	n	%	n	%
Management after *ex-vivo* tumour sample retrieved										
HIVEC with MMC	3	7.7	1	14.3	1	20.0	1	5.9	0	0
Intravesical BCG	10	25.6	0	0	1	20.0	9	52.9	0	0
Any intravesical therapy	13	33.3	1	14.3	2	40.0	10	58.8	0	0
RC only	10	25.6	0	0	0	0	4	23.5	6	60.0
NAC + RC	1	2.6	0	0	0	0	0	0.0	1	10.0
Any RC	11	28.2	0	0	0	0	4	23.5	7	70.0
Radiotherapy	2	5.1	0	0	0	0	0	0.0	2	20.0
Surveillance only	11	28.2	6	85.7	3	60.0	2	11.8	0	0
BSC	2	5.1	0	0	0	0	1	5.9	1	10.0
No invasive treatment	13	33.3	6	85.7	3	60.0	3	17.7	1	10.0
Local recurrence after initial management										
Recurrence – yes	12	30.8	3	42.9	3	60.0	5	29.4	NA	NA
Multiple recurrences	6	15.4	0	0	2	40.0	3	17.6	NA	NA
Subsequent treatment*	6	15.4	1	14.3	1	20.0	4	23.5	NA	NA
Progression after initial management										
Progression** – yes	6	15.4	0	0	1	20.0	3	17.6	2	20.0
Subsequent treatment*	3	7.7	0	0	0	0	2	11.8	1	10.0
Mortality										
Cancer specific deaths	4	10.3	0	0	0	0	2	11.8	2	20.0
Overall deaths	5	12.8	0	0	0	0	2	11.8	3	30.0

*EAU – European Association of Urology; LR NMIBC – low-risk non-muscle invasive bladder cancer; IR NMIBC – intemediate-risk non-muscle invasive bladder cancer; HR NMIBC – high-risk non-muscle invasive bladder cancer; MIBC – muscle-invasive bladder cancer; HIVEC – heated intravesical chemotherapy; MMC – Mitomycin C; BCG - Bacillus Calmette-Guerin; RC – radical cystectomy; NAC – neoadjuvant chemotherapy; BSC – best supportive care. *intravesical/systemic treatment, or radical surgery (not simply TURBT) after initial management; **for NMIBC this is defined as moving from a low grade to a high-grade tumour, or progression from Ta to >Ta stage; for MIBC this is defined as the presence of locoregional or distal metastases during follow up.*

5.2.4 DEFINING POSITIVE CTG RESPONSE

Ex-vivo high throughput drug screening in BC is a novel concept, and there is a paucity of data in the literature to determine thresholds for positive response from primary BC tissue, unlike immortal cell lines, which are much more well-established (263). Several different metrics can be used to define positive response to a drug treatment. Firstly, two common metrics that are used to summarise a dose response curve - IC_{50} and EC_{50}. IC_{50} which represents the dose which is required for 50% reduction in cell count from controls and EC_{50} represents the dose reflecting the midpoint of the sigmoid dose response curve (211,219). An alternative metric is the area under dose-response curve (AUC), which is more robust to experimental noise than IC_{50} and EC_{50} (211,219,220), and regardless of the shape of the dose

response curve, provides a single numerical value that can summarise response. Hence, AUC was chosen as the dose response metric for this study.

5.2.5 EXPLORING DRUG ACTIVITY IN THE SCREEN

Standard high-throughput methodology for larger drug studies often uses a primary and secondary screening to eliminate inactive compounds and explore the active compounds in more detail (220). When defining activity thresholds, a balance must be met between setting a low threshold, in which there is a risk of defining inactive drugs as active (false positives); and setting the threshold too high, potentially excluding active compounds (false negatives).

To explore the distribution of AUC responses in more detail, all AUC values for all compounds tested on all tumours were plotted (Figure 17: A); this included screening 12 patient tumours for 21 drugs on BB1 plates (n=252 AUC values) and screening 27 patient tumours for 22 drugs on BB2 plates (n=594 AUC values). A total of 846 drug response AUC values were generated across the 39 malignant bladder tumours. The results were not normally distributed (Figure 17: B), with a median (IQR) AUC of 0.858 (0.663-0.975). Across BB1 and BB2, there were 15 common drugs, which is a relatively small screen; but combining the common drugs increased the number of BC results available. To avoid over-exclusion of potentially effective compounds, an exclusion threshold for efficacy was defined at the 75th percentile of all AUC responses (0.975). Any compounds with a mean/median AUC greater than 0.975 were defined as “inactive”; these drugs were subsequently excluded from drug hit and phenotype analysis (Table 12). In the remainder of this chapter, the methods and drug response profiles discussed are focussed on the 15 common compounds tested unless otherwise stated.

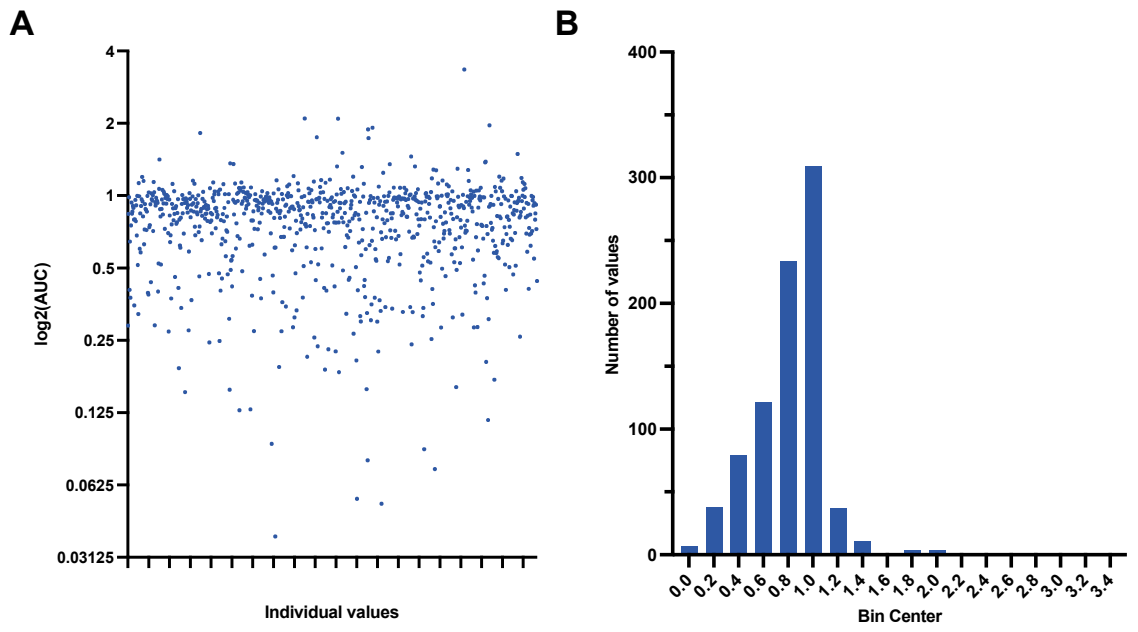

Figure 17: A. Scatter plot of all AUC values, to all drugs, across the 39 malignant bladder tumours; B. Frequency distribution histogram of AUC values for all drugs, all 39 malignant bladder tumours showing skewed distribution. AUC – area under dose-response curve.

Table 12: Common drug response thresholds generated by mapping the distribution of AUC for all 39 malignant bladder tumours

Drug	Normal distribution	Mean/Median AUC*
Cisplatin	Yes	0.370
Vinblastine	Yes	0.472
MMC	Yes	0.609
Docetaxel	Yes	0.746
Paclitaxel	Yes	0.852
Gemcitabine	Yes	0.883
Etoposide	Yes	0.933
Doxorubicin	No	0.916
AZD2014	No	0.323
AZD8186	No	0.747
Nutlin-3a	No	0.834
AZD5356	No	0.878
Lenvatinib	No	1.015
AZD4547	No	1.025
Erdafitinib	No	1.095

*AUC – area under curve; MMC – mitomycin C. *based on histogram distribution*

5.2.6 AUC NORMALISATION

As the drugs had differing potencies across the bladder tumour spectrum, it was necessary to normalise the data for compounds deemed as active. Several methods are available for data normalisation (Figure *18*). Firstly, min-max normalisation (264), where the minimum and maximum values are defines as 0 and 1, respectively, and each value between those are allocated a fraction or percentage value. Next, Z-score normalisation, which uses mean and standard deviation of the data set to normalise the values around 0 (265). Finally, robust or modified Z-score (rZ_{auc}) normalisation, which uses the median and each values' deviation from the median to normalise data around 0. For many drugs in this screen, the AUC values were not normally distributed (Table 12) and as shown in Figure *18*: A, several drugs had outlier AUC values that could skew the normalised data. Hence, as the rZ_{auc} uses the median, and is more robust to outlier results, this was chosen as the normalisation process for the data. The following formula was used to calculate robust Z scores (265):

$$\text{Robust Z score} = (0.6745(x_i - \tilde{x}))/\text{MAD}$$

$\tilde{x}$ = sample median; x_i = value being normalised; $\text{MAD} = \tilde{x}(x_i - \tilde{x})$

If the median absolute deviation (MAD) returned as 0, then calculation of the robust Z score is not be possible. In these rare circumstances, a standard Z score would be calculated.

5.2.7 SPECIAL CONSIDERATIONS FOR AZD2014

The dose for AZD2014 was reduced between drug plate bladder batch 1 (BB1) (top concentration 5μM) and drug plate bladder batch 2 (BB2) (top concentration 2μM) over concerns that the novel compound seemed very effective and to ensure the results weren't solely due to toxicity. The median (IQR) AUC values were not significantly different between BB1 and BB2 at 0.304 and 0.344, respectively (Mann Whitney U p=0.964). AUCs cannot be directly compared between groups when the drug doses are altered. Hence, normalisation scores were derived for each individual batch (n=12 for BB1 and n=27 for BB2), which then facilitated direct comparison once the data had been normalised.

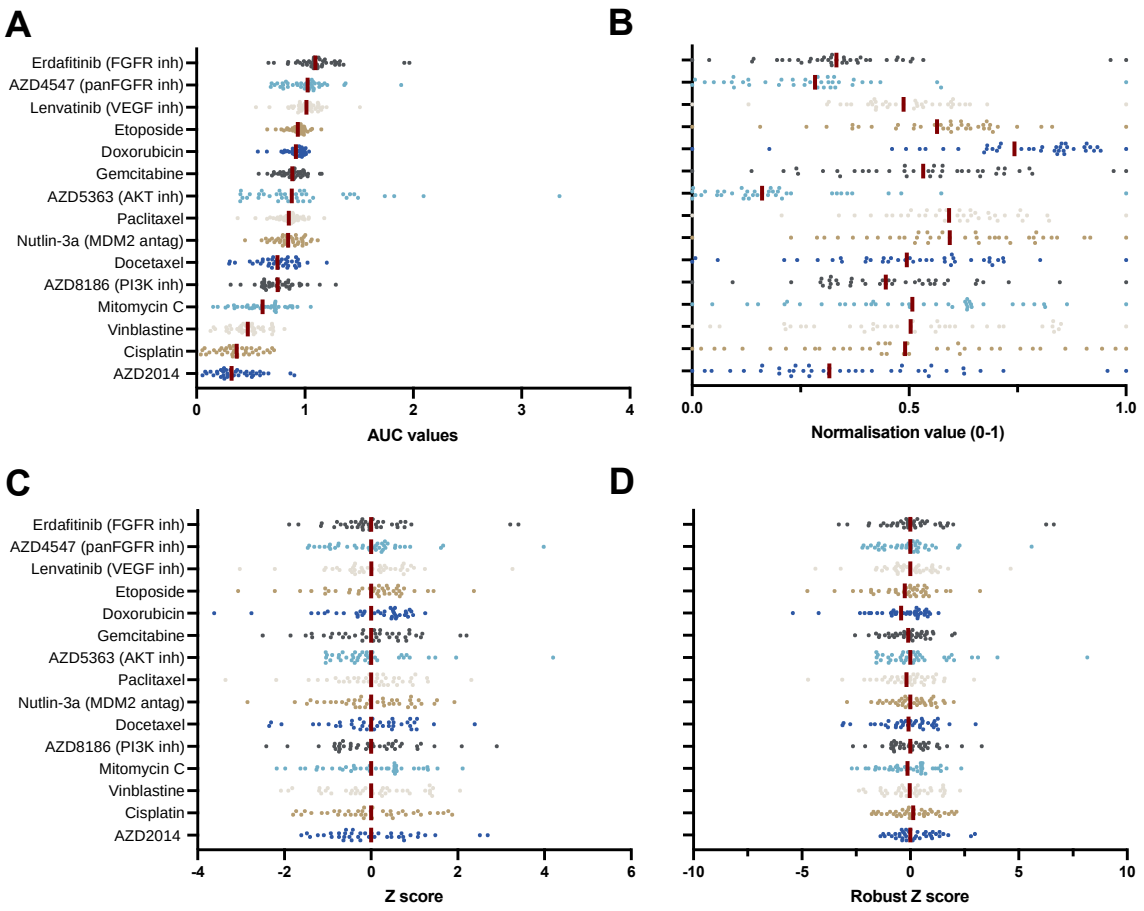

Figure 18: For all dot plots, each individual dot indicates the drug response for each individual tumour, where red lines indicate the mean or median response depending on normality of distribution; A. Raw AUC values for all tumours for each drug; B. Min-max normalisation, where all raw AUC values were transformed so that the lowest value = 0 and the highest value = 1; C. Z score normalisation (formula = (x-mean)/standard deviation, where x = the single data value; D. Robust Z score normalisation (formula = 0.6745(xi – x̃) / MAD), where xi = single data value; x̃ = median of the dataset; MAD = median of absolute differences between individual values of the cohort and group median. AUC – area under dose-response curve.*

5.2.8 CLUSTERING OF DRUG AND TUMOUR RESPONSES

To explore the differential clusters of tumours and drug responses, unsupervised clustering of rZ_{auc} data using K means was performed using the “cluster” package in R (266). The K means method aims to divide the group into K number of clusters, where each cluster has a distinct centroid, and are defined by their Euclidean distance (the square root of the sum of square differences) from the centroid (267). The elbow method is then used to explore the optimal

number of clusters (k); this uses the square of the distance between the sample points in each cluster and the centroid for a large series of K values. The sum of squared errors is calculated for each K value and plotted, with the optimal cluster presenting an 'elbow' shape inflection point (267). Briefly, the data was first transformed (as described in section 5.2.6). First, Euclidean distance was calculated (Figure *19*: A&B) before exploring differential K mean cluster patterns (Figure *19*: C&D). The elbow method suggested that the optimal number of clusters for drugs tested was 3 and for tumours screened was 4 (Figure *19*: E&F).

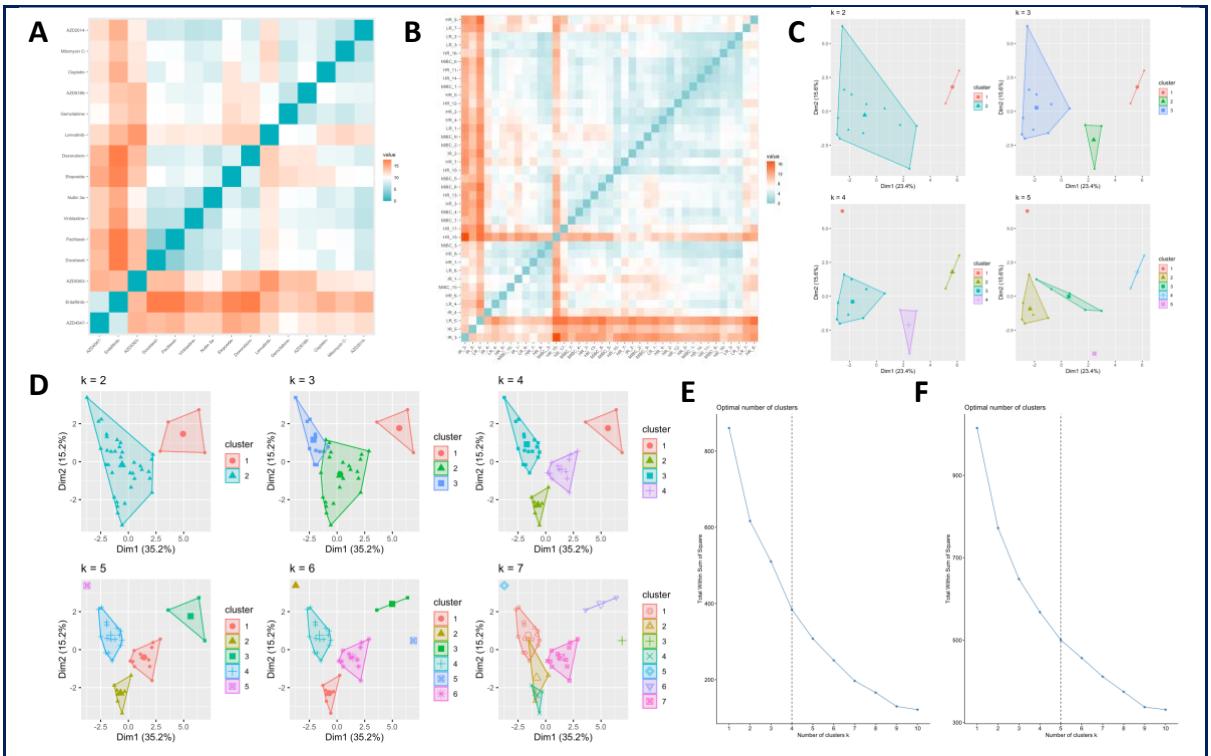

Figure 19: A. Euclidean distances matrix produced using the rZ_{auc} data drugs tested in the ex-vivo screen; B. Euclidean distances matrix produced using the rZ_{auc} data drugs tested in the ex-vivo screen; C. Differential cluster groups for drugs tested in the ex-vivo screen using K =2, K=3, K=4, K=5; D. Differential cluster groups for tumours tested in the ex-vivo screen using K =2, K=3, K=4, K=5, K=6, K=7; E. Graphical representation of the optimal number of clusters of drugs screened (calculated using the elbow method); F. Graphical representation of the optimal number of clusters of tumours screened (calculated using the elbow method).

Final cluster plots and the corresponding heatmap are shown in *Figure 20*. In terms of drug clusters (*Figure 20*: A), drugs with similar mechanisms of action were in close proximity; for example, Erdafitinib and AZD4547, two fibroblast growth factor receptor (FGFR) inhibitors grouped in cluster 2 (green), and docetaxel and paclitaxel were positioned in very close proximity within cluster 4 (magenta). AZD5363 (blue) clustered in isolation. Tumours were clustered into five phenotypic groups with differential resistance profiles (*Figure 20*: B&C).

Investigating the tumour clustering (*Figure 20*: B&C) HR_15 clustered in isolation (cluster 4, blue) and was one of the most resistant tumours in the screen. LR_5, IR_5, and IR_3 clustered together (cluster 1, orange) and were three of the most sensitive tumours, but all showed very poor response to drug cluster 2 (FGFR inhibition). Clusters 2, 3 and 4 (gold, green, and blue) consisted of almost unanimously G3 or above tumours (22/24, 91.7%), compared to only 2 (2/15, 13.3%) in cluster 1 and 5 (red and magenta) (Fisher's exact, $p<0.0001$). Clusters 2, 3, and 4, were also more likely to be ≥T1 stage (19/24, 79.1% versus 2/15, 13.3%, Fisher's exact $p<0.0001$), but there was no significant difference in the number of MIBCs. Tumour cluster 2 were more responsive to drug clusters 1 and 2, suggesting that this group may be amenable to receptor tyrosine kinase inhibition (FGFR, PI3K and VEGF inhibitors), whereas tumour clusters 3 and 4 seemed to be multi-drug resistant. Tumour clusters 1 and 5, were more chemosensitive. Tumours in cluster 5 were also more globally responsive to AKT inhibition.

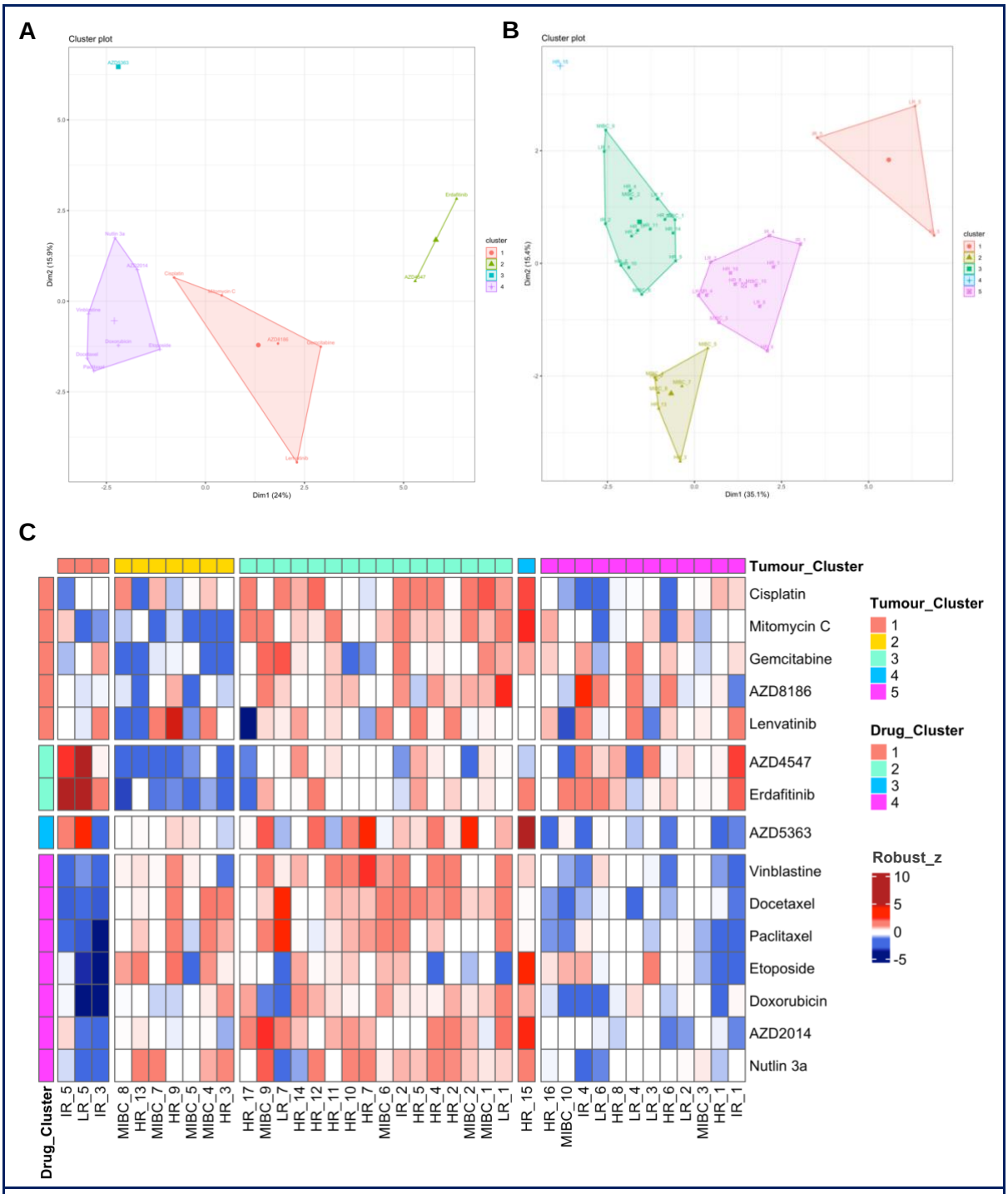

Figure 20: A. Final cluster plot of drugs based on elbow method for clustering of normalised drug response AUC values; B. Final cluster plot of tumours based on elbow method for clustering of normalised drug response AUC values; C. Heatmap of robust Z score AUC values for 15 tested common drug compounds (y axis) across 39 bladder tumours (x axis). Navy/blue indicates very good response to the drug, red/burgundy suggests a very poor response. Rows were divided by drug clusters and columns divided by tumour clusters, as previously described.

5.2.9 *EX-VIVO* DRUG RESPONSE PHENOTYPES

After removing the three "ineffective" compounds (Lenvatinib, Erdafitinib, and AZD4547, as per section 5.2.5), 12 common drugs across 39 tumours were evaluated in more depth. A positive drug response, described as a 'hit', was defined as an rZ_{auc} of less than 0 and a non-response was defined as a rZ_{auc} greater than or equal to 0. Global drug sensitivity or resistance scores per tumour were determined by the number of drug hits. The median (IQR) drug hits per tumour was 6 (3-9) (*Figure 21*: A). Tumours with a sensitive *ex-vivo* phenotypic signature were defined as those with 6 or more drug hits (n=20); tumours with a resistant signature were defined as those with less than 6 drug hits (*Figure 21*: B). Sensitive and resistant *ex-vivo* phenotypic tumour groups had a median (IQR) number of drug hits of 9 (8-9) and 3 (2-4), respectively.

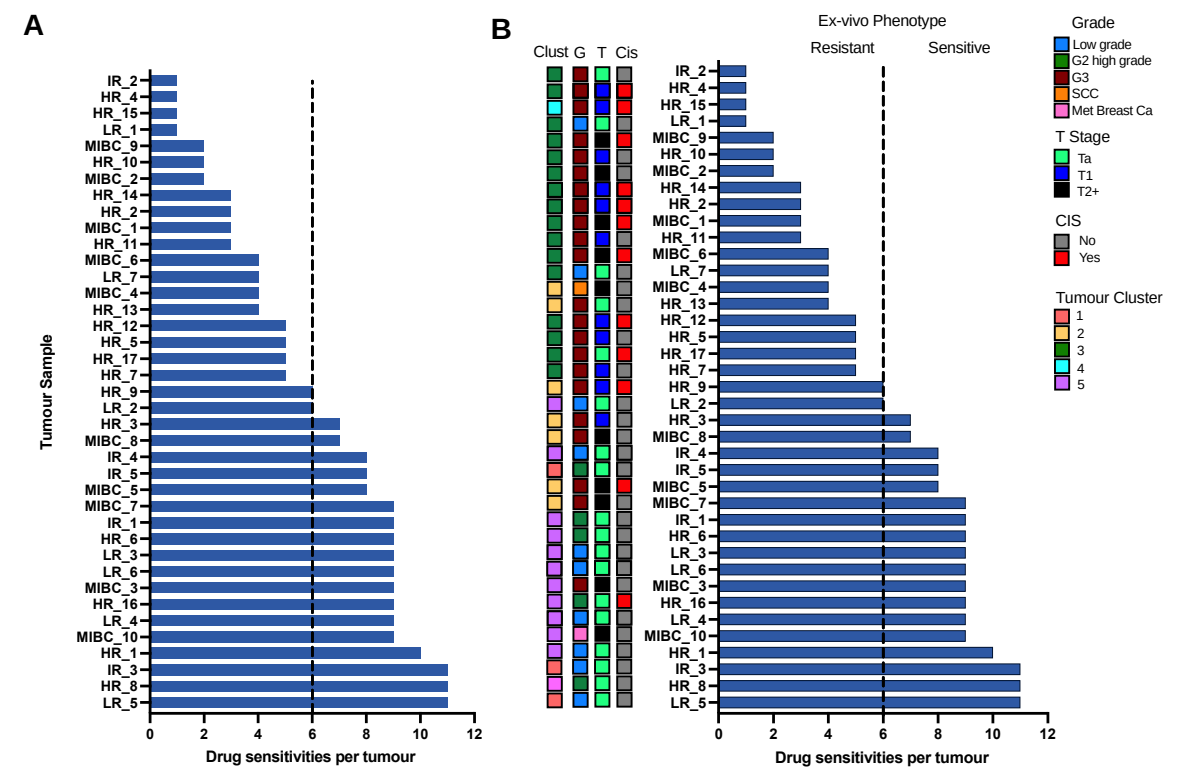

Figure 21: A –bar chart showing the number of positive drug 'hits' ($rZ_{auc} < 0$) per tumour; median number of 'hits' indicated by the black dotted line; B – the same bar graph has been annotated with grade, stage, carcinoma-in-situ, and cluster status of individual tumours; the cohort have been divided, using the median number of hits, into sensitive (green) and resistant (red) ex-vivo determined phenotypes. G – grade; T – tumour stage; CIS – carcinoma-in-situ; SCC – squamous cell carcinoma; Met Breast Ca – metastatic breast cancer; Clust – ex-vivo phenotypic tumour cluster.

5.2.10 *EX-VIVO* PHENOTYPIC SIGNATURES HAVE DIFFERING CLINICAL CHARACTERISTICS

Patient and tumour characteristics for each *ex-vivo* determined phenotypic group (EVP) are described in

Table 13: Patient and tumour characteristics for *ex-vivo* determined sensitive and resistant phenotypic signatures for 39 malignant bladder tumours

. As shown, the resistant EVP were significantly younger (Mann Whitney U, p=0.025) and had significantly less females in the cohort (Fisher's exact, p=0.044). In terms of tumour characteristics, the resistant EVP had a higher proportion of patients with grade 3 tumours (Fisher's exact, p=0.0002), associated carcinoma-in-situ (CIS) (Fisher's exact, p=0.041), and ≥T1 tumours (Fisher's exact, p=0.025). Interestingly, there was no difference in the number of smokers per group, the number of MIBCs per group, nor the EAU risk class (LR and IR NMIBC versus HR NMIBC and MIBCs). In terms of clinical outcomes, there was no difference in the recurrence, progression, metastases, or deaths between the sensitive and resistant EVPs. As the sensitive EVP had a significantly higher proportion of patients who received no invasive treatment after diagnosis (11/20, 55.5% versus 2/19, 10.5%; p=0.0057), these patients were removed and the data re-analysed; this revealed that there were more recurrences observed in the resistant group (4/17, 23.5% versus 1/9, 11.1%), but the difference was not statistically significant (p=0.63).

Table 13: Patient and tumour characteristics for *ex-vivo* determined sensitive and resistant phenotypic signatures for 39 malignant bladder tumours					
	Sensitive EVP (n=20)		Resistant EVP (n=19)		P value
	n	%	n	%	
Demographics					
Age – years (IQR)	77 (73-84)		71 (67-76)		**0.025**
Female sex	7	35.0	1	5.3	**0.044**
Never smoked	7	35.0	7	36.8	>0.99
Tumour characteristics					
Grade					
- G3 tumour	6	30.0	17	89.5	**0.0002**
- Associated CIS	3	15.0	9	47.4	**0.041**
Stage					
- ≥ T1	7	35.0	14	73.7	**0.025**
EAU 2022 Risk Classification					
- HR NMIBC/MIBC	11	55.0	16	84.2	0.082
First treatment received					
HIVEC + MMC	1	5.0	2	10.5	0.61
Intravesical BCG	3	15.0	7	36.8	0.15
Any intravesical therapy	4	20.0	9	47.4	0.096
RC only	3	15.0	7	36.8	0.15
NAC + RC	1	5.0	0	0.0	>0.99
Any RC	4	20.0	7	36.8	0.15
Radiotherapy	1	5.0	1	5.3	>0.99
Surveillance only	8	40.0	1	5.3	**0.020**
BSC	3	15.0	1	5.3	0.61
No invasive treatment	11	55.0	2	10.5	**0.0057**
Clinical outcomes					
Recurrence	7	35.0	5	26.3	0.73
Recurrence after treatment*	1	11.1	4	23.5	0.63
Progression	4	20.0	2	10.5	0.66
Progression after treatment*	2	22.2	1	5.8	0.26
Metastases	3	15.0	2	10.5	>0.99
Death	4	20.0	1	5.3	0.34

EVP – ex-vivo phenotype; IQR – interquartile range; EAU – European Association of Urology; HR NMIBC – high-risk non-muscle invasive bladder cancer; MIBC – muscle-invasive bladder cancer; HIVEC – heated intravesical chemotherapy; MMC – Mitomycin C; BCG - Bacillus Calmette-Guerin; RC – radical cystectomy; NAC – neoadjuvant chemotherapy; BSC – best supportive care. *patients who received surveillance or best supportive care only were removed from each group leaving n=9 in sensitive group and n=17 in the resistant group

5.2.11 *EX-VIVO* PDC SCREENING IDENTIFIES ALTERNATIVE DRUG SENSITIVITIES FOR INDIVIDUAL DRUG-RESISTANT COHORTS

A key challenge in the management of BC patients is the issue of treatment resistance. Using the *ex-vivo* BC screening results, it was possible to identify drug-resistant cohorts for each compound tested. Through exploring these drug resistant cohorts in more depth, alternative drug sensitivity patterns were determined (*Figure 22*: A). The mammalian target of rapamycin (mTOR) and docetaxel resistant tumours were the most multi-drug resistant. There was evidence of cross-resistance patterns between drugs with similar mechanisms of action, for example, paclitaxel resistant tumours were also resistant to docetaxel. As cisplatin resistance is a critical barrier in treating patients with BC, this group was explored in more depth. Interestingly, 55.0% (11/20) of cisplatin-resistant tumours were sensitive to PI3K inhibition (AZD8186) and 50.0% (10/20) to AKT inhibition (AZD5363) and mTOR inhibition (AZD2014). The group seemed to be a divided between cisplatin-resistant tumours that were responsive to other therapies and those that were multi-drug resistant (*Figure 22*: B). All of the cisplatin-resistant tumours that were also multi-drug resistant were classified as *ex-vivo* phenotype cluster 3 or 4.

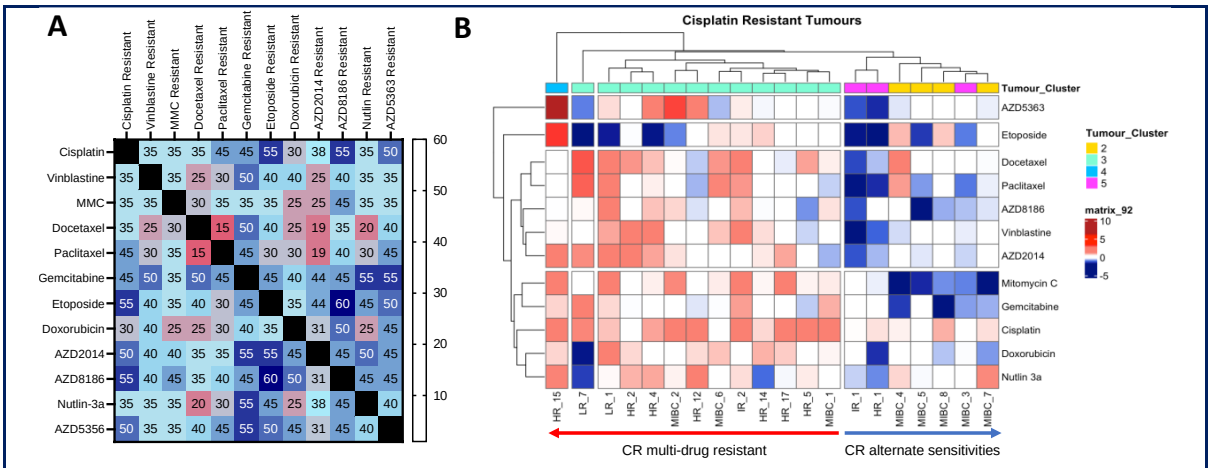

Figure 22: A – Matrix of alternative drug sensitivities for each individual drug resistant cohort (x axis). Each box shows the percentage of tumours within the resistant drug cohort that were sensitive to other agents in the screen (y axis); dark blue indicates a high proportion of alternative sensitivity and red indicates a low proportion of alternative sensitivity; B – heatmap of cisplatin resistant (CR) tumours and their responses to other drugs in the ex-vivo screen; navy/blue indicates good response to the drug, red/burgundy suggests poor response; columns have been annotated with ex-vivo phenotypic tumour clusters.

5.2.12 PROLIFERATIVE RESPONSES OF *EX-VIVO* PROCESSED BLADDER TUMOURS TO NOVEL THERAPIES

In a small group of tumours, it was noted that *ex-vivo* PDCs had proliferative responses (higher AUC compared to vehicle controls) to a subset of compounds. Proliferative response was defined as a raw AUC value greater than 1.25. The proliferative effect was only observed in response to novel receptor tyrosine kinase inhibitors, including: FGFR, AKT, PI3K, and VEGF inhibitors. Across the common drug screen (15 drugs, 39 tumours) a total of 22 proliferative responses were observed in 14 (14/39, 35.9%) different tumours, where six (6/39, 15.4%) had multiple proliferative responses (Figure 23). Three tumours showed common proliferation to both AZD4547, a potent inhibitor of FGFR1-3 (268), and Erdafitinib, a potent inhibitor of FGFR 1-4 (104). Erdafitinib, however, had a much higher number of proliferative responses compared to AZD4547 (8/39, 20.5% and 3/39, 7.7%), respectively), which may reflect its additional activity on FGFR4. AZD5363, a potent pan-AKT kinase inhibitor (269), had the highest number of proliferative responses in nine (9/39, 23.1%) different tumours, and occurred in conjunction with Erdafitinib or AZD4547 proliferation in four (4/39, 10.3%) cases.

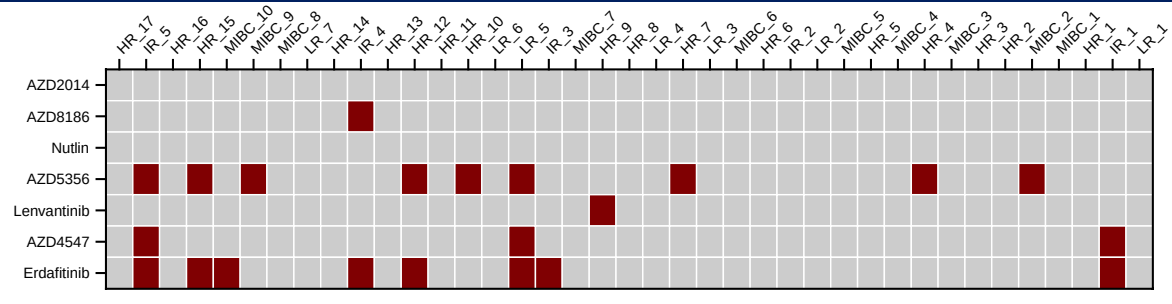

Figure 23: Heatmap of raw AUC values for novel inhibitors in the drug screen. The red squares indicate the tumours which have expressed a proliferative response (AUC >1.25) to a drug treatment.

Clinical outcomes in these tumours were generally poor. In the NMIBC proliferative tumours (11/14, 78.6%) that underwent bladder sparing treatments (ie did not have RC), seven (7/9, 77.8%) experienced recurrence; two further NMIBC patients underwent primary RC, one of whom progressed to metastases. Hence, 72.7% (8/11) of NMIBC proliferative tumours either recurred or progressed during follow-up. In patients who had MIBC proliferative tumours (3/14, 21.4%), two received radical treatment (RC or radical radiotherapy) and remained disease free; whereas, one patient rapidly progressed and died of the disease. In total, 64.3% (9/14) of patients with proliferative *ex-vivo* signatures experienced clinical recurrence, progression,

metastases, or death events due to their BC; this was significantly higher than to the non-proliferation tumours (9/14, 64.3% versus 7/24, 29.2%, Chi-squared p=0.034).

5.2.13 CORRELATION WITH PATIENT CLINICAL RESPONSES: CASES SERIES AND REPORTS

5.2.13.1 HEATED INTRAVESICAL CHEMOTHERAPY WITH MMC (HIVEC WITH MMC)

A total of three patients received adjuvant hyperthermic intravesical chemotherapy (HIVEC) with mitomycin C (MMC) after TURBT where *ex-vivo* tumour screening was performed. One patient, IR_2, had previously been treated with intravesical BCG, developed three further recurrences after HIVEC with MMC, consistent with a heavily resistant EVP and high levels of resistance to MMC (Figure 24: IR_2). Two further patients, LR_1 and HR_1 received HIVEC with MMC to good effect, with no further recurrences. HR_1 was deemed phenotypically sensitive to MMC, which corresponds with the clinical outcome and had a generally sensitive EVP (Figure 24: HR_1); whereas LR_1 was deemed phenotypically resistant to MMC. LR_1 has not developed any subsequent recurrences, which would be inconsistent with the observed *ex-vivo* phenotype.

Four further patients received HIVEC with MMC after an interval tumour recurrence (subsequent tumour after *ex-vivo* screen sample acquired). IR_3 and LR_2 had received no interval treatment, however, HR_14 and HR_15 had received adjuvant intravesical BCG. IR_3 was the only patient not to develop a subsequent recurrence after HIVEC with MMC treatment, which is consistent with the *ex-vivo* phenotypic screening results (Figure 25: IR_3). However, these results may be confounded by the fact that IR_3 displayed a particularly sensitive EVP and that HR_14 and HR_15 underwent interval intravesical treatment failure with BCG, suggesting aggressive phenotypes.

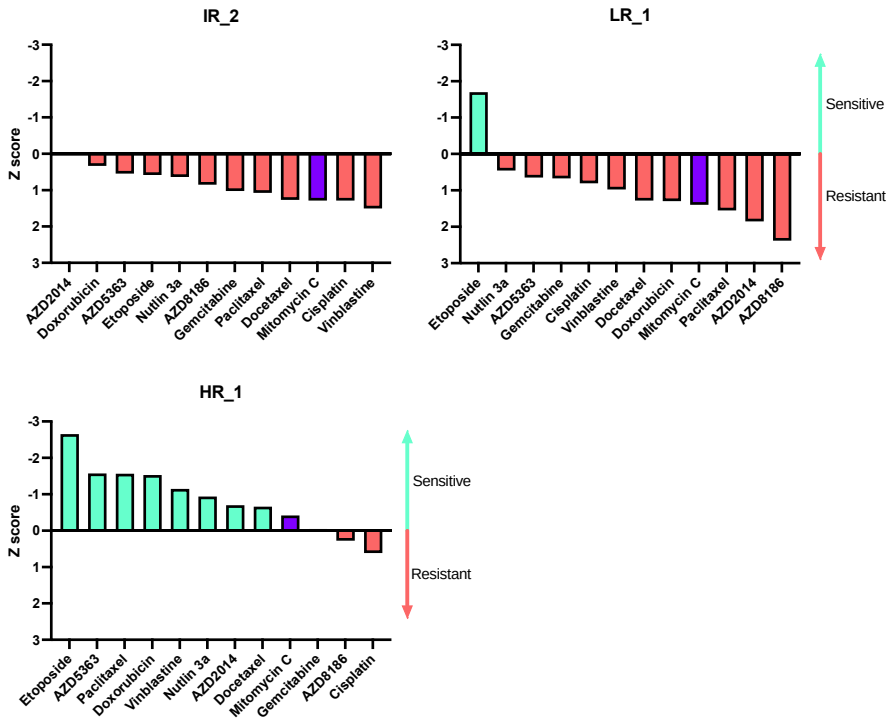

Figure 24: Ex-vivo determined phenotypic drug responses for IR_2, LR_1, and HR_1 showing robust Z scored AUC data ordered by drug sensitivity. Green indicates drug sensitivity, red indicates drug resistance, and MMC results are highlighted in purple.

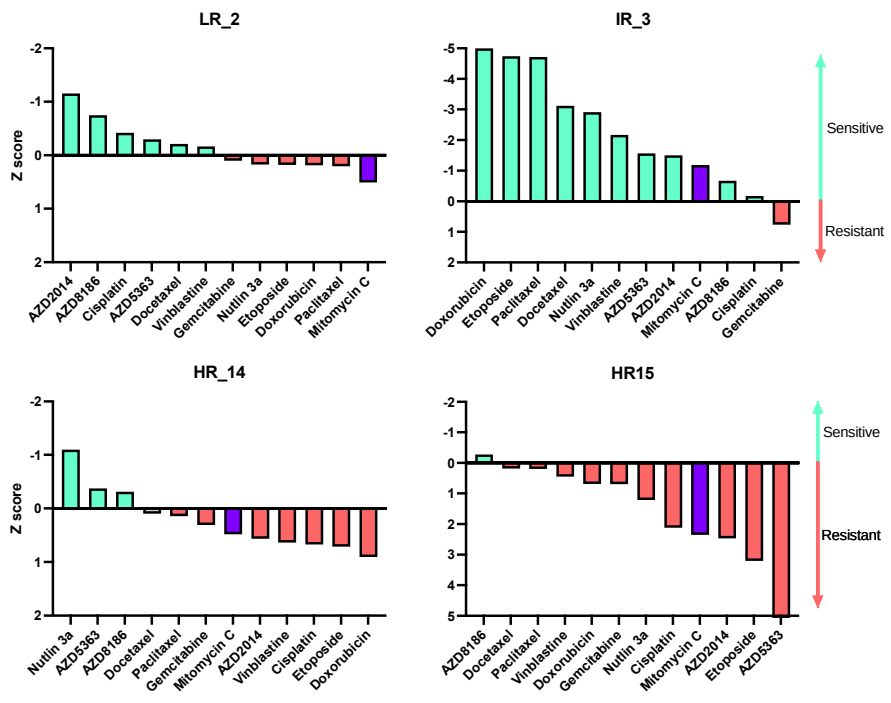

Figure 25: Ex-vivo determined phenotypic drug responses for LR_2, IR_3, HR_14, and HR_15 showing robust Z scored AUC data ordered by drug sensitivity. Green indicates drug sensitivity, red indicates drug resistance, and MMC results are highlighted in purple.

5.2.13.2 NEOADJUVANT CHEMOTHERAPY

MIBC_1 was the only patient to receive neoadjuvant chemotherapy (NAC) with cisplatin and gemcitabine before RC. At the time of RC, this patient still had a muscle invasive tumour residing in his bladder despite NAC, which is consistent with the lack of phenotypic response seen to those compounds *ex-vivo* (Figure 26). As the tumour was completely excised at RC, this patient has not experienced any progression events at 29 months follow-up; however, would be at high risk of progression events in the long term, with few available treatment options should this occur. Interestingly, this tumour was sensitive two novel compounds AZD2014 (mTOR inhibitor) and AZD5363 (AKT inhibitor), as well as paclitaxel.

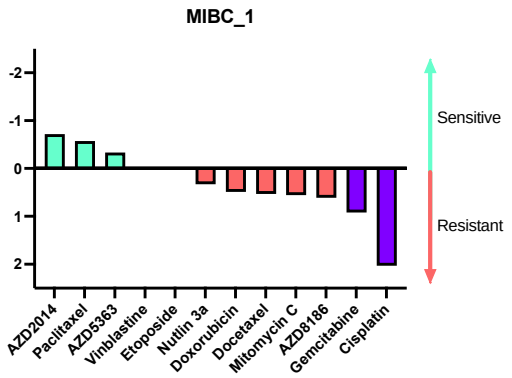

Figure 26: Ex-vivo determined phenotypic drug responses for MIBC_1 showing robust Z scored AUC data ordered by drug sensitivity. Green indicates drug sensitivity, red indicates drug resistance, and gemcitabine and cisplatin results are highlighted in purple.

5.2.13.3 PALLIATIVE SYSTEMIC THERAPY

Two patients progressed to metastatic disease requiring palliative systemic therapy. Both patients (HR_10 and MIBC_7) progressed after RC without NAC. HR_10 was treated with palliative systemic cisplatin-gemcitabine when metastases were identified, with stable disease at the time of submission, suggesting concordance with the *ex-vivo* phenotype (Figure 27). Whereas, MIBC_7 was treated with palliative systemic gemcitabine-carboplatin chemotherapy when metastases were identified, but progressed and died despite treatment. MIBC_7's ex-vivo phenotypic profile showed a mixed response – with sensitivity to gemcitabine, but resistance to cisplatin, suggesting non-concordance when comparing to *in-vivo* response (Figure 27). MIBC_7 may have benefited from alternative treatment, based on the *ex-vivo* phenotypic sensitivity profile shown.

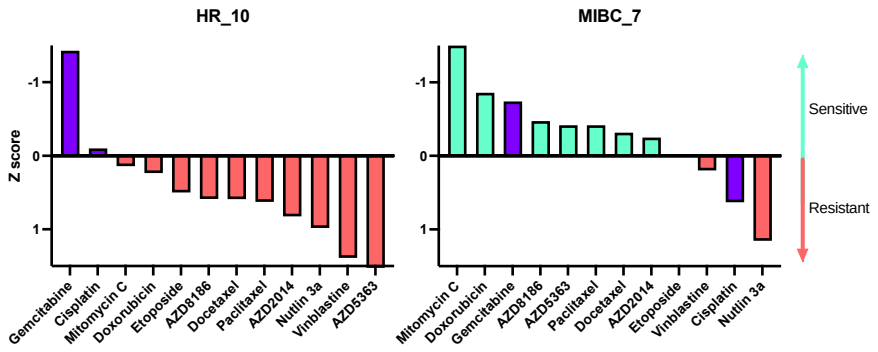

Figure 27: Ex-vivo determined phenotypic drug responses for HR_10 and MIBC_7 showing robust Z scored AUC data ordered by drug sensitivity. Green indicates drug sensitivity, red indicates drug resistance, and gemcitabine and cisplatin results are highlighted in purple.

5.3 DISCUSSION

We are entering an era where precision oncology is the benchmark for how we should be treating patients with cancer. The key is navigating away from '*one size fits all*' approaches and using alternative strategies to personalise treatments in the clinic. One method is looking at genomic biomarkers of response; this has been successful in a handful of cancer types, for example, epidermal growth factor receptor (EGFR) inhibition in non-small cell lung cancer (270) or B-Raf (BRAF) proto-oncogene inhibition in melanoma (271). However, these biomarker-driven therapies are only available to selected patients, may fail (in isolation) to identify therapeutic targets (272), and often have poor response rates across cancer types (23% response rate across all biomarker-driven basket clinical trials (273)). Hence, using alternative models to improve the success of personalised therapy are needed.

Using immortal cell line (ICL) assays to screen anti-cancer compounds is a well-established process and has advanced our understanding of cancer biology, as well as, in vitro mechanisms and biomarkers of large scale drug response (or resistance) (263,274,275). More recently, BC-specific cell line encyclopaedias have been developed, which can be mapped to molecular subtypes and have been utilised to predict differential treatment response (126,127,225,276). These libraries provide an invaluable resource for researchers, particularly when annotated with detailed phenotypic drug response and genomic sequencing data (263). However, identification of successful compounds often leads to several subsequent phases of translational experimentation (including the use of animals) before assessment in clinical trials. For example, Ertl et al. (225) performed genomic characterisation of 32 BC ICLs, before performing high-throughput drug screening (>1700 compounds) on 23 ICLs that spanned the molecular landscape of the disease. Having identified a potential candidate drug, they then repeated the phenotypic testing using ICLs, patient-derived cell lines (PDCLs), and then patient-derived xenografts (PDXs). Although this provides complementary layers of scientific evidence supporting the candidate drug, this translational workflow would not be implementable in a clinical cancer pathway to predict patient response, nor direct patient treatment.

In this study, *ex-vivo* high-throughput screening of BC PDCs has been shown to successfully deliver personalised drug response profiles for 75.9% (41/54) of tumours screened. These individual phenotypic reports highlight key differential treatment response patterns that do not align with traditional risk classification systems, and susceptibility of certain tumours to novel compounds. Although clinical outcome correlation at this stage was lacking, owing to the short follow-up and low number of events, the logistical and methodological success of this platform

have highlighted its potential as a preclinical treatment prediction model and novel drug discovery platform, with endpoint results that can be returned within a clinically relevant timeframe.

Logistically, the study was a success with excellent patient recruitment and tumour tissue acquisition, demonstrating both feasibility and proof of concept. During an 18-month patient recruitment phase, a total of 78 patients consented to participate in the study. Only two patients who were approached did not want to take part, which reaffirms that patients are keen to partake in cancer research activity and to donate their tissue for research purposes (277–279); this was also consistent with the patient and public involvement focus group work performed as part of the EVIDENT consortium at the start of this PhD. The methodological success rate of generating BC PDCs and subsequently screening them was 75.9%, which is consistent with the literature for propagation of bladder tumour tissues in 2D and 3D culture (133,280). The tumour drop off rate likely reflects variable tissue characteristics, diathermy tissue damage, and the challenges of propagating primary tumour tissue, as discussed in Chapter 4.

The overall cohort included 41 tissue specimens, of which 39 were malignant bladder tumours. The cohort was all inclusive, spanning a range of BC grades, stages, and thus EAU risk classes. Positive smoking history (ex or current smoker) was present in 25 (25/41, 61.0%) patients recruited, which is a key attributable risk factor for BC development (3). Interestingly, 12 (12/41, 29.3%) patients developed BC as a second malignancy, which is higher than previously reported (281). In eligible patients, management reflected international guidance (8,9), except that only one patient with MIBC who went on to have RC received NAC. This is lower than expected; in some cases this reflected patient choice, but in others it was due to ineligibility, non-urothelial histology, and the complex nature of providing NAC during the COVID-19 pandemic. Recurrence and progression events were relatively low for this cohort, making clinical outcome correlation challenging.

After defining positive CTG response, it was possible to cluster patient and drug responses using Euclidean and K mean methodology. There were four drug clusters and five tumour clusters established. Drugs with similar mechanisms of action (Erdafitinib and AZD4547, Docetaxel and Paclitaxel) and standard of care compounds (SOC) (Cisplatin, Gemcitabine, and MMC) seemed to be grouped in close proximity, providing reassurance for the validity of drug responses observed. Interestingly, AZD8186 (PI3K inhibitor) clustered closely to standard of care compounds, suggesting this could potentially be an effective therapeutic agent to explore (BKM120, a pan-PI3K inhibitor is currently being explored in metastatic platinum-refractory patients in a phase 2 clinical trial (NCT01551030). AZD5363 (AKT

inhibitor) clustered in isolation, likely relating to the high proportion of proliferative responses observed.

Tumours were clustered into five phenotypic groups with differential resistance profiles (*Figure 20*: B&C). HR_15 clustered in isolation (cluster 4) and was one of the most resistant tumours in the screen. LR_5, IR_5, and IR_3 clustered together (cluster 1) and were three of the most sensitive tumours, but all showed very poor response to drug cluster 2 (FGFR inhibitors). Clusters 2, 3 and 4 (gold, green, and blue) consisted of almost unanimously G3 or above tumours (22/24, 91.7%), compared to only 2 (2/15, 13.3%) in cluster 1 and 5 (red and magenta) (Fisher's exact, $p<0.0001$). Clusters 2, 3, and 4, were also more likely to be ≥T1 stage (79.1% versus 13.3%, Fisher's exact $p<0.0001$), but there was no significant difference in the number of MIBCs. Tumour clusters 3 and 4 were typically multi-drug resistant and clusters 1 and 5 were more chemosensitive. Tumour cluster 5 were also more globally responsive to AKT inhibition. These phenotypic response clusters may provide scope to modify treatment strategies. Not only can individual compounds be allocated to sensitive tumours to deliver personalised treatment recommendations, but tumour clusters may infer resistant biology. For example, patients with tumours that lie in clusters (3 and 5) may benefit from early radical surgery due to the poor global drug responses in these groups.

To explore global patterns of sensitivity and resistance in this cohort, *ex-vivo* phenotypes were generated based on the number of pan-screen drug hits. Those that had 6 or more drug hits across the screen were defined as sensitive, and those with less, were defined as resistant. As expected, the tumours in the resistant cohort were significantly more likely to be higher grade (G3, $p=0.0002$), have associated CIS ($p=0.041$), and have higher degree of invasiveness (≥ T1, $p=0.025$). The number of MIBCs were split equally between the groups, although one of the MIBCs in the sensitive group was actually a muscle invasive metastatic breast cancer, which has differing cancer biology and may be responsive to an array of chemotherapies, hormonal therapies, and biological therapies depending on the molecular status (282). There was also no statistical difference between groups regarding EAU risk class (LR and IR NMIBC versus HR NMIBC and MIBCs), although there was a higher proportion of HR NMIBC and MIBCs in the resistant cohort (84.2% versus 55.0%, $p=0.082$).

Although the sensitive and resistant EVPs showed differences in *ex-vivo* drug responses, there were no significant differences identified in patient clinical outcomes (recurrence, progression, metastases, and death events). It is worth noting here that these cohorts are small, and so significant differences are difficult to elicit with low event numbers. In addition, there were confounding variables between the groups. For example, the sensitive group had a higher proportion of patients who received no invasive treatment after TURBT, and the

resistant EVP seem to have been more aggressively managed with a slightly higher proportion of patients receiving curative radical surgery (36.8% versus 20%). Hence, although the resistant and sensitive EVPs showed diverging *ex-vivo* phenotypic sensitivities, at this stage, with short-term follow-up (18 months), the groups did not differ significantly in terms of clinical outcomes.

It was also possible to explore drug-specific phenotypes, with particular reference to drug-resistant groups, for example, cisplatin-resistant tumours. Cisplatin is an alykylating chemotherapeutic which forms the cornerstone of treatment for locally advanced and metastatic BC. It is first-line treatment for patients with MIBC in neo-adjuvant and adjuvant settings, and is used to treat metastatic disease (8). However, clinical response to cisplatin is unpredictable, with no current validated biomarkers (283) and significant associated toxicity (61). Here, it was possible to explore alternative drug sensitivities for *ex-vivo* defined cisplatin-resistant tumours. The cisplatin-resistant group contained 8 (8/10, 80%) of the MIBCs, again reinforcing that cisplatin-resistance is a key problem in aggressive BC, with a need to identify alternative effective therapies. The *ex-vivo* screening platform identified a subset of cisplatin-resistant tumours with a number of alternative drug sensitivities. Interestingly, most (5/7, 71.4%) of the tumours with alternative sensitivities were MIBCs and two of the most effective alternative agents were novel targeted inhibitors (PI3K and AKT inhibitors). The remaining tumours were seen to be multi-drug resistant. The clinical implications of this would be particularly important for those undergoing cisplatin-based NAC prior to RC. Patients with cisplatin and multi-drug resistant tumours, may opt to be triaged directly to RC, to avoid ineffective neoadjuvant treatment, whereas, cisplatin-resistant tumours with alternate sensitivities may opt for an amended NAC regimen based on their individualised drug response profiles.

Finally, a subset of tumours were identified that displayed proliferative responses to a group of targeted therapies (inhibitors of FGFR, AKT, PI3K, and VEGF). These responses occurred in over one-third of tumours (14/39, 35.9%), most of which were NMIBC (11/14, 78.6%). It was concerning that this phenotypic signature was associated with high recurrence and progression event rates in 64.3% (9/14), which was significantly higher than the non-proliferation group (7/24, 29.2%, Chi-squared p=0.034). A similar phenomenon was observed in an *ex-vivo* drug screening study in 12 AML patients, where blast cell proliferation occurred in response to several different compounds (284). One proposed mechanism for the proliferative responses is the complex biological crosstalk between different receptor tyrosine kinase (RTK) members. When a cancer cell is treated by a single RTK inhibitor, it may undergo rapid tumour cell reprogramming leading to de-repression of other RTKs, bypassing the inhibition; or marked changes in RTK dominance, which may lead to epithelial-to-

mesenchymal transition and changes in paracrine and autocrine signalling, which may alter growth and invasiveness in response to targeted inhibition (285). This complex biological phenomena has been described in mechanistic work performed in lung cancer (286–288), glioblastoma (289), head and neck squamous cell carcinoma (290,291), melanoma (292), and breast cancer (293). Clinically, this certainly raises concern about the use of targeted agents in clinical practice that may potentially accelerate the disease course; for example, currently there is a phase 2 clinical trial exploring efficacy of erdafitinib in *FGFR3* mutant NMIBC (NCT04172675). In a clinical context, when proliferative responses are observed during *ex-vivo* screening, it could be used as a negative biomarker and to inform on treatments that should be avoided.

Ex-vivo high throughput drug screening has therefore provided insight into tumour phenotypic responses, potential novel candidate therapies, and has identified clinically relevant treatment-resistant subgroups. However, there are several limitations that require discussion. First and foremost, this study was not conducted as an interventional clinical trial, so the *ex-vivo* phenotypic responses were not used to dictate patient treatment. Hence, by default, the clinical outcomes are only observational. Secondly, due to the limitations imposed by COVID-19, tumour tissue collection was initially suspended. Once the study reopened, it was imperative to include as many eligible patients as possible to develop the methodology and explore its potential in BC. However, this 'all-comers' approach has several shortcomings, most notably that only 4 (4/39, 10.3%) patients received treatment after tumour sampling that corresponded with compounds in the *ex-vivo* screen. Due to the pathological breadth of tumours acquired, and the relatively short follow-up, the number of recurrence and progression events were low; meaning that correlation of clinical endpoints with *ex-vivo* phenotypic sensitivities did not yield significant differences. Therefore, only a small number of tumours that underwent *ex-vivo* processing could be compared to the *in-vivo* clinical responses observed in the patients from which the tumours were yielded. At this stage, there was mixed concordance between ex-vivo response profiles and in-vivo responses, as described in Section 5.2.13. When analysing some of the drug response profiles in more detail, some tumours were responsive to many different treatments, for example, MIBC_7 (Figure 27). A consensus strategy of how to approach this problem would need to be established to ensure the process of choosing treatments was ethically sound. Snijder et al., who treated patients with advanced haematological malignancies using *ex-vivo* approaches, proposed using the most effective candidate treatments identified by *ex-vivo* based screening, so long as they were clinically available and considered safe given the patient's underlying medical comorbidities (198).

Another limitation to highlight is that combination treatments were not explored in this initial evaluation of the feasibility of *ex-vivo* drug screening in BC. Exploring drug combinations required meticulous drug plate dose planning, a greater number of viable tumour cells to seed on the expanded required drug combinations, and complex computation models to map synergy, antagonistic, or non-interacting effects (294). As GC combination chemotherapy is standard of care for patients with MIBC, an essential part of the future work will include exploring the feasibility of combination drug mapping through the *ex-vivo* platform.

CHAPTER 6

WHOLE EXOME SEQUENCING OF *EX-VIVO* PROCESSED BLADDER CANCERS

6.1 INTRODUCTION

Cancer is diagnosed in over 19 million people and kills over 10 million people on an annual basis (1), making it the second leading cause of death worldwide. With incidence and mortality rates thought to increase over the next 20 years, huge efforts have been launched to better understand and treat the disease. One example, of this is through advances in cancer genomics, where next generation sequencing (NGS) has transformed our understanding of cancer biology. The completion of the first human genome characterisation in 2004 (295) provided a roadmap whereby individual or grouped cancer samples could be cross-examined using NGS and *in silico* techniques. International collaborative genomic efforts soon followed through consortia such as The Cancer Genome Atlas (TCGA) and the International Cancer Genome Consortium (ICGC).

Carcinogenesis of cells is a complex biological process. With regards to genomics, mechanisms of cancer development and propagation include, but are not limited to: mutations or deletions of tumour suppressor genes (TSG), activation or overexpression of oncogenes, dysregulation of genetic repair mechanisms, and dysfunctional signalling pathways. NGS encompasses multiple different methods of tumour and normal tissue evaluation that aim to explore these underpinning mechanisms. The most common approaches include whole genome sequencing (WGS), whole exome sequencing (WES), and whole transcriptome sequencing (RNA-seq). WES, unlike WGS, only captures the exonic, protein-coding regions, which accounts for approximately 2% of the whole genome (296). Although WES is, by default, less comprehensive than WGS, exonic regions of the genome contain most of the known disease-driving mutations (296). WES also yields lower volumes of data, hence, requires less time, money, and expertise to analyse (and store) data (297,298). Hence, WES has been used more frequently in cancer research because it provides a summary of clinically relevant and actionable mutations, whilst being more cost, time, and data efficient. RNA-seq, on the other hand, explores the transcriptome, providing another layer of biological information regarding protein expression, epigenetic regulation, and downstream processes implicated in cancer pathways.

In this study, WES was chosen over WGS as the modality of NGS for tumour tissue examination, for the reasons described above. WES allows for identification of mutations in nucleic acids in exonic regions, which may lead to subsequent alterations in amino acid protein sequences and changes in protein function that can contribute to carcinogenic properties of a cell. For example, mutations in exons coding for TSGs, such as, *TP53*, *BRCA*, and *PTEN* proteins, may weaken or halt their activity (299). Whereas, mutations in exons coding for

oncogenes, such as, *FGFR3*, *PIK3CA*, and *KRAS*, may drive pathogenic behaviour (299). In a recent pan-cancer WES study of over 9,000 patient tumour samples, 299 consensus cancer driver genes were identified, 87 of which have roles in two or more cancer types (300); a list which is regularly expanding to include more samples, more genes, and a wider breadth of cancer types.

Bladder cancer (BC) has benefited from both pan-cancer and BC-specific genomic studies. From a pan-cancer perspective, identification of common cancer-wide mutations provides scope to deliver appropriately powered clinical trials exploring novel biomarker-driven treatments across cancer types (basket trials). For example, *FGFR3* was identified as a common oncogenic driver, which led to the development of FGFR inhibitors. BC benefited from this in the form of Erdafitinib, an FGFR inhibitor that was initially trialled in a phase 1 basket trial for advanced solid tumours harbouring FGFR mutations (301). Patients with advanced urothelial carcinoma showed the most promising responses, hence, a phase 2 trial was established in patients with *FGFR2/3* positive, pre-treated, metastatic urothelial carcinoma (104). The success of Erdafitinib in this cohort is now being evaluated as a phase 3 trial (NCT03390504), as well as, being trialled in patients with Bacillus Calmette-Guérin (BCG) unresponsive high-risk non-muscle invasive BC (HR NMIBC) (NCT04172675).

More in-depth, BC-specific genomic studies have broadened our horizons of the molecular disparities across the disease spectrum and within distinct clinical subtypes (27–36). For example, in the UROMOL non-muscle invaive BC (NMIBC) study (31), the authors used transcriptomic, genomic, and proteomic analysis of 862 NMIBCs to define four molecular classes (Class 1, 2a, 2b, and 3), which did not map directly to traditional clinical risk classifications. These molecular subtypes exhibited differential mutations, gene expression, regulatory pathways, immuno-stromal signatures, and clinical outcomes. In addition, groups 1 and 3 were identified as potential candidates for FGFR-targeting therapy and groups 2a and 2b better candidates for immunotherapy or radical cystectomy (RC).

Similar efforts have been exerted in muscle invasive BC (MIBC). Kamoun et al. (35) identified 6 distinct molecular subtypes of MIBC using transcriptomic profiles from 1,750 MIBCs. Again, these tumours displayed differing clinico-pathological features, levels of infiltrating micro-environment components, treatment responses, and outcomes. As such, there is scope for these molecular subtypes to be utilised in future to deliver more intricate risk stratification and tailored management strategies to patients in the clinic. Currently, the predictive utility and impact of directing neoadjuvant therapy in MIBC by genomic subtypes is being investigated in a multi-centre, phase 2, randomised trial that is due to start recruiting in Sheffield in 2023 (ISRCTN17378733). These examples highlight the power of understanding cancer genomics

in advancing biological insight, patient risk stratification, drug development, and personalised cancer therapy.

To gain a better understanding of molecular phenotypes and the biological mechanisms of response and resistance to treatment in this cohort of BC patient-derived *ex-vivo* cultures PDCs, WES of stored tumour tissue was performed for almost all (40/41, 97.6%) bladder tumour samples with endpoint CellTiter-Glo® (CTG) data available. Through additional WES analysis, the aim was to identify potential candidate genomic biomarkers of phenotypic response and non-response to treatment; to provide target credentialling for novel therapies; and to provide further molecular insight into the heterogeneity of drug responses in this BC cohort.

6.2 RESULTS

6.2.1 WHOLE EXOME SEQUENCING QUALITY MEASURES

In total, 100µL of DNA extraction solution was collected for all 40 samples. The median (inter-quartile range (IQR)) DNA concentration was 29.6 (14.5-43.25) ng/µL, with an average DNA Integrity Number (DIN) of 6.61. DNA samples were sent to MACROGEN Europe, who performed library preparation, quality assurance, and WES, as described in section 3.3.5. Post sequencing quality measures were assessed, as per recommended Samtools specifications (302), using median depth of coverage (DP), quality scores (QUAL), and quality divided by depth of coverage (QD) (provided by Dr Quayle during analysis). Overall quality descriptives of the cohort sequences included median depth of coverage (DP) 116, quality score (QUAL) 1336, and quality divided by the unfiltered depth of coverage (QD) 11.9, respectively. These metrics demonstrate the sequencing was of sufficient quality for subsequent downstream analysis. *In the remainder of this chapter, the data refers to the WES analysis for 38 malignant BCs with endpoint CTG results (two benign lymph nodes were removed).*

6.2.2 FILTERING STRATEGY

As there were no paired (matching) normal tissues to assist with filtering germline variants, the data was initially filtered using the 1,000 genome project dataset (218) and converted to MAF format by Dr Quayle (all subsequent analysis was performed by me as part of this PhD

thesis). At this stage, the number of variants called when aligned to the reference genome was still high displaying over 90,000 mutations across the cohort, many of which were multi-hit and mutated in all samples (Appendix 6, Section 9.6); in addition, the tumour mutational burden was higher than any other comparable The Cancer Genome Atlas (TCGA) cohort (Appendix 6, Section 9.6). Hence, further filtering of the WES data was required. First further population level variants were removed by filtering using the GENOMAD dataset, which is the largest open-access genome database (303). All mutations with an GENOMAD allelic frequency of >1% were removed (as these are observed in >1% of the general population and are thought to represent benign germline single nucleotide polymorphisms (SNP) with low probability of being deleterious).

Further filters were applied to explore significant, frequently mutated genes. A panel of genes was created using frequently mutated genes in BC using publicly available BC datasets in cbioportal (304,305). These genes were filtered using OncoKB^{TM} function, a cancer knowledge database that annotates genetic information with clinically relevant data regarding actionable mutations and food and drug administration (FDA)-approved therapies (306). All mutated genes present in ≥5% of the cbioportal BC datasets were included in the panel (n=80). These were then supplemented with a consensus pan-cancer gene mutation panel curated from WES of over 9,000 tumours across 33 TCGA datasets using a pan-software computational approach (300) (additional 249 genes). The curated gene panel (n=329) is summarised in (Appendix 7, Section 9.7). The final filtering event was using ANNOVAR annotations to remove suspected benign mutations. ANNOVAR is a publicly available, human genomic variant database that aggregates genomic variant information to generate clinical significance interpretations (307). In this step, all mutations that were deemed to be “benign” were removed. Any mutations present in over 80% of tumours were removed, as these likely represent sequencing artefacts.

6.2.3 SUMMARY OF WHOLE EXOME SEQUENCING FINDINGS

6.2.3.1 FREQUENTLY MUTATED GENES

Of the targeted panel generated, 167 (167/329, 50.8%) genes were mutated in this cohort. In total, there were 359 mutations across the 167 genes, which are summarised in *Figure 28*. The median (IQR) number of mutations per sample was 8.5 (5-13.3). Most mutations were missense, followed by nonsense, and splice site. Nucleotide transitions were more common

than transversions (median 54.5% versus 45.6%, respectively). The most frequent mutations were in *FGFR3* (26.3%), followed by *LRP1B* (21.1%), *TP53* (18.4%), *PCLO* (18.4%), and *PLXNB2* (18.4%) (*Figure 28*). *FGFR3* mutations were only observed in NMIBCs. Conversely, *TP53* mutations were only identified in HR NMIBCs and MIBCs. *LRP1B*, *PCLO*, and *PLNXB2* mutations are less well reported in BC and were distributed across the disease spectrum.

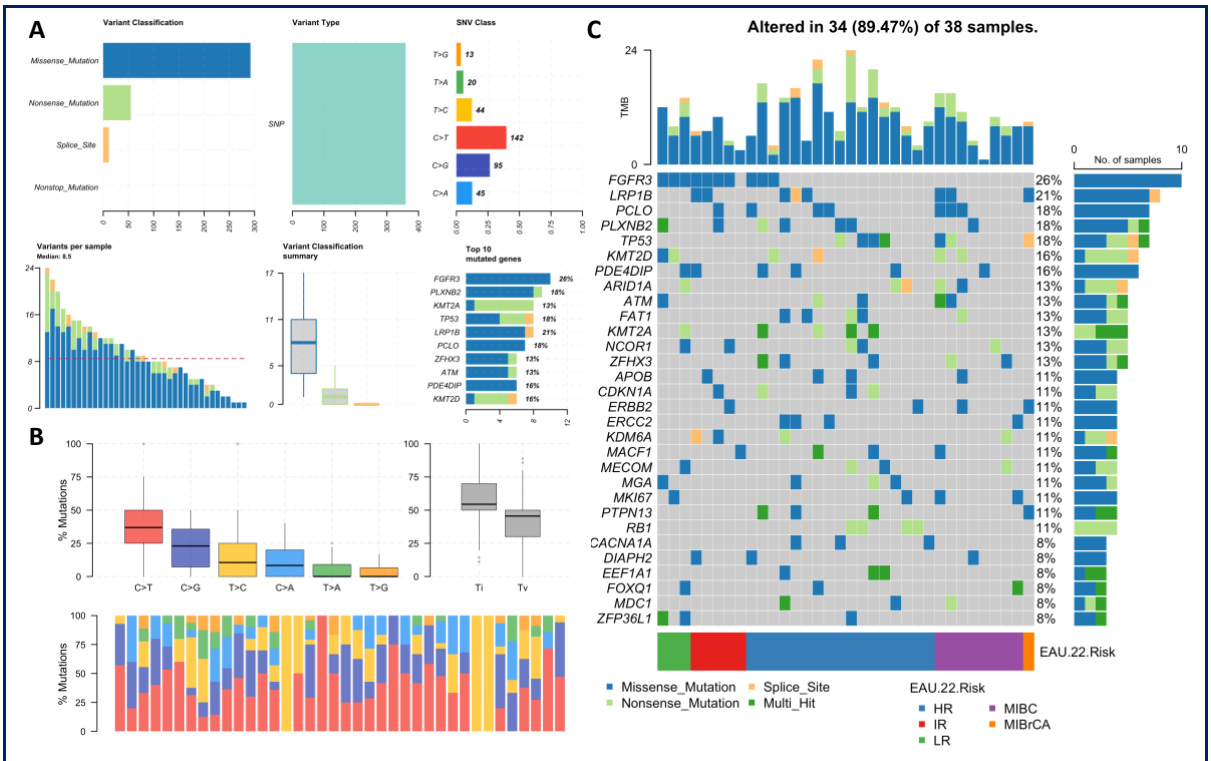

Figure 28: A – Summary plot of the variant classification, variant type, single nucleotide variant class, and number of variants per sample; B – TiTv summary plot showing the proportion of transitions and transversions per tumour and across the cohort; C – Oncoplot summary of top 30 mutated genes across the cohort, which were mutated in 34/38 (89%) samples, annotated by European Association of Urology 2022 clinical risk score.

6.2.3.2 FREQUENTLY MUTATED PATHWAYS

Understanding the interplay between cancer signalling pathways permits a better understanding of tumour crosstalk. It also generates data to support targeted therapy and combination therapy when there are parallel pathway mutations present. Mutations in the receptor tyrosine kinase (RTK-RAS) signalling (22/38, 57.9%), NOTCH (9/38, 26.3%), TP53 (8/38, 23.7%), cell cycle (7/38, 18.4%), and hippo pathways (7/38, 18.4%) were the most frequent in this cohort (Table 14). The proportion of tumours harbouring mutated pathway genes was lower than presented in recent pan-cancer analysis (308), which likely reflects

differential genetic analysis strategies and sample sizes. Within the RTK-RAS pathway (*Figure 29*), 16 (16/38, 42.1%) tumours harboured one RTK-RAS pathway mutation and six (6/38, 15.8%) harboured multiple pathway mutations. The most frequent mutations were *FGFR3* in 26.3% (10/38) and *ERBB2*/*3* mutations in 18.4% (7/38). One patient harboured both a *BRAF* and *NRAS* mutation, neither of which are commonly mutated in BC. When exploring all drug sensitivities for Bladder Batch 2, which included a MEK inhibitor (AZD6244), this *BRAF* mutant tumour was responsive, highlighting the potential for targeted therapy in this population.

Table 14: Summary of TCGA oncogenic pathway mutations identified in this cohort of patient bladder tumours, generated using OncogenicPathways function, maftools package, R (213)

Pathway	Genes in pathway	Affected genes in pathway; n (%)	Number of samples with mutation in pathway; n (%)
RTK-RAS	85	15 (17.6)	22 (57.8)
NOTCH	71	7 (9.9)	10 (26.3)
TP53	6	2 (33.3)	9 (23.7)
Hippo	38	2 (5.3)	7 (18.4)
Cell Cycle	15	2 (13.3)	7 (18.4)
PI3K	29	4 (13.8)	6 (15.8)
MYC	13	1 (7.7)	4 (10.5)
WNT	68	3 (4.4)	4 (10.5)
TGF-Beta	7	3 (4.3)	3 (7.9)
NRF2	3	2 (66.7)	2 (5.3)

TCGA – The Cancer Genome Atlas.

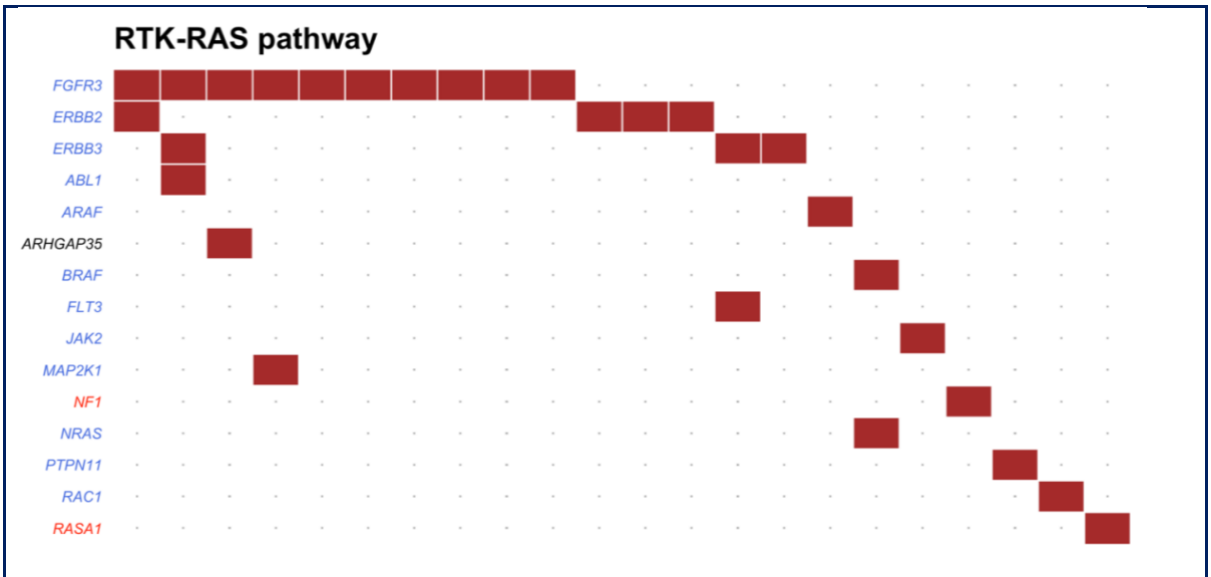

Figure 29: Summary of mutated genes in the RTK-RAS oncogenic pathway. In total, 22 (22/38, 57.9%) tumours harboured mutations in this pathway, of which 6 (15.8%) had multiple mutations. Genes in blue indicates an oncogene; genes in red indicate a tumour suppressor gene; genes in black indicate unknown mechnism. Red squares show individual tumours with a mutation in the allocated gene.

6.2.3.3 CO-OCCURRING AND MUTUALLY EXCLUSIVE GENES

After exploring the types of genetic mutations, it can be useful to explore the relationships between those mutations (co-occurrence and mutual exclusivity) (309). There were few mutually exclusive genes in this cohort, but several were co-occurring (*Figure 30*). Common co-occurring genes included *PTPRB* and *ERBB3*, *KMT2A* and *CDKN1A*, *EPHA3* and *APOB*, *CHD3* and *MKI67*, and *SPEN* and *RB1*. The co-occurring genes are mostly related to cell cycle regulation, which are observed in more aggressive BCs (34,35), although these specific co-occurrences are not described. *FGFR* mutations did not significantly co-occur with any other genes, which can be a common event NMIBC (310).

gene1	gene2	pValue	OR	Adjusted pValue	Event
PTPRD	ERBB3	0.0043	Inf	0.21	Co_Occurence
KMT2A	CDKN1A	0.0045	37.0	0.21	Co_Occurence
EPHA3	APOB	0.0085	Inf	0.36	Co_Occurence
CHD3	MKI67	0.0085	Inf	0.36	Co_Occurence
SPEN	RB1	0.0085	Inf	0.36	Co_Occurence
FOXQ1	ERBB3	0.0126	45.5	0.51	Co_Occurence
KMT2A	CIC	0.0142	Inf	0.51	Co_Occurence
FAT1	MSH6	0.0142	Inf	0.51	Co_Occurence
FAT1	SPEN	0.0142	Inf	0.51	Co_Occurence
NCOR1	SPEN	0.0142	Inf	0.51	Co_Occurence
PLXNB2	CDKN1A	0.0152	19.4	0.53	Co_Occurence
KMT2D	ATM	0.0207	13.2	0.70	Co_Occurence
EPHA3	KMT2D	0.0213	Inf	0.70	Co_Occurence
ZFP36L1	MECOM	0.0247	26.0	0.77	Co_Occurence
PMS2	RB1	0.0247	26.0	0.77	Co_Occurence
EPHA3	PCLO	0.0299	Inf	0.89	Co_Occurence
MSH6	PLXNB2	0.0299	Inf	0.89	Co_Occurence
ATM	PCLO	0.0346	9.8	0.97	Co_Occurence
ATM	TP53	0.0346	9.8	0.97	Co_Occurence
RHOB	ATM	0.0403	18.0	0.97	Co_Occurence
ERBB3	KMT2A	0.0403	18.0	0.97	Co_Occurence
FOXQ1	KMT2A	0.0403	18.0	0.97	Co_Occurence
ZFP36L1	KMT2A	0.0403	18.0	0.97	Co_Occurence
TSC1	NCOR1	0.0403	18.0	0.97	Co_Occurence
ZFP36L1	NCOR1	0.0403	18.0	0.97	Co_Occurence
EEF1A1	ZFHX3	0.0403	18.0	0.97	Co_Occurence
MDC1	ZFHX3	0.0403	18.0	0.97	Co_Occurence
PTPN13	CDKN1A	0.0475	13.7	1.00	Co_Occurence
PTPN13	MGA	0.0475	13.7	1.00	Co_Occurence

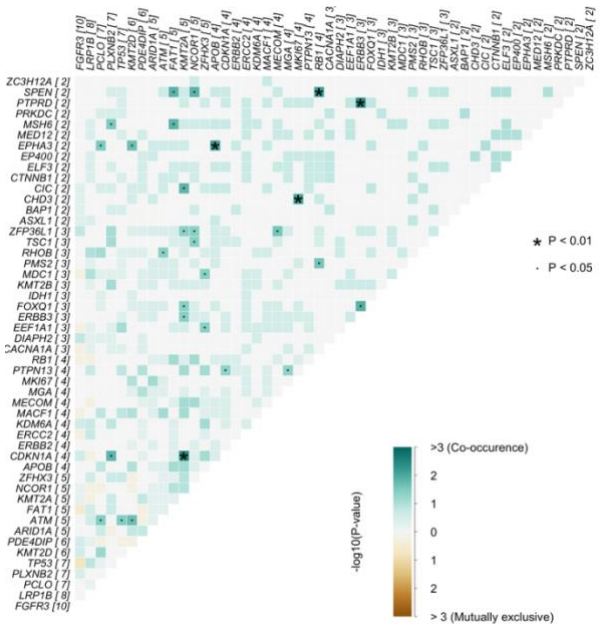

Figure 30: Table of co-occurring genes with associated p values, odd's ratios (OR), and adjusted p values with associated matrix plot showing significantly co-occurring genes.

6.2.3.4 APOBEC SIGNATURE ENRICHMENT

The apolipoprotein B mRNA-editing enzyme catalytic polypeptide (APOBEC) family consists of 11 cytosine deaminases and may be responsible for hypermutations associated with cancer development (311). APOBEC signatures are highly enriched in BC (311), and have recently been highlighted as a potential candidate biomarker for response to a systemic therapies (312). It was possible to calculate the APOBEC tCw TCW>T/G load for 35 samples, as described by Roberts et al. (311) (as enrichment cannot be calculated for tumours with only one identified mutation). In total, nine (23.7%) were classified as APOBEC enriched (Figure 31). There was no significant difference in mutational load between non-APOBEC and APOBEC enriched samples (t-test p>0.05). There were no significant differentially mutated

genes with respect to APOBEC enrichment. The majority (7/9, 77.8%) of the APOBEC enriched tumours were from ex, or current smoking patients; although this was not significantly higher than the non-enriched group (12/29, 58.6%, Fisher's exact p=0.44). The proportion of APOBEC-enriched tumours did not differ by clinical class (NMIBC 7/28, 25.0% versus MIBC 2/10, 20%, respectively, Fisher's exact p>0.99) nor sensitive and resistant EVP (6/19, 31.6% versus 3/19, 15.8%, respectively, Fisher's exact p=0.45).

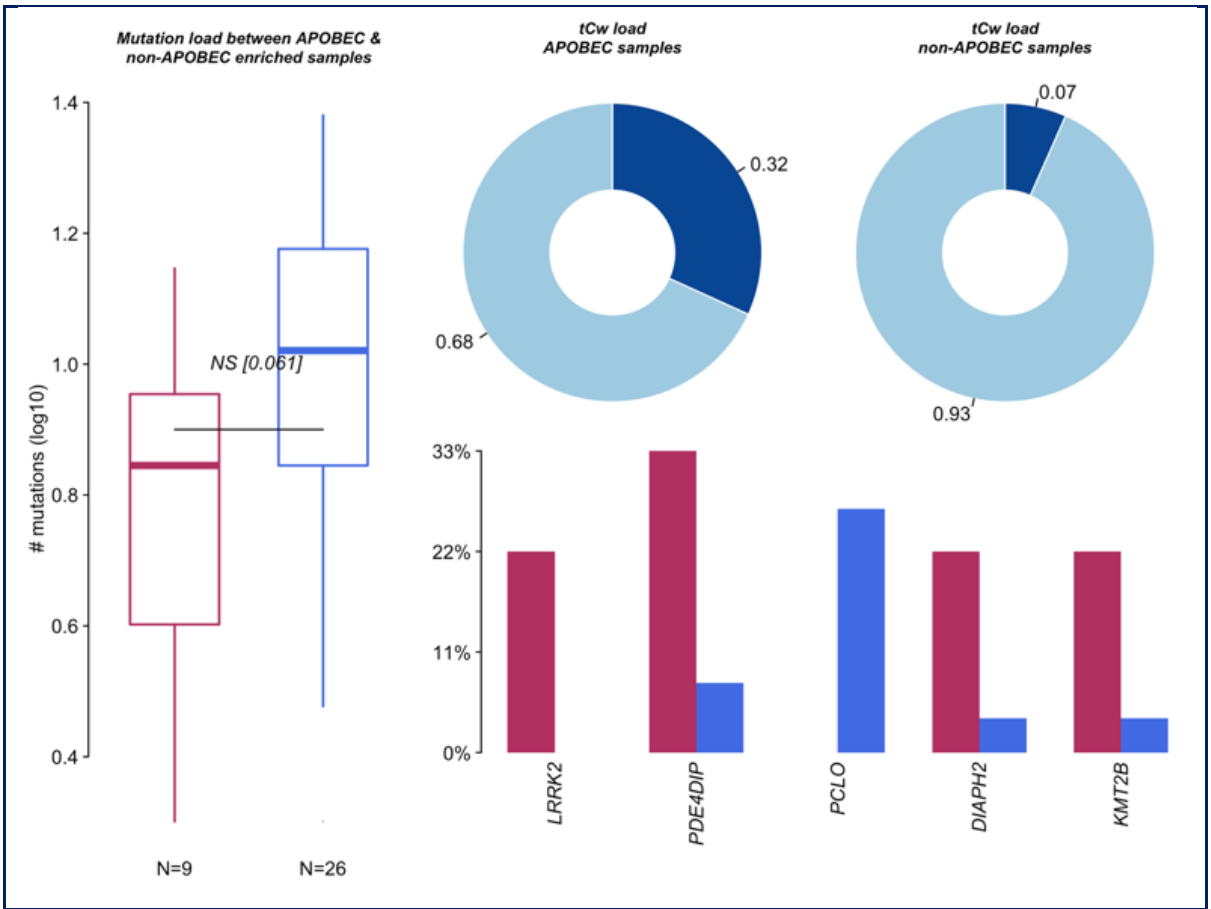

Figure 31: APOBEC enrichment analysis of tumours with >1 mutation (n=35) showing no significant difference in mutational load between APOBEC enriched and non-APOBEC enriched tumours, and no significant differentially mutated genes between the groups.

6.2.3.5 COSMIC SIGNATURE EXPRESSION

Exploring the combination of multiple superimposed mutational signatures is becoming increasingly common because we struggle to describe the complex nature of cancer through one isolated mutation alone. There are 96 classes of single base substitutions (SBS) (considered in the context of the 5′ and 3′ flanking nucleotides), where mutational signatures are calculated from the multinomial distributions of mutation counts over these categories (313). The Catalogue of Somatic Mutations in Cancer (COSMIC) database contains a reference set of signatures, some of which can be linked to specific mutagenic processes.

Currently, there are 60 mutational SBS signatures described (313). Using non-negative matrix factorisation, it was possible to explore similarities between this cohort of tumours and COSMIC signatures (using the cophenetic correlation metric). Two COSMIC signatures had a cosine similarity of greater than 0.7 – SBS5 and SBS3 (Figure 32).

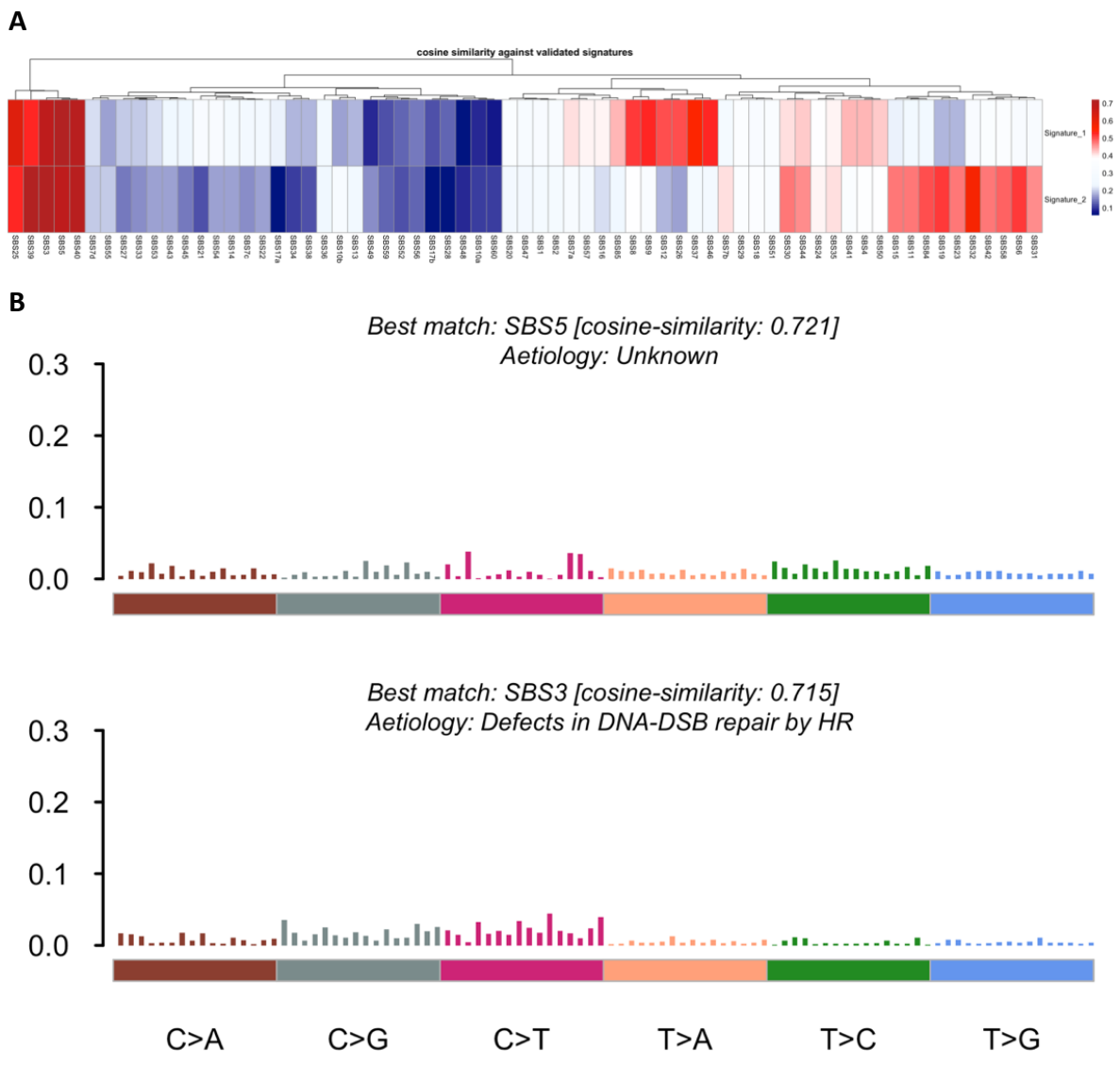

Figure 32: A – heatmap of cosine similarity scores between WES analysis of bladder tumours and 60 known COSMIC signature profiles; B – the two most highly matched COSMIC signatures (SBS5 and SBS3) with this BC cohort by cosine similarity. SBS – single base substitution; DSB – double strand breaks; HR – homologous recombination.

The cause of COSMIC signature SBS5 is currently unknown, but as it is reported across all cancer types, it is thought to be triggered by endogenous mutagenic processes (314). In addition, across all cancers, it is associated with increasing age (315). However, in BC, the link to age has not been shown as significant; given recent reports in lung cancer where the

high smoking cluster had significantly higher contributions of SBS5 (than the low smoking cluster), it is possible that this mutation in BC could be related to smoking. SBS3 is associated with defective homologous-recombination-based DNA repair (313); this can sensitise tumours to platinum-based therapy and poly(adenosine diphosphate [ADP]–ribose) polymerase (PARP) inhibitors (316).

6.2.4 GENETIC MUTATIONS BY PATIENT AND TUMOUR CHARACTERISTICS

Differences in mutated genes were explored by patient and tumour characteristics including: age (<75 years, n=18 versus ≥75 years, n=20), sex (men, n=31 versus women, n=7), smoking status (never, n=14 versus ever or current, n=24), grade (G3, n=24 versus <G3, n=14), stage (Ta, n=17 versus ≥T1, n=21), presence of carcinoma-in-situ (CIS) (yes, n=21 versus no, n=17), and risk class (non-muscle invasive BC (NMIBC), n=28 versus MIBC, n=10). With regards to patient characteristics (Figure *33*: A-C), *APOB* was the only genetic mutation that was enriched in the younger patients (4/18, 22.2% versus 0/20, 0%, Fisher's exact p=0.042), as were hippo pathway related genes (6/18, 33.3% versus 1/20, 5.0%, Fisher's exact p=0.038); *MSH6*, *TET2*, *TLR4*, and *UBR5* were enriched in women (2/7, 28.7% versus 0/31, 0%, Fisher's exact p=0.030), although the proportion of women in this cohort was small (n=7); and *MDC1* was enriched in never smokers (3/14, 21.4% versus 0/24, 0%, Fishers' exact p=0.043).

With regards to tumour characteristics (Figure *33*: D-F), *FGFR3* mutations were more frequent in lower grade tumours (7/14, 50.0% versus 3/24, 12.5%, Fisher's exact p=0.021) and *TP53* mutations were more frequent in higher grade (G3) tumours (0/14, 0% versus 7/24, 29.2%, Fisher's exact p=0.033). All *FGFR3* mutations were found in NMIBCs (10/28, 35.7% versus 0/10, 0%, Fisher's exact p=0.038), which were almost unanimously Ta tumours (9/17, 52.9% versus 1/21, 4.8%, Fisher's exact p=0.009). There were no significantly enriched mutations in higher stage tumours, MIBCs, nor tumours with CIS.

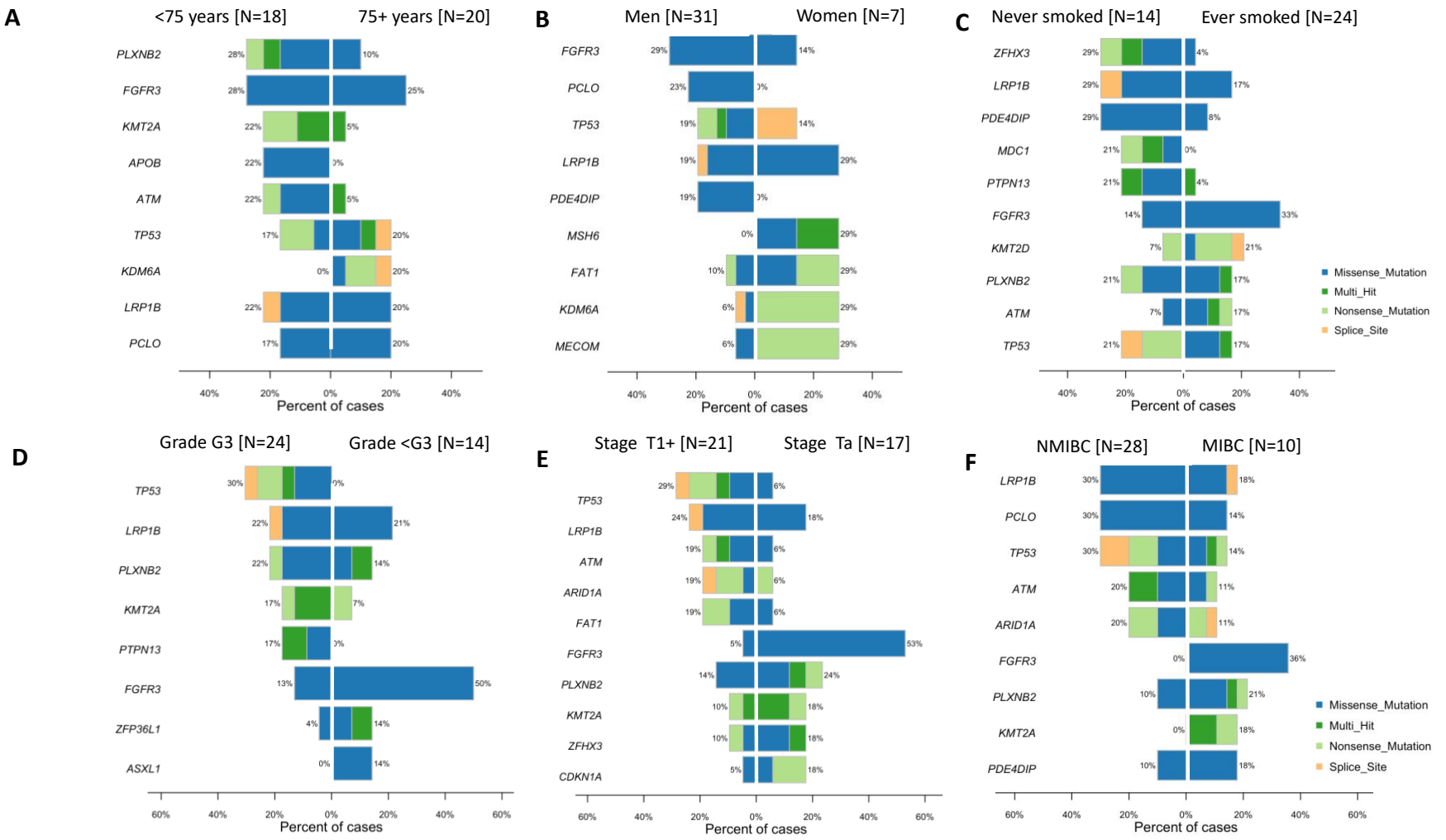

Figure 33: co-bar plots of differentially mutated genes by patient characteristics. A - younger (<75 years) versus older (75+ years); B – men versus women; C – never versus ever smokers; D – grade G3 versus grade <G3; E – stage T1+ versus stage Ta; F – NMIBC versus MIBC. NMIBC – non-muscle invasive bladder cancer; MIBC – muscle invasive bladder cancer.

6.2.5 GENETIC MUTATIONS BY SENSITIVE AND RESISTANT *EX-VIVO* PHENOTYPES

When performing WES correlation to *ex-vivo* determined drug sensitivities, mutational differences between sensitive and resistant *ex-vivo* phenotypes (EVPs) (as described in section 5.2.9) were explored. Tumours expressing the resistant EVP had significantly more mutations per tumour than the sensitive EVP (11.4 versus 7.5, t-test p=0.036, *Figure 34*: A). The two phenotypic groups had differential genotypes (*Figure 34*: B). For example, the resistant EVP had significantly higher proportion of *ARID1A* and *KMT2A* mutations (both 5/19, 26.3% versus 0/19, 0%, Fisher's exact p=0.046). *TP53* was also more frequently mutated in the resistant EVP (6/19, 31.5% versus 1/19, 5.3%), but this was not significantly different (Fisher's exact, p=0.090). The resistant EVP had significantly higher cell cycle pathway mutations (*CDKN1A/B, CDKN2A/B/C, CCNE1, CCND1/2/3, CDK2/4/6, RB1, E2F1/3*)(308) than the sensitive phenotype (7/19, 36.8% versus 0/19, 0%, Fisher's exact p=0.008). Tumour APOBEC enrichment was split equally between the two groups (4/19, 21.1% in resistant EVP versus 5/19, 26.3% in sensitive EVP) and there was close similarity in COSMIC signature enrichment – with both groups expressing SBS5 and SBS3.

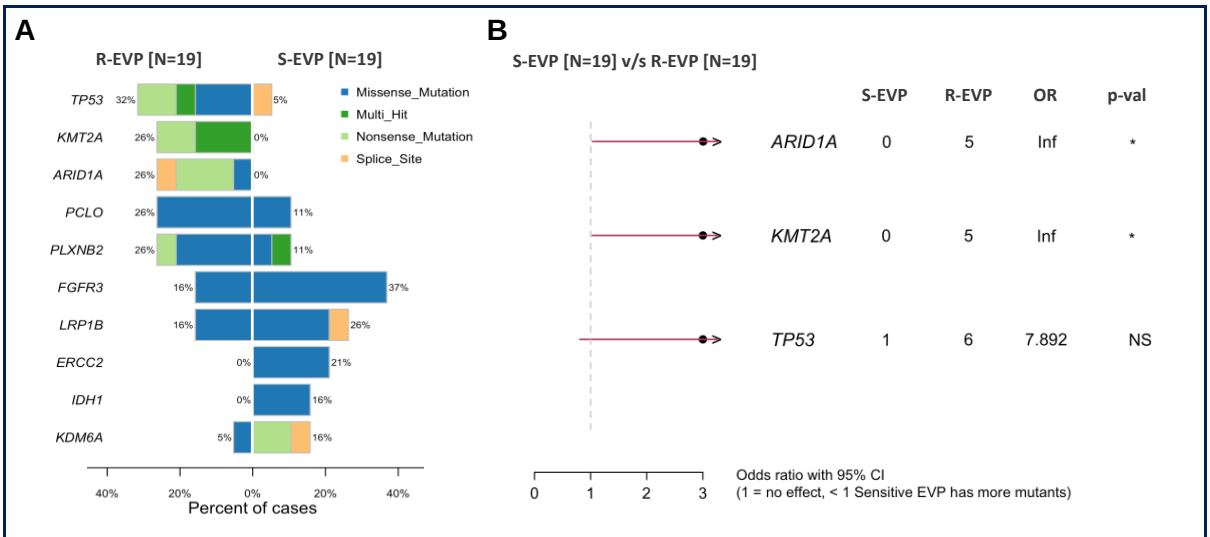

Figure 34: A –co-bar plot summary showing differential expression of genes between sensitive and resistant EVP cohorts and proportions of mutations observed; B – forest plot showing differentially mutated genes and their corresponding odds ratios and p values between sensitive and resistant EVPs. R-EVP – resistant ex-vivo phenotype; S-EVP – sensitive ex-vivo phenotype; OR = odds ratio; p-val – p value; ∗ = p<0.05, NS – not significant.

6.2.6 GENETIC SIGNATURES PREDICTIVE OF OUTCOME

The 'survGroup' function in maftools (213) was used to identify significant associations between survival outcomes (recurrence, progression, metastases, and death) and mutations in this cohort, using a minimum threshold of five mutated samples across the cohort to collate candidate genes for assessment (n=13, *TP53, PLXNB2, PCLO, FAT1, PDE4DIP, KMT2A, ATM, ARID1A, ZFHX3, NCOR1, FGFR3, KMT2D,* and *LRP1B*). Due to the small cohort, and low number of events during the follow-up period, there were no significant associations with survival outcomes across the cohort.

6.2.7 GENETIC DIFFERENCES IN DRUG-SPECIFIC *EX-VIVO* RESPONSE COHORTS

6.2.7.1 CISPLATIN SENSITIVE AND RESISTANT *EX-VIVO* PHENOTYPES

As described in section 0, cisplatin resistance in BC is a challenging clinical problem. When comparing genomics between cisplatin resistant and cisplatin sensitive tumours, there were common mutations across both groups, for example, *TP53* and *FGFR3* shown in Figure 35: A. However, *MGA* was identified as more frequently mutated in the cisplatin sensitive group (4/18, 22.2% versus 0/20, 0%, Fisher's exact p=0.042)(*Figure 35*: B). *MGA* (MAX gene-associated protein) is a TSG in the MYC pathway (308), hence, why the MYC pathway mutations were enriched in parallel (4/18 (22.2%) versus 0/20 (0%), Fisher's exact p=0.042) (*Figure 35*: C). The cisplatin resistant tumours could then be further divided in terms of their pan-screen phenotypic responses, dichotomised into two subgroups: cisplatin resistant tumours with alternative drug sensitivities and cisplatin resistant tumours that were multi-drug resistant (*Figure 36*: A). There were a higher proportion of cisplatin resistant and multi-drug resistant tumours with *TP53*, *PCLO*, *PLXNB2*, *KMT2A*, and *ARID1A* mutations (*Figure 36*: B). These mutations were not observed in the cisplatin resistant with alternative sensitivities group.

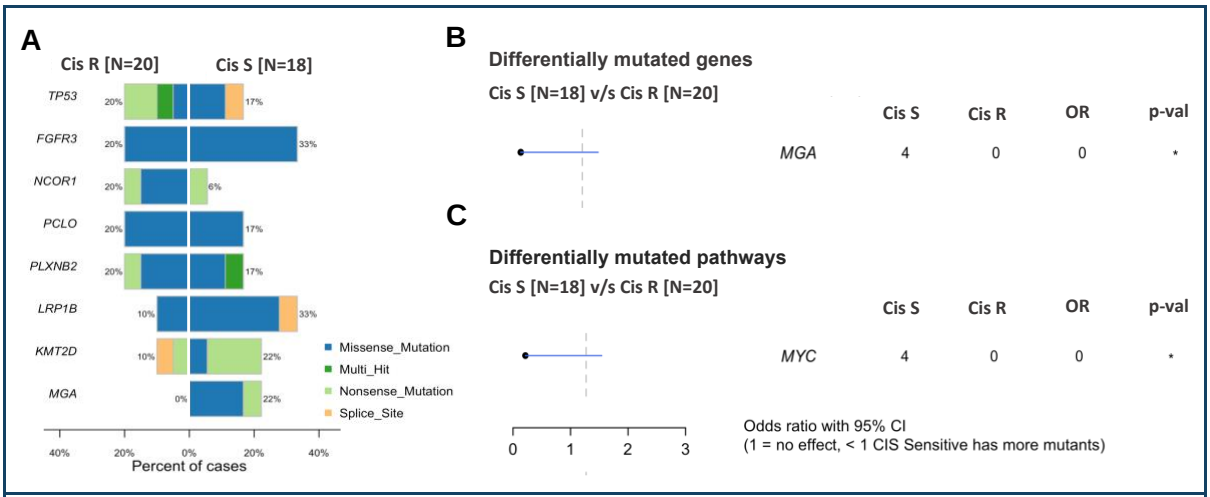

Figure 35: A – co-bar plot summary showing differential expression of genes between cisplatin resistant and cisplatin sensitive cohorts; B – forest plot showing the differentially mutated genes and their corresponding odds ratios and p values; C – forest plot showing the differentially mutated pathways and their corresponding odds ratios and p values. Cis S – cisplatin sensitive phenotype; Cis R – cisplatin resistant phenotype; OR – odds ratio; p-val – p value; ∗ = p<0.05.

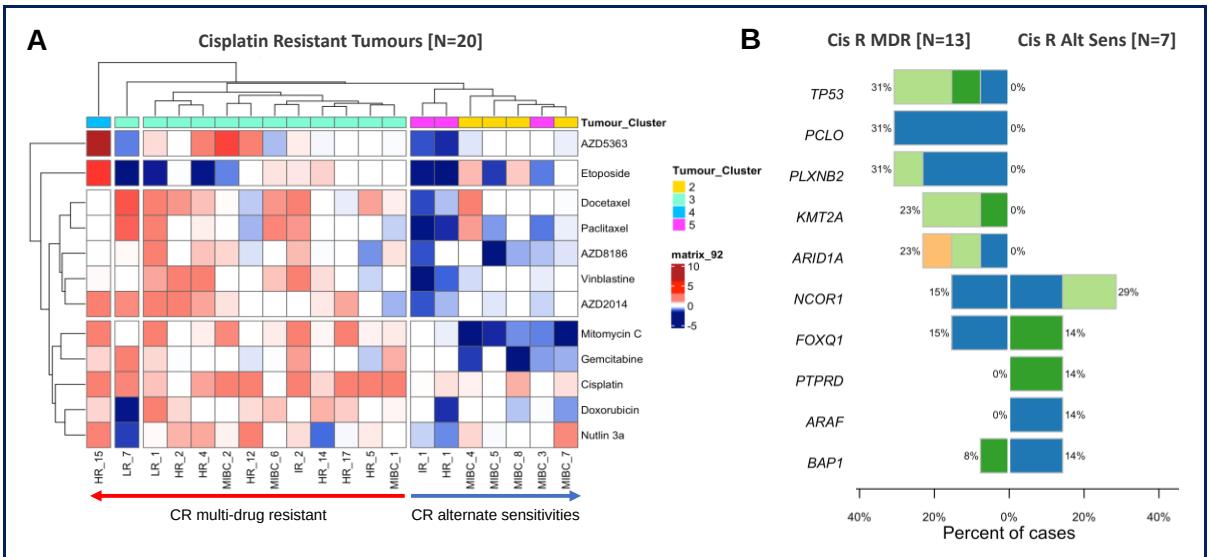

Figure 36: A – heatmap of cisplatin resistant tumour alternative drug hits (blue = hit, white = no hit), showing a split between cisplatin resistant tumours with alternative sensitivities (right) and cisplatin resistant tumours that are multi-drug resistant (left); B – co-bar plot of differentially mutated genes between the cisplatin resistant and multi-drug resistant group and the cisplatin resistant with alternative sensitivities group. CR – cisplatin resistant; Cis R MDR – cisplatin resistant multi-drug resistant phenotype; Cis R Alt Sens – cisplatin resistant with alternative sensitivities phenotype; OR – odds ratio; p-val – p value; ∗ = p<0.05.

6.2.7.2 OTHER STANDARD-OF-CARE DRUG SENSITIVE AND RESISTANT GROUPS

Differential genetic mutations were explored between *ex-vivo* determined drug sensitive and resistant cohorts. There were no significant differentially mutated genes between mitomycin C (MMC), Doxorubicin, Etoposide and Gemcitabine sensitive and resistant cohorts. Vinblastine, Docetaxel, and Paclitaxel sensitive and resistant groups had differentially mutated genes (*Figure 37*). *ERCC2* mutations were more common in Vinblastine sensitive tumours (4/18, 22.2% versus 0/20, 0%, Fisher's exact, p=0.042). In Docetaxel and Paclitaxel resistant tumours, *ARID1A* mutations were more frequent (5/20, 25% versus 0/18, 0%, Fisher's exact p=0.048 and 5/19, 26.3% versus 0/19, 0%, Fisher's exact p=0.046, respectively).

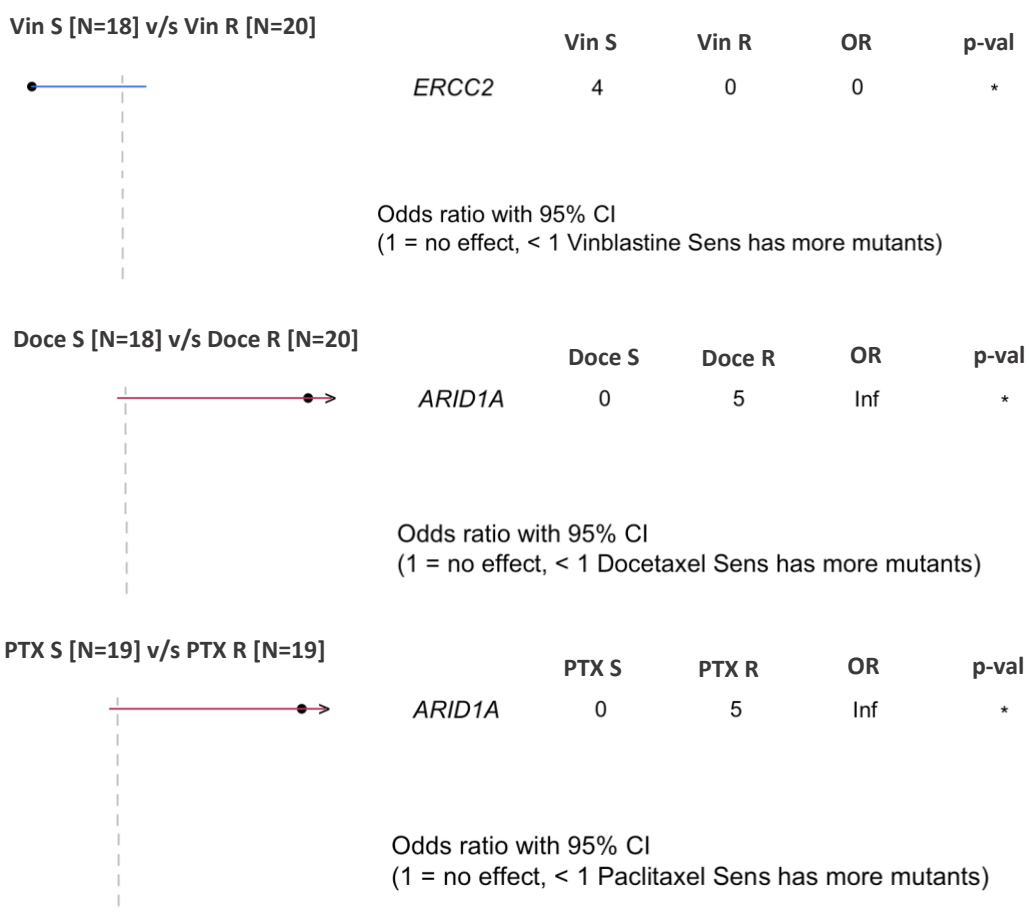

Figure 37: Forest plots showing significant differentially mutated genes between drug resistant and drug sensitive groups for standard of care chemotherapies. Vin S – vinblastine sensitive phenotype; Vin R – vinblastine resistant phenotype; Doce S – docetaxel sensitive phenotype; Doce R – docetaxel resistant phenotype; PTX S – paclitaxel sensitive phenotype; PTX R – paclitaxel resistant phenotype; OR – odds ratio; p-val – p value; ∗ = p<0.05.

6.2.7.3 NOVEL DRUG SENSITIVE AND RESISTANT GROUPS

All of the novel effective drugs in the screen showed differential mutation patterns between sensitive and resistant EVPs, as shown in Figure 38. The mTOR inhibitor (AZD2014) resistant phenotype was significantly enriched for *ARID1A*, *KMT2A*, and *APOB* mutations (5/16, 31.3% versus 0/22, 0%, Fisher's exact, p=0.0087; 5/16, 31.3% versus 0/22, 0%, Fisher's exact p=0.0087; and 4/16, 25.0% versus 0/22, 0%, Fisher's exact p=0.025, respectively). The PI3K inhibitor (AZD8186) sensitive phenotype had significantly more *PTPN13* mutations (4/18, 22.2% versus 0/20, 0%, Fisher's exact, p=0.042). The AKT inhibitor (AZD5363) resistant phenotype had significantly more *TP53* mutations (7/20, 35.0% versus 0/18, 0%, Fisher's exact p=0.0087), whereas the sensitive phenotype were enriched for *ERCC2* (4/18, 22.2% versus 0/20, 0%, Fisher's exact p=0.042). The nutlin-3a resistant group had a higher proportion of *FAT1* mutations (5/19, 26.3% versus 0/19, 0%, Fisher's exact p=0.046).

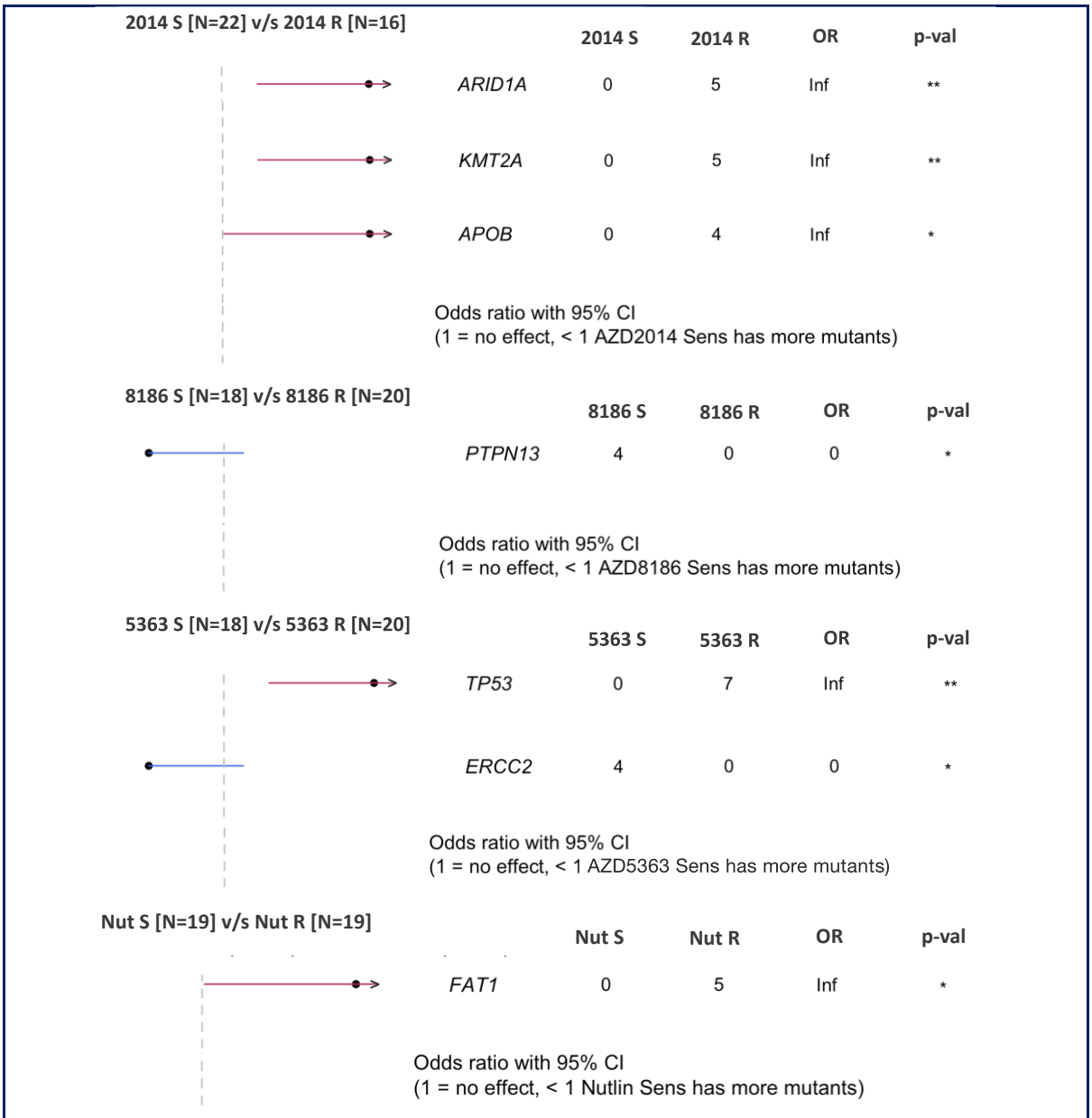

*Figure 38: Forest plots showing significant differentially mutated genes between drug resistant and drug sensitive groups for novel therapies. 2014 S – AZD2014 sensitive phenotype; 2014 R – AZD2014 resistant phenotype; 8186 S – AZD8186 sensitive phenotype; 8186 R – AZD8186 resistant phenotype; 5363 S – AZD5363 sensitive phenotype; 5363 R – AZD5363 resistant phenotype; Nut S – nutlin sensitive phenotype; Nut R – nutlin resistant phenotype; OR – odds ratio; p-val – p value; * = p<0.05; ** = p<0.01.*

6.2.8 PROLIFERATIVE PHENOTYPE

As described in section 5.2.12, 14 (14/39, 35.9%) tumour displayed proliferative phenotypic responses to several novel targeted therapies. Proliferative tumours did not have significantly more mutations per tumour (Mann-Whitney U, p=0.88) and they did not harbour significantly higher proportions of receptor tyrosine kinase (RTK) mutations than non-proliferative tumours (7/14 (50%) versus 12/24 (50%), Chi-squared p>0.99). Similarly, there was no difference in APOBEC enrichment between the groups (4/14 (28.6%) versus 5/24 (20.8%), Fisher's exact p=0.70). Proliferative tumours however did have differential COSMIC signature enrichment, with higher cosine similarity scores for SBS40 (cosine-similarity 0.722) and SBS39 (cosine-similarity 0.659), which have unknown aetiology; whereas the non-proliferative group mirrored the whole cohort with COSMIC signatures SBS3 (cosine-similarity 0.684) and SBS5 (cosine-similarity 0.646).

6.2.9 ACTIONABLE NOVEL MUTATIONS WITH HIGH PREVALENCE IN THIS COHORT

6.2.9.1 FGFR3 MUTATIONS

As described previously, there were 10 (26.3%) *FGFR3* mutant tumours, which were typically lower grade, Ta tumours. Of *FGFR3* mutated tumours, seven (7/10, 70.0%) resided in the sensitive EVP group with a median (IQR) of 9 (4-11) drug hits per tumour. Common alternate SOC drug hits identified for this cohort using the *ex-vivo* platform, which may be used for intravesical instillation included: Docetaxel (7/10, 70%), Paclitaxel (7/10, 70%), Etoposide (7/10, 70%), MMC (6/10, 60.0%), and Doxorubicin (6/10, 60.0%). These tumours also responded favourably to nutlin-3a (8/10, 80.0%), as all were wild-type for *TP53*, and to AZD2014 (7/10, 70.0%) (mTOR inhibitor). Although Erdafitinib was deemed an ineffective compound in the screen-wide analysis, drug response data were analysed for this specific *FGFR3* mutant population.

Only 30.0% (3/10) of patients with *FGFR3* mutations responded to Erdafitinib; this is not discordant to clinical trial data using erdafitinib in patients with FGFR2/3 mutated urothelial cancer (40%) (104) or other FGFR1-4 mutated solid cancer types (30%) (317). Figure *39* shows the locations of *FGFR3* mutations in the ten mutated tumours, where six (60%) had S249C (TCC > TGC) mutations, which is the most common *FGFR3* mutation seen in BC patients and is a known oncogenic driver (318–322). It affects the extracellular domain of the

receptor causing ligand-independent dimerization and downstream transduction (323). The remaining *FGFR3* mutations in this cohort were Y373C (n=2), R248C (n=1), and one G370C (n=1) all of which are less common, but have been described in BC series (322,324,325). R248C has a similar mechanism to S249C causing extracellular domain dimerization, whereas G370C (326) and Y373C (327) mutations leave cysteine residues at the transmembrane domain. None of these mutations affect the kinase domains of the FGFR3 receptor, which has been used as an exclusion criteria in clinical trials (317), and all of the observed point mutations were included in the BLC2001 trial (104).

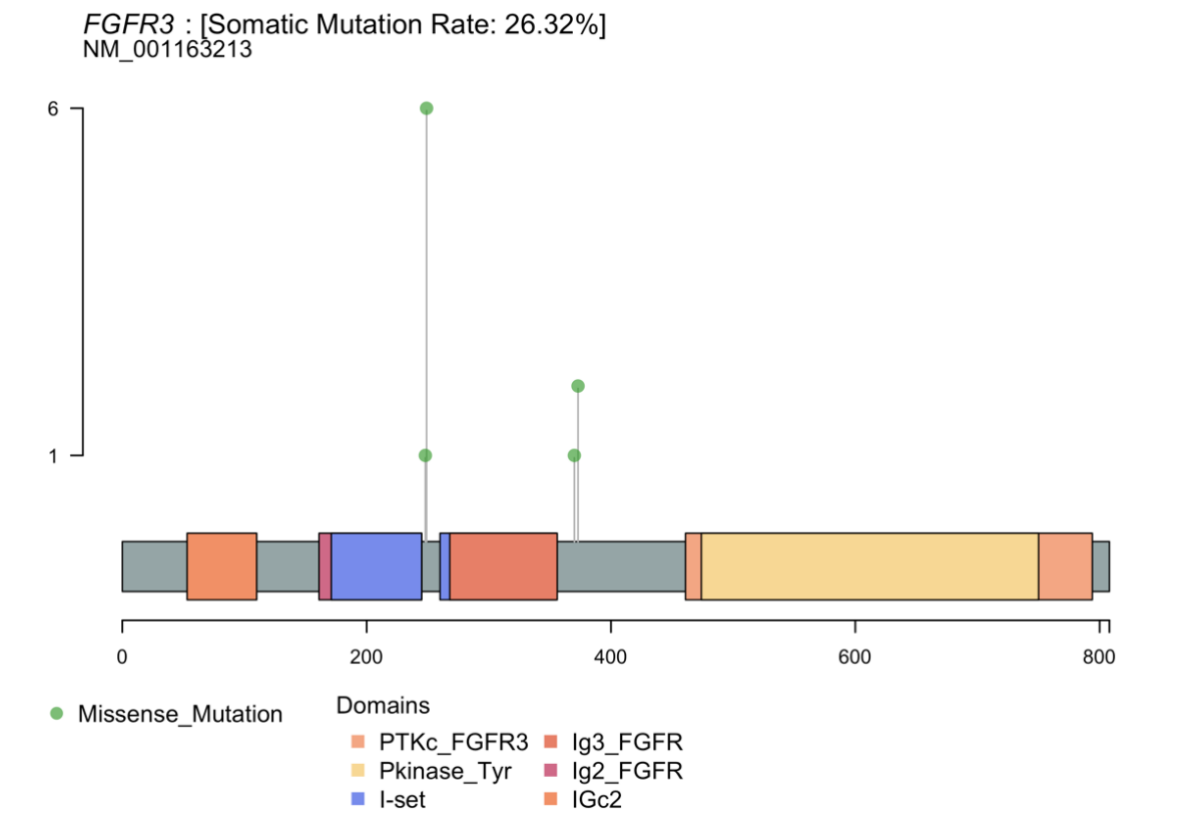

Figure 39: Lollipop plot showing the locations of different FGFR3 point mutations. Green dots highlight missense mutations; there were no other types of mutations identified. The different FGFR3 receptor domains are highlighted in the figure key.

All the patients who responded to Erdafitinib had S249C mutations, and as described above, a response rate of 30% is consistent with what has been previously observed in urothelial cancer (104). Lack of response could result from mutations occurring at gatekeeper residues that prevent receptor-drug binding; or, more likely in this case, 'bypass' signalling through alternative mutated RTK pathways that reactivate downstream cascades (328). However, no correlation with alternate pathway mutations were identified in this study.

6.2.9.2 TP53 MUTATIONS

In this cohort, 7 (18.4%) patients harboured tumour protein 53 (*TP53)* mutations and were found more frequently in high grade and higher stage tumours, where six (85.7%) expressed resistant EVP. Figure 40 summarises the location of *TP53* mutations. Two of these were nonsense mutations, the remainder were missense. One patient had both a missense (p.E180K) and nonsense mutation (p.R306*), the latter of which was the only mutation occurring outside of the DNA binding domain. *TP53*^{R306*} causes truncation of the tetramer domain leading to loss of functionality (329), whereas the E180K variant is only thought to cause partial loss of function (330). The R306* nonsense mutation is rarely reported in BC, but more commonly in colorectal adenocarcinoma and ductal breast cancer (321).

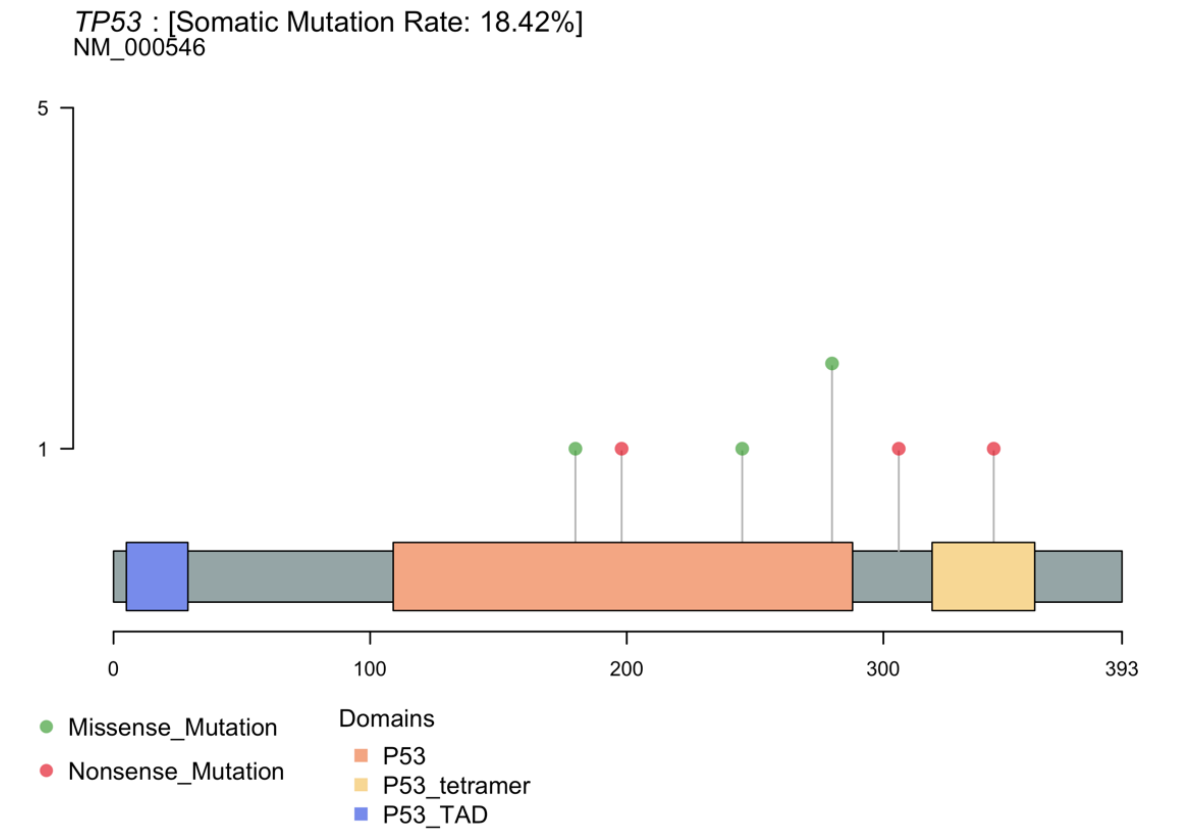

Figure 40: Lollipop plot showing the locations of different TP53 point mutations. Green dots highlight missense mutations and red dots highlight nonsense mutations. The different TP53 receptor domains are highlighted in the figure key.

The *TP53* tumours had a median (IQR) number of 5 (2-5) alternative drug hits. Most of these were to Gemcitabine (5/7, 71.4%), Etoposide (5/7, 71.4%), and the PI3K inhibitor AZD8186 (5/7, 71.4%). As anticipated, only one (14.2%) of the *TP53* mutant tumours responded to nutilin-3a, which acts on *TP53* wild-type tumours; this patient actually had a pre-treated

metastatic breast cancer deposit that was invading the detrusor muscle of the bladder, with a rare *TP53* p.X187_splice mutation.

6.3 DISCUSSION

The combination of improved access to NGS and enhanced *in silico* analytical techniques has hugely advanced our understanding of the genetic underpinnings of cancer development, survival, and progression. Enhanced biological knowledge fosters a climate for the improvement of treatment-response biomarkers and development of mutation-specific drug targets to advance patient care. For example, NGS analysis of pan-cancer tumour samples has shown that 62-94% have actionable mutations with dedicated drug targets (208–210). In appropriately selected patients, molecularly guided therapy may improve outcomes such as progression-free and overall survival (209,210,331,332); however, there are still many barriers to delivering these targeted agents to patients in the clinic (208,333), where actual response rates remain low (6-21%) (209,332). BC patients, however, represent very few participants in the aforementioned studies (333), which may reflect challenges in patient recruitment, tissue sampling, and its high tumour mutational burden (334,335). Consistent with that, treatment paradigms for patients with BC have not changed in 20-30 years, aside from recent advances in *FGFR3* targeted therapy that have not yet been introduced to clinical care.

In this chapter, WES data from 38 malignant bladder tumours have been examined against clinicopathological parameters, clinical outcomes, and *ex-vivo* phenotypic drug screening results, revealing biological insight into sensitivity and resistance patterns. Mutated genes, pathways, and COSMIC signatures known to be implicated in BC were enriched in these tumours, including *FGFR3* and *TP53* mutations, enrichment of RTK-RAS pathway genes, and frequent SBS5 COSMIC signature mutations. As expected, genotypes differed by patient and tumour characteristics. It was also observed that sensitive and resistant *ex-vivo* phenotypes (EVPs) had differential mutational profiles. For example, resistant EVP tumours had significantly higher numbers of mutations per tumour, and were enriched for *ARID1A*, *KMT2A*, and cell cycle pathway mutations. In addition, when exploring specific drug-resistant profiles, *ARID1A* was again enriched in several drug-resistant cohorts.

Across the cohort, there was a median of 8.5 mutations per tumour, spanning 167 (167/329, 50.8%) of the targeted panel. The most common mutations were in the Fibroblast Growth Factor Receptor 3 (*FGFR3*) gene. The most frequent mutations of *FGFR3* in BC are S249C, R248C, G372C, S373C, and K652E (319,320). FGFR mutations are commonplace in NMIBC (320), and in this cohort, 10 (26.3%) patients had *FGFR3* mutations, which were enriched in lower grade, Ta tumours. These features suggest alignment with molecular UROMOL subtypes class 1 or 3 (31). Concordant with this, *FGFR3* mutated tumours seemed responsive to SOC intravesical chemotherapies, with over 60.0% responding to Docetaxel, Paclitaxel,

Etoposide, MMC and Doxorubicin. Contradictory to the UROMOL study, *FGFR3* mutations were significantly associated with poorer RFS, where six (6/10, 60.0%) developed recurrence, five (5/10, 50.0%) of whom experienced multiple recurrences. This likely reflects confounding factors, as 50.0% (5/10) of these patients received no adjuvant therapy, and 30.0% (3/10) were classified as resistant EVP.

Although Erdafitinib was deemed an ineffective compound in the screen-wide analysis, when correlated with *FGFR3* genomic data, 30.0% (3/10) patients were deemed to have responded; this data is consistent with response rates in FGFR2/3 positive urothelial cancers (104) and across cancer types (317) when evaluated in clinical trials. All patients who responded to erdafitinib in this study had S249C mutations, potentially highlighting this as a candidate point mutation biomarker for erdafitinib therapy. Lack of response reflects the complex biology of solid cancers, where far-reaching mutational networks interplay to overcome the inhibition of one inhibited receptor; for example, cancers may initiate 'bypass' signalling through alternative mutated RTK networks, when one pathway is inhibited, to reactivate downstream cascades (328). In this study, concomitant RTK mutations were not identified due to the low number of patients with *FGFR3* mutations, but this would certainly be pertinent to explore, particularly in non-responders to erdafitinib in clinical trials.

The *TP53* gene is a TSG encoding the p53 transcription factor responsible for regulation of cell cycle activity, apoptosis, senescence, DNA repair, and metabolism (336). *TP53* is the most commonly mutated gene in human cancer, typically as missense mutations at the DNA binding domain, which may result in loss of function or gain in oncogenic activity (336,337). In this cohort, *TP53* mutations were identified in opposing patient and tumour populations to those with *FGFR3* mutations, which is commonplace in BC (338). For example, seven (7/38, 18.4%) patients harboured *TP53* mutations, which were observed unanimously in G3 tumours ($p=0.037$), and 85.7% (6/7) in ≥T1 stage ($p=0.090$), as would be expected in BC patients (31,35). Interestingly, one patient had both missense (p.E180K) and nonsense (p.R306*) mutations, the latter of which was the only mutation occurring outside of the DNA binding domain; this patient's tumour was a heavily squamous-differentiated HR NMIBC, which showed extremely aggressive behaviour and metastasised within 13 months. Alternative sensitivities in *TP53*-mutated tumours included Gemcitabine, Etoposide, and PI3K inhibition (AZD8186).

Other common mutations in this cohort (*LRP1B, PCLO*, and *PLXNB2*) are less well reported in BC (34–36,339) and likely reflect the inclusion of pan-cancer consensus genes in the targeted panel. However, these genes may provide information that could assist in patient selection for treatment. For example, *LRP1B* (encoding the Low-density lipoprotein (LDL)

receptor-related protein 1B) is a TSG that was mutated in 21.1% (8/38) of this cohort. *LRP1B* is frequently mutated in lung-SCC (296) and in a small BC cohort has been associated with higher-grade disease (340); findings in this study were consistent with that, where 87.5% (7/8) of *LRP1B* mutated tumours were high-grade. Pan-cancer data has highlighted that *LRP1B* mutated tumours may exert enhanced immunotherapy responses (341), which may suggest that these patients would be susceptible to intravesical BCG or immune checkpoint inhibitor therapy. Similarly, *PCLO* (encoding the piccolo presynaptic cytomatrix protein (342)) is frequently mutated in oesophageal squamous cell carcinoma (SCC) and malignant melanoma (342,343), but only occurs in 8-12% of BCs that are typically lower-risk (344). Conversely, in this study, *PCLO* mutations occurred unanimously in high grade tumours. *PCLO* mutated tumours are thought to pathogenically activate PI3K/AKT pathways (345), and interestingly, these tumours were frequently responsive to the AKT inhibitor AZD5363.

Understanding the interplay between cancer signalling pathways permits a better understanding of tumour crosstalk and the potential to overcome drug resistance by actioning several parallel signalling pathways. For example, tumours frequently host tandem RTK-RAS and Hippo pathways mutations, or TP53 and cell-cycle mutations, which can lead to synergistic activation of downstream cascades (308). The RTK-RAS pathways is the most frequently mutated across all cancers, but in BC, RTK-RAS pathway mutations are superseded by cell-cycle related genes (64% versus 81%, respectively) (308). The most frequently altered pathways in this study were RTK-RAS, NOTCH, TP53, and cell-cycle related pathways – the most frequently targeted by standard of care and novel investigational therapies (308). The proportion of RTK-RAS pathway mutations were similar to that described in the TCGA pan-cancer oncogenic pathways study at 57.9%, but TP53 (23.7%) and cell cycle (18.4%) related mutations were much lower (308), likely owing to differences in gene filtering, analytical methods, and sample size.

Within the RTK-RAS pathway, high proportions of *FGFR3* mutations (10/38, 26.3%) and *ERBB2/3* mutations (7/38, 18.4%) provide an exciting therapeutic opportunity. *ERBB2* mutations are more common in MIBCs (34) and represent an opportunity for molecularly guided therapy with HER2 targeting agents, such as, Trastuzumab, which is used in ERBB2-amplified breast cancer (346). Six (6/7, 85.7%) of the *ERBB* mutated tumours were HG and three (3/7, 42.9%) muscle-invasive – including one HER2-expressing, trastuzumab-treated, breast cancer that subsequently metastasised to the bladder. Another interesting combination of mutations was in a tumour harbouring *BRAF* and *NRAS* mutations, which are not frequently seen in BC. This tumour was seen to respond to the MEK inhibitor (AZD6244) (full Bladder Batch 2 data not shown, rZ_{auc} -0.81 corresponding to a positive drug hit), which is a known treatment for *BRAF*-mutant melanoma (347). These examples provide support that WES of

BCs can identify actionable mutations which can be cross-examined with phenotypic drug screening to identify potential candidates for novel therapies.

As described in Chapter 5, CTG analysis of *ex-vivo* drug screening revealed resistant and sensitive EVPs. The resistant EVP represents a challenging cohort of tumours to manage, with high levels of resistance across the screened candidate compounds, and thus, fewer neoadjuvant and adjuvant therapies to offer. To better understand the mechanisms of resistance, the genotypes between resistant and sensitive EVPs were compared. Resistant tumours had a significantly higher number of mutations per tumour ($p=0.036$), consistent with the Goldie-Coldman hypothesis that higher rates of mutations per tumour mathematically increase the likelihood of higher proportions of resistant clones (348). Aside from upregulation of cell-cycle related genes in the resistant EVP, two specific genes were significantly enriched – *KMT2A* and *ARID1A*, both of which are epigenetic regulators.

KMT2A (Lysine methyltransferase 2 family A) mutations are common in haematological malignancies and occur in up to 5% of solid cancers (349). In BC, *KMT2A* mutations occur more frequently in advanced BC in 11-30% (34,350). The *ARID1A* (AT-rich interaction domain 1A) gene encodes for the protein that creates the DNA-binding subunit of the SWItch/Sucrose Non-Fermentable (SWI/SNF) complex, which are epigenetic regulators functioning in chromatin remodelling (351), and is thought to act as a TSG. *ARID1A* mutations are present in one-fifth of cancers (352) and are present in 25-29% of BCs (353), the majority of which are truncating mutations (304). Mutations in these genes have been linked to chemoresistance across cancer types. For example, *ARID1A* mutations have been linked to chemoresistance in BC (354), biliary tract cancer (355), ovarian cancer (356–358) and squamous cell carcinomas (359); and *KMT2A* mutations have been linked to chemoresistance in BC cells lines (360).

In this study, *ARID1A* mutations were also highlighted as a marker of taxane chemoresistance. Interestingly, data has emerged to suggest that both of these mutations, whilst linked to chemoresistance, may also confer a pattern of enhanced immunotherapy response (361–364). *ARID1A* was also identified as one of the most clinically actionable mutations (Appendix 8, Section 9.8), as these tumours are susceptible to synthetic lethality through treatment with DNA damaging agents and targeted therapies (365). Hence, providing a unique opportunity in using these genomic biomarkers for repurposing of anti-cancer agents or identifying novel effective compounds in phenotypically resistant tumours.

Finally, it was possible to compare individual drug resistant and sensitive genotypes, to explore possible candidate genes that may indicate underlying biological mechanisms of

response. For example, cisplatin sensitive tumours were enriched for *MGA* mutations. *MGA* is a tumour suppressor gene located in the MYC pathway (308). MGA loss-of-function mutations are common in multiple cancer types, leading to uncontrolled activation of MYC signalling, increased growth and cellular proliferation (366). Interestingly, in this cohort, *MGA* mutations were more common in cisplatin-sensitive tumours, which may be more reflective of tumour stage (all were NMIBCs). When exploring the cisplatin-resistant EVP in more detail, tumours seemed to branch into two further phenotypes: those that were multi-drug resistant, and those that displayed sensitivity to other compounds in the screen. More frequently mutated genes in the multi-drug resistant group included *TP53, PCLO, PLXNB2, KMT2A*, and *ARID1A*. *TP53* mutant tumours have been well described as chemo-resistant (32), which is highlighted in the multi-drug resistant cohort. *PCLO*, *PLXNB2*, *KMT2A* and *ARID1A* are less well documented in the literature. However, as described above, *KMT2A* and *ARID1A* mutant tumours may be susceptible to immunotherapies, repurposed DNA damaging, and novel agents. Clinical implications here are mainly focussed on advanced BCs – where the standard of care is platinum-cased neoadjuvant chemotherapy (NAC), adjuvant chemotherapy (AC), or first-line palliative therapy in the metastatic setting. For example, an upcoming clinical trial exploring molecular subtype-directed neoadjuvant chemotherapy in MIBC patients (ISRCTN17378733) could be enhanced with supplementary *ex-vivo* phenotypic drug response data.

As for the cohort of tumours with proliferative responses to therapy (14/39, 35.9%), the whole exome sequencing and analysis strategy used did not provide further insight on potential molecular mechanisms. For example, the tumours did not have significantly higher numbers of mutations, did not have more mutations in RTK pathway genes, and had similar APOBEC enrichment scores to non-proliferative phenotypes. Currently, the differences in COSMIC signature enrichment (SBS40 and SBS39 rather than SBS3 and SBS5) remain of unknown significance. Further work using modified WES analytical techniques may help to further explore this unusual phenotypic group, to better understand the molecular biology of their proliferative responses to novel targeted inhibitors.

CHAPTER 7

DISCUSSION OF RESULTS

7.1 SUMMARY DISCUSSION

Bladder cancer (BC) is a common disease with high associated morbidity and mortality. This is particularly true for patients with advanced BC. Broadly speaking, treatments for BC have changed very little over the last 30 years and currently there are no validated molecular or phenotypic risk stratification tools that are in clinical use. Hence, not only is BC common, but outcomes are not improving. Research is required to personalise patient and treatment selection approaches, to maximise efficacy and minimise undue treatment toxicity (including cost). Research efforts in this field have been largely divided into those using molecular data and those using pre-clinical BC models to advance our current treatment paradigms. With huge advances in our genomic understanding of BC in recent years, molecularly-guided therapy seems a promising approach; however, there are many barriers to delivering these complex treatment pathways in the clinic and the efficacy of molecularly-guided treatment has not been successful in across all cancer types (122). An array of pre-clinical models have been used to explore direct phenotypic drug responses on BC cells or patient tissues, with the aim of replicating *in vivo* tumour characteristics; sadly, translational success of to date has been poor and implementation of predictive pre-clinical models into clinical cancer pathways to direct patient treatment is extremely difficult.

Ex vivo drug screening allows for the testing of anti-cancer compounds directly on freshly retrieved, patient-specific tumour cells or tissues. Adopting this methodology for high-throughput candidate compound selection is primarily based on the concept that if drugs are inactive when placed in direct contact with tumour cells, then they are unlikely to be effective when given to patients (200). *Ex-vivo* high-throughput drug screening using patient derived *ex-vivo* cultures (PDCs) is a relatively novel approach, which has been performed across a number of liquid (haematological)(196–199) and solid tumours (134–138,201–205). In addition, there is growing evidence to suggest that this model can be used to accurately predict patient responses to therapy and even direct patient treatment (135–137,198,199).

Ex-vivo high throughput drug screening in BC seems logistically feasible, with transurethral resection of bladder tumours (TURBT) allowing direct access and there being several windows of opportunity to access tissue, with clearly defined clinical endpoints. This could maximise the impact of such a model. In addition, high-throughput screening can assist in identifying novel compounds, tested for efficacy directly on patient tumour tissue, which may expand the number of treatments available to patients with BC. Hence, the purpose of this thesis was to explore the following hypothesis: *Ex-vivo high throughput drug screening in BC is logistically and methodologically feasible and can be used to explore differential responses to standard*

of care and novel therapies to personalise patient treatment selection. Figure 41 summarises the PhD aims, experimental approach, and relevant thesis chapters.

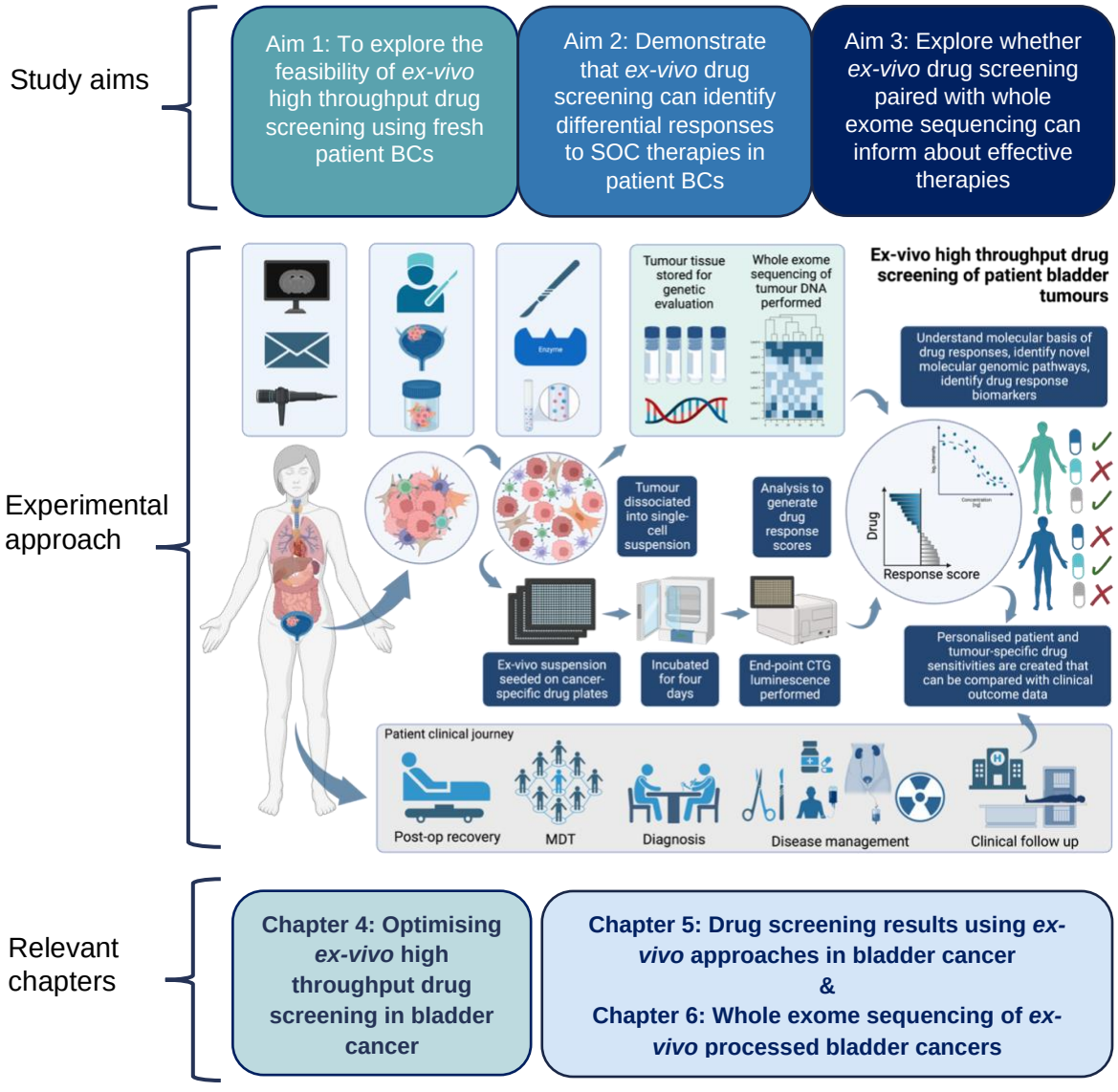

Figure 41: Overview of aims and approaches used in this study to explore ex-vivo high throughput drug screening in patient bladder cancers. BC – bladder cancer; SOC – standard of care; CTG - CellTiter-Glo®; MDT – multi-disciplinary team.

7.2 SUMMARY OF FINDINGS

Although *ex-vivo* high throughput drug screening has been documented in other solid cancers, the use of BC PDCs to screen standard of care and novel compounds has not yet been described. In this study, the combination of *ex-vivo* high throughput drug screening and parallel whole exome sequencing, allowed for individual tumour responses to be explored whilst highlighting potential molecular mechanisms indicative of *ex-vivo* sensitivity and resistance.

The first aim of my PhD was to explore the feasibility of *ex-vivo* high throughput drug screening using BC PDCs, through optimisation of *ex-vivo* tissue processing methodology *de novo*. Patient recruitment and tumour tissue acquisition was excellent, reflecting the high-volume throughput of patients with BC at a specialist uro-oncology surgical centre and patient acceptability to participate. However, differential tumour sample consistencies and characteristics meant that standardising experimental procedures was challenging. Nonetheless, it was possible to deliver patient-specific drug sensitivity profiles, using CellTiter-Glo® (CTG) endpoint analysis, for 69.5% (41/59) of acquired tumours; this is consistent with the literature for propagation of 2D and 3D BCs in culture (133,280) and reflects the challenges with tissue quality at time of acquisition, particularly due to electrocautery damage.

Having established that *ex-vivo* high throughput drug screening in BC was feasible, the next step was to evaluate differential phenotypic responses to treatment expressed by BC PDCs. Tumours and drugs could be clustered based on *ex-vivo* response profiles. In particular, sensitive and resistant *ex-vivo* phenotypic signatures (EVPs) showed correlation with expected clinical phenotypes. For example, resistant EVP tumours were more likely to be higher grade (grade 3, $p=0.0002$), higher stage (≥ T1, $p=0.025$), and have associated carcinoma-in-situ (CIS) ($p=0.041$) – all of which would indicate more aggressive and resistant tumour behaviour. However, due to the short follow-up duration (median 18 months), low number of patients treated with neoadjuvant or adjuvant therapy, and low numbers of recurrence and progression events, no differences were observed in clinical outcomes between sensitive and resistant EVPs. Molecularly, the two groups also had differing genotypes. The resistant EVP tumours had significantly more mutations per tumour, and were enriched for mutations in *ARID1A*, *KMT2A*, and cell cycle regulatory genes; all of which biologically support the observation of resistant phenotypic behaviour (354–360).

It was also possible to explore individual drug-response cohorts in more detail, such as those that were cisplatin-resistant. Understanding cisplatin-resistance and developing novel therapeutic strategies for patients with cisplatin-resistant disease is of critical importance in a number of platinum-treated cancer types, one of which is BC (367). As anticipated, most muscle invaive BCs (MIBCs) resided in the cisplatin-resistant phenotypic group. Interestingly, when exploring the cisplatin-resistant group's alternative drug response profiles, there was dichotomisation of the group into those with alternative sensitivities and those that were multi-drug resistant. Although comparative group numbers were small, it again seemed that cisplatin-resistant and multi-drug resistant tumours had differential genotypes to those with alternative sensitivities, harbouring higher proportions of *TP53, PCLO, PLXNB2, KMT2A*, and *ARID1A* mutations. Most patients in the group with alternative sensitivities were MIBCs, which could have potential implications on choosing neoadjuvant therapy in the window of opportunity between TURBT and radical cystectomy (RC) (Figure 42). Alternatively, in tumours that were phenotypically cisplatin-resistant and were also multi-drug resistant, this could be an indication that the patient may be best managed with immediate radical treatment (surgery or radiotherapy) (Figure 42). With future clinical trials in MIBC looking to deliver neoadjuvant treatment based on molecular subtype (ISRCTN17378733), supplementary *ex-vivo* screening of BC tissue could provide complementary phenotypic drug response data to enhance patient selection and treatment stratification.

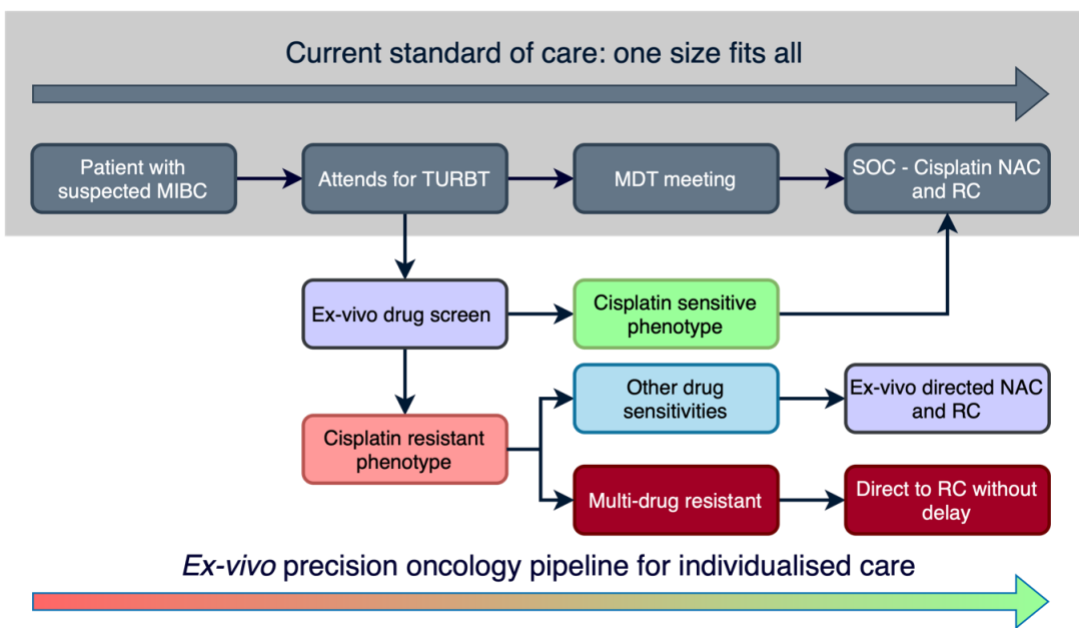

Figure 42: Hypothetical patient pipeline with integration of ex-vivo high-throughput drug screening integrated to deliver personalised care for muscle invasive bladder cancer (MIBC) patients. TURBT – transurethral resection of bladder tumour; MDT – multidisciplinary meeting; SOC – standard of care; Cis – cisplatin; NAC – neoadjuvant chemotherapy; RC – radical cystectomy.

One particular subset of patients exhibited proliferative responses to a range of novel targeted inhibitors (14/39, 35.9%); this group had a significantly higher proportion of recurrence or progression events (9/14, 64.3%) than the non-proliferative cohort (7/24, 29.2%) (Chi-squared p=0.034). The phenomenon has been described in other solid cancers (286–293), but also in patient acute myeloid leukaemia samples in another *ex-vivo* screening study (284). Although mechanisms for such proliferative responses have been hypothesised (285), the whole exome sequencing (WES) analysis strategy used in this study did not provide further biological insight. Further work using modified WES analytical techniques may help to explore this unusual phenotypic group, to better understand the molecular biology of their proliferative responses to novel targeted inhibitors. Clinically, this information highlights the additional benefits of direct phenotypic screening directly on patient tumour tissues, whereby proliferative responses could be used as a negative biomarker to inform on treatments that should be avoided.

7.3 STUDY LIMITATIONS

As described in Chapter 4, one of the key challenges when working with primary BC tissue, in an unselected cohort, was the variability in tissue characteristics. The rationale, in this study, for recruiting patients in an unrefined fashion was primarily to assess methodological feasibility of *ex-vivo* high throughput drug screening in BC (Aim 1). In addition, the research and clinical pressures incurred during the COVID-19 pandemic meant that all willing participants were recruited to the study to maximise research outputs through a very difficult period. Moving forward with the study, as documented in a recently successful Weston Park Cancer Charity grant, the aim is to identify a more refined cohort of patients with suspected MIBC who are fit to receive radical treatment. Firstly, this will likely address some of the tissue variance issues; and secondly, will allow for the recruitment of a group of patients in which treatment and progression events are more likely to occur during follow-up, to better facilitate correlation analyses.

In this study, the low numbers of treatment and recurrence or progression events make it difficult to ascertain whether the observed *ex-vivo* phenotypic drug responses, or indeed phenotypic signatures, correlate with patient outcomes. In particular, some of the observed ex-vivo phenotypes conflicted with the in-vivo patient responses. Technical factors, as discussed in Chapter 5, could have contributed to these discrepancies, but it is also important to consider sampling bias. Sampling bias is particularly important when correlating results with more advanced disease states, as the population clones sampled from the primary tumour,

may not be genetically and/or phenotypically matched to those at the invasive or micrometastatic front of the disease (368). At this stage, the results must be interpreted with caution, given the low event rate and its ability to be used as a predictive treatment selection tool in BC.

In addition, as described in Chapter 5, it will be essential to explore tumour responses to combination treatments, particularly gemcitabine-cisplatin (GC) combination therapy, which is standard of care for patients with MIBC. Although modelling this is more technically and analytically complex, and will require more viable tumour material to complete, it will provide drug combination response sensitivity and drug synergy anlayses that are more reflective of the in vivo treatment processes patients experience in the clinic. Hopefully, this will provide more insight on the ex-vivo drug screening platform's ability to predict in vivo responses.

Currently, the phenotypic data presented in this thesis is limited to 15 common drugs across the two drug plate batches for the 39 malignant BCs acquired. The nature of the PhD required primary tumour tissue to be used to complete parallel optimisation and validation experiments alongside the drug screen to evaluate feasibility. After preliminary review of drug responses prior to production of Bladder Batch 2 drug plates, the EVIDENT consensus was to make several changes, removing potentially ineffective compounds and adding more novel discovery compounds. In hindsight, this reduced the ability to compare drug response metrics between the two drug batches, meaning that only common compounds could be evaluated in totality (n=15). However, given the preliminary data, there is certainly scope for scalability to increase the number of compounds screened. One potential option moving forward would be to have a primary "validation plate" containing longer dose ranges of standard-of-care compounds for correlation with patient treatment response data; and a secondary "discovery plate" with a higher number of compounds (reduced concentration ranges and dose replicates) that can be used to explore novel effective compounds, should there be sufficient live tumour cells to do so.

As will be described in the Chapter 8: Future Work, using CTG is beneficial in terms of ease, time-efficiency, and relatively low cost. However, as an endpoint assay it is not without limitation. The CTG assay uses adenosine triphosphate as crude proxy for number of viable cells, providing a quantitative comparator value between treatment and control wells. However, there are two key limiting assumptions that are made. Firstly, that there is a linear relationship between number of live cells and CTG luminescence values and that this is consistent across different tissue types; secondly, that different intra-tumoral cell types are metabolically equivalent. Hence, caution must be taken when interpreting CTG results when using complex tumour suspensions that contain differential cell types. In addition, CTG

analysis cannot differentiate between intra-tumoural cell types found within ex-vivo tumour suspensions, which may have contributed to some of the variability in responses observed. Further work will include exploring different endpoint assays that provide more granular, single-cell metrics of drug response, such as immunofluorescence microscopy.

With regards to whole exome sequencing, the main challenge was that matched normal tissue was not acquired for patients, making it more difficult and less precise to filter out germline variants. After initial 1,000 genome project and GENOMAD filters were applied, the data outputs still suggested that there was a lot of noise; hence, further filtering strategies were applied to focus more closely on significantly mutated genes in cancer. Hence, this study reflects a more targeted sequencing approach, which limits the discovery potential of WES, as unknown genes, or those of uncertain significance may have been lost through the filtering process. In the next phase of the EVIDENT study, paired whole blood samples will be retrieved to accompany individual tumours, so that patient-specific germline variants can be removed in a more robust fashion.

Although the addition of exome sequencing in this study did provide key insight into specific drug responses, it should be highlighted that exome analysis alone does not tell the whole story. The addition of transcriptomic analysis would have provided invaluable data regarding protein expression, and may have allowed for mapping of this cohort to contemporary molecular classifications. One reason for choosing WES, was the potential to map the coding regions of the genome at relatively low cost, compared to whole-transcriptome sequencing.. At the time of extraction, there were heightened courier regulations after the UK left the European Union, which had the potential to delay transportation to Macgrogen Europe. Hence, given that RNA is less stable than DNA, DNA extraction for WES was chosen and the option of least risk. Unfortunately, there was not the time or the finances to complete both.

The final limitation I would like to discuss is the lack of urinary microbiome (urobiome) in triaging treatment response used in this model. Loss of the healthy urinary bacteria has been linked to conditions that cause chronic inflammation of the urothelium, such as intersitial cystitis, bladder overactivity, and urge incontinence (369). Thus, urinary dysbiosis may contribute to the carcinogensis of some BCs and researchers are currently exploring the urinary microbiome as a potential way to screen patients who may be at a higher risk of BC development (370). Although not completely understood, the urine microbiome is though to contribute to immunomodulatory responses, which is particularly relevant in the context of intravesical immunotherapy response in BC patients, such as to intravesical BCG (369). In this *ex-vivo* model, surgically exised tumour material is removed from its native urobiome and

cultured in growth media. Standard conditions include the addition of penicillin-streptomycin antibiotic therapy in growth media to minimise bacterial overgrowth during incubation. The implications of this on *ex-vivo* tumour treatment response are unknown.

7.4 LEARNING POINTS

Considering the above limitations and the data presented, many lessons have been learned throughout the course of this study, some of which could help modify the pipeline moving forward.

For example, as described above, this was a feasibility and methodological development study, hence, the BC patient cohort was unrefined. Not only did this mean that there was a low event rate (due to the natural history of tumour types being collected) that limited outcome analysis, but it also meant that the tumours acquired were heterogenous. In future, and as has been described in the Weston Park Cancer Charity grant protocol, a more refined cohort of patients will be approached to participate in future. Recruitment will focus on patients with suspected MIBC, who are fit enough to undergo neoadjuvant chemotherapy (NAC) and RC. This particular group of patients have more refined endpoints (NAC response rate, residual tumour at RC, and subsequent clinical progression, metastases, or death) and should have tumours that are less heterogenous in tissue characteristics.

Secondly, one particular limiting aspect of tumour tissue acquisition was the confounder of diathermy artifact on the tumour specimens. All different modalities of tumour tissue acquisition (radiological biopsy, surgical biopsy, surgical resection specimen) have their benefits and drawbacks. However, in this study, it was felt that excessive electrocautery use intra-operatively may have contributed to downstream poor viability. Although it is not possible to change the clinical pathway or the operative procedure for patients, having a good working relationship with the surgical team and encouraging minimal use of diathermy for research sample acquisition will be important moving forward. Alternatively, biopsy of the tumour prior to electrocautery resection could potentially avoid this issue, but will likely lead to lower tissue volume.

In terms of genomic data, for the next group of participants it will be essential to collect matched normal samples (blood or tissue) for comparison when performing sequencing. This will allow for more refined removal of germline variants, which created a challenge when analysing WES data in this study. By confidently removing matched germline variants, filtering using population databases and targeted genomic panels will not likely be necessary; this will open the door for more in-depth genomic data retrieval to identify novel exploratory biomarkers of phenotypic response.

Finally, as described in the limitations section, because of the optimisation process, as well as limited time, resources, and technical support, the number of drugs in the current screen was limited. The ambition moving forward is to expand the number of drugs screened per tumour sample, using validation and exploratory libraries. Another critical step will be to explore whether immunotherapy drug screening can be explored using the *ex-vivo* platform. Immunotherapy indications are rapidly expanding across the cancer spectrum – including BC. Hypothetically, if immune infiltrates were seeded (or otherwise inoculated) onto the drug plates within the complex PDC suspensions, and were combined with an immunotherapy compound, then responses may be observed. More sophisticated endpoint assays may be required in this setting, to first confirm the presence of immune complement within the cell suspension and secondly explore how they interact with the tumour cells. CTG, unfortunately, cannot provide that granularity. However, alternative endpoint assays, as will be discussed in the Future Work Chapter (Section 8.1), may provide the means for immunotherapies to be explored.

CHAPTER 8

FUTURE WORK

8.1 EXPLORING HIGH CONTENT IMMUNOFLUORESCENCE MICROSCOPY AS AN ENDPOINT MODALITY FOR *EX-VIVO* DRUG SCREEING

8.1.1 INTRODUCTION

The preceding chapters have highlighted key successes when using a metabolic assay to acquire personalised drug sensitivity profiles using *ex-vivo* processed patient bladder cancers (BCs). However, there are a range of alternative endpoint assays that can be used to deliver more granular drug sensitivity data. One alternative, that has shown success in the field of *ex-vivo* high throughput screening, is high content immunofluorescence microscopy (IFM). IFM allows for automated high-quality microscopic visualisation of individual cells, and their cellular components, using targeted antibodies (with an associated fluorophore emission). Unlike metabolic cytotoxicity assays, IFM provides more granular information regarding single cell and spatial metrics, meaning that cell-on-cell interactions can be explored. IFM protocols can be adapted per cancer type to explore distinctive cellular lineages within complex tumour *ex-vivo* cultures, through the staining of differential cell proteins (136,371). In addition, the ability to label non-cancerous cells within a complex tumour suspension provides an internal toxicity control for drug-response data (137,371).

The most robust evidence to support the use of *ex-vivo* high throughput IFM drug screening to direct patient therapy is in haematological cancers. Although phase 3 clinical trial data are lacking, early phase clinical trials have shown potential in providing cancer-specific cytotoxicity profiles that can be used to individualise patient treatment in the clinic. For example, Snijder et al. (198) conducted a single-arm, open-label, pilot study, using “pharmacoscopy” (IFM drug screening) of mononuclear cells collected from patients (n=57) with late stage (no further treatments available) haematological cancers. Through labelling of *ex-vivo* blast cells, on-target and off-target toxicity profiles were generates for 139 compounds. Of the initial cohort, 17 (29.8%) were eligible for prospective treatment using IFM-directed therapy, where 88% (15/17) achieved complete or partial response, compared to only 38% (5/13) of patients in a parallel observational cohort (clinician-led therapy). An expanded cohort (n=56) of patients were recruited for IFM-based therapy in this setting, demonstrating a 1.3-fold increase in

progression-free survival (compared to previous treatment) in 53.6% of patients (30/56) (199). These trials highlight how *ex-vivo* high-throughput IFM drug screening may be used to deliver personalised therapy with enhanced clinical responses.

Although it is challenging to implement such methodology in solid cancers, for the reasons discussed in Chapter 4, IFM-based *ex-vivo* high throughput screening has been described in three rare cancers (epithelial–myoepithelial carcinoma, recurrent thymoma, and Kruckenberg tumours) (136–138). Rare cancers account for 24% of all cancers in Europe (372) and represent a group of patients with unique therapeutic challenges due to a paucity of biological knowledge, evidence-based treatments, and access to interventional clinical trials. Hence, patients often have few treatment options available to them and have particularly poor clinical outcomes (372). *Ex-vivo* high throughput drug screening in such cases may provide bespoke therapeutic treatment options in patients with no standard of care treatments available.

In these rare cancer case reports, IFM-based screening through differential antibody labelling of tumour-derived epithelial, mesenchymal, or myoepithelial cells, delivered cell-type-specific cytotoxicity profiles to over 130 compounds per cancer. Patients with adequate performance status and no therapeutic options available, who were ineligible for treatment on clinical trials, were treated with *ex-vivo* directed therapy (off-label). These patients had advanced, heavily pre-treated, chemo-refractory disease and had received multiple previous lines of therapy. For example, a patient with an advanced taxane and platinum-refractory Krukenberg tumour (138) was treated with sunitinib due to its selective cytotoxicity towards cytokeratin 19 expressing tumour cells and immunomodulatory effect on both tumour and ascitic cells *ex-vivo*. Similarly, a patient with a recurrent chemotherapy-resistant thymoma showed *ex-vivo* sensitivity to epidermal growth factor receptor (EGFR) therapy that selectively targeted epithelial rather than stromal cells; the patient's tumour had immunohistochemistry confirmed strong membranous EGFR expression and was treated with cetuximab therapy (137). In a mixed-lineage rare salivary gland carcinoma (136), there were differential *ex-vivo* phenotypic responses to treatment based on the two intra-tumoral cell lineages. Epithelial and myoepithelial labelled cells had diverging responses to mTOR and MEK inhibitors. Although the patient was not treated with combination therapy, this phenotypic data highlights the potential to explore novel drug class combinations, or sequential treatment. All of the above patients had showed clinical response to *ex-vivo* directed therapy, with duration of responses lasting between 5-13 months.

Of all the *ex-vivo* approaches discussed in Section 1.3, IFM-*ex-vivo* phenotypic drug screening is the only model to have directed patient treatment. The potential to deliver more granular single cell and spatial metrics, as well as cell-type specific drug responses is particularly novel.

In this section of future work, I will discuss a provisional assessment of the feasibility of using IFM-based *ex-vivo* endpoint analysis in BC.

8.1.2 DIFFERENCES BETWEEN CTG AND IFM ASSAYS

CellTiter-Glo® (CTG) is a metabolic assay that uses endpoint cell lysis to release cellular adenosine triphosphate; this generates a luciferase reaction to produce oxyluciferin and release luminescence, which can be quantified in relation to the amount of adenosine triphosphate present. The amount of adenosine triphosphate present is thought to be a surrogate for metabolic activity, and thus can be compared between drug and control wells to generate dose response curves. In addition, CTG evaluation may be sensitive even at very low cell counts (as low as 10 cells per well according to manufacturer data) and can be used for non-adherent cell types. Conversely, IFM has the potential to directly visualise and classify different cell types, delivering more granular metrics of viability and drug response. To facilitate this, there are several pre-imaging steps which must be completed, including: cellular fixation, permeabilisation, blocking, and antibody incubation (373), which increase the complexity of the assay when compared to CTG.

Table 15: Differences between metabolic CTG and immunofluorescence endpoint assays describes the differences between the two endpoint analysis methods.

The first step in comparing the two methods was to explore the difference between CTG results and IFM DAPI (4', 6-diamidino-2-phenylindole) counts. DAPI is a nuclear counterstain that emits blue fluorescence upon binding to the AT region of DNA (374) and can be used in living or fixed cell states (375). DAPI counterstaining does not require permeabilisation or blocking steps, making it the simplest form of image-based *ex-vivo* screening, and therefore, the most appropriate first step in evaluating the IFM methodology and comparison to CTG. *For the subsequent experiments that are described in this section, DAPI IFM was used as the endpoint output modality unless otherwise stated.*

Table 15: Differences between metabolic CTG and immunofluorescence endpoint assays		
	CTG metabolic assay	IF analysis
Assay sensitivity	Sensitive from above 10 cells per well	Depends on cell adherence, seeding density, and area of well imaged
Adherent versus non-adherent cells	Both	Typically, only adherent cells (non-adherent may be washed away)
Area of well analysed	Whole well	Depends on tile strategy (often only a proportion of well imaged)
Time required for assay	Luciferase reaction Luminescence read	Pre-imaging fixation and antibody staining, microscope imaging and analysis
Technical requirements	Single protocol, minimal technical training	Several protocols, high-content microscopy and image analysis training
Post-processing requirements	Minimal	Images need to be analysed using advanced AI software
End-point result	Single parameter (ATP) readout	Multiple metrics of growth, survival, and drug response (including TME)
Cell-type specific responses	No	Yes, if antibody staining protocols optimised
Cost	Assay reagent (CTG), luminescence plate reader	Antibodies, microscope, analysis time, data storage

CTG - CellTiter-Glo®; IF – immunofluorescence; ATP – adenosine triphosphate, TME – tumour microenvironment.

8.1.3 PROVISIONAL METHODOLOGY

8.1.3.1 IFM FIXING AND STAINING PROTOCOL

After a four-day incubation period, *ex-vivo* processed tumours underwent fixation and staining. This consists of four components: fixation, permeabilisation, blocking, and antibody incubation (373). Fixation prevents degradation of cells and preserves morphology, whilst maintaining the ability to combine with surface receptors or secreted antibodies. Paraformaldehyde (PFA) does this by forming intra and intermolecular methylene cross-links. Permeabilisation with detergents, such as, Triton-X or Tween-20 allows for fluorophore-labelled antibodies to combine to intra-cellular targets. Blocking agents, such as bovine serum albumin (BSA), are then used to prevent non-specific binding of antibodies, which are fluorophore-labelled antibody with pre-defined excitation and emission wavelengths. Briefly, processed patient-derived *ex-vivo* cultures (PDCs) were fixed on the 384-well plates using 4% PFA in phosphate buffered saline (PBS) and 0.6% Triton™ X-100 solution. 45µL of combined PFA and Triton™ X-100 solution was dispensed into each well and incubated at room temperature for 30 minutes. The total volume per well (cell media and PFA/Triton X-100 solution) was aspirated and discarded before performing a PBS wash and storing at 4°C until IFM. For antibody labelling, the PBS from each well was removed and 10µL cancer-specific antibodies were added (at differential concentrations, in PBS and 0.05% Tween® 20 solution with 1% BSA). In this study, Cytokeratin 19 (Santa-Cruz, A53-B/A2 Alexa Fluor® 647, sc-6278 AF647) was used to label epithelial cells and Vimentin (Santa-Cruz, 5G3F10 Alexa Fluor® 546, sc-66002 AF546) was used to label stromal cells.

8.1.3.2 HIGH-CONTENT IFM PROTOCOL

High-content IFM was performed using the ZEISS Celldiscoverer 7 automated microscope. Drug plates were loaded and imaged using 10X magnification, which provided high-quality cellular imaging, whilst maximising well coverage. In brief, each plate was manually calibrated using the Brightfield microscopy setting. The tile strategy was determined, and each antibody matched to their corresponding emission fluorophore. The focus strategy was calibrated using the DAPI channel, performing quality-control checks at corner wells. The automated image process used the reference DAPI definite focus protocol, running in a snake-like pattern from top left to top right (usually B2 towards B23), and then back (usually C23 towards C2).

8.1.3.3 IFM IMAGE-ANALYSIS PROTOCOL

ZEISS ZEN analysis software version 3.0 was used for quantitative analysis of image features, offering the capability of both global thresholding and deep-learning technology. Global thresholding allows the observer to set standardised parameters for systematic detection of nuclei and fluorophore characteristics across each image scene. Intellesis, the deep-learning programme available on ZEN, is initially observer-trained (using an extracted training set for each tumour, where the analysis programme adapts through sequential learning) before being applied to autonomously detect the learned image features. This deep-learning mechanism allows for more in-depth cellular segmentation and more reliable and adaptable image feature capture – particularly for suboptimal image scenes (for example, where there may be debris within the image scene, or suboptimal antibody staining).

For use of Intellesis software, a training set of the first 50-100 consecutive images were extracted. The software was trained through repeated annotation of DAPI stained nuclei and background (Figure 43: A). A range of high- and low-quality scenes were selected for annotation to maximise the network's exposure to features, enhancing the deep-learning algorithm. The tumour-specific algorithm was then applied to the whole drug-plate image set. DAPI selection and segmentation was generated by the Intellesis feature (Figure 43: B), with a minimum confidence threshold for nuclei capture of 60% (Figure 43: C). Cell-type segmentation, inferred by differential fluorophore emission, was analysed using a "zone-of-influence" (ZOI) around the labelled parent DAPI nucleus. Fluorophore dichotomisation was histogram-based where lower and upper values were established through visual inspection. Further conditions for cellular inclusion were refined by alteration of additional feature thresholds, such as: area, circularity, intensity mean values, and roundness. The measurement outputs included counts per well for DAPI and fluorophore annotated cells.

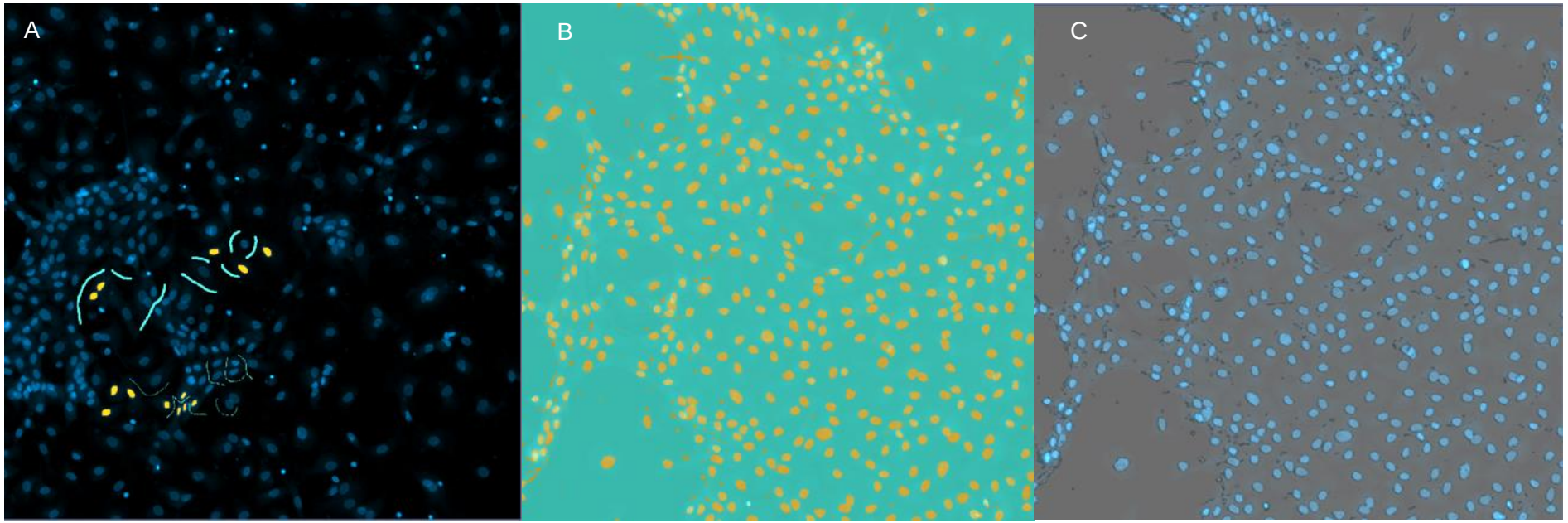

Figure 43: Example image of ZEISS ZEN Intellesis training software used to label and segregate cellular nuclei. A - 10x image of an BC PDC showing DAPI-stained nuclei (blue); the user sequentially trains the programme by labelling nuclei in orange and background in turquoise. B – after training the programme, it then provides an image showing the nuclear segmentation. C – it also provides an estimate of nuclei confidence that can be used as a gating feature.

8.1.4 RESULTS

8.1.4.1 IFM MAGNIFICATION AND TILE STRATEGIES

Using the Zeiss CD7 microscope allowed for high quality images to be taken, but changing the magnification, number of images per well, and the number of channels imaged, all impacted on throughput. Considering these factors, first, a consensus decision had to be made regarding the quality of images required for downstream analysis. The *ex-vivo* consortium agreed that 10x and 20x images provided adequate quality cellular images. Next, the well coverage per magnification was explored. The individual well area on Perkin-Elmer Cell Carrier Ultra (384-well plate) is 10.6mm^2 (3.26mm x 3.26mm) (376). 10x images covered an area of 0.51mm^2 (0.712 x 0.712mm), whereas, 20x images covered only 0.16mm^2 (0.394mm x 0.394mm). Hence, 10x images provided enhanced well coverage, without affording image quality. Next, it was important to decide on the number of image scenes ("tiles") acquired per well. At 10x, 5-tiles, 9-tiles, and 12-tiles covered 24.1%, 43.3%, and 57.7% of the well area, respectively. However, incremental tile increases afforded additional microscopy time, analysis requirements, and data storage cost (Table 16).

Table 16: Benefits and drawbacks of different tile strategies used for DAPI only analysis

Tile approach	5-Tile	9-Tile	12-Tile
Well coverage (%)	24.1	43.3	57.7
Microscopy time	1-1.5h	1.5-2h	2-3h
Images per plate	1,540	2,772	3,696
Analysis time	+	++	+++
Data storage	+	++	+++

DAPI - 4′,6-diamidino-2-phenylindole.

Given the increased time, data storage, and cost required to image using a 12-tile strategy, 5 or 9 tile approaches were explored. To determine the variability of each approach, DAPI counts were analysed in dimethylsulfoxide (DMSO) control wells for three different *ex-vivo* processed PDCs using both 5 and 9 tiles approaches. Table 17 shows that there was a trend towards improved reproducibility (lower coefficient of variance (COV)) with a 9-tile approach. Comparison of DAPI area under dose-response curve (AUC) drug responses between different tile strategies showed excellent correlation. This data suggests that although the 9-

tile strategy did not alter the drug-responses observed, it improved the reproducibility of the assay.

Table 17: Evaluation of differences in co-efficient of variation and drug responses when *ex-vivo* bladder PDCs were images at 5 and 9 tiles per well

Tumour Sample	Tile approach	Mean (SD)	COV (%)	Correlation of AUC values (R^2)
BT 7.0	5	360 (78)	21.66	0.99
	9	725 (127)	17.50	
BT 9.0	5	448 (60)	13.46	>0.99
	9	767 (89)	11.66	
BT 8.9	5	256 (62)	24.24	>0.95
	9	542 (117)	21.49	

PDC – patient-derived ex-vivo culture; SD – standard deviation; COV – coefficient of variance; AUC – area under dose-response curve.

8.1.4.2 SEEDING DENSITY ASSESSMENT

As described in section 4.2.2.9, it was important to explore the optimal seeding density for IFM analysis, to determine the limitations of the assay reproducibility and potential implications on PDC growth parameters. It was anticipated there would be more DMSO variation (COV) when using DAPI IFM compared to CTG due to the more complex post-incubation methodological processing. Figure 44 shows the DAPI counts per DMSO well at different seeding densities for three different BC PDCs.

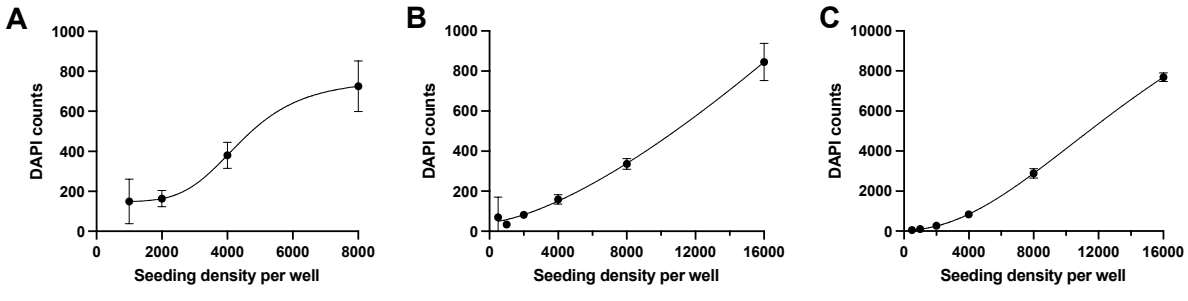

Figure 44: Trends in endpoint DAPI IFM analysis of ex-vivo processed bladder tumour tissue seeded at different seeding densities in 0.05% DMSO control vehicle media. A – BT 7.0, 28 replicates per seeding density (1000 to 8000 cells per well); B – EVD0015, 14 replicates per seeding density (1000 to 16000 cells per well); C – EVD0031, 14 replicates per seeding density (1000 to 16000 cells per well). DAPI - 4′,6-diamidino-2-phenylindole.

For BT 7.0, there was a flattening of the curve between 4000 and 8000 cells per well, with no improvement in the COV value, whereas this was not the case for EVD0015 and EVD0031, where higher seeding densities continued to reduce the COV (Table 18). This could be a result of differing biology, as EVD0015 and EVD0031 were both NMIBCs and BT 7.0 was a muscle invasive BC (MIBC). On further inspection of the DAPI IFM images, BT 7.0 cells also showed a different growth pattern, with tightly aggregated and overlapping cells at higher seeding densities (Figure 45: A). This made nuclear segmentation more difficult, unlike the more two-dimensional "cell-line-like" growth patterns of EVD0015 and EVD0031 (Figure 45: B&C). These results suggest that higher seeding densities may improve the reproducibility of the assay for those with non-aggregated growth patterns, however, may be inhibitory to downstream analysis for others. Hence, reaffirming the challenges discussed in Chapter 4.

Table 18: Co-efficient of variation between seeding density titration replicates for two *ex-vivo* bladder tumour cell suspensions

Tumour	Seeding Density	Mean (SD) DAPI counts	COV DAPI
BT 7.0	1000	150 (112)	74.73
	2000	163 (40)	24.59
	4000	381(65)	17.21
	8000	726 (127)	17.49
EVD0015	1000	33 (9)	26.96
	2000	82 (13)	15.59
	4000	159 (24)	14.79
	8000	336 (27)	8.04
EVD0031	1000	105 (15)	14.03
	2000	271 (30)	11.04
	4000	840 (52)	6.22
	8000	2889 (236)	8.17
	16000	7686 (214)	2.79

SD – standard deviation; COV – coefficient of variance; DAPI - 4';6-diamidino-2-phenylindole.

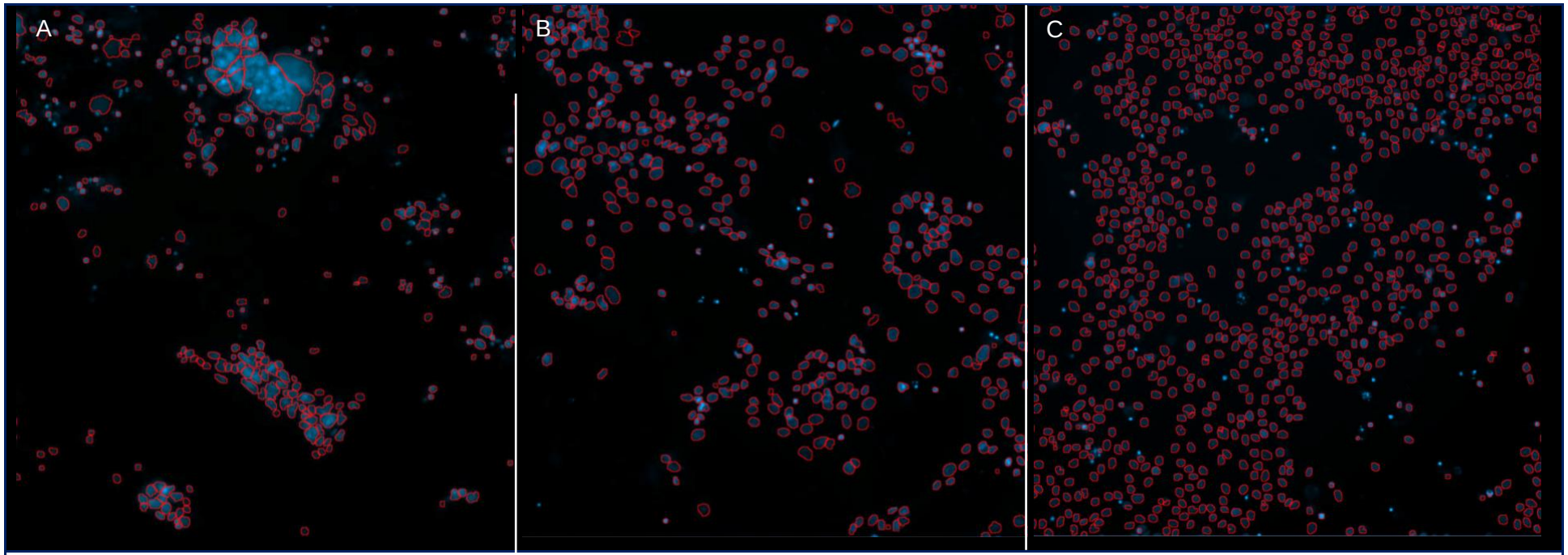

Figure 45: A – BT 7.0 10x DAPI IFM images with overlaid segmentation annotation; B – EVD0015 10x DAPI IFM images with overlaid segmentation annotation; C – EVD0031 10x DAPI IFM images with overlaid segmentation annotation. Blue indicates 4′,6-diamidino-2-phenylindole (DAPI) emission suggesting nuclear staining; black indicates background; red lines highlight the identification of individual nuclei by the ZEISS ZEN analytical software.

8.1.4.3 SEEDING DENSITY COMPARISON BETWEEN CTG AND IFM DAPI

For one tumour, seeding density CTG and DAPI IFM endpoint results were available at the time of submission (Figure 46). These results suggest that CTG was more reproducible at both lower and higher seeding densities than IFM for that tumour. This could reflect that at lower seeding densities (1000-2000 cell per well) the number of cells identified using DAPI IFM was too low (Table 18)(as less than half of the well was being imaged using a 9-tile strategy) leading to higher variability. At higher seeding densities, higher variability in DAPI IFM likely reflected clustering of cells described in Figure 45: A, which made image segmentation more challenging, hence, higher variability. These results highlight the potential drawbacks of using IFM instead of CTG. First, it may not provide reproducible outputs at low cell seeding density, which could be a problem for smaller or less viable samples. Secondly, as there are numerous pre-imaging manipulations, non-adherent cells may be inadvertently washed away or disrupted. And finally, the post-imaging steps to yield endpoint results may be impacted by tumour-specific growth patterns, which can be challenging to segment during analysis. Hence, when deciding between endpoint CTG of IFM analysis, Brightfield microscopy prior to making this decision could identify some of aforementioned variables to determine the most appropriate endpoint modality.

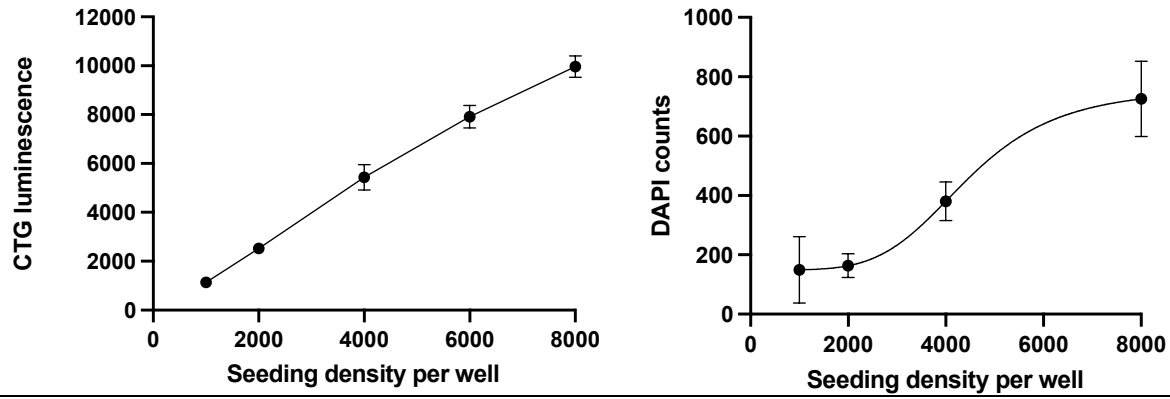

Figure 46: BT 7.0 endpoint CTG (left) and DAPI IFM (right) DMSO replicates plotted at different seeding densities (1000 to 8000 cells per well, 28 replicates per seeding density). CTG - CellTiter-Glo®; DAPI - 4′,6-diamidino-2-phenylindole.

8.1.4.4 EXPLORING IFM CELL-TYPE SPECIFIC ANALYSIS

As described in the section 8.1.1, one of the key added benefits when using IFM is the ability to identify multiple subpopulations of cells with differential lineages. Thus, alongside preliminary DAPI IFM reproducibility analysis, differential antibody stains were explored as

potential candidate BC-specific markers. Cytokeratins are intermediate filament forming proteins of epithelial cells, which are cell-type, differentiation-state, and functional-state dependent (377). Hence, cytokeratin-specific antibody stains have been used for many years in clinical histopathology to differentiate between tumour types. Additionally, cytokeratin-targeted antibodies labelled with an immunofluorescent fluorophore can be used to visualise epithelial cells during IFM.

Cytokeratin-19 (CK19) is a keratin protein that forms part of the cytoskeletal scaffold in epithelial cells and its expression often retained by cancers (377,378). CK19 is expressed by almost all (92-100%) urothelial cancers (377,378), which make up the majority of BCs. To confirm that CK19 was an appropriate candidate antibody target, the EJ urothelial cancer cell line (379) was stained with a range of different conjugated cytokeratin antibodies at a concentration of 1:400. Optimal cytoplasmic staining was observed using CK19, whereas CK7, CK14 and CK20 were suboptimal (Figure 47).

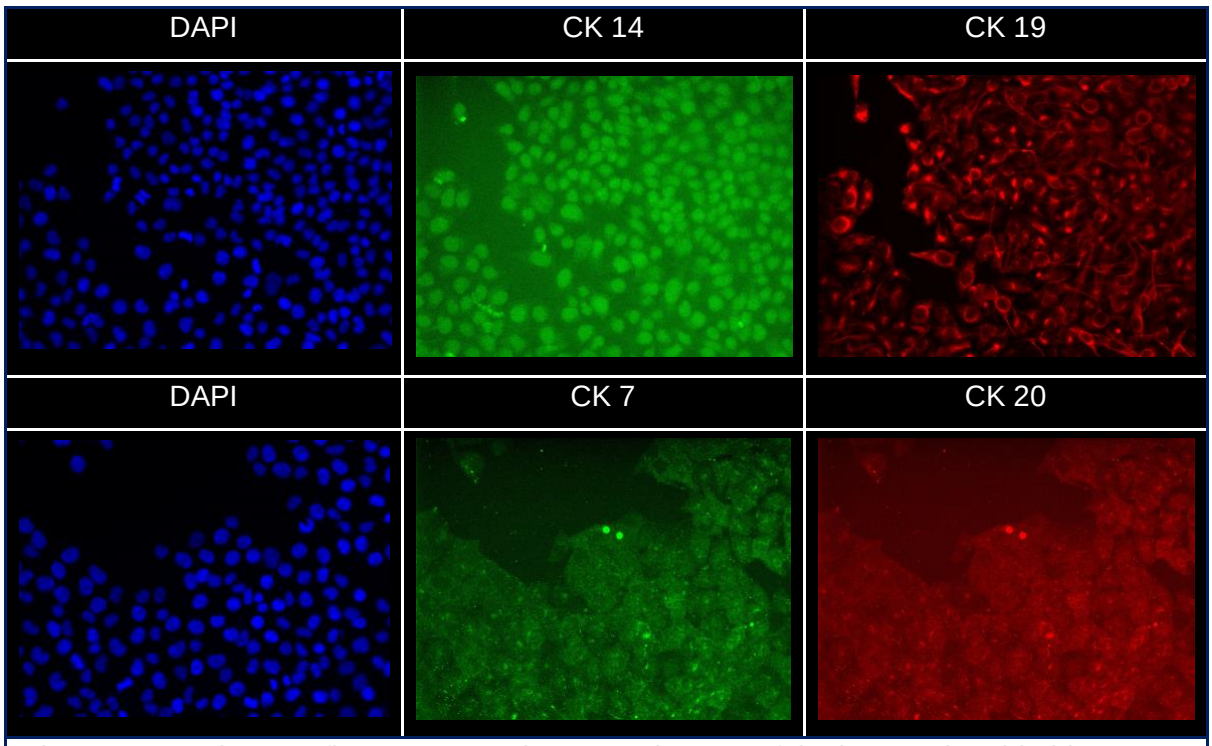

Figure 47: 20x immunofluorescence microscopy images of the immortal EJ bladder cancer cell line stained with 1:1000 DAPI, 1:400 CK14, 1:400 CK19, 1:400 CK7, and 1:4000 CK20, showing optimal cytokeratin staining with the CK19 antibody. CK – cytokeratin.

Having chosen CK19, it was important to explore the quality of staining at different antibody concentrations. As 1:400 antibody concentration had been sufficient in the EJ cell line, an antibody titration experiment was performed using a processed BC PDC between 1:50 to

1:400 CK19 concentration. Figure 48 shows example images of CK19 staining across the spectrum of antibody concentrations in EVD0031. As there was very little difference in staining quality, these results suggest that a concentration of 1:400 would be sufficient to label BC PDC cells, whilst minimising antibody volume required and hence cost of the staining process.

A similar process was performed to look at alternative cell types within the PDC suspensions. Mesenchymal cells are commonly present within solid tumours, either as normal infiltrating fibroblasts, cancer-associated fibroblasts (380), or cells undergoing epithelial to mesenchymal transition, which allows them to migrate, adopt stem-cell-like properties, and become more resistant to chemotherapies (380–383). Vimentin is a type III intermediate filament protein and plays a role in organelle placement, adhesion, and migration. It is highly expressed by fibroblasts of all types (380) and it has been identified that higher vimentin expression (using immunohistochemistry analysis) in resected BCs is associated with more aggressive disease phenotypes, such as, muscle invasive BC (MIBC) or metastatic BC, and poorer clinical outcomes (382,384).

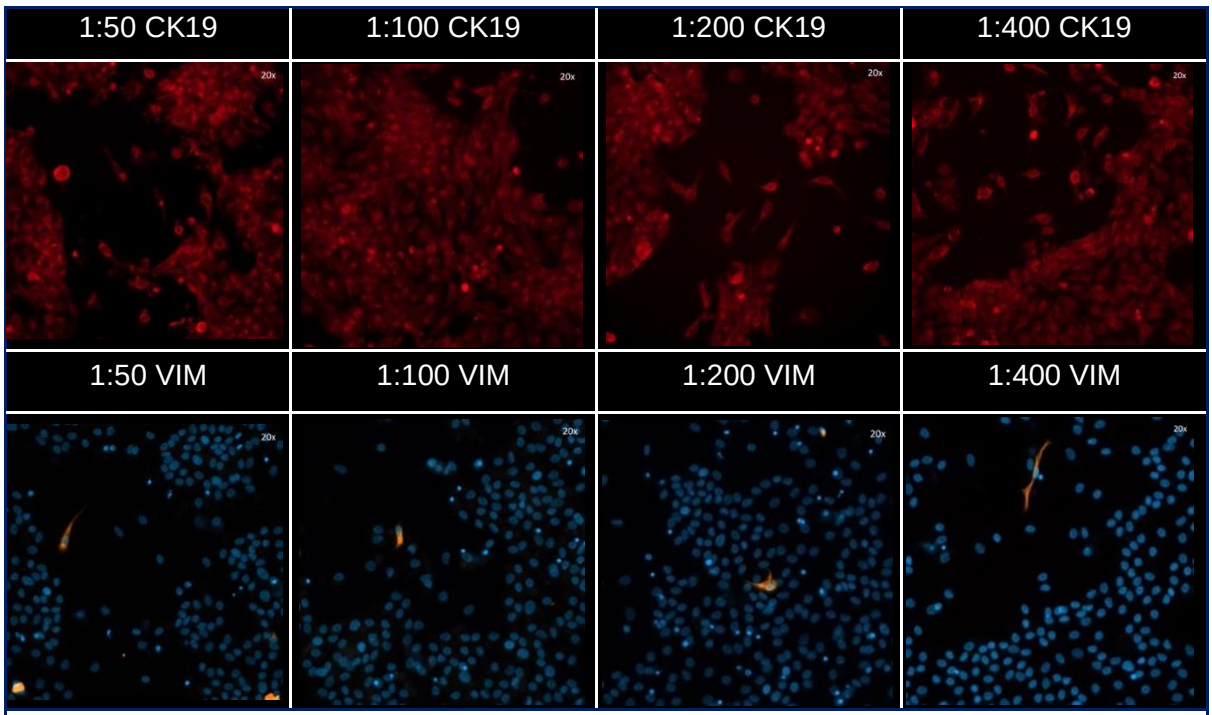

Figure 48: 20x immunofluorescence microscopy images of EVD0031 primary ex-vivo bladder tumour tissue stained with 1:50 to 1:400 concentrations of CK19 and Vimentin, showing very little difference across the dilution series. CK – cytokeratin; VIM – vimentin.

As it is known that some BCs express this protein, vimentin was chosen as a preliminary antibody to explore whether differential cell lineages could be identified within BC PDCs suspensions during IFM. A concentration of 1:400 was chosen, as there was no difference in

staining quality between 1:50 and 1:400 concentrations of antibody (Figure 48). Using the 1:400 concentrations for CK19 and vimentin, and 1:1000 for DAPI antibody staining, the IFM staining quality was evaluated across a range of *ex-vivo* processed BC PDCs. There was consistent CK19 positive staining across a the spectrum of BCs sampled, from low-risk NMIBC (LR NMIBC) and intermediate-risk NMIBC (IR NMIBC), to high-risk NMIBC (HR NMIBC), to MIBC (Figure 49), consistent with the literature (377,378). Again, this data supports the choice of CK19 to identify urothelial cancer epithelial cells in *ex-vivo* processed BC PDCs. In addition, it was possible to identify vimentin stained cells that were not stained with CK19; these mesenchymal cells were particularly abundant in the MIBC, compared to the NMIBCs – consistent with the findings of immunohistochemistry studies (382,384).

8.1.4.5 METHODOLOGICAL FEASIBILITY OF IFM ASSAY

Using the methodology above, the feasibility of *ex-vivo* IFM imaging was explored. Of the 39 malignant BCs with endpoint CTG results, 26 (26/39, 69.2%) tumours had sufficient PDC material to attempt IFM image analysis by seeding tumour cells into 28 DMSO only wells. A total of 21 (21/26, 80.8%) had sufficient image quality to perform single-cell analysis, and of these, 17 (17/26, 65.4%) had a per well DAPI COV that met the methodological quality threshold (≤0.25). Table 19 describes the differentially labelled single-cell counts in the DMSO control wells and their corresponding COV values. Median (IQR) DAPI counts per well between methodological successes (n=17) and failures (n=4) were 389 (236-862) and 95 (54-546), respectively (Mann-Whitney U p=0.052). Across the 17 successful tumours, there were significantly more tumour epithelial cells (TCs) within the images than stromal cells (SCs): median (interquartile range (IQR)) TC and SC counts were 365 (154-830) and 38 (10-67), respectively (Mann-Whitney U, p<0.0001). SC counts were typically low (resulting in high COV values), which reflects the biology of this predominant NMIBC group that have tumours primarily of epithelial origin.

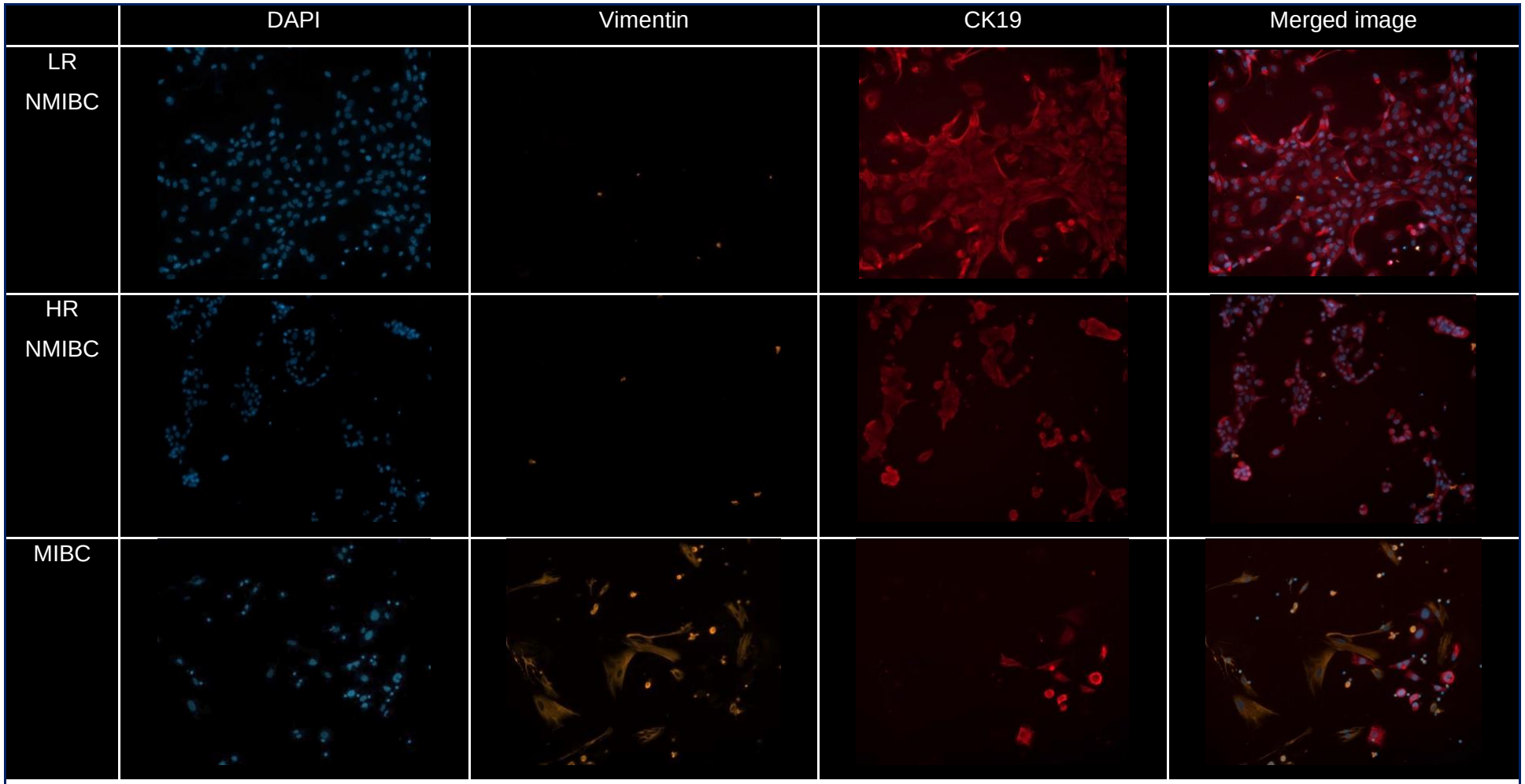

Figure 49: 10x images of primary processed ex-vivo bladder tumour tissues across the disease spectrum (low/intermediate risk, high risk, and muscle-invasive BC) showing positive CK19 immunofluorescence staining throughout, but with variable populations. Of note, the muscle invasive BC had lowed CK19 staining and a much higher proportion of vimentin staining, than the other two classes. LR NMIBC – low-risk non muscle invasive BC; HR – high risk non-muscle invasive BC; MIBC – muscle invasive BC; DAPI - 4′,6-diamidino-2-phenylindole; CK – cytokeratin.

Table 19: Differential single cell counts per DMSO well and variation between DMSO wells for the 21 *ex-vivo* processed drug plates with adequate images to analyse

Tumour code	Clinical code	Median counts per DMSO well			COV of cell counts between DMSO			TC:SC ratio
		DAPI	TC	SC	DAPI	TC	SC	
EVD0016	IR_5	351.0	365.0	10.0	14.7	19.2	97.1	36.5
EVD0015	HR_16	378.0	388.0	23.5	12.2	19.6	126.1	16.5
EVD0014	HR_15	261.5	178.5	13.5	10.8	25.0	129.8	13.2
EVD0009	MIBC_9	141.5	104.5	19.0	13.5	19.0	43.0	4.6
EVD0007	MIBC_8	261.0	61.5	207.0	15.5	54.0	23.1	0.3
EVD0005	LR_7	1924.0	1703.0	44.0	21.6	24.2	198.2	38.7
9.2	IR_4	2807.0	2846.5	171.0	22.0	22.0	52.6	16.6
9.0	HR_12	828.5	909.0	9.0	13.0	16.0	72.7	101.0
8.9	HR_11	668.5	640.5	43.0	21.2	23.1	29.1	14.9
8.8	HR_10	170.0	156.5	9.0	16.1	19.0	46.5	17.4
8.7	LR_6	894.5	751.0	352.5	8.3	40.4	43.9	2.1
8.6	LR_5	210.0	96.5	37.5	19.5	25.4	25.5	2.6
8.5	IR_3	569.0	205.0	81.5	13.8	52.8	48.1	2.5
8.2	HR_9	145.5	151.0	51.5	22.2	28.8	69.3	2.9
7.3	HR_7	690.5	614.5	5.0	19.1	18.7	120.1	122.9
7.0	MIBC_6	389.0	214.5	40.0	19.6	27.5	28.6	5.4
6.8	IR_2	1897.5	1711.5	5.0	12.7	14.2	195.0	342.3
8.4	MIBC_7	45.0	36.5	3.0	39.9	44.5	72.7	12.2
8.1	HR_8	692.0	369.5	15.0	34.5	37.0	62.7	24.6
6.6	LR_2	81.5	58.5	8.0	32.0	39.0	149.7	7.3
6.0	MIBC_3	108.0	52.5	10.5	30.6	43.0	44.4	5.0

DAPI - 4',6-diamidino-2-phenylindole; SC – stromal cell (Vimentin+); TC – tumour epithelial cell (CK19+); DMSO – dimethyl sulfoxide; TC:SC ratio – ratio of tumour cells to stromal cells within a DMSO control well; highlighted in red are tumours that had higher SC counts than TC counts; highlighted in grey are the tumours where DAPI COV did not reach the quality standard.

8.1.5 DISCUSSION AND CONCLUSIONS

This chapter describes provisional experiences using *ex-vivo* high throughput IFM analysis for BC PDCs. Although further optimisation and validation is required, these data highlight that methodological throughput to endpoint DAPI IFM is feasible in almost two-thirds of processed bladder tumours (17/26, 65.4%). Figure 49 highlights that differential cell lineage visualisation was possible in some tumours, with clear differential staining using CK19 and vimentin. However, stromal cells were sparsely present across the predominantly NMIBC cohort, where low overall counts led to high variability. Only one tumour (1/17, 5.9%) tumour met the COV threshold for stromal cell (SC) counts; this tumour was a MIBC with a tumour cell to stromal cell ratio of 0.3. Reasons for low SC counts could simply reflect the biology of this predominantly NMIBCs cohort, where tumours are typically papillary outgrowth of the urothelium, rather than solid tumours invading into the detrusor muscle; alternatively, the vimentin labelled populations may be less adherent than the tumour cell (TC) populations, thus more prone to being lost in pre-microscopy washes. Furthermore, it would be useful to explore alternative mesenchymal antibody markers across the spectrum of BCs acquired. It is also worth noting that in some circumstances, the total TC and SC median counts equated to more than the DAPI median (for example, IR_4) (Table 19). Reasons for this could be due to suboptimal antibody staining or challenges with the post-imaging analysis (training Zeiss to select differentially labelled cells). On the whole, this difference between total count, and the sum of TC/SC counts, fell within 10%.

Future work towards optimising this aspect of this study protocol will include:

1. Optimisation of antibody selection and staining protocols to minimise non-specific antibody binding and to improve the delineation of intra-tumoral differential cell populations (where present);
2. Exploring modifications to the plating or fixing methodology that may minimise the loss of non-adherent cell types; for example, brief centrifugation of suspensions prior to fixing, or by coating the wells with charged substrates that assist with adhesion, such as polylysine (385);
3. Optimisation of image analysis to include improved nuclear segmentation techniques and more robust protocols for the identification and differentiation of fluorophore labels;
4. Standardisation of post-processing bioinformatic pipelines that will assist with streamlining the IFM high-throughput protocol and increasing reproducibility to minimise inter-tumour and inter-operator variability.

8.2 EXPLORING THE USE OF *EX-VIVO* HIGH-THROUGHPUT DRUG SCREENING IN KIDNEY CANCER

8.2.1 INTRODUCTION

Although not the primary objective of this PhD, the Ex-VIvo DetErmiNed cancer Therapy (EVIDENT) study (NCT05231655) aims to deliver proof-of-concept data to support the use of *ex-vivo* high throughput drug screening in a range of cancer types. Currently, the EVIDENT consortium has focussed on recruiting patients with BC, kidney cancer (KC), glioblastoma, melanoma, sarcoma, and head and neck cancers; however, there is scope to expand the number of tumour types, adapting the methodology to develop cancer-specific standard operating procedures and analysis pipelines. Through the assessment and clinical validation of cancer and tumour-specific *ex-vivo* drug responses, EVIDENT aims to generate enough data to progress towards an early phase clinical trial, where *ex-vivo* directed treatment can be compared to standard of care treatment. The remainder of this chapter will summarise preliminary *ex-vivo* high-throughput drug screening results for the first ten KC patients recruited through this PhD.

Each year, KC affects 431,288 patients globally, with 179,368 dying from the disease (1). KC is common in Europe (386) and the age-standardised incidence of KC in the UK alone has doubled since 1993 (387). In England, KC now affects over 10,000 patients per year (388). Most KCs are renal cell carcinomas (RCC), of which the most common subtype is clear cell RCC (ccRCC) (388). Despite increased access to diagnostic imaging and advances in anti-cancer therapy, age-standardised mortality rates have not improved (388). Approximately one-fifth (18%) of new cases of KC in the UK present with metastases (Stage 4) at diagnosis, which has a median survival of six months (388). Even in patients who have locally advanced (Stage 3) KC, survival rates at 5-years remain poor (20%)(389). Several novel therapies have been introduced in the last decade to treat metastatic KC, including targeted (TK, VEGF, mTOR, FGFR) and immune-checkpoint inhibitors. However, predictive biomarkers and individualised approaches to select the best treatment, in the correct sequence, are currently lacking. Hence, there is a need to improve treatment selection algorithms and outcomes for patients with KC in the UK, particularly those with the most advanced disease states.

8.2.2 METHODS

The primary objective of this pilot study was to explore the methodological feasibility of *ex-vivo* high-throughput drug screening in KC. Patients were identified and recruited as previously described for BC (Section 3.1). In brief, patients who were due to undergo surgical removal of their KC (radical nephrectomy (RN)) were approached and asked if they would like to participate in the study (EVIDENT, STH20854). Kidneys containing tumour were transported as whole organs to histopathology immediately for tumour sampling by a trained clinician (Figure 50). Warm ischaemic time was documented for all tumours, defined as the time from renal artery clamping to tumour sampling. Whole kidneys were sliced in the coronal plane, taking time to preserve diagnostic hilar structures (Figure 50). Tumour was macroscopically distinct from healthy renal parenchyma and care was taken to retrieve samples from more viable areas (that were not fibrotic or haemorrhagic). Tumour samples were then transported directly to the laboratory in plain RPMI-1640 (Lonza) for *ex-vivo* tumour processing.

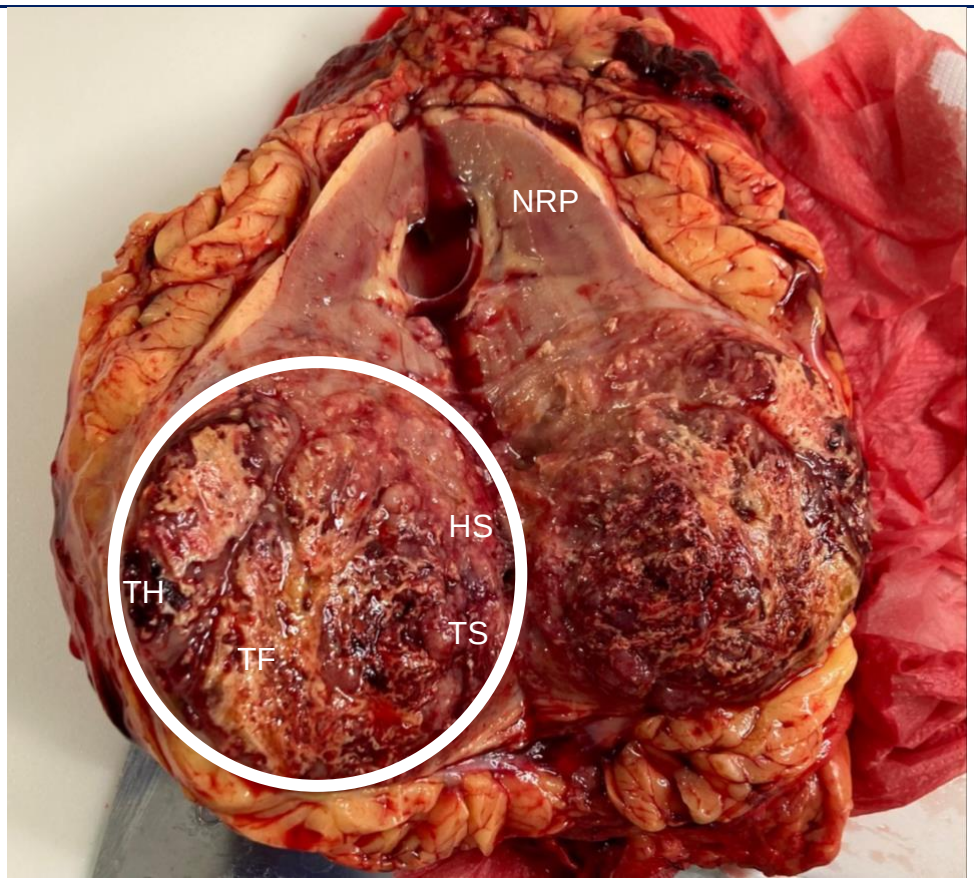

Figure 50: Image of kidney sliced lateral to medial whilst maintaining the hilar structures (HS). The tumour (circled in white) can be differentiated macroscopically from normal renal parenchyma (NRP) tissue. There are visible areas of intrinsic tumour haemorrhage (TH) and tumour fibrosis (TF). The tumour sample (TS) was taken from a macroscopically more viable part of the tumour.

8.2.3 RESULTS

8.2.3.1 PATIENT AND TUMOUR CHARACTERISTICS

All patients approached consented to participate in the study, suggesting high levels of acceptability (consistent with patient and public engagement activity performed prior to initiating this arm of the EVIDENT study). Clinical and pathological features of patient samples acquired are described in Table 20. Median (IQR) age was 68 (53-73) years. As expected, most (6/10, 60%) patients had ccRCCs, one (1/10, 10%) had a papillary RCC, and one (1/10, 10%) had a chromophobe RCC. Most patients with RCC (6/7, 85.7%) were classed as having high-risk tumours. Interestingly, two (2/10, 20%) of the resected tumours were metastatic uveal melanomas to the kidney, which are extremely rare (390).

Table 20: Clinical and pathological characteristics of the first ten consecutive patients recruited for *ex-vivo* processing of renal tumours

Tumour ID	Code	Sex	Age	Histopathology	Histological variant	Mayo risk score
EVD0001	RCC1	F	48	PRCC	Yes	High (11)
EVD0003	RCC2	M	79	CCRCC	No	Intermediate (3)
EVD0006	RCC3	M	71	CCRCC	No	High (6)
EVD0008	MM1	F	55	UM	NA	NA
EVD0011	MM2	M	77	UM	NA	NA
EVD0012	RCC4	M	48	CCRCC	Yes	High (11)
EVD0017	RCC5	F	57	CCRCC	No	High (9)
EVD0022	RCC6	M	71	CCRCC	No	High (3)
EVD0023	RCC7	F	72	ChRCC	Yes	Not scored
EVD0028	RCC8	M	65	CCRCC	Yes	High (8)

M – male; F – female; CCRCC – clear cell RCC; ChRCC – chromaphobe RCC; PRCC – papillary RCC; UM – metastatic uveal melanoma to the kidney.

8.2.3.2 ADAPTED *EX-VIVO* TISSUE PROCESSING PROTOCOL

Methods used for tumour dissociation, cell seeding, incubation, and endpoint assays were adapted from the methods used in BCs (Section 3.3.2). Media and supplementation remained unchanged to keep consistency between *ex-vivo* approaches. Renal tumour tissue processing

characteristics are shown in Table 8. All tumours were acquired via RN. Median (IQR) tumour warm ischaemic time was 75 (44-98) minutes. Unlike the predominantly soft, papillary bladder tumours, most (7/10, 70%) KCs were solid. Median (IQR) tumour sample volume was 1,911 (1,079-2202)mm^3. Median (IQR) time in enzyme was 68 (30-113) minutes, but solid tumours required significantly longer to reach a single cell suspension than soft or gelatinous tumours (Mann-Whitney U, p=0.008). The median (IQR) percentage viability of processed suspensions was low, at 28% (26-40%).

When comparing these values to *ex-vivo* processed BCs, KC samples were significantly larger (Mann-Whitney U p<0.0001), took longer to dissociate (Mann-Whitney U, p=0.004), and had lower percentage viability (Mann-Whitney U, p=0.016). Although KC samples yielded significantly higher total live cell counts than BCs (Mann-Whitney U, p<0.0001), the live cell yield: volume (LY:V) ratio was not significantly different (Mann-Whitney U, p=0.17). It was also noted that 5 (5/8, 62.5%) of the RCCs had visible immune infiltrates present during tissue processing (observed as a buffy coat during centrifugation and/or identification using Brightfield microscopy); this was not something that had been observed when processing patient BCs.

Table 21: Renal tumour tissue sample pre and post-processing characteristics

Tumour Code	Tumour description	WIT (mins)	Volume (mm3)	Immune cells	Enzyme	Time (mins)	Viability (%)	Total live cells	LY:V
RCC1	Solid	60	2,450	-	TrypLE	40	63	20,336,400	8,301
RCC2	Solid	40	1,500	++	C/D	100	25	21,510,000	14,340
RCC3	Solid	90	728	+++	Acc	75	28	10,620,000	14,588
MM1	Soft, pulpy	120	954	-	TyrpLE	30	33	12,960,000	13,585
MM2	Soft, black	60	2,105	-	TyrpLE	30	26	14,640,000	6,955
RCC4	Gelatinous	90	2,136	-	TyrpLE	30	59	55,080,000	25,787
RCC5	Solid	45	1,120	-	Acc	100	31	7,832,000	6,993
RCC6	Solid	30	1,725	++	C/D	150	25	9,350,000	5,420
RCC7	Solid	90	2,096	+	Acc	60	27	40,200,000	19,179
RCC8	Solid	150	2,400	+	C/D	240	27	38,000,000	15,833

WIT – warm ischaemic time; RN – radical nephrectomy; C/D – collagenase/dispase; Acc – Accutase

8.2.3.3 METHODOLOGICAL SUCCESS

The primary objective of this pilot study was to evaluate whether KC samples could be processed using similar *ex-vivo* methodology to BCs and reach reproducible endpoint results. Methodological success was assessed by evaluating the COV in endpoint CTG values between DMSO control wells, as defined in section 5.2.1. Median (IQR) CTG COV values for the first ten KCs processed was 0.056 (0.051-0.098), suggesting very good reproducibility. Using a threshold for quality of COV ≤0.25, all ten KCs (100%) were defined as methodological successes.

8.2.3.4 PRELIMINARY DRUG RESPONSE DATA

Although not the primary objective of this pilot study, it was interesting to explore CTG drug response data across the ten KC samples processed using *ex-vivo* methodology. Bespoke KC plates had not been created for the purpose of this pilot study, so *ex-vivo* processed KC PDCs were seeded on BC drug plates (Bladder Batch 2). Using similar methodology described in section 5.2.6, the RCC area under dose-response curve (AUC) values were normalised and plotted (Figure 51). Although only descriptive at this stage, it seemed apparent that there were some outlier drug responses.

For example, RCC4, a 48-year old male with an aggressive RCC histological variant, with one of the highest Mayo scores, showed almost screen-wide resistance, with only a moderate response to Fulvestrant (an oestrogen receptor inhibitor). The two malignant uveal melanomas had similar drug response profiles, and as expected, both showed an enhanced response to AZD6244, the MEK inhibitor, which is approved for the treatment of BRAF-positive malignant melanoma (203). MM2 seemed to be very responsive to a range of targeted inhibitors, but more chemoresistant, whereas, MM1 showed an opposing profile. Several tumours showed a moderate response to Pembrolizumab (RCC5, RCC6, MM2), however, at this stage, this did not seem to correlate with the observed proportion of immune complement within the cellular milieu at the time of tumour processing – warranting further evaluation. As next generation sequencing (NGS) data was lacking for these tumours, novel treatment responses could not be compared to genomic profiles of these individual KCs.

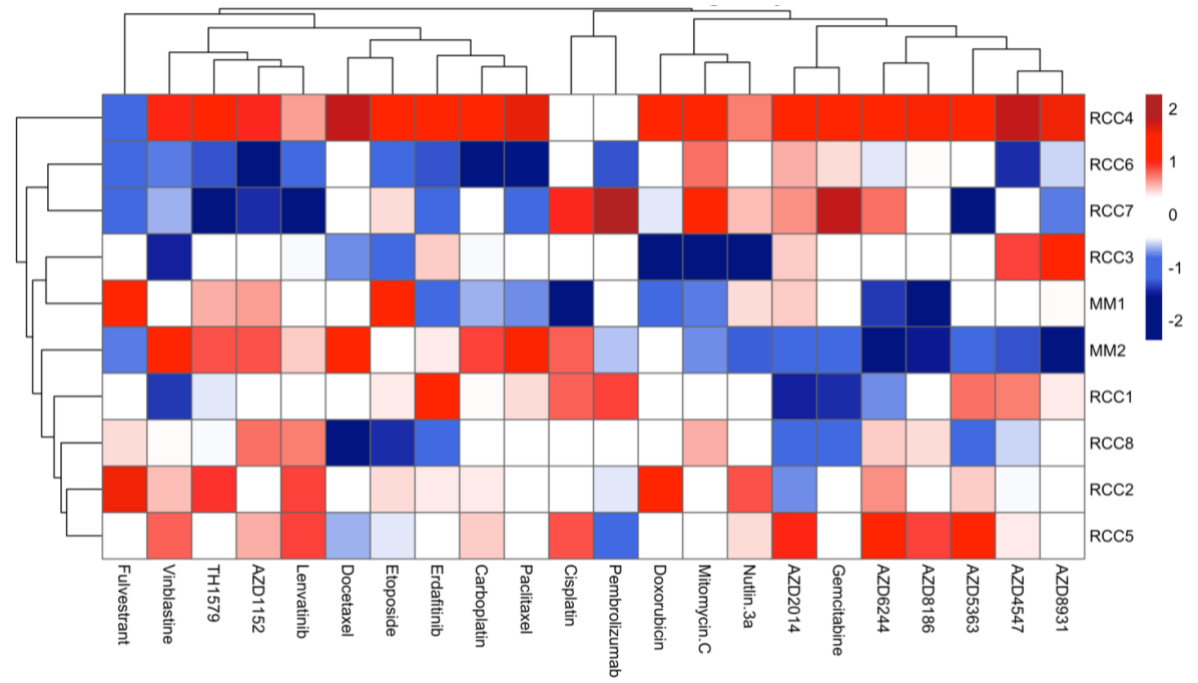

Figure 51: Heatmap of robust Z score AUC values for 22 tested compounds (x axis) across 10 kidney tumours (y axis). Navy/blue indicates very good response to the drug, red/burgundy suggests a very poor response. Heirarchical clustering was used to group drugs and tumours.

Table 22 and Figure 52 show the differences between mean/median raw AUC values for BC and KCs. As anticipated, the KCs were typically less responsive to standard of care chemotherapies than BCs. AZD2014, the mTOR inhibitor, had the most potent effect on KC PDCs, although this was less pronounced than in BC; of note, alternative mTOR inhibitors, including everolimus, have historically been used in the treatment of patients with metastatic KC prior to immunotherapies through targeting of the von-Hippel-Lindau pathway (391–393). Although raw AUC values remained high for Lenvatinib, a multi-tyrosine kinase inhibitor that has been recommended in the treatment of metastatic ccRCC in combination with pembrolizumab (394), was significantly more active than in BC. Generally high AUC values in these *ex-vivo* KC samples could reflect the differing biology of tumours treated, that the drug plates were not bespoke to the treatment of KCs, and differing PDC compositions to that of processed BCs. Interestingly, the proliferative responses seen in 14 (14/39, 35.9%) of the patient BCs, were not observed in KC.

Table 22: Common drug response thresholds generated by mapping the distribution of AUC for all 39 malignant bladder tumours versus 10 malignant kidney tumours processed

Drug	Mean/Median AUC BC	Mean/Median AUC KC	Difference p-value
Cisplatin	0.370	0.745	**<0.0001**
Vinblastine	0.472	0.843	**<0.0001**
MMC	0.609	0.744	**0.028**
Docetaxel	0.746	0.920	**0.006**
Paclitaxel	0.852	0.961	**0.020**
Gemcitabine	0.883	0.828	0.20
Etoposide	0.933	0.994	**0.049**
Doxorubicin	0.916	0.961	0.16
AZD2014	0.323	0.641	**<0.0001**
AZD8186	0.747	0.790	0.36
Nutlin-3a	0.834	0.904	0.24
AZD5356	0.878	0.833	0.63
Levantinib	1.015	0.927	**0.007**
AZD4547	1.025	0.918	0.13
Erdafitinib	1.095	0.880	**<0.0001**

AUC – area under dose-response curve; BC – bladder cancer; KC – kidney cancer.

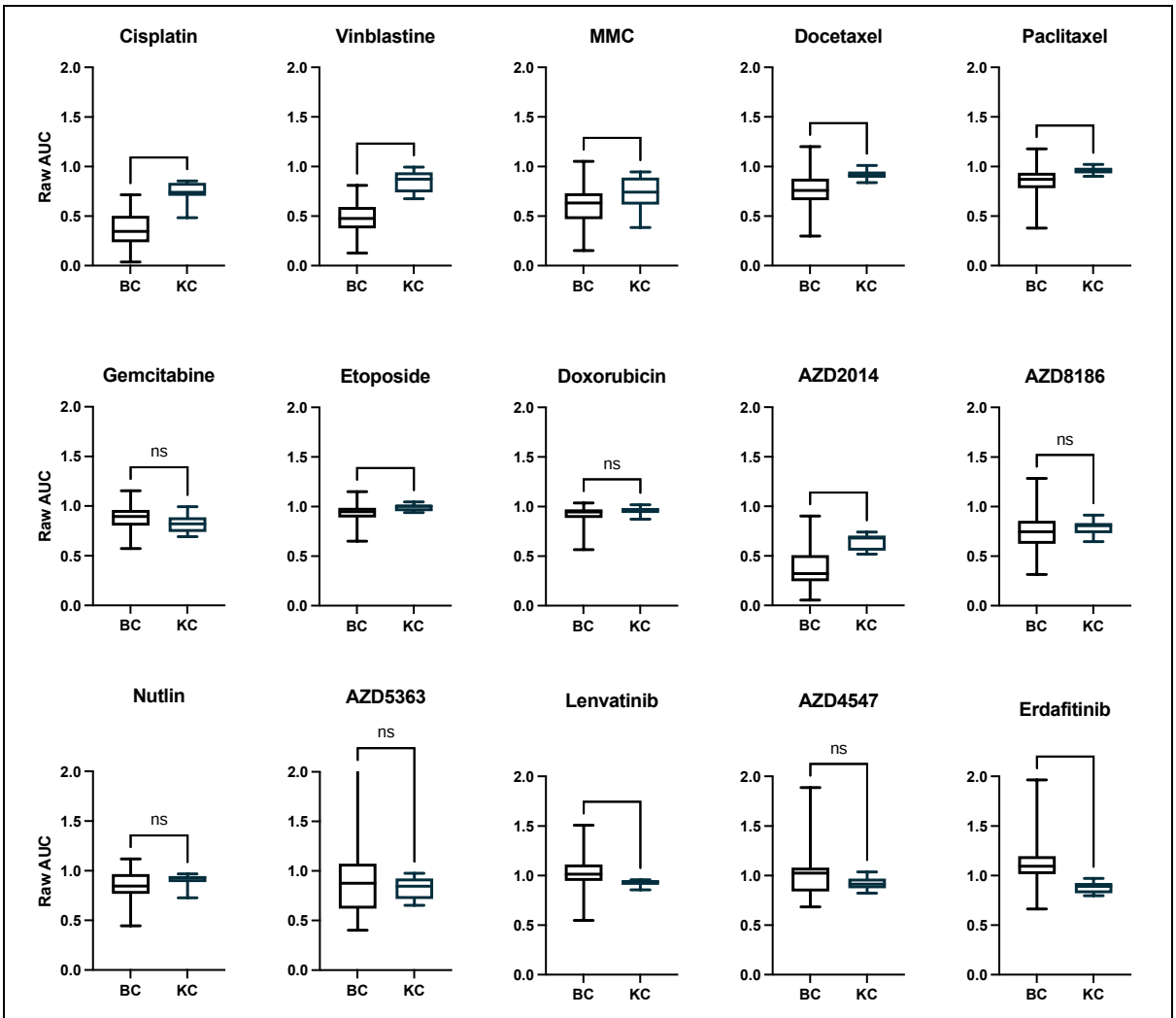

*Figure 52: Comparison of raw area under dose-response curve (AUC) values per common drug screened between BCs (n=39) and KCs (n=10). (Mann-Whitney U comparison. NS – non-significant; * - p<0.05; ** - p<0.01; *** - p<0.001; **** - p<0.0001). BC - bladder cancer; KC – kidney cancer.*

8.2.3.5 PRELIMINARY IFM ANALYSIS

Again, performing IFM-based analysis in this pilot study was not the primary aim; however, for several tumours, exploratory image analysis was performed. Unlike BCs, RCCs do not typically express CK19 (395). ccRCCs may positively express vimentin, CA-IX, or broad pan-cytokeratins (PanCK) (395,396); less common subtypes, such as papillary RCCs, may have variable expression. Immunofluorescence experiments performed on primary *ex-vivo* processed KC tissue showed diffuse positive staining for vimentin in both clear cell and papillary RCC subtypes, but differential PanCK staining (Figure 53); this is consistent with the literature as 87-100% of clear cell and papillary subtypes express vimentin (395,397). In

addition, there is both intra-tumoural differential cell morphologies, and clear differential morphology between the two tumour subtypes.

As described in the literature, another advantage of IFM-based *ex-vivo* screening is the ability to explore special cell-on-cell interactions. One feature that was unique to KCs, was the presence of immune complement within some of the *ex-vivo* PDCs. To explore whether the immune complement could be differentially identified using IFM, the pan-leucocyte marker CD45 was used (Santa-Cruz, 30-F11 Alexa Fluor® 594, sc-53665 AF594). Figure 54 is a 50x image taken of the *ex-vivo* processed RCC EVD0006 from a pembrolizumab treated well. From this image, there are clear morphological differences between tumour cells (Vimentin+) and smaller surrounding immune complement. Although the antibody staining using CD45 is suboptimal here, it can be seen that some of the smaller immune complement have taken up the antibody stain and are in close proximity to the larger tumour cells. Figure 54 suggests that if immune complement are present within the *ex-vivo* processed PDC, they can be captured using IFM and may be distinguished from tumour cells using morphological and antibody fluorophore metrics; this is particularly exciting for *ex-vivo* drug screening in KC, as it suggests that there may be scope to explore immunotherapy responses, which are the standard of care treatment for patients with advanced or metastatic disease.

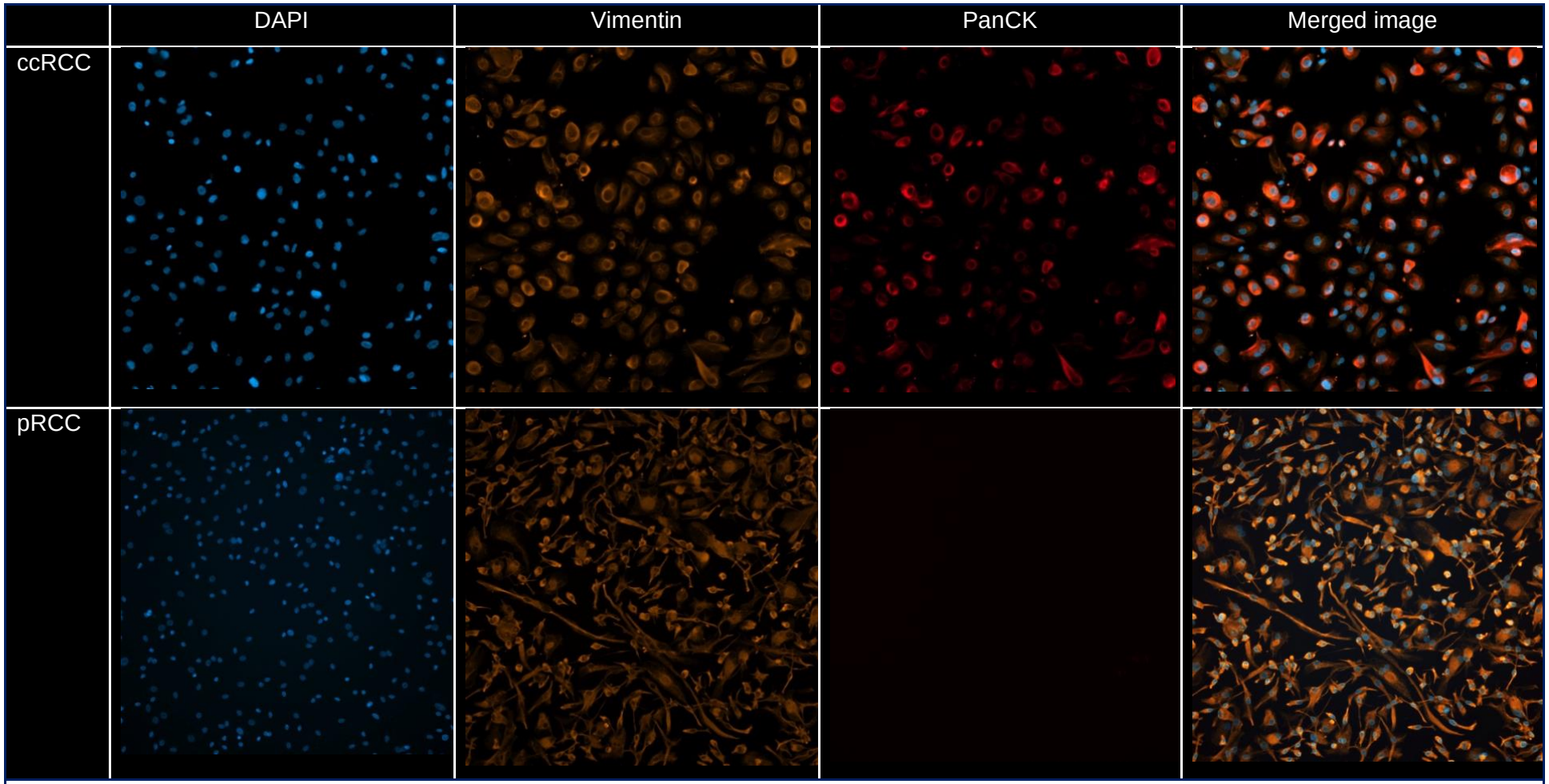

Figure 53: Positive vimentin staining and differential PanCK staining in two different RCC histological subtypes. Images are 10x magnification. ccRCC – clear cell RCC; pRCC – papillary RCC; DAPI - 4′,6-diamidino-2-phenylindole; PanCK – pan-cytokeratin.

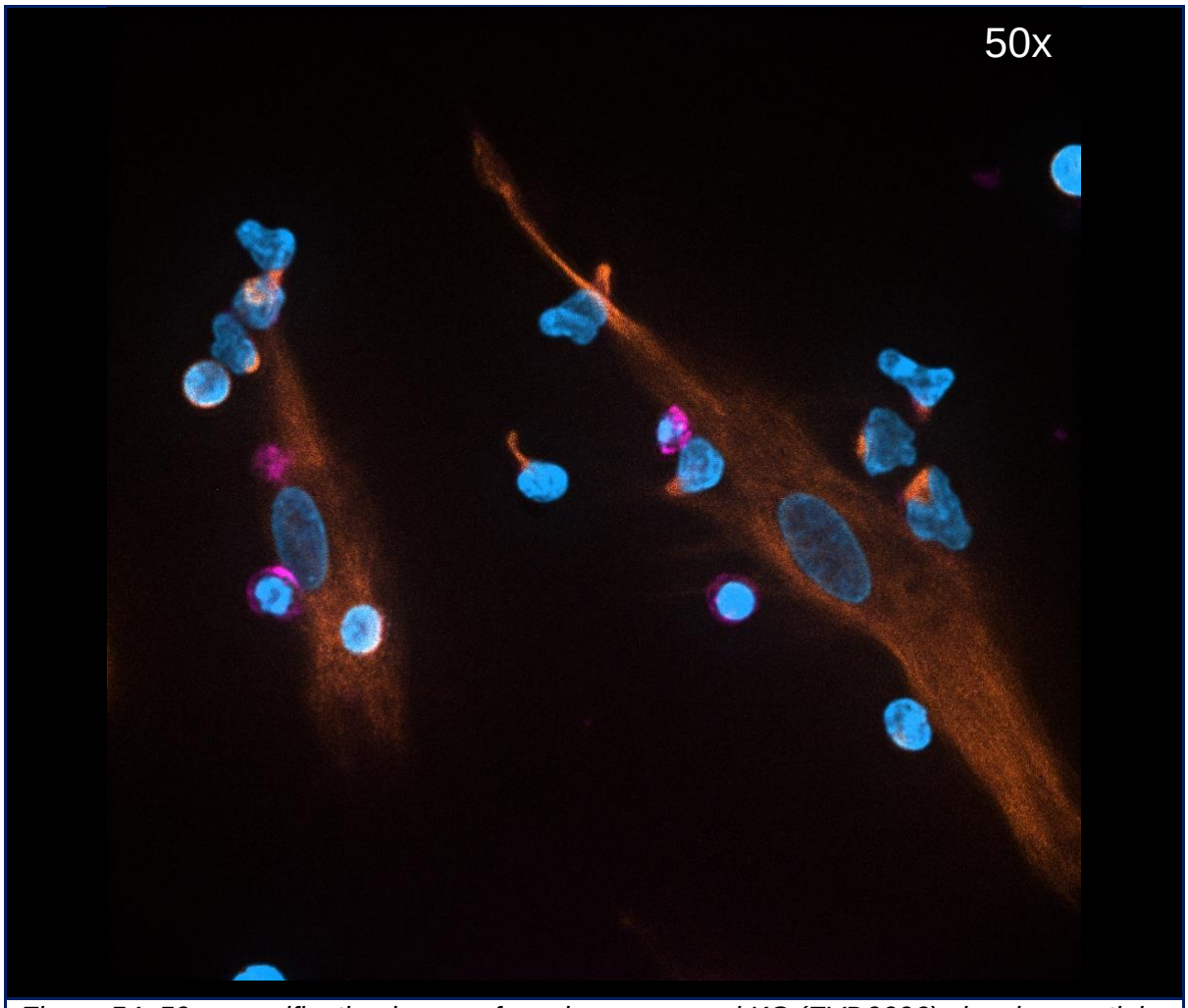

Figure 54: 50x magnification image of ex-vivo processed KC (EVD0006) showing spatial interaction between tumour cells (vimentin, orange) and immune complement (CD3, magenta). 4′,6-diamidino-2-phenylindole (DAPI)-stained nuceli appear blue.

8.2.4 DISCUSSION AND CONCLUSIONS

The primary aim of this pilot *ex-vivo* study in KC was to explore the methodological feasibility of throughput from patient tumour to quality assured endpoint CTG results. Impressively, all (10/10, 100%) of *ex-vivo* processed KCs met the defined quality assurance threshold, suggesting that the *ex-vivo* methodology can be adapted for different cancer types and that KCs potentially process with greater success than BCs. The processing methodology, as expected, had to be adapted to ensure that single cell suspensions could be yielded. In particular, KC samples acquired were typically solid and required significantly longer enzymatic dissociation periods than BCs. KCs also had lower percentage viability than BCs,

which could reflect the effects of warm ischaemia or impact of longer enzymatic incubation on tumour cells; again, highlighting some of the challenges when working with primary human tumour material. Currently, there is no clear consensus on the optimal dissociation enzyme or minimum dissociation time for KC samples. Given that collagenase enzymatic cocktails have been described in the literature to successfully yield viable suspensions from renal tumour tissue (398), these will be used moving forward with tumour dissociation.

One particularly interesting finding during tumour tissue processing was the abundance of immune complement present in some of the renal tumours. Although antibody staining was suboptimal at this stage, it was possible to identify immune complement during IFM processing through CD45 labelling and morphological differentiation Figure 54. Further work to optimise differential antibody labelling of tumour and immune cells withing suspension are required. Furthermore, it may also be possible to explore spatial interactions of the immune complement and tumour cells using IFM methods; hence, there is scope to evaluate the immunomodulatory potential of different compounds, including immunotherapies. One methodological implication limiting this would be that immune complement are non-adherent, and thus could be inadvertently removed from the cellular melieu with the addition of washing steps. However, this methodology has previously been used to derive ex-vivo 'pharmacoscopy' profiles for patients with haematological malignancies (399). Additional centrifugation steps prior to fixing and staining procedures may help to move live cells to the well bottom to minimise the likelihood of inadvertent washing/aspiration. Furthermore, this particular 2D *ex-vivo* model does not have the potential to recapitulate tumour vasculature, unlike some other 3D, tissue slice, and explant platforms (400). Hence, similar to other traditional in vitro models, may limit the ability of this model to accurately predict the anti-angiogenic effects of standard KC systemic treatments.

Although not the primary objective of this study, as all tumours met quality assurance thresholds for CTG, it was possible to explore differential drug responses mirroring the BC methodology. Although only descriptive at this stage, given the small number of tumours within the cohort, differential response profiles across the spectrum of disease could be identified. For example, RCC4 displayed very aggressive phenotypic features with almost no drug hits across the screen and the two malignant melanomas grouping in close proximity with similar responses to the MEK inhibitor AZD6244. One potential pitfall of using CTG in these cases, as described in Chapter 7, is the inability to differentiate between cell types; hence, in cases where there is an abundance of immune complement identified, the drug responses observed could correspond to immunotoxicity rather than tumour cell cytotoxicity. Therefore, for the *ex-*

vivo screening of KC drug responses, IFM-based methodology would seem the more appropriate assay, once optimised.

9. REFERENCES

1. Sung H, Ferlay J, Siegel RL, Laversanne M, Soerjomataram I, Jemal A, et al. Global Cancer Statistics 2020: GLOBOCAN Estimates of Incidence and Mortality Worldwide for 36 Cancers in 185 Countries. CA Cancer J Clin. 2021 May 1;71(3):209–49.

2. Jubber I, Ong S, Bukavina L, Black PC, Compérat E, Kamat AM, et al. Epidemiology of Bladder Cancer in 2023: A Systematic Review of Risk Factors. Eur Urol. 2023;84(2):176–90.

3. Cumberbatch MGK, Jubber I, Black PC, Esperto F, Figueroa JD, Kamat AM, et al. Epidemiology of Bladder Cancer: A Systematic Review and Contemporary Update of Risk Factors in 2018. Eur Urol. 2018 Dec 1;74(6):784–95.

4. Cumberbatch MGK, Cox A, Teare D, Catto JWF. Contemporary Occupational Carcinogen Exposure and Bladder Cancer. JAMA Oncol. 2015 Dec 1;1(9):1282.

5. Catto JWF, Rogers Z, Downing A, Mason SJ, Jubber I, Bottomley S, et al. Lifestyle Factors in Patients with Bladder Cancer: A Contemporary Picture of Tobacco Smoking, Electronic Cigarette Use, Body Mass Index, and Levels of Physical Activity. Eur Urol Focus. 2023;9(6):974–82.

6. Nassar AH, Abou Alaiwi S, AlDubayan SH, Moore N, Mouw KW, Kwiatkowski DJ, et al. Prevalence of pathogenic germline cancer risk variants in high-risk urothelial carcinoma. Genet Med 2019 224. 2019 Dec 17;22(4):709–18.

7. Rothman N, Garcia-Closas M, Chatterjee N, Malats N, Wu X, Figueroa JD, et al. A multi-stage genome-wide association study of bladder cancer identifies multiple susceptibility loci. Nat Genet. 2010 Nov 1;42(11):978–84.

8. Witjes J, Bruins H, Carrión A, Cathomas R, Compérat E, Efstathiou J, et al. Muscle-invasive and Metastatic Bladder Cancer EAU Guidelines on. 2022;

9. Compérat E, Gontero P, Liedberg F, Masson-Lecomte A, Mostafid AH, Palou J, et al. Non-muscle-invasive Bladder Cancer (TaT1 and CIS) EAU Guidelines on. 2022;

10. Humphrey PA, Moch H, Cubilla AL, Ulbright TM, Reuter VE. The 2016 WHO Classification of Tumours of the Urinary System and Male Genital Organs—Part B: Prostate and Bladder Tumours. Eur Urol. 2016 Jul 1;70(1):106–19.

11. Dahm P, Gschwend JE. Malignant Non-Urothelial Neoplasms of the Urinary Bladder: A Review. Eur Urol. 2003 Dec 1;44(6):672–81.

12. El-Sebaie M, Saad M, Grahame Z, Mokhtar A. Squamous cell carcinoma of the bilharzial and non-bilharzial urinary bladder: a review of etiological features, natural history, and management. Rev Artic Int J Clin Oncol. 2005;10:20–5.

13. Babjuk M, Burger M, Compérat E, Gontero P, Liedberg F, Masson-Lecomte A, et al. Non-muscle-invasive Bladder Cancer (TaT1 and CIS) EAU Guidelines on. 2022.

14. Bryan RT, Liu W, Pirrie SJ, Amir R, Gallagher J, Hughes AI, et al. Comparing an Imaging-guided Pathway with the Standard Pathway for Staging Muscle-invasive Bladder Cancer: Preliminary Data from the BladderPath Study. Eur Urol. 2021 Jul 1;80(1):12–5.

15. Conroy S, Hubbard R, Noon AP, Hussain SA, Griffin J, Kennish S, et al. Case of the month from the University of Sheffield, UK: Expediting definitive treatment in patients with invasive bladder cancer: an MRI-guided pathway. BJU Int. 2022 Jun 1;129(6):691–4.

16. Zeng Y, Wang A, Lv W, Wang Q, Jiang S, Pan X, et al. Recent development of urinary biomarkers for bladder cancer diagnosis and monitoring. Clin Transl Discov. 2023 Apr 1;3(2):e183.

17. Maas M, Todenhöfer T, Black PC. Urine biomarkers in bladder cancer — current status and future perspectives. Nat Rev Urol 2023. 2023 May 24;1–18.

18. Mostofi F, Sobin L, Torloni H, Organization WH. Histological typing of urinary bladder tumours. Geneva, Switzerland; 1973.

19. Delahunt B, Cheville JC, Martignoni G, Humphrey PA, Magi-Galluzzi C, McKenney J, et al. The International Society of Urological Pathology (ISUP) Grading System for Renal Cell Carcinoma and Other Prognostic Parameters. Am J Surg Pathol. 2013 Oct;37(10):1490–504.

20. Brierley J, Gospodarowicz MK, Wittekind C. TNM classification of malignant tumours. 8th ed. Wiley-Blackwell; 2016. 253 p.

21. Sylvester RJ, van der Meijden APM, Oosterlinck W, Witjes JA, Bouffioux C, Denis L, et al. Predicting Recurrence and Progression in Individual Patients with Stage Ta T1 Bladder Cancer Using EORTC Risk Tables: A Combined Analysis of 2596 Patients from Seven EORTC Trials. Eur Urol. 2006 Mar;49(3):466–77.

22. D'Andrea D, Shariat SF, Soria F, Mari A, Mertens LS, Di Trapani E, et al. The Impact of Primary Versus Secondary Muscle-invasive Bladder Cancer at Diagnosis on the Response to Neoadjuvant Chemotherapy. Eur Urol Open Sci. 2022 Jul 1;41:74–80.

23. Ge P, Wang L, Lu M, Mao L, Li W, Wen R, et al. Oncological Outcome of Primary and Secondary Muscle-Invasive Bladder Cancer: A Systematic Review and Meta-analysis. Sci Rep. 2018 Dec 1;8(1):7543.

24. Sylvester RJ, Rodríguez O, Hernández V, Turturica D, Bauerová L, Bruins HM, et al. European Association of Urology (EAU) Prognostic Factor Risk Groups for Non–muscle-invasive Bladder Cancer (NMIBC) Incorporating the WHO 2004/2016 and WHO 1973 Classification Systems for Grade: An Update from the EAU NMIBC Guidelines Panel. Eur Urol. 2021 Apr 1;79(4):480–8.

25. Woo S, Panebianco V, Narumi Y, Del Giudice F, Muglia VF, Takeuchi M, et al. Diagnostic Performance of Vesical Imaging Reporting and Data System for the Prediction of Muscle-invasive Bladder Cancer: A Systematic Review and Meta-analysis. Eur Urol Oncol. 2020 Jun 1;3(3):306–15.

26. Girard A, Vila Reyes H, Shaish H, Grellier JF, Dercle L, Salaün PY, et al. The Role of 18F-FDG PET/CT in Guiding Precision Medicine for Invasive Bladder Carcinoma. Front Oncol. 2020 Oct 6;10:6.

27. Sjodahl G, Lauss M, Lovgren K, Chebil G, Gudjonsson S, Veerla S, et al. A Molecular Taxonomy for Urothelial Carcinoma. Clin Cancer Res. 2012 Jun 15;18(12):3377–86.

28. Hedegaard J, Lamy P, Nordentoft I, Algaba F, Høyer S, Ulhøi BP, et al. Comprehensive Transcriptional Analysis of Early-Stage Urothelial Carcinoma. Cancer Cell. 2016 Jul 11;30(1):27–42.

29. Hurst CD, Alder O, Platt FM, Droop A, Stead LF, Burns JE, et al. Genomic Subtypes of Non-invasive Bladder Cancer with Distinct Metabolic Profile and Female Gender Bias in KDM6A Mutation Frequency. Cancer Cell. 2017 Nov 13;32(5):701-715.e7.

30. van Kessel KEM, van der Keur KA, Dyrskjøt L, Algaba F, Welvaart NYC, Beukers W, et al. Molecular Markers Increase Precision of the European Association of Urology Non–Muscle-Invasive Bladder Cancer Progression Risk Groups. Clin Cancer Res. 2018 Apr 1;24(7):1586–93.

31. Lindskrog SV, Prip F, Lamy P, Taber A, Groeneveld CS, Birkenkamp-Demtröder K, et al. An integrated multi-omics analysis identifies prognostic molecular subtypes of non-muscle-invasive bladder cancer. Nat Commun 2021 121. 2021 Apr 16;12(1):1–18.

32. Choi W, Porten S, Kim S, Willis D, Plimack ER, Hoffman-Censits J, et al. Identification of Distinct Basal and Luminal Subtypes of Muscle-Invasive Bladder Cancer with Different Sensitivities to Frontline Chemotherapy. Cancer Cell. 2014 Feb 10;25(2):152–65.

33. Seiler R, Ashab HAD, Erho N, van Rhijn BWG, Winters B, Douglas J, et al. Impact of Molecular Subtypes in Muscle-invasive Bladder Cancer on Predicting Response and Survival after Neoadjuvant Chemotherapy. Eur Urol. 2017 Oct;72(4):544–54.

34. Robertson AG, Kim J, Al-Ahmadie H, Bellmunt J, Guo G, Cherniack AD, et al. Comprehensive Molecular Characterization of Muscle-Invasive Bladder Cancer. Cell. 2017 Oct 19;171(3):540-556.e25.

35. Kamoun A, de Reyniès A, Allory Y, Sjödahl G, Robertson AG, Seiler R, et al. A Consensus Molecular Classification of Muscle-invasive Bladder Cancer. Eur Urol. 2020 Apr 1;77(4):420–33.

36. Tan TZ, Rouanne M, Tan KT, Huang RY-J, Thiery J-P. Molecular Subtypes of Urothelial Bladder Cancer: Results from a Meta-cohort Analysis of 2411 Tumors. Eur Urol. 2019;75(3):423–32.

37. Hedegaard J, Lamy P, Nordentoft I, Algaba F, Høyer S, Ulhøi BP, et al. Comprehensive Transcriptional

Analysis of Early-Stage Urothelial Carcinoma. Cancer Cell. 2016 Jul 11;30(1):27–42.

38. Neuzillet Y, Van Rhijn BWG, Prigoda NL, Bapat B, Liu L, Bostrom PJ, et al. FGFR3 mutations, but not FGFR3 expression and FGFR3 copy-number variations, are associated with favourable non-muscle invasive bladder cancer. Virchows Arch. 2014;465(2):207–13.

39. Linton KD, Rosario DJ, Thomas F, Rubin N, Goepel JR, Abbod MF, et al. Disease Specific Mortality in Patients with Low Risk Bladder Cancer and the Impact of Cystoscopic Surveillance. J Urol. 2013 Mar;189(3):828–33.

40. Sylvester RJ, Oosterlinck W, Holmang S, Sydes MR, Birtle A, Gudjonsson S, et al. Systematic Review and Individual Patient Data Meta-analysis of Randomized Trials Comparing a Single Immediate Instillation of Chemotherapy After Transurethral Resection with Transurethral Resection Alone in Patients with Stage pTa-pT1 Urothelial Carcinoma. Eur Urol. 2016;69:231–44.

41. NICE. Bladder cancer: risk classification in non-muscle-invasive bladder cancer. 2015;(February).

42. Tan WS, Steinberg G, Witjes JA, Li R, Shariat SF, Roupret M, et al. Intermediate-risk Non–muscle-invasive Bladder Cancer: Updated Consensus Definition and Management Recommendations from the International Bladder Cancer Group. Eur Urol Oncol. 2022 Oct 1;5(5):505–16.

43. Malmström P-U, Sylvester RJ, Crawford DE, Friedrich M, Krege S, Rintala E, et al. An Individual Patient Data Meta-Analysis of the Long-Term Outcome of Randomised Studies Comparing Intravesical Mitomycin C versus Bacillus Calmette-Guérin for Non–Muscle-Invasive Bladder Cancer. Eur Urol. 2009 Aug 1;56(2):247–56.

44. Oddens J, Brausi M, Sylvester R, Bono A, Van De Beek C, Van Andel G, et al. Final results of an EORTC-GU cancers group randomized study of maintenance bacillus Calmette-Guérin in intermediate- and high-risk Ta, T1 papillary carcinoma of the urinary bladder: one-third dose versus full dose and 1 year versus 3 years of maintenance. Eur Urol. 2013 Mar;63(3):462–72.

45. Zhao H, Chan VWS, Castellani D, Chan EOT, Ong WLK, Peng Q, et al. Intravesical Chemohyperthermia vs. Bacillus Calmette-Guerin Instillation for Intermediate- and High-Risk Non-muscle Invasive Bladder Cancer: A Systematic Review and Meta-Analysis. Front Surg , 8 , Artic 775527 . 2021 Nov 23;8.

46. Morales A. BCG: A throwback from the stone age of vaccines opened the path for bladder cancer immunotherapy. Can J Urol. 2017;24(3).

47. Martínez-Piñeiro L, Portillo JA, Fernández JM, Zabala JA, Cadierno I, Moyano JL, et al. Maintenance Therapy with 3-monthly Bacillus Calmette-Guérin for 3 Years is Not Superior to Standard Induction Therapy in High-risk Non-muscle-invasive Urothelial Bladder Carcinoma: Final Results of Randomised CUETO Study 98013. Eur Urol. 2015 Aug 1;68(2):256–62.

48. Schmidt S, Kunath F, Coles B, Draeger DL, Krabbe LM, Dersch R, et al. Intravesical Bacillus Calmette-Guérin versus mitomycin C for Ta and T1 bladder cancer. Cochrane database Syst Rev. 2020 Jan 8;1(1).

49. Cambier S, Sylvester RJ, Collette L, Gontero P, Brausi MA, Van Andel G, et al. EORTC Nomograms and Risk Groups for Predicting Recurrence, Progression, and Disease-specific and Overall Survival in Non-Muscle-invasive Stage Ta-T1 Urothelial Bladder Cancer Patients Treated with 1-3 Years of Maintenance Bacillus Calmette-Guérin. Eur Urol. 2016 Jan 1;69(1):60–9.

50. Bandari J, Maganty A, MacLeod LC, Davies BJ. Manufacturing and the Market: Rationalizing the Shortage of Bacillus Calmette-Guérin. Eur Urol Focus. 2018 Jul 1;4(4):481–4.

51. Oughton JB, Poad H, Twiddy M, Collinson M, Hiley V, Gordon K, et al. Radical cystectomy (bladder removal) against intravesical BCG immunotherapy for high-risk non-muscle invasive bladder cancer (BRAVO): a protocol for a randomised controlled feasibility study. BMJ Open. 2017 Aug 11;7(8):e017913.

52. Clements MB, Atkinson TM, Dalbagni GM, Li Y, Vickers AJ, Herr HW, et al. Health-related Quality of Life for Patients Undergoing Radical Cystectomy: Results of a Large Prospective Cohort. Eur Urol. 2022 Mar 1;81(3):294–304.

53. Mason SJ, Downing A, Wright P, Hounsome L, Bottomley SE, Corner J, et al. Health-related quality of life after treatment for bladder cancer in England. Br J Cancer. 2018 May 14;118(11):1518–28.

54. Catto JWF, Downing A, Mason S, Wright P, Absolom K, Bottomley S, et al. Quality of Life After Bladder

Cancer: A Cross-sectional Survey of Patient-reported Outcomes. Eur Urol. 2021 May 1;79(5):621–32.

55. Jubber I, Rogers Z, Catto JW, Bottomley S, Glaser A, Downing A, et al. Sexual Activity, Function and Dysfunction After a Diagnosis of Bladder Cancer. J Sex Med. 2022 Sep 1;19(9):1431–41.

56. Catto JWF, Gordon K, Collinson M, Poad H, Twiddy M, Johnson M, et al. Radical cystectomy against intravesical BCG for high-risk high-grade nonmuscle invasive bladder cancer: Results from the randomized controlled BRAVO-feasibility study. J Clin Oncol. 2021;39(3):202–14.

57. Sherif A, Holmberg L, Rintala E, Mestad O, Nilsson J, Nilsson S, et al. Neoadjuvant Cisplatinum Based Combination Chemotherapy in Patients with Invasive Bladder Cancer: A Combined Analysis of Two Nordic Studies. Eur Urol. 2004;

58. Grossman HB, Natale RB, Tangen CM, Speights VO, Vogelzang NJ, Trump DL, et al. Neoadjuvant chemotherapy plus cystectomy compared with cystectomy alone for locally advanced bladder cancer. N Engl J Med. 2003;349(9):859–66.

59. Yin M, Joshi M, Meijer RP, Glantz M, Holder S, Harvey HA, et al. Neoadjuvant Chemotherapy for Muscle-Invasive Bladder Cancer: A Systematic Review and Two-Step Meta-Analysis. Oncologist. 2016;

60. von der Maase H, Sengelov L, Roberts JT, Ricci S, Dogliotti L, Oliver T, et al. Long-Term Survival Results of a Randomized Trial Comparing Gemcitabine Plus Cisplatin, With Methotrexate, Vinblastine, Doxorubicin, Plus Cisplatin in Patients With Bladder Cancer. J Clin Oncol. 2005 Jul 20;23(21):4602–8.

61. Pfister C, Gravis G, Fléchon A, Chevreau C, Mahammedi H, Laguerre B, et al. Dose-Dense Methotrexate, Vinblastine, Doxorubicin, and Cisplatin or Gemcitabine and Cisplatin as Perioperative Chemotherapy for Patients With Nonmetastatic Muscle-Invasive Bladder Cancer: Results of the GETUG-AFU V05 VESPER Trial. J Clin Oncol. 2022 Mar 7;JCO2102051.

62. Rosenblatt R, Sherif A, Rintala E, Wahlqvist R, Ullén A, Nilsson S, et al. Pathologic downstaging is a surrogate marker for efficacy and increased survival following neoadjuvant chemotherapy and radical cystectomy for muscle-invasive urothelial bladder cancer. Eur Urol. 2012;

63. Sonpavde G, Goldman BH, Speights VO, Lerner SP, Wood DP, Vogelzang NJ, et al. Quality of pathologic response and surgery correlate with survival for patients with completely resected bladder cancer after neoadjuvant chemotherapy. Cancer. 2009;

64. Vetterlein MW, Wankowicz SAM, Seisen T, Lander R, Löppenberg B, Chun FKH, et al. Neoadjuvant chemotherapy prior to radical cystectomy for muscle-invasive bladder cancer with variant histology. Cancer. 2017 Nov 15;123(22):4346–55.

65. Veskimäe E, Espinos EL, Bruins HM, Yuan Y, Sylvester R, Kamat AM, et al. What Is the Prognostic and Clinical Importance of Urothelial and Nonurothelial Histological Variants of Bladder Cancer in Predicting Oncological Outcomes in Patients with Muscle-invasive and Metastatic Bladder Cancer? A European Association of Urology Muscle Invasive and Metastatic Bladder Cancer Guidelines Panel Systematic Review. Eur Urol Oncol. 2019 Nov 1;2(6):625–42.

66. Basile G, Bandini M, Gibb EA, Ross JS, Raggi D, Marandino L, et al. Neoadjuvant Pembrolizumab and Radical Cystectomy in Patients with Muscle-Invasive Urothelial Bladder Cancer: 3-Year Median Follow-Up Update of PURE-01 Trial. Clin Cancer Res. 2022 Dec 1;28(23):5107–14.

67. Szabados B, Kockx M, Assaf ZJ, van Dam PJ, Rodriguez-Vida A, Duran I, et al. Final Results of Neoadjuvant Atezolizumab in Cisplatin-ineligible Patients with Muscle-invasive Urothelial Cancer of the Bladder. Eur Urol. 2022 Aug 1;82(2):212–22.

68. Booth CM, Siemens DR, Li G, Peng Y, Kong W, Berman DM, et al. Curative Therapy for Bladder Cancer in Routine Clinical Practice: A Population-based Outcomes Study. Clin Oncol. 2014 Aug;26(8):506–14.

69. Witjes JA, Bruins HM, Cathomas R, Compérat EM, Cowan NC, Gakis G, et al. European Association of Urology Guidelines on Muscle-invasive and Metastatic Bladder Cancer: Summary of the 2020 Guidelines. Eur Urol. 2021 Jan 1;79(1):82–104.

70. Catto JWF, Khetrapal P, Ricciardi F, Ambler G, Williams NR, Al-Hammouri T, et al. Effect of Robot-Assisted Radical Cystectomy With Intracorporeal Urinary Diversion vs Open Radical Cystectomy on 90-Day Morbidity and Mortality Among Patients With Bladder Cancer: A Randomized Clinical Trial. JAMA. 2022 Jun 7;327(21):2092–103.

71. Nielsen ME, Mallin K, Weaver MA, Palis B, Stewart A, Winchester DP, et al. Association of hospital

volume with conditional 90-day mortality after cystectomy: an analysis of the National Cancer Data Base. BJU Int. 2014;114(1):46–55.

72. Bruins HM, Veskimae E, Hernandez V, Imamura M, Neuberger MM, Dahm P, et al. The Impact of the Extent of Lymphadenectomy on Oncologic Outcomes in Patients Undergoing Radical Cystectomy for Bladder Cancer: A Systematic Review. Eur Urol. 2014;66:1065–77.

73. Karl A, Carroll PR, Gschwend JE, Knüchel R, Montorsi F, Stief CG, et al. The Impact of Lymphadenectomy and Lymph Node Metastasis on the Outcomes of Radical Cystectomy for Bladder Cancer. Eur Urol. 2009 Apr;55(4):826–35.

74. Gschwend JE, Heck MM, Lehmann J, Rübben H, Albers P, Wolff JM, et al. Extended Versus Limited Lymph Node Dissection in Bladder Cancer Patients Undergoing Radical Cystectomy: Survival Results from a Prospective, Randomized Trial. Eur Urol. 2019 Apr 1;75(4):604–11.

75. NICE. Bladder cancer: diagnosis and management. 2015.

76. Giacalone NJ, Shipley WU, Clayman RH, Niemierko A, Drumm M, Heney NM, et al. Long-term Outcomes After Bladder-preserving Tri-modality Therapy for Patients with Muscle-invasive Bladder Cancer: An Updated Analysis of the Massachusetts General Hospital Experience. Eur Urol. 2017;

77. Milosevic M, Gospodarowicz M, Zietman A, Abbas F, Haustermans K, Moonen L, et al. Radiotherapy for Bladder Cancer. Urology. 2007;69(1, Supplement):80–92.

78. Sondergaard J, Holmberg M, Jakobsen AR, Agerbæk M, Muren LP, Hoyer M. A comparison of morbidity following conformal versus intensity-modulated radiotherapy for urinary bladder cancer. Acta Oncol (Madr). 2014;

79. Huddart RA, Hall E, Lewis R, Porta N, Crundwell M, Jenkins PJ, et al. Patient-reported Quality of Life Outcomes in Patients Treated for Muscle-invasive Bladder Cancer with Radiotherapy ± Chemotherapy in the BC2001 Phase III Randomised Controlled Trial[Formula presented]. Eur Urol. 2020 Feb 1;77(2):260–8.

80. James ND, Hussain SA, Hall E, Jenkins P, Tremlett J, Rawlings C, et al. Radiotherapy with or without chemotherapy in muscle-invasive bladder cancer. N Engl J Med. 2012;

81. Hoskin PJ, Rojas AM, Bentzen SM, Saunders MI. Radiotherapy with concurrent carbogen and nicotinamide in bladder carcinoma. J Clin Oncol. 2010;

82. Hall E, Hussain SA, Porta N, Lewis R, Crundwell M, Jenkins P, et al. Chemoradiotherapy in Muscle-invasive Bladder Cancer: 10-yr Follow-up of the Phase 3 Randomised Controlled BC2001 Trial. Eur Urol. 2022 Sep 1;82(3):273–9.

83. Suer E, Hamidi N, Gokce MI, Gulpinar O, Turkolmez K, Beduk Y, et al. Significance of second transurethral resection on patient outcomes in muscle-invasive bladder cancer patients treated with bladder-preserving multimodal therapy. World J Urol. 2016;

84. Fahmy O, Khairul-Asri MG, Schubert T, Renninger M, Malek R, Kübler H, et al. A systematic review and meta-analysis on the oncological long-term outcomes after trimodality therapy and radical cystectomy with or without neoadjuvant chemotherapy for muscle-invasive bladder cancer. Urologic Oncology: Seminars and Original Investigations. 2018.

85. Ding H, Fan N, Ning Z, Ma D. Trimodal Therapy vs. Radical Cystectomy for Muscle-Invasive Bladder Cancer: A Meta-Analysis. Front Oncol. 2020 Oct 14;10.

86. Leow JJ, Martin-Doyle W, Rajagopal PS, Patel CG, Anderson EM, Rothman AT, et al. Adjuvant Chemotherapy for Invasive Bladder Cancer: A 2013 Updated Systematic Review and Meta-Analysis of Randomized Trials. Eur Urol. 2014 Jul;66(1):42–54.

87. Burdett S, Fisher DJ, Vale CL, Bono A V., Clarke NW, Cognetti F, et al. Adjuvant Chemotherapy for Muscle-invasive Bladder Cancer: A Systematic Review and Meta-analysis of Individual Participant Data from Randomised Controlled Trials. Eur Urol. 2022 Jan 1;81(1):50–61.

88. Bajorin DF, Witjes JA, Gschwend JE, Schenker M, Valderrama BP, Tomita Y, et al. Adjuvant Nivolumab versus Placebo in Muscle-Invasive Urothelial Carcinoma. N Engl J Med. 2021 Jun 3;384(22):2102–14.

89. Bellmunt J, Hussain M, Gschwend JE, Albers P, Oudard S, Castellano D, et al. Adjuvant atezolizumab versus observation in muscle-invasive urothelial carcinoma (IMvigor010): a multicentre, open-label,

randomised, phase 3 trial. Lancet Oncol. 2021 Apr 1;22(4):525.

90. Rosenberg JE, Carroll PR, Small EJ. Update on chemotherapy for advanced bladder cancer. Journal of Urology. 2005.

91. Pfister C, Gravis G, Fléchon A, Soulié M, Guy L, Laguerre B, et al. Randomized Phase III Trial of Dose-dense Methotrexate, Vinblastine, Doxorubicin, and Cisplatin, or Gemcitabine and Cisplatin as Perioperative Chemotherapy for Patients with Muscle-invasive Bladder Cancer. Analysis of the GETUG/AFU V05 VESPER Trial Secondary Endpoints: Chemotherapy Toxicity and Pathological Responses. Eur Urol. 2021 Feb 1;79(2):214–21.

92. Galsky MD, Hahn NM, Rosenberg J, Sonpavde G, Hutson T, Oh WK, et al. Treatment of patients with metastatic urothelial cancer "Unfit" for cisplatin-based chemotherapy. Journal of Clinical Oncology. 2011.

93. De Santis M, Bellmunt J, Mead G, Kerst JM, Leahy M, Maroto P, et al. Randomized phase II/III trial assessing gemcitabine/carboplatin and methotrexate/carboplatin/vinblastine in patients with advanced urothelial cancer who are unfit for cisplatin-based chemotherapy: EORTC study 30986. J Clin Oncol. 2012;

94. Galsky MD, Arija JÁA, Bamias A, Davis ID, De Santis M, Kikuchi E, et al. Atezolizumab with or without chemotherapy in metastatic urothelial cancer (IMvigor130): a multicentre, randomised, placebo-controlled phase 3 trial. Lancet. 2020 May 16;395(10236):1547–57.

95. Powles T, Csőszi T, Özgüroğlu M, Matsubara N, Géczi L, Cheng SYS, et al. Pembrolizumab alone or combined with chemotherapy versus chemotherapy as first-line therapy for advanced urothelial carcinoma (KEYNOTE-361): a randomised, open-label, phase 3 trial. Lancet Oncol. 2021 Jul 1;22(7):931–45.

96. Powles T, van der Heijden MS, Castellano D, Galsky MD, Loriot Y, Petrylak DP, et al. Durvalumab alone and durvalumab plus tremelimumab versus chemotherapy in previously untreated patients with unresectable, locally advanced or metastatic urothelial carcinoma (DANUBE): a randomised, open-label, multicentre, phase 3 trial. Lancet Oncol. 2020 Dec 1;21(12):1574–88.

97. Powles T, Park SH, Voog E, Caserta C, Valderrama BP, Gurney H, et al. Avelumab Maintenance Therapy for Advanced or Metastatic Urothelial Carcinoma. N Engl J Med. 2020 Sep 24;383(13):1218–30.

98. Witjes A, Lebret T, Compérat EM, Cowan NC, De Santis M, Bruins HM, et al. Updated 2016 EAU Guidelines on Muscle-invasive and Metastatic Bladder Cancer. Eur Urol. 2017;

99. Oing C, Rink M, Oechsle K, Seidel C, Von Amsberg G, Bokemeyer C. Second Line Chemotherapy for Advanced and Metastatic Urothelial Carcinoma: Vinflunine and beyond - A Comprehensive Review of the Current Literature. Journal of Urology. 2016.

100. Raggi D, Miceli R, Sonpavde G, Giannatempo P, Mariani L, Galsky MD, et al. Second-line single-agent versus doublet chemotherapy as salvage therapy for metastatic urothelial cancer: A systematic review and meta-analysis. Ann Oncol. 2016;

101. Powles T, Durán I, van der Heijden MS, Loriot Y, Vogelzang NJ, De Giorgi U, et al. Atezolizumab versus chemotherapy in patients with platinum-treated locally advanced or metastatic urothelial carcinoma (IMvigor211): a multicentre, open-label, phase 3 randomised controlled trial. Lancet (London, England). 2018;391(10122):748–57.

102. Bellmunt J, de Wit R, Vaughn DJ, Fradet Y, Lee J-L, Fong L, et al. Pembrolizumab as Second-Line Therapy for Advanced Urothelial Carcinoma. N Engl J Med. 2017 Mar 16;376(11):1015–26.

103. Powles T, Rosenberg JE, Sonpavde GP, Loriot Y, Durán I, Lee J-L, et al. Enfortumab Vedotin in Previously Treated Advanced Urothelial Carcinoma. N Engl J Med. 2021 Mar 25;384(12):1125–35.

104. Loriot Y, Necchi A, Park SH, Garcia-Donas J, Huddart R, Burgess E, et al. Erdafitinib in Locally Advanced or Metastatic Urothelial Carcinoma. N Engl J Med. 2019 Jul 25;381(4):338–48.

105. Catto JWF, Mandrik O, Quayle LA, Hussain SA, McGrath J, Cresswell J, et al. Diagnosis, treatment and survival from bladder, upper urinary tract, and urethral cancers: real-world findings from NHS England between 2013 and 2019. BJU Int. 2023 Feb 7;12:14.

106. Sylvester RJ, van der Meijden APM, Oosterlinck W, Witjes JA, Bouffioux C, Denis L, et al. Predicting Recurrence and Progression in Individual Patients with Stage Ta T1 Bladder Cancer Using EORTC Risk Tables: A Combined Analysis of 2596 Patients from Seven EORTC Trials. Eur Urol. 2006 Mar

1;49(3):466–77.

107. Reesink DJ, van de Garde EMW, Peters BJM, van der Nat PB, Los M, Horenblas S, et al. Treatment patterns and clinical outcomes of chemotherapy treatment in patients with muscle-invasive or metastatic bladder cancer in the Netherlands. Sci Rep. 2020 Dec 25;10(1):15822.

108. Petrelli F, Coinu A, Cabiddu M, Ghilardi M, Vavassori I, Barni S. Correlation of Pathologic Complete Response with Survival After Neoadjuvant Chemotherapy in Bladder Cancer Treated with Cystectomy: A Meta-analysis. Eur Urol. 2014 Feb;65(2):350–7.

109. Noon AP, Albertsen PC, Thomas F, Rosario DJ, Catto JWF. Competing mortality in patients diagnosed with bladder cancer: evidence of undertreatment in the elderly and female patients. Br J Cancer. 2013 Apr 16;108(7):1534–40.

110. Eylert M, Hounsome L, Persad R, Bahl A, Jefferies E, Verne J, et al. Falling bladder cancer incidence from 1990 to 2009 is not producing universal mortality improvements. J Clin Urol. 2014 Mar 9;7(2):90–8.

111. Ferlay J, Shin HR, Bray F, Forman D, Mathers C, Parkin DM. Estimates of worldwide burden of cancer in 2008: GLOBOCAN 2008. Int J Cancer. 2010;127(12):2893–917.

112. Matulay JT, Soloway M, Witjes JA, Buckley R, Persad - R, Lamm DL, et al. Risk-adapted management of low-grade bladder tumours: recommendations from the International Bladder Cancer Group (IBCG). BJU Int. 2020 Apr 1;125(4):497–505.

113. Musat MG, Kwon CS, Masters E, Sikirica S, Pijush DB, Forsythe A. Treatment Outcomes of High-Risk Non-Muscle Invasive Bladder Cancer (HR-NMIBC) in Real-World Evidence (RWE) Studies: Systematic Literature Review (SLR). Clin Outcomes Res CEOR. 2022;14:35.

114. Ploussard G, Shariat SF, Dragomir A, Kluth LA, Xylinas E, Masson-Lecomte A, et al. Conditional Survival After Radical Cystectomy for Bladder Cancer: Evidence for a Patient Changing Risk Profile over Time. Eur Urol. 2014 Aug 1;66(2):361–70.

115. Vlaming M, Kiemeney LALM, van der Heijden AG. Survival after radical cystectomy: progressive versus de novo muscle invasive bladder cancer. Cancer Treat Res Commun. 2020 Dec 4;100264.

116. Shah B, Mandal R. Survival trends in metastatic bladder cancer in the United States: A population based study. J Cancer Res Ther. 2015 Jan 1;11(1):124.

117. Yeung C, Dinh T, Lee J. The Health Economics of Bladder Cancer: An Updated Review of the Published Literature. Pharmacoeconomics. 2014 Nov 24;32(11):1093–104.

118. Cox E, Saramago P, Kelly J, Porta N, Hall E, Tan WS, et al. Effects of Bladder Cancer on UK Healthcare Costs and Patient Health-Related Quality of Life: Evidence From the BOXIT Trial. Clin Genitourin Cancer. 2020 Aug 1;18(4):e418.

119. Leal J, Luengo-Fernandez R, Sullivan R, Witjes JA. Economic Burden of Bladder Cancer Across the European Union. Eur Urol. 2016 Mar;69(3):438–47.

120. Saunders CL, Abel GA, Lyratzopoulos G. Inequalities in reported cancer patient experience by socio-demographic characteristic and cancer site: evidence from respondents to the English Cancer Patient Experience Survey. Eur J Cancer Care (Engl). 2015 Jan 1;24(1):85–98.

121. Edmondson AJ, Birtwistle JC, Catto JWF, Twiddy M. The patients' experience of a bladder cancer diagnosis: a systematic review of the qualitative evidence. J Cancer Surviv. 2017 Aug 17;11(4):453–61.

122. Sabnis AJ, Bivona TG. Principles of Resistance to Targeted Cancer Therapy: Lessons from Basic and Translational Cancer Biology. Trends Mol Med. 2019/01/29. 2019;25(3):185–97.

123. Paul SM, Mytelka DS, Dunwiddie CT, Persinger CC, Munos BH, Lindborg SR, et al. How to improve R&D productivity: the pharmaceutical industry's grand challenge. Nat Rev Drug Discov. 2010 Mar 19;9(3):203–14.

124. Johnson JI, Decker S, Zaharevitz D, Rubinstein L V., Venditti JM, Schepartz S, et al. Relationships between drug activity in NCI preclinical in vitro and in vivo models and early clinical trials. Br J Cancer. 2001 May 18;84(10):1424–31.

125. Williams ST, Wells G, Conroy S, Gagg H, Allen R, Rominiyi O, et al. Precision oncology using ex vivo technology: a step towards individualised cancer care? Expert Rev Mol Med. 2022 Oct 3;1–48.

126. Zuiverloon TCM, de Jong FC, Costello JC, Theodorescu D. Systematic Review: Characteristics and Preclinical Uses of Bladder Cancer Cell Lines. Bl Cancer. 2018 Apr 26;4(2):169–83.

127. Nickerson ML, Witte N, Im KM, Turan S, Owens C, Misner K, et al. Molecular analysis of urothelial cancer cell lines for modeling tumor biology and drug response. Oncogene. 2017 Jan 5;36(1):35–46.

128. Warrick JI, Walter V, Yamashita H, Chung E, Shuman L, Amponsa VO, et al. FOXA1, GATA3 and PPARɣ Cooperate to Drive Luminal Subtype in Bladder Cancer: A Molecular Analysis of Established Human Cell Lines. Sci Rep. 2016;6:38531.

129. Williams PD, Lee JK, Theodorescu D. Molecular credentialing of rodent bladder carcinogenesis models. Neoplasia. 2008 Aug;10(8):838–46.

130. Lepikhova T, Karhemo PR, Louhimo R, Yadav B, Murumägi A, Kulesskiy E, et al. Drug-Sensitivity Screening and Genomic Characterization of 45 HPV-Negative Head and Neck Carcinoma Cell Lines for Novel Biomarkers of Drug Efficacy. Mol Cancer Ther. 2018/07/05. 2018;17(9):2060–71.

131. Stringer BW, Day BW, D'Souza RCJ, Jamieson PR, Ensbey KS, Bruce ZC, et al. A reference collection of patient-derived cell line and xenograft models of proneural, classical and mesenchymal glioblastoma. Sci Rep. 2019/03/22. 2019;9(1):4902.

132. Kim M, Mun H, Sung CO, Cho EJ, Jeon HJ, Chun SM, et al. Patient-derived lung cancer organoids as in vitro cancer models for therapeutic screening. Nat Commun. 2019/09/07. 2019;10(1):3991.

133. Kettunen K, Boström PJ, Lamminen T, Heinosalo T, West G, Saarinen I, et al. Personalized Drug Sensitivity Screening for Bladder Cancer Using Conditionally Reprogrammed Patient-derived Cells. Eur Urol. 2019 Oct 1;76(4):430–4.

134. Crystal AS, Shaw AT, Sequist L V, Friboulet L, Niederst MJ, Lockerman EL, et al. Patient-derived models of acquired resistance can identify effective drug combinations for cancer. Science. 2014 Dec 19;346(6216):1480–6.

135. Rantala JK, Arjonen A, Hakkarainen H, Kononen J, Rantala JK, Hollmén M, et al. Ex Vivo Modelling of Therapy Efficacy for Rare Krukenberg Tumors – A Report of Two Cases. Clin Oncol Res. 2020 Jul 1;2020(7):1–8.

136. Mäkelä R, Arjonen A, Suryo Rahmanto A, Härmä V, Lehtiö J, Kuopio T, et al. Ex vivo assessment of targeted therapies in a rare metastatic epithelial-myoepithelial carcinoma. Neoplasia. 2020 Jul 6;22(9):390–8.

137. Arjonen A, Mäkelä R, Härmä V, Rintanen N, Kuopio T, Kononen J, et al. Image-based ex vivo drug screen to assess targeted therapies in recurrent thymoma. Lung Cancer. 2020/05/11. 2020;145:27–32.

138. Mäkelä R, Arjonen A, Härmä V, Rintanen N, Paasonen L, Paprotka T, et al. Ex vivo modelling of drug efficacy in a rare metastatic urachal carcinoma. BMC Cancer. 2020 Dec 23;20(1):590.

139. John BA, Said N. Insights from animal models of bladder cancer: recent advances, challenges, and opportunities. Oncotarget. 2017 Aug 22;8(34):57766–81.

140. Lamont FR, Tomlinson DC, Cooper PA, Shnyder SD, Chester JD, Knowles MA. Small molecule FGF receptor inhibitors block FGFR-dependent urothelial carcinoma growth in vitro and in vivo. Br J Cancer. 2011 Jan 4;104(1):75–82.

141. Szepeshazi K, Schally A V., Keller G, Block NL, Benten D, Halmos G, et al. Receptor-targeted therapy of human experimental urinary bladder cancers with cytotoxic LH-RH analog AN-152 (AEZS-108). Oncotarget. 2012;3(7):686–99.

142. Hayashi T, Seiler R, Oo HZ, Jäger W, Moskalev I, Awrey S, et al. Targeting HER2 with T-DM1, an antibody cytotoxic drug conjugate, is effective in HER2 over expressing bladder cancer. J Urol. 2015 Oct 1;194(4):1120–31.

143. Inoue K, Slaton JW, Davis DW, Hicklin DJ, McConkey DJ, Karashima T, et al. Treatment of Human Metastatic Transitional Cell Carcinoma of the Bladder in a Murine Model with the Anti-Vascular Endothelial Growth Factor Receptor Monoclonal Antibody DC101 and Paclitaxel. Clin Cancer Res. 2000;6(7).

144. Yang X, Kessler E, Su LJ, Thorburn A, Frankel AE, Li Y, et al. Diphtheria toxin-epidermal growth factor fusion protein DAB 389EGF for the treatment of bladder cancer. Clin Cancer Res. 2013 Jan 1;19(1):148–

57.

145. Ruan JL, Hsu JW, Browning RJ, Stride E, Yildiz YO, Vojnovic B, et al. Mouse Models of Muscle-invasive Bladder Cancer: Key Considerations for Clinical Translation Based on Molecular Subtypes. Vol. 2, European Urology Oncology. Elsevier B.V.; 2019. p. 239–47.

146. Noguera-Ortega E, Secanella-Fandos S, Eraña H, Gasión J, Rabanal RM, Luquin M, et al. Nonpathogenic Mycobacterium brumae Inhibits Bladder Cancer Growth In Vitro, Ex Vivo, and In Vivo. Eur Urol Focus. 2016 Apr 1;2(1):67–76.

147. Potts KG, Irwin CR, Favis NA, Pink DB, Vincent KM, Lewis JD, et al. Deletion of F4L (ribonucleotide reductase) in vaccinia virus produces a selective oncolytic virus and promotes anti-tumor immunity with superior safety in bladder cancer models . EMBO Mol Med. 2017 May;9(5):638–54.

148. Noguera-Ortega E, Rabanal RM, Gómez-Mora E, Cabrera C, Luquin M, Julián E. Intravesical Mycobacterium brumae triggers both local and systemic immunotherapeutic responses against bladder cancer in mice. Sci Rep. 2018 Dec 1;8(1):1–9.

149. Wang L, Saci A, Szabo PM, Chasalow SD, Castillo-Martin M, Domingo-Domenech J, et al. EMT- and stroma-related gene expression and resistance to PD-1 blockade in urothelial cancer. Vol. 9, Nature communications. Lippincott Williams and Wilkins; 2018. p. 3503.

150. Ciamporcero E, Shen H, Ramakrishnan S, Yu Ku S, Chintala S, Shen L, et al. YAP activation protects urothelial cell carcinoma from treatment-induced DNA damage. Oncogene. 2016 Mar 24;35(12):1541–53.

151. Wang F, Zhang H, Ma AH, Yu W, Zimmermann M, Yang J, et al. COX-2/sEH dual inhibitor PTUPB potentiates the antitumor efficacy of cisplatin. Mol Cancer Ther. 2018 Feb 1;17(2):474–83.

152. Ooki A, Del Carmen Rodriguez Pena M, Marchionni L, Dinalankara W, Begum A, Hahn NM, et al. YAP1 and COX2 coordinately regulate urothelial cancer stem-like cells. Cancer Res. 2018 Jan 1;78(1):168–81.

153. Martin KA, Hum NR, Sebastian A, He W, Siddiqui S, Ghosh PM, et al. Methionine adenosyltransferase 1a (MAT1A) enhances cell survival during chemotherapy treatment and is associated with drug resistance in bladder cancer PDX mice. Int J Mol Sci. 2019 Oct 2;20(20):4983.

154. Kita Y, Hamada A, Saito R, Teramoto Y, Tanaka R, Takano K, et al. Systematic chemical screening identifies disulfiram as a repurposed drug that enhances sensitivity to cisplatin in bladder cancer: a summary of preclinical studies. Br J Cancer. 2019 Dec 10;121(12):1027–38.

155. Guo J, Lv J, Chang S, Chen Z, Lu W, Xu C, et al. Inhibiting cytoplasmic accumulation of HuR synergizes genotoxic agents in urothelial carcinoma of the bladder. Oncotarget. 2016;7(29):45249–62.

156. Wei L, Chintala S, Ciamporcero E, Ramakrishnan S, Elbanna M, Wang J, et al. Genomic profiling is predictive of response to cisplatin treatment but not to PI3K inhibition in bladder cancer patient-derived xenografts. Oncotarget. 2016;7(47):76374–89.

157. Cirone P, Andresen CJ, Eswaraka JR, Patrick ·, Lappin B, Cedo ·, et al. Patient-derived xenografts reveal limits to PI3K/mTOR-and MEK-mediated inhibition of bladder cancer. Cancer Chemother Pharmacol. 2014;3:525–38.

158. Pan CX, Zhang H, Tepper CG, Lin TY, Davis RR, Keck J, et al. Development and characterization of bladder cancer patient- derived xenografts for molecularly guided targeted therapy. PLoS One. 2015 Aug 13;10(8):e0134346.

159. Zeng XS, Y. Z, W. Y, H. Z, T.-Y. L, W. S, et al. The phosphatidylinositol 3-kinase pathway as a potential therapeutic target in bladder cancer. Clin Cancer Res. 2017;23(21):6580–91.

160. Wu M, Sheng L, Cheng M, Zhang H, Jiang Y, Lin S, et al. Low doses of decitabine improve the chemotherapy efficacy against basal-like bladder cancer by targeting cancer stem cells. Oncogene. 2019 Jul 4;38(27):5425–39.

161. Bernardo C, Santos LL. Patient-derived bladder cancer xenografts. In: Methods in Molecular Biology. Humana Press Inc.; 2018. p. 169–75.

162. He F, Mo L, Zheng XY, Hu C, Lepor H, Lee EY, et al. Deficiency of pRb family proteins and p53 in invasive urothelial tumorigenesis. Cancer Res. 2009/12/03. 2009;69(24):9413–21.

163. Ahmad I, Patel R, Liu Y, Singh LB, Taketo MM, Wu XR, et al. Ras mutation cooperates with beta-catenin activation to drive bladder tumourigenesis. Cell Death Dis. 2011/03/04. 2011;2:e124.

164. Puzio-Kuter AM, Castillo-Martin M, Kinkade CW, Wang X, Shen TH, Matos T, et al. Inactivation of p53 and Pten promotes invasive bladder cancer. Genes Dev. 2009/03/06. 2009;23(6):675–80.

165. Seager CM, Puzio-Kuter AM, Patel T, Jain S, Cordon-Cardo C, Mc Kiernan J, et al. Intravesical delivery of rapamycin suppresses tumorigenesis in a mouse model of progressive bladder cancer. Cancer Prev Res. 2009/12/03. 2009;2(12):1008–14.

166. Camargo JA, Passos GR, Ferrari KL, Billis A, Saad MJA, Reis LO. Intravesical Immunomodulatory Imiquimod Enhances Bacillus Calmette-Guérin Downregulation of Nonmuscle-invasive Bladder Cancer. Clin Genitourin Cancer. 2018;16(3):e587–93.

167. Fantini D, Glaser AP, Rimar KJ, Wang Y, Schipma M, Varghese N, et al. A Carcinogen-induced mouse model recapitulates the molecular alterations of human muscle invasive bladder cancer. Oncogene. 2018 Apr 25;37(14):1911–25.

168. Rebouissou S, Bernard-Pierrot I, De Reyniès A, Lepage M-L, Krucker C, Chapeaublanc E, et al. EGFR as a potential therapeutic target for a subset of muscle-invasive bladder cancers presenting a basal-like phenotype. Sci Transl Med. 2014;6(244):244ra91.

169. Durek C, Brandau S, Ulmer AJ, Flad H-D, Jocham D, Bohle A. Bacillus-Calmette-Guerin (BCG) and 3D tumors: an in vitro model for the study of adhesion and invasion. J Urol. 1999;162(2):600–5.

170. Kilani RT, Tamimi Y, Karmali S, Mackey J, Hanel EG, Wong KK, et al. Selective cytotoxicity of gemcitabine in bladder cancer cell lines. Anticancer Drugs. 2002;13:557–66.

171. Lottner C, Knuechel R, Bernhardt G, Brunner H. Distribution and subcellular localization of a water-soluble hematoporphyrin-platinum(II) complex in human bladder cancer cells. Cancer Lett. 2004;215:167–77.

172. Moibi JA, Mak AL, Sun B, Moore RB. Urothelial cancer cell response to combination therapy of gemcitabine and TRAIL. Int J Oncol. 2011/05/04. 2011;39(1):61–71.

173. Ojha R, Jha V, Singh S, Bhattacharyya S. Autophagy inhibition suppresses the tumorigenic potential of cancer stem cell enriched side population in bladder cancer. Biochim Biophys Acta. 2014 Nov 1;1842(11):2073–86.

174. Yoshida T, Sopko NA, Kates M, Liu X, Joice G, Mcconkey DJ, et al. Impact of spheroid culture on molecular and functional characteristics of bladder cancer cell lines. Oncol Lett. 2019 Nov 1;18(5):4923–9.

175. Kim MJ, Chi BH, Yoo JJ, Ju YM, Whang YM, Chang IH. Structure establishment of three-dimensional (3D) cell culture printing model for bladder cancer. PLoS One. 2019 Oct 1;14(10):e0223689.

176. Yoshida T, Okuyama H, Nakayama M, Endo H, Nonomura N, Nishimura K, et al. High-dose chemotherapeutics of intravesical chemotherapy rapidly induce mitochondrial dysfunction in bladder cancer-derived spheroids. Cancer Sci. 2015 Jan 1;106(1):69.

177. Hyung Lee S, Hu W, Matulay JT, Silva M V, Owczarek TB, Kim K, et al. Tumor evolution and drug response in patient-derived organoid models of bladder cancer. Cell. 2018;173(2):515–28.

178. Lee SH, Hu W, Matulay JT, Silva M V., Owczarek TB, Kim K, et al. Tumor Evolution and Drug Response in Patient-Derived Organoid Models of Bladder Cancer. Cell. 2018;173(2):515-528.e17.

179. Karekla E, Liao WJ, Sharp B, Pugh J, Reid H, Quesne JL, et al. Ex Vivo Explant Cultures of Non-Small Cell Lung Carcinoma Enable Evaluation of Primary Tumor Responses to Anticancer Therapy. Cancer Res. 2017/02/17. 2017;77(8):2029–39.

180. Kelly JD, Williamson KE, Weir HP, Mcmanus DT, Hamilton PW, Keane PF, et al. Induction of apoptosis by mitomycin-C in an ex vivo model of bladder cancer. 2000;

181. Schmittgen TD, Wientjes MG, Badalament RA, Au2 JL-S. Pharmacodynamics of Mitomycin C in Cultured Human Bladder Tumors. Cancer Res. 1991;51:3849–56.

182. Bolenz C, Ikinger E-M, Ströbel P, Trojan L, Steidler A, Fernández MI, et al. Topical Chemotherapy in Human Urothelial Carcinoma Explants: A Novel Translational Tool for Preclinical Evaluation of

Experimental Intravesical Therapies. Eur Urol. 2009;56(3):504–11.

183. Muthuswamy R, Wang L, Pitteroff J, Gingrich JR, Kalinski P. Combination of IFNα and poly-I:C reprograms bladder cancer microenvironment for enhanced CTL attraction. J Immunother Cancer. 2015;3:6.

184. Ojha R, Singh SK, Bhattacharyya S. JAK-mediated autophagy regulates stemness and cell survival in cisplatin resistant bladder cancer cells. Biochim Biophys Acta. 2016;1860:2484–97.

185. Van Den Tempel N, Naipal KAT, Raams A, Van Gent DC, Franckena M, Boormans JL, et al. Ex vivo assays to predict enhanced chemosensitization by hyperthermia in urothelial cancer of the bladder. PLoS One. 2018;13(12):e0209101.

186. Neal JT, Li X, Zhu J, Giangarra V, Grzeskowiak CL, Ju J, et al. Organoid Modeling of the Tumor Immune Microenvironment. Cell. 2018 Dec 13;175(7):1972-1988.e16.

187. Van De Merbel AF, Van Der Horst G, Van Der Mark MH, Van Uhm JIM, Van Gennep EJ, Kloen P, et al. An ex vivo tissue culture model for the assessment of individualized drug responses in prostate and bladder cancer. Front Oncol. 2018;8(OCT).

188. Relph K, Annels N, Smith C, Kostalas M, Pandha H. Oncolytic Immunotherapy for Bladder Cancer Using Coxsackie A21 Virus: Using a Bladder Tumor Precision-Cut Slice Model System to Assess Viral Efficacy. Methods Mol Biol. 2020;2058:249–59.

189. Annels NE, Arif M, Simpson GR, Denyer M, Moller-Levet C, Mansfield D, et al. Oncolytic Immunotherapy for Bladder Cancer Using Coxsackie A21 Virus. Mol Ther - Oncolytics. 2018 Jun 29;9:1–12.

190. Workman P, Aboagye EO, Balkwill F, Balmain A, Bruder G, Chaplin DJ, et al. Guidelines for the welfare and use of animals in cancer research. Br J Cancer. 2010 May 5;102(11):1555.

191. The University of Sheffield. Facts and figures on animal research [Internet]. 2023 [cited 2023 Jul 18]. Available from: https://www.sheffield.ac.uk/research-services/ethics-integrity/animal-research/facts

192. United States Environmental Protection Agency. Laboratories for the 21st Century: An Introduction to Low-Energy Design. 2008.

193. Urbina MA, Watts AJR, Reardon EE. Labs should cut plastic waste too. Nat 2015 5287583. 2015 Dec 23;528(7583):479–479.

194. Greever C, Ramirez-Aguilar K, Connelly J. Connections between laboratory research and climate change: what scientists and policy makers can do to reduce environmental impacts. FEBS Lett. 2020 Oct 1;594(19):3079–85.

195. The University of Sheffield. Green Impact Statement [Internet]. 2023 [cited 2023 Jul 18]. Available from: https://www.sheffield.ac.uk/sustainability/green-impact

196. Swords RT, Azzam D, Al-Ali H, Lohse I, Volmar CH, Watts JM, et al. Ex-vivo sensitivity profiling to guide clinical decision making in acute myeloid leukemia: A pilot study. Leuk Res. 2017/11/28. 2018;64:34–41.

197. Malani D, Kumar A, Brück O, Kontro M, Yadav B, Hellesøy M, et al. Implementing a Functional Precision Medicine Tumor Board for Acute Myeloid Leukemia. Cancer Discov. 2021/11/19. 2022;12(2):388–401.

198. Snijder B, Vladimer GI, Krall N, Miura K, Schmolke AS, Kornauth C, et al. Image-based ex-vivo drug screening for patients with aggressive haematological malignancies: interim results from a single-arm, open-label, pilot study. Lancet Haematol. 2017/11/21. 2017;4(12):e595–606.

199. Kornauth C, Pemovska T, Vladimer GI, Bayer G, Bergmann M, Eder S, et al. Functional Precision Medicine Provides Clinical Benefit in Advanced Aggressive Hematological Cancers and Identifies Exceptional Responders. Cancer Discov. 2021 Oct 11;candisc.0538.2021.

200. Blom K, Nygren P, Alvarsson J, Larsson R, Andersson CR. Ex Vivo Assessment of Drug Activity in Patient Tumor Cells as a Basis for Tailored Cancer Therapy. J Lab Autom. 2016 Feb 5;21(1):178–87.

201. Martin SZ, Wagner DC, Hörner N, Horst D, Lang H, Tagscherer KE, et al. Ex vivo tissue slice culture system to measure drug-response rates of hepatic metastatic colorectal cancer. BMC Cancer. 2019 Dec 1;19(1):1030.

202. Novo SM, Wedge SR, Stark LA. Ex vivo treatment of patient biopsies as a novel method to assess

colorectal tumour response to the MEK1/2 inhibitor, Selumetinib. Sci Rep. 2017;7(1):12020.

203. Flørenes VA, Flem-Karlsen K, McFadden E, Bergheim IR, Nygaard V, Nygård V, et al. A Three-dimensional Ex Vivo Viability Assay Reveals a Strong Correlation Between Response to Targeted Inhibitors and Mutation Status in Melanoma Lymph Node Metastases. Transl Oncol. 2019 Jul;12(7):951–8.

204. Friedman AA, Xia Y, Trippa L, Le LP, Igras V, Frederick DT, et al. Feasibility of Ultra-High-Throughput Functional Screening of Melanoma Biopsies for Discovery of Novel Cancer Drug Combinations. Clin Cancer Res. 2017 Aug 15;23(16):4680–92.

205. Skaga E, Kulesskiy E, Brynjulvsen M, Sandberg CJ, Potdar S, Langmoen IA, et al. Feasibility study of using high-throughput drug sensitivity testing to target recurrent glioblastoma stem cells for individualized treatment. Clin Transl Med. 2019 Dec 30;8(1):1–15.

206. Kelly JD, Williamson KE, Weir HP, McManus DT, Hamilton PW, Keane PF, et al. Induction of apoptosis by mitomycin-C in an ex vivo model of bladder cancer. BJU Int. 2001 Dec 24;85(7):911–7.

207. van de Merbel AF, van der Horst G, van der Mark MH, van Uhm JIM, van Gennep EJ, Kloen P, et al. An ex vivo Tissue Culture Model for the Assessment of Individualized Drug Responses in Prostate and Bladder Cancer. Front Oncol. 2018;8:400.

208. Beltran H, Eng K, JM M, Sigaras A, Romanel A, Rennert H, et al. Whole-Exome Sequencing of Metastatic Cancer and Biomarkers of Treatment Response. JAMA Oncol. 2015;1(4):466–74.

209. Kato S, Kim KH, Lim HJ, Boichard A, Nikanjam M, Weihe E, et al. Real-world data from a molecular tumor board demonstrates improved outcomes with a precision N-of-One strategy. Nat Commun. 2020 Dec 1;11(1).

210. Kris MG, Johnson BE, Berry LD, Kwiatkowski DJ, Iafrate AJ, Wistuba II, et al. Using multiplexed assays of oncogenic drivers in lung cancers to select targeted drugs. JAMA. 2014 May 21;311(19):1998–2006.

211. Clark NA, Hafner M, Kouril M, Williams EH, Muhlich JL, Pilarczyk M, et al. GRcalculator: an online tool for calculating and mining dose-response data. BMC Cancer. 2017 Oct 24;17(1):698.

212. Kolde R. Package “pheatmap.” 2022.

213. Mayakonda A, Lin DC, Assenov Y, Plass C, Koeffler HP. Maftools: efficient and comprehensive analysis of somatic variants in cancer. Genome Res. 2018 Nov 1;28(11):1747–56.

214. Gagg H, Williams ST, Conroy S, Myers KN, McGarrity-Cottrell C, Jones C, et al. Ex-vivo drug screening of surgically resected glioma stem cells to replace murine avatars and provide personalise cancer therapy for glioblastoma patients. F1000Research 2023 12954. 2023 Aug 8;12:954.

215. Arjonen A, Mäkelä R, Härmä V, Rintanen N, Kuopio T, Kononen J, et al. Image-based ex vivo drug screen to assess targeted therapies in recurrent thymoma. Lung Cancer. 2020;145:27–32.

216. Riss TL, Moravec RA, Niles AL, Duellman S, Benink HA, Worzella TJ, et al. Cell Viability Assays. Assay Guid Man. 2016 Jul 1;

217. Garcia M, Juhos S, Larsson M, Olason PI, Martin M, Eisfeldt J, et al. Sarek: A portable workflow for whole-genome sequencing analysis of germline and somatic variants. F1000Research. 2020 Sep 4;9:63.

218. Overbeek R, Begley T, Butler RM, Choudhuri J V., Chuang HY, Cohoon M, et al. The subsystems approach to genome annotation and its use in the project to annotate 1000 genomes. Nucleic Acids Res. 2005;33(17):5691–702.

219. Beam A, Motsinger-Reif A. Beyond IC50s: Towards Robust Statistical Methods for in vitro Association Studies. J Pharmacogenomics Pharmacoproteomics. 2014;5(1):1000121.

220. Shockley KR. Quantitative high-throughput screening data analysis: challenges and recent advances. Drug Discov Today. 2015;20(3):296.

221. Al-Khayal K, Vaali-Mohammed MA, Elwatidy M, Bin Traiki T, Al-Obeed O, Azam M, et al. A novel coordination complex of platinum (PT) induces cell death in colorectal cancer by altering redox balance and modulating MAPK pathway. BMC Cancer. 2020 Jul 23;20(1).

222. De Mattos SF, Villalonga P, Clardy J, Lam EWF. FOXO3a mediates the cytotoxic effects of cisplatin in

colon cancer cells. Mol Cancer Ther. 2008 Oct 1;7(10):3237.

223. Ahmed D, Eide PW, Eilertsen IA, Danielsen SA, Eknæs M, Hektoen M, et al. Epigenetic and genetic features of 24 colon cancer cell lines. Oncogenesis. 2013;2(9):e71.

224. Larsson P, Engqvist H, Biermann J, Werner Rönnerman E, Forssell-Aronsson E, Kovács A, et al. Optimization of cell viability assays to improve replicability and reproducibility of cancer drug sensitivity screens. Sci Reports 2020 101. 2020 Apr 2;10(1):1–12.

225. Ertl IE, Lemberger U, Ilijazi D, Hassler MR, Bruchbacher A, Brettner R, et al. Molecular and Pharmacological Bladder Cancer Therapy Screening: Discovery of Clofarabine as a Highly Active Compound. Eur Urol (in Press. 2022;

226. PUCK TT, CIECIURA SJ, ROBINSON A. GENETICS OF SOMATIC MAMMALIAN CELLS : III. LONG-TERM CULTIVATION OF EUPLOID CELLS FROM HUMAN AND ANIMAL SUBJECTS. J Exp Med. 1958 Nov 11;108(6):945.

227. Subbiahanadar Chelladurai K, Selvan Christyraj JD, Rajagopalan K, Yesudhason BV, Venkatachalam S, Mohan M, et al. Alternative to FBS in animal cell culture - An overview and future perspective. Heliyon. 2021 Aug 1;7(8).

228. Ackermann T, Tardito S. Cell culture medium formulation and its implications in cancer metabolism. Trends in cancer. 2019 Jun 6;5(6):329.

229. Yakisich JS, Azad N, Kaushik V, Iyer AK V. Cancer Cell Plasticity: Rapid Reversal of Chemosensitivity and Expression of Stemness Markers in Lung and Breast Cancer Tumorspheres. J Cell Physiol. 2017 Sep 1;232(9):2280.

230. Groothuis FA, Heringa MB, Nicol B, Hermens JLM, Blaauboer BJ, Kramer NI. Dose metric considerations in in vitro assays to improve quantitative in vitro–in vivo dose extrapolations. Toxicology. 2015 Jun 5;332:30–40.

231. Lehtomaki KI, Lahtinen LI, Rintanen N, Kuopio T, Kholova I, Makela R, et al. Clonal Evolution of MEK/MAPK Pathway Activating Mutations in a Metastatic Colorectal Cancer Case. Anticancer Res. 2019 Nov 1;39(11):5867–77.

232. Kettunen K, Boström PJ, Lamminen T, Heinosalo T, West G, Saarinen I, et al. Personalized Drug Sensitivity Screening for Bladder Cancer Using Conditionally Reprogrammed Patient-derived Cells. Eur Urol. 2019/07/02. 2019;76(4):430–4.

233. Abugomaa A, Elbadawy M, Yamanaka M, Goto Y, Hayashi K, Mori T, et al. Establishment of 2.5D organoid culture model using 3D bladder cancer organoid culture. Sci Rep. 2020 Dec 1;10(1).

234. Karekla E, Liao WJ, Sharp B, Pugh J, Reid H, Le Quesne J, et al. Ex Vivo explant cultures of non-small cell lung carcinoma enable evaluation of primary tumor responses to anticancer therapy. Cancer Res. 2017 Apr 15;77(8):2029–39.

235. Liu X, Zhang T, Wang R, Shi P, Pan B, Pang X. Insulin-Transferrin-Selenium as a Novel Serum-free Media Supplement for the Culture of Human Amnion Mesenchymal Stem Cells. Ann Clin Lab Sci. 2019;49(1):73–71.

236. Ding T, Luo A, Yang S, Lai Z, Wang Y, Shen W, et al. Effects of Basal Media and Supplements on Diethylstilbestrol-Treated Immature Mouse Primary Granulosa Cell Growth and Regulation of Steroidogenesis In Vitro. Reprod Domest Anim. 2012 Jun 1;47(3):355–64.

237. Caneparo C, Chabaud S, Fradette J, Bolduc S. Evaluation of a Serum-Free Medium for Human Epithelial and Stromal Cell Culture. Int J Mol Sci. 2022;23(17).

238. Warburg O. On the origin of cancer cells. Science (80-). 1956 Feb 24;123(3191):309–14.

239. Cantor JR, Sabatini DM. Cancer Cell Metabolism: One Hallmark, Many Faces. Cancer Discov. 2012 Oct;2(10):881.

240. Reichard A, Asosingh K. Best Practices for Preparing a Single Cell Suspension from Solid Tissues for Flow Cytometry. Cytom Part A. 2019 Feb 1;95(2):219–26.

241. Mashni J, Godoy G, Haarer C, Dalbagni G, Reuter VE, Ahmadie H Al, et al. Prospective evaluation of plasma kinetic bipolar resection of bladder cancer: Comparison to monopolar resection and pathologic

findings. Int Urol Nephrol. 2014 Sep 1;46(9):1699–705.

242. Lagerveld BW, Koot RAC, Smits GAHJ. Thermal artifacts in bladder tumors following loop endoresection: electrovaporization v electrocauterization. J Endourol. 2004 Aug;18(6):583–6.

243. Piccinini F, Tesei A, Arienti C, Bevilacqua A. Cell Counting and Viability Assessment of 2D and 3D Cell Cultures: Expected Reliability of the Trypan Blue Assay. Biol Proced Online. 2017 Jul 20;19(1).

244. Tennant JR. EVALUATION OF THE TRYPAN BLUE TECHNIQUE FOR DETERMINATION OF CELL VIABILITY. Transplantation. 1964;2(6):685–94.

245. Douglas S. Auld PD, Peter A. Coassin BS, Nathan P. Coussens PD, Hensley P, Klumpp-Thomas C, Michael S, et al. Microplate Selection and Recommended Practices in High-throughput Screening and Quantitative Biology. Assay Guid Man. 2020 Jun 1;

246. Barrett TA, Wu A, Zhang H, Levy MS, Lye GJ. Microwell engineering characterization for mammalian cell culture process development. Biotechnol Bioeng. 2010 Feb 1;105(2):260–75.

247. Huang AH, Motlekar NA, Stein A, Diamond SL, Shore EM, Mauck RL. High-throughput screening for modulators of mesenchymal stem cell chondrogenesis. Ann Biomed Eng. 2008 Nov 13;36(11):1909–21.

248. Boehnke K, Iversen PW, Schumacher D, Lallena MJ, Haro R, Amat J, et al. Assay Establishment and Validation of a High-Throughput Screening Platform for Three-Dimensional Patient-Derived Colon Cancer Organoid Cultures. J Biomol Screen. 2016 Oct 1;21(9):931–41.

249. Ray AM, Salim N, Stevens M, Chitre S, Abdeen S, Washburn A, et al. Exploiting the HSP60/10 chaperonin system as a chemotherapeutic target for colorectal cancer. Bioorg Med Chem. 2021 Jun 15;40:116129.

250. Liebens V, Defraine V, Fauvart M. A whole-cell-based high-throughput screening method to identify molecules targeting Pseudomonas aeruginosa persister cells. Methods Mol Biol. 2016;1333:113–20.

251. Driehuis E, Kretzschmar K, Clevers H. Establishment of patient-derived cancer organoids for drug-screening applications. Nat Protoc 2020 1510. 2020 Sep 14;15(10):3380–409.

252. Larsen BM, Kannan M, Langer LF, Leibowitz BD, Bentaieb A, Cancino A, et al. A pan-cancer organoid platform for precision medicine. Cell Rep. 2021 Jul 27;36(4):109429.

253. Dranchak P, Moran JJ, MacArthur R, Lopez-Anido C, Inglese J, Svaren J. Genome-edited cell lines for high-throughput screening. Methods Mol Biol. 2018;1755:1–17.

254. Kulesskiy E, Saarela J, Turunen L, Wennerberg K. Precision Cancer Medicine in the Acoustic Dispensing Era: Ex Vivo Primary Cell Drug Sensitivity Testing. J Lab Autom. 2016 Feb 1;21(1):27–36.

255. Sazonova E V., Chesnokov MS, Zhivotovsky B, Kopeina GS. Drug toxicity assessment: cell proliferation versus cell death. Cell Death Discov 2022 81. 2022 Oct 14;8(1):1–11.

256. Grasso S, Tristante E, Saceda M, Carbonell P, Mayor-López L, Carballo-Santana M, et al. Resistance to Selumetinib (AZD6244) in Colorectal Cancer Cell Lines is Mediated by p70S6K and RPS6 Activation. Neoplasia. 2014;16(10):845.

257. Nelson CM, Chen CS. Cell-cell signaling by direct contact increases cell proliferation via a PI3K-dependent signal. FEBS Lett. 2002 Mar 13;514(2–3):238–42.

258. Heng BC, Bezerra PP, Preiser PR, Alex Law SK, Xia Y, Boey F, et al. Effect of cell-seeding density on the proliferation and gene expression profile of human umbilical vein endothelial cells within ex vivo culture. Cytotherapy. 2011 May 1;13(5):606–17.

259. Parker RF. Action of Penicillin on Staphylococcus. Effect of Size of Inoculum on the Test for Sensitivity. Proc Soc Exp Biol Med. 1946;63(2):443–6.

260. Ohnuma T, Arkin H, Holland JF. Effects of cell density on drug-induced cell kill kinetics in vitro (inoculum effect). Br J Cancer. 1986 Sep;54(3):415.

261. Hall BG, Acar H, Nandipati A, Barlow M. Growth Rates Made Easy. Mol Biol Evol. 2014 Jan 1;31(1):232–8.

262. Johnson KE, Howard G, Mo W, Strasser MK, Lima EABF, Huang S, et al. Cancer cell population growth

kinetics at low densities deviate from the exponential growth model and suggest an Allee effect. PLOS Biol. 2019 Aug 5;17(8):e3000399.

263. Yang W, Soares J, Greninger P, Edelman EJ, Lightfoot H, Forbes S, et al. Genomics of Drug Sensitivity in Cancer (GDSC): a resource for therapeutic biomarker discovery in cancer cells. Nucleic Acids Res. 2013 Jan 1;41(Database issue).

264. De Livera AM, Sysi-Aho M, Jacob L, Gagnon-Bartsch JA, Castillo S, Simpson JA, et al. Statistical methods for handling unwanted variation in metabolomics data. Anal Chem. 2015 Apr 7;87(7):3606–15.

265. Seo S. A Review and Comparison of Methods for Detecting Outliers in Univariate Data Sets. 2006.

266. Maechler M, Rousseeuw P, Struyf A, Hubert M, Hornik K. cluster: Cluster Analysis Basics and Extensions. 2022.

267. Yuan C, Yang H. Research on K-Value Selection Method of K-Means Clustering Algorithm. J 2019, Vol 2, Pages 226-235. 2019 Jun 18;2(2):226–35.

268. Saka H, Kitagawa C, Kogure Y, Takahashi Y, Fujikawa K, Sagawa T, et al. Safety, tolerability and pharmacokinetics of the fibroblast growth factor receptor inhibitor AZD4547 in Japanese patients with advanced solid tumours: a Phase I study. Invest New Drugs. 2017 Aug 1;35(4):451.

269. Davies BR, Greenwood H, Dudley P, Crafter C, Yu DH, Zhang J, et al. Preclinical pharmacology of AZD5363, an inhibitor of AKT: Pharmacodynamics, antitumor activity, and correlation of monotherapy activity with genetic background. Mol Cancer Ther. 2012 Apr 1;11(4):873–87.

270. Bria E, Milella M, Cuppone F, Novello S, Ceribelli A, Vaccaro V, et al. Outcome of advanced NSCLC patients harboring sensitizing EGFR mutations randomized to EGFR tyrosine kinase inhibitors or chemotherapy as first-line treatment: a meta-analysis. Ann Oncol. 2011 Oct 1;22(10):2277–85.

271. Hauschild A, Grob JJ, Demidov L V., Jouary T, Gutzmer R, Millward M, et al. Dabrafenib in BRAF-mutated metastatic melanoma: A multicentre, open-label, phase 3 randomised controlled trial. Lancet. 2012 Jul 28;380(9839):358–65.

272. Pauli C, Hopkins BD, Prandi D, Shaw R, Fedrizzi T, Sboner A, et al. Personalized In Vitro and In Vivo Cancer Models to Guide Precision Medicine. Cancer Discov. 2017/03/24. 2017;7(5):462–77.

273. Haslam A, Olivier T, Tuia J, Prasad V. Umbrella review of basket trials testing a drug in tumors with actionable genetic biomarkers. BMC Cancer. 2023 Dec 1;23(1):1–8.

274. Shoemaker RH. The NCI60 human tumour cell line anticancer drug screen. Nat Rev Cancer 2006 610. 2006 Oct;6(10):813–23.

275. Barretina J, Caponigro G, Stransky N, Venkatesan K, Margolin AA, Kim S, et al. The Cancer Cell Line Encyclopedia enables predictive modelling of anticancer drug sensitivity. Nature. 2012 Mar 29;483(7391):603–7.

276. Earl J, Rico D, Carrillo-de-Santa-Pau E, Rodríguez-Santiago B, Méndez-Pertuz M, Auer H, et al. The UBC-40 Urothelial Bladder Cancer cell line index: a genomic resource for functional studies. BMC Genomics. 2015 Dec 22;16(1):403.

277. Moorcraft SY, Marriott C, Peckitt C, Cunningham D, Chau I, Starling N, et al. Patients' willingness to participate in clinical trials and their views on aspects of cancer research: results of a prospective patient survey. Trials. 2016 Jan 9;17(1).

278. Bryant J, Sanson-Fisher R, Fradgley E, Regan T, Hobden B, Ackland SP. Oncology patients overwhelmingly support tissue banking. BMC Cancer. 2015 May 17;15(1):1–8.

279. Unger JM, Hershman DL, Till C, Minasian LM, Osarogiagbon RU, Fleury ME, et al. "When Offered to Participate": A Systematic Review and Meta-Analysis of Patient Agreement to Participate in Cancer Clinical Trials. JNCI J Natl Cancer Inst. 2021 Mar 1;113(3):244–57.

280. Lee SH, Hu W, Matulay JT, Silva M V, Owczarek TB, Kim K, et al. Tumor Evolution and Drug Response in Patient-Derived Organoid Models of Bladder Cancer. Cell. 2018/04/07. 2018;173(2):515-528 e17.

281. Donin NM, Filson CP, Drakaki A, Tan HJ, Castillo A, Kwan L, et al. Risk of second primary malignancies among cancer survivors in the United States, 1992 through 2008. Cancer. 2016 Oct 1;122(19):3075–86.

282. Łukasiewicz S, Czeczelewski M, Forma A, Baj J, Sitarz R, Stanisławek A. Breast Cancer—Epidemiology, Risk Factors, Classification, Prognostic Markers, and Current Treatment Strategies—An Updated Review. Cancers 2021, Vol 13, Page 4287. 2021 Aug 25;13(17):4287.

283. Taber A, Christensen E, Lamy P, Nordentoft I, Prip F, Lindskrog SV, et al. Molecular correlates of cisplatin-based chemotherapy response in muscle invasive bladder cancer by integrated multi-omics analysis. Nat Commun 2020 111. 2020 Sep 25;11(1):1–15.

284. Swords RT, Azzam D, Al-Ali H, Lohse I, Volmar CH, Watts JM, et al. Ex-vivo sensitivity profiling to guide clinical decision making in acute myeloid leukemia: A pilot study. Leuk Res. 2018 Jan 1;64:34–41.

285. Kleczko EK, Heasley LE. Mechanisms of rapid cancer cell reprogramming initiated by targeted receptor tyrosine kinase inhibitors and inherent therapeutic vulnerabilities. Mol Cancer. 2018 Feb 19;17(1).

286. Ware KE, Marshall ME, Heasley LR, Marek L, Hinz TK, Hercule P, et al. Rapidly Acquired Resistance to EGFR Tyrosine Kinase Inhibitors in NSCLC Cell Lines through De-Repression of FGFR2 and FGFR3 Expression. PLoS One. 2010;5(11):e14117.

287. Sharifnia T, Rusu V, Piccioni F, Bagul M, Imielinski M, Cherniack AD, et al. Genetic modifiers of EGFR dependence in non-small cell lung cancer. Proc Natl Acad Sci U S A. 2014 Dec 30;111(52):18661–6.

288. Lee HJ, Zhuang G, Cao Y, Du P, Kim HJ, Settleman J. Drug Resistance via Feedback Activation of Stat3 in Oncogene-Addicted Cancer Cells. Cancer Cell. 2014 Aug 11;26(2):207–21.

289. Akhavan D, Pourzia AL, Nourian AA, Williams KJ, Nathanson D, Babic I, et al. De-repression of PDGFRβ transcription promotes acquired resistance to EGFR tyrosine kinase inhibitors in glioblastoma patients. Cancer Discov. 2013 May;3(5):534–47.

290. Kleczko EK, Kim J, Keysar SB, Heasley LR, Eagles JR, Simon M, et al. An Inducible TGF-β2-TGFβR Pathway Modulates the Sensitivity of HNSCC Cells to Tyrosine Kinase Inhibitors Targeting Dominant Receptor Tyrosine Kinases. PLoS One. 2015 May 6;10(5).

291. Singleton KR, Kim J, Hinz TK, Marek LA, Casás-Selves M, Hatheway C, et al. A receptor tyrosine kinase network composed of fibroblast growth factor receptors, epidermal growth factor receptor, v-erb-b2 erythroblastic leukemia viral oncogene homolog 2, and hepatocyte growth factor receptor drives growth and survival of head and neck squamous carcinoma cell lines. Mol Pharmacol. 2013 Apr;83(4):882–93.

292. Song C, Piva M, Sun L, Hong A, Moriceau G, Kong X, et al. Recurrent tumor cell–intrinsic and –extrinsic alterations during mapki-induced melanoma regression and early adaptation. Cancer Discov. 2017 Nov 1;7(11):1248–65.

293. Stuhlmiller TJ, Miller SM, Zawistowski JS, Nakamura K, Beltran AS, Duncan JS, et al. Inhibition of Lapatinib-Induced Kinome Reprogramming in ERBB2-Positive Breast Cancer by Targeting BET Family Bromodomains. Cell Rep. 2015 Apr 21;11(3):390–404.

294. He L, Kulesskiy E, Saarela J, Turunen L, Wennerberg K, Aittokallio T, et al. Methods for High-throughput Drug Combination Screening and Synergy Scoring. Methods Mol Biol. 2018;1711:351.

295. Abdellah Z, Ahmadi A, Ahmed S, Aimable M, Ainscough R, Almeida J, et al. Finishing the euchromatic sequence of the human genome. Nature. 2004 Oct 21;431(7011):931–45.

296. Bailey MH, Meyerson WU, Dursi LJ, Wang LB, Dong G, Liang WW, et al. Retrospective evaluation of whole exome and genome mutation calls in 746 cancer samples. Nat Commun 2020 111. 2020 Sep 21;11(1):1–27.

297. Xiao W, Ren L, Chen Z, Fang LT, Zhao Y, Lack J, et al. Toward best practice in cancer mutation detection with whole-genome and whole-exome sequencing. Nat Biotechnol 2021 399. 2021 Sep 9;39(9):1141–50.

298. Schwarze K, Buchanan J, Taylor JC, Wordsworth S. Are whole-exome and whole-genome sequencing approaches cost-effective? A systematic review of the literature. Genet Med 2018 2010. 2018 Feb 15;20(10):1122–30.

299. Lee EYHP, Muller WJ. Oncogenes and Tumor Suppressor Genes. Cold Spring Harb Perspect Biol. 2010;2(10).

300. Bailey MH, Tokheim C, Porta-Pardo E, Sengupta S, Bertrand D, Weerasinghe A, et al. Comprehensive Characterization of Cancer Driver Genes and Mutations. Cell. 2018 Apr 4;173(2):371.

301. Tabernero J, Bahleda R, Dienstmann R, Infante JR, Mita A, Italiano A, et al. Phase I dose-escalation study of JNJ-42756493, an oral pan-fibroblast growth factor receptor inhibitor, in patients with advanced solid tumors. J Clin Oncol. 2015 Oct 20;33(30):3401–8.

302. Danecek P, Bonfield JK, Liddle J, Marshall J, Ohan V, Pollard MO, et al. Twelve years of SAMtools and BCFtools. Gigascience. 2021 Jan 29;10(2):1–4.

303. Chen S, Francioli LC, Goodrich JK, Collins RL, Wang Q, Alföldi J, et al. A genome-wide mutational constraint map quantified from variation in 76,156 human genomes. bioRxiv. 2022 Oct 10;2022.03.20.485034.

304. Cerami E, Gao J, Dogrusoz U, Gross BE, Sumer SO, Aksoy BA, et al. The cBio cancer genomics portal: an open platform for exploring multidimensional cancer genomics data. Cancer Discov. 2012 May;2(5):401–4.

305. Gao J, Aksoy BA, Dogrusoz U, Dresdner G, Gross B, Sumer SO, et al. Integrative analysis of complex cancer genomics and clinical profiles using the cBioPortal. Sci Signal. 2013 Apr 2;6(269).

306. Chakravarty D, Gao J, Phillips S, Kundra R, Zhang H, Wang J, et al. OncoKB: A Precision Oncology Knowledge Base. https://doi.org/101200/PO1700011. 2017 May 16;(1):1–16.

307. Wang K, Li M, Hakonarson H. ANNOVAR: functional annotation of genetic variants from high-throughput sequencing data. Nucleic Acids Res. 2010 Sep 1;38(16):e164–e164.

308. Sanchez-Vega F, Mina M, Armenia J, Chatila WK, Luna A, La KC, et al. Oncogenic Signaling Pathways in The Cancer Genome Atlas. Cell. 2018 Apr 5;173(2):321-337.e10.

309. Zhang J, Wu LY, Zhang XS, Zhang S. Discovery of co-occurring driver pathways in cancer. BMC Bioinformatics. 2014 Aug 9;15(1):1–14.

310. Iyer G, Al-Ahmadie H, Schultz N, Hanrahan AJ, Ostrovnaya I, Balar A V., et al. Prevalence and Co-Occurrence of Actionable Genomic Alterations in High-Grade Bladder Cancer. J Clin Oncol. 2013 Sep 9;31(25):3133.

311. Roberts SA, Lawrence MS, Klimczak LJ, Grimm SA, Fargo D, Stojanov P, et al. An APOBEC Cytidine Deaminase Mutagenesis Pattern is Widespread in Human Cancers. Nat Genet. 2013 Sep;45(9):970.

312. Glaser AP, Fantini D, Wang Y, Yu Y, Rimar KJ, Podojil JR, et al. APOBEC-mediated mutagenesis in urothelial carcinoma is associated with improved survival, mutations in DNA damage response genes, and immune response. Oncotarget. 2018 Jan 1;9(4):4537.

313. Alexandrov LB, Kim J, Haradhvala NJ, Huang MN, Tian Ng AW, Wu Y, et al. The repertoire of mutational signatures in human cancer. Nat 2020 5787793. 2020 Feb 5;578(7793):94–101.

314. Moore L, Cagan A, Coorens THH, Neville MDC, Sanghvi R, Sanders MA, et al. The mutational landscape of human somatic and germline cells. Nat 2021 5977876. 2021 Aug 25;597(7876):381–6.

315. Alexandrov LB, Jones PH, Wedge DC, Sale JE, Campbell PJ, Nik-Zainal S, et al. Clock-like mutational processes in human somatic cells. Nat Genet. 2015 Dec 1;47(12):1402.

316. Stewart MD, Vega DM, Arend RC, Baden JF, Barbash O, Beaubier N, et al. Homologous Recombination Deficiency: Concepts, Definitions, and Assays. Oncologist. 2022;27(3):167.

317. Pant S, Schuler M, Iyer G, Witt O, Doi T, Qin S, et al. Erdafitinib in patients with advanced solid tumours with FGFR alterations (RAGNAR): an international, single-arm, phase 2 study. Lancet Oncol. 2023 Aug 1;24(8):925–35.

318. Qing J, Du X, Chen Y, Chan P, Li H, Wu P, et al. Antibody-based targeting of FGFR3 in bladder carcinoma and t(4;14)-positive multiple myeloma in mice. J Clin Invest. 2009 May 1;119(5):1216–29.

319. Knowles MA. Novel therapeutic targets in bladder cancer: mutation and expression of FGF receptors. Future Oncol. 2008 Feb;4(1):71–83.

320. Shi MJ, Meng XY, Lamy P, Banday AR, Yang J, Moreno-Vega A, et al. APOBEC-mediated Mutagenesis as a Likely Cause of FGFR3 S249C Mutation Over-representation in Bladder Cancer. Eur Urol. 2019 Jul 1;76(1):9–13.

321. Sweeney SM, Cerami E, Baras A, Pugh TJ, Schultz N, Stricker T, et al. AACR Project GENIE: Powering

Precision Medicine through an International Consortium. Cancer Discov. 2017;7(8):818–31.

322. Hernández S, López-Knowles E, Lloreta J, Kogevinas M, Amorós A, Tardón A, et al. Prospective study of FGFR3 mutations as a prognostic factor in nonmuscle invasive urothelial bladder carcinomas. J Clin Oncol. 2006 Aug 1;24(22):3664–71.

323. Garje R, An J, Obeidat M, Kumar K, Yasin HA, Zakharia Y. Fibroblast Growth Factor Receptor (FGFR) Inhibitors in Urothelial Cancer. Oncologist. 2020 Nov 1;25(11):e1711.

324. Al-Ahmadie HA, Iyer G, Janakiraman M, Lin O, Heguy A, Tickoo SK, et al. Somatic mutation of Fibroblast Growth Factor Receptor-3 (FGFR3) defines a distinct morphologic subtype of high-grade urothelial carcinoma. J Pathol. 2011 Jun;224(2):270.

325. van Rhijn BWG, van Tilborg AAG, Lurkin I, Bonaventure J, de Vries A, Thiery JP, et al. Novel fibroblast growth factor receptor 3 (FGFR3) mutations in bladder cancer previously identified in non-lethal skeletal disorders. Eur J Hum Genet 2002 1012. 2002 Dec 3;10(12):819–24.

326. Cappellen D, De Oliveira C, Ricol D, de Medina S, Bourdin J, Sastre-Garau X, et al. Frequent activating mutations of FGFR3 in human bladder and cervix carcinomas. Nat Genet 1999 231. 1999;23(1):18–20.

327. Gallo LH, Nelson KN, Meyer AN, Donoghue DJ. Functions of Fibroblast Growth Factor Receptors in cancer defined by novel translocations and mutations. Cytokine Growth Factor Rev. 2015 Aug 1;26(4):425–49.

328. Krook MA, Reeser JW, Ernst G, Barker H, Wilberding M, Li G, et al. Fibroblast growth factor receptors in cancer: genetic alterations, diagnostics, therapeutic targets and mechanisms of resistance. Br J Cancer. 2021 Mar 3;124(5):880.

329. Hainaut P, Pfeifer GP. Somatic TP53 Mutations in the Era of Genome Sequencing. Cold Spring Harb Perspect Med. 2016 Nov 1;6(11).

330. Klimovich B, Merle N, Neumann M, Elmshäuser S, Nist A, Mernberger M, et al. p53 partial loss-of-function mutations sensitize to chemotherapy. Oncogene 2021 417. 2021 Dec 14;41(7):1011–23.

331. Radovich M, Kiel PJ, Nance SM, Niland EE, Parsley ME, Ferguson ME, et al. Clinical benefit of a precision medicine based approach for guiding treatment of refractory cancers. Oncotarget. 2016;7(35):56491–500.

332. Stockley TL, Oza AM, Berman HK, Leighl NB, Knox JJ, Shepherd FA, et al. Molecular profiling of advanced solid tumors and patient outcomes with genotype-matched clinical trials: the Princess Margaret IMPACT/COMPACT trial. Genome Med. 2016 Oct 25;8(1).

333. Morash M, Mitchell H, Beltran H, Elemento O, Pathak J. The Role of Next-Generation Sequencing in Precision Medicine: A Review of Outcomes in Oncology. J Pers Med. 2018 Sep 17;8(3).

334. Chalmers ZR, Connelly CF, Fabrizio D, Gay L, Ali SM, Ennis R, et al. Analysis of 100,000 human cancer genomes reveals the landscape of tumor mutational burden. Genome Med. 2017 Apr 19;9(1):1–14.

335. Campbell PJ, Getz G, Korbel JO, Stuart JM, Jennings JL, Stein LD, et al. Pan-cancer analysis of whole genomes. Nat 2020 5787793. 2020 Feb 5;578(7793):82–93.

336. Kotler E, Shani O, Goldfeld G, Lotan-Pompan M, Tarcic O, Gershoni A, et al. A Systematic p53 Mutation Library Links Differential Functional Impact to Cancer Mutation Pattern and Evolutionary Conservation. Mol Cell. 2018 Jul 5;71(1):178-190.e8.

337. Hu J, Cao J, Topatana W, Juengpanich S, Li S, Zhang B, et al. Targeting mutant p53 for cancer therapy: direct and indirect strategies. J Hematol Oncol 2021 141. 2021 Sep 28;14(1):1–19.

338. Neuzillet Y, Paoletti X, Ouerhani S, Mongiat-Artus P, Soliman H, de The H, et al. A Meta-Analysis of the Relationship between FGFR3 and TP53 Mutations in Bladder Cancer. PLoS One. 2012 Dec 13;7(12):e48993.

339. The Cancer Genome Atlas Network. Comprehensive molecular characterization of urothelial bladder carcinoma. Nature. 2014 Mar 29;507(7492):315–22.

340. Langbein S, Szakacs O, Wilhelm M, Sukosd F, Weber S, Jauch A, et al. Alteration of the LRP1B Gene Region Is Associated with High Grade of Urothelial Cancer. Lab Investig. 2002 May 1;82(5):639–43.

341. Chen H, Chong W, Wu Q, Yao Y, Mao M, Wang X. Association of LRP1B mutation with tumor mutation burden and outcomes in melanoma and non-small cell lung cancer patients treated with immune check-point blockades. Front Immunol. 2019;10(MAY):1113.

342. Ren C hua, Ruan Y. Expression and clinical significance of five major genes in cutaneous melanoma based on TCGA database. Hum Pathol Case Reports. 2020 Sep 1;21:200411.

343. Frattini M, Molinari F, Epistolio S. The role of Piccolo in cancer treatment: relationship with EGFR and related therapies, and a marker for new targeted therapies. J Thorac Dis. 2017 Nov 1;9(11):4240–3.

344. Zhang M, Zhu J, Zhang P, Li L, Min M, Li T, et al. Development and validation of cancer-associated fibroblasts-related gene landscape in prognosis and immune microenvironment of bladder cancer. Front Oncol. 2023 Jun 15;13.

345. Qiu Z, Lin A, Li K, Lin W, Wang Q, Wei T, et al. A novel mutation panel for predicting etoposide resistance in small-cell lung cancer. Drug Des Devel Ther. 2019;13:2021.

346. Romond EH, Perez EA, Bryant J, Suman VJ, Geyer CE, Davidson NE, et al. Trastuzumab plus Adjuvant Chemotherapy for Operable HER2-Positive Breast Cancer. N Engl J Med. 2005 Oct 20;353(16):1673–84.

347. Flaherty KT, Robert C, Hersey P, Nathan P, Garbe C, Milhem M, et al. Improved survival with MEK inhibition in BRAF-mutated melanoma. N Engl J Med. 2012 Jul 12;367(2):107–14.

348. Goldie JH, Coldman AJ. A mathematic model for relating the drug sensitivity of tumors to their spontaneous mutation rate. Cancer Treat Rep. 1979 Nov 1;63(11–12):1727–33.

349. Castiglioni S, Di Fede E, Bernardelli C, Lettieri A, Parodi C, Grazioli P, et al. KMT2A: Umbrella Gene for Multiple Diseases. Genes 2022, Vol 13, Page 514. 2022 Mar 15;13(3):514.

350. Clinton TN, Chen Z, Wise H, Lenis AT, Chavan S, Donoghue MTA, et al. Genomic heterogeneity as a barrier to precision oncology in urothelial cancer. Cell Rep. 2022 Dec 20;41(12):111859.

351. Mullen J, Kato S, Sicklick JK, Kurzrock R. Targeting ARID1A mutations in cancer. Cancer Treat Rev. 2021 Nov 1;100:102287.

352. Helming KC, Wang X, Roberts CWM. Vulnerabilities of mutant SWI/SNF complexes in cancer. Cancer Cell. 2014;26(3):309–17.

353. Rehman H, Chandrashekar DS, Balabhadrapatruni C, Nepal S, Balasubramanya SAH, Shelton AK, et al. ARID1A-deficient bladder cancer is dependent on PI3K signaling and sensitive to EZH2 and PI3K inhibitors. JCI Insight. 2022 Aug 22;7(16).

354. Jiang Y, Situai Y, Deng H, Zhang H, Huang C, Wang L, et al. ARID1A Inactivation Increases Expression of circ0008399 and Promotes Cisplatin Resistance in Bladder Cancer. Curr Med Sci 2023. 2023 May 5;1–12.

355. Lee SH, Cheon J, Lee S, Kang B, Kim C, Shim HS, et al. ARID1A Mutation from Targeted NGS Predicts Primary Resistance to Gemcitabine and Cisplatin Chemotherapy in Advanced Biliary Tract Cancer. Cancer Res Treat. 2023 May 3;

356. Luo Q, Wu X, Zhang Y, Shu T, Ding F, Chen H, et al. ARID1A ablation leads to multiple drug resistance in ovarian cancer via transcriptional activation of MRP2. Cancer Lett. 2018 Jul 28;427:9–17.

357. Katagiri A, Nakayama K, Rahman MT, Rahman M, Katagiri H, Nakayama N, et al. Loss of ARID1A expression is related to shorter progression-free survival and chemoresistance in ovarian clear cell carcinoma. Mod Pathol 2012 252. 2011 Nov 18;25(2):282–8.

358. Stewart JR, Poradosu E, Woods A, Shemesh S, Clarke P, Te Poele R, et al. 8P NXP800 versus cisplatin in ARID1a-mutated ovarian clear cell carcinoma xenograft models. ESMO Open. 2023 Feb 1;8(1):100862.

359. Luo Q, Wu X, Chang W, Zhao P, Nan Y, Zhu X, et al. ARID1A prevents squamous cell carcinoma initiation and chemoresistance by antagonizing pRb/E2F1/c-Myc-mediated cancer stemness. Cell Death Differ. 2019 Dec 12;27(6):1981–97.

360. Wu S, Yang Z, Ye R, An D, Li C, Wang Y, et al. Novel variants in MLL confer to bladder cancer recurrence identified by whole-exome sequencing. Oncotarget. 2016 Jan 1;7(3):2629.

361. Jiang T, Chen X, Su C, Ren S, Zhou C. Pan-cancer analysis of ARID1A Alterations as Biomarkers for Immunotherapy Outcomes. J Cancer. 2020;11(4):776–80.

362. Goswami S, Chen Y, Anandhan S, Szabo PM, Basu S, Blando JM, et al. ARID1A mutation plus CXCL13 expression act as combinatorial biomarkers to predict responses to immune checkpoint therapy in mUCC. Sci Transl Med. 2020 Jun 17;12(548).

363. Wang L, Qu J, Zhou N, Hou H, Jiang M, Zhang X. Effect and biomarker of immune checkpoint blockade therapy for ARID1A deficiency cancers. Biomed Pharmacother. 2020 Oct 1;130:110626.

364. Zhang R, Wu HX, Xu M, Xie X. KMT2A/C mutations function as a potential predictive biomarker for immunotherapy in solid tumors. Biomark Res. 2020 Dec 1;8(1):71.

365. Mandal J, Mandal P, Wang TL, Shih IM. Treating ARID1A mutated cancers by harnessing synthetic lethality and DNA damage response. J Biomed Sci 2022 291. 2022 Sep 19;29(1):1–15.

366. Llabata P, Mitsuishi Y, Choi PS, Cai D, Francis JM, Torres-Diz M, et al. Multi-omics analysis identifies MGA as a negative regulator of the MYC pathway in lung adenocarcinoma. Mol Cancer Res. 2020 Apr 1;18(4):574–84.

367. Ranasinghe R, Mathai ML, Zulli A. Cisplatin for cancer therapy and overcoming chemoresistance. Heliyon. 2022 Sep 1;8(9).

368. Clinton TN, Chen Z, Wise H, Lenis AT, Chavan S, Donoghue MTA, et al. Genomic heterogeneity as a barrier to precision oncology in urothelial cancer. Cell Rep. 2022 Dec 12;41(12):111859.

369. Friedrich V, Choi HW. The Urinary Microbiome: Role in Bladder Cancer and Treatment. Diagnostics. 2022 Sep 1;12(9).

370. Babjuk M, Burger M, Capoun O, Cohen D, Compérat EM, Dominguez Escrig JL, et al. European Association of Urology Guidelines on Non-muscle-invasive Bladder Cancer (Ta, T1, and Carcinoma in Situ). Eur Urol. 2022 Jan 1;81(1):75–94.

371. Vladimer GI, Snijder B, Krall N, Bigenzahn JW, Huber KVM, Lardeau C-H, et al. Global survey of the immunomodulatory potential of common drugs. Nat Chem Biol. 2017 Jun 24;13(6):681–90.

372. Gatta G, Capocaccia R, Botta L, Mallone S, De Angelis R, Ardanaz E, et al. Burden and centralised treatment in Europe of rare tumours: results of RARECAREnet—a population-based study. Lancet Oncol. 2017 Aug;18(8):1022–39.

373. Im K, Mareninov S, Diaz MFP, Yong WH. An introduction to Performing Immunofluorescence Staining. Methods Mol Biol. 2019;1897:299.

374. Kapuscinski J. DAPI: a DNA-specific fluorescent probe. Biotech Histochem. 1995;70(5):220–33.

375. Cummings BS, Wills LP, Schnellmann RG. Measurement of Cell Death in Mammalian Cells. Curr Protoc Pharmacol. 2004 Sep 9;0 12(1).

376. PerkinElmer. Dimensions of CellCarrier-384 Ultra.

377. Menz A, Bauer R, Kluth M, Marie von Bargen C, Gorbokon N, Viehweger F, et al. Diagnostic and prognostic impact of cytokeratin 19 expression analysis in human tumors: a tissue microarray study of 13,172 tumors. Hum Pathol. 2021 Sep 1;115:19–36.

378. Karantza V. Keratins in health and cancer: more than mere epithelial cell markers. Oncogene. 2011 Jan 1;30(2):127.

379. Johnen G, Rozynek P, von der Gathen Y, Bryk O, Zdrenka R, Johannes C, et al. Cross-Contamination of a UROtsa Stock with T24 Cells - Molecular Comparison of Different Cell Lines and Stocks. PLoS One. 2013 May 17;8(5):e64139.

380. Nurmik M, Ullmann P, Rodriguez F, Haan S, Letellier E. In search of definitions: Cancer-associated fibroblasts and their markers. Int J Cancer. 2020 Feb 15;146(4):895–905.

381. Monteiro-Reis S, Lobo J, Henrique R, Jerónimo C. Epigenetic Mechanisms Influencing Epithelial to Mesenchymal Transition in Bladder Cancer. Int J Mol Sci. 2019 Jan 2;20(2).

382. Vasaikar S V., Deshmukh AP, den Hollander P, Addanki S, Kuburich NA, Kudaravalli S, et al. EMTome:

a resource for pan-cancer analysis of epithelial-mesenchymal transition genes and signatures. Br J Cancer 2020 1241. 2020 Dec 10;124(1):259–69.

383. Baumgart E, Cohen MS, Neto BS, Jacobs MA, Wotkowicz C, Rieger-Christ KM, et al. Identification and prognostic significance of an epithelial-mesenchymal transition expression profile in human bladder tumors. Clin Cancer Res. 2007 Mar 15;13(6):1685–94.

384. Lobo J, Monteiro-Reis S, Guimarães-Teixeira C, Lopes P, Carneiro I, Jerónimo C, et al. Practicability of clinical application of bladder cancer molecular classification and additional value of epithelial-to-mesenchymal transition: Prognostic value of vimentin expression. J Transl Med. 2020 Aug 5;18(1):1–12.

385. Mazia D, Schatten G, Sale W. ADHESION OF CELLS TO SURFACES COATED WITH POLYLYSINE Applications to Electron Microscopy. J Cell Biol. 1975;66:198–200.

386. Bukavina L, Bensalah K, Bray F, Carlo M, Challacombe B, Karam JA, et al. Epidemiology of Renal Cell Carcinoma: 2022 Update. Eur Urol. 2022 Nov 1;82(5):529–42.

387. Smittenaar CR, Petersen KA, Stewart K, Moitt N. Cancer incidence and mortality projections in the UK until 2035. Br J Cancer. 2016 Oct 10;115(9):1147.

388. Conroy S, Catto JWF, Bex A, Brown JE, Cartledge J, Fielding A, et al. Diagnosis, treatment, and survival from kidney cancer: real-world National Health Service England data between 2013 and 2019. BJU Int. 2023;

389. Ljungberg, B, Albiges L, Bensalah K, Bex A, Giles R.H., Hora M, Kuczyk MA, Lam T, Marconi L, Merseburger AS, Powles T, Staehler M VA. Renal Cell Carcinoma EAU Guidelines on. 2018.

390. Levin BM, Boulos FI, Herrell SD. Metastatic ocular melanoma to the kidney 20 years after initial diagnosis. Urology. 2005;66(3):658.e11-658.e12.

391. Kohno J, Matsui Y, Yamasaki T, Shibasaki N, Kamba T, Yoshimura K, et al. Role of mammalian target of rapamycin inhibitor in the treatment of metastatic epithelioid angiomyolipoma: a case report. Int J Urol. 2013 Sep;20(9):938–41.

392. Motzer RJ, Barrios CH, Kim TM, Falcon S, Cosgriff T, Harker WG, et al. Phase II randomized trial comparing sequential first-line everolimus and second-line sunitinib versus first-line sunitinib and second-line everolimus in patients with metastatic renal cell carcinoma. J Clin Oncol. 2014;

393. Patel PH, Chadalavada RSV, Chaganti RSK, Motzer RJ. Targeting von Hippel-Lindau pathway in renal cell carcinoma. Clin Cancer Res. 2006;

394. Motzer R, Alekseev B, Rha S-Y, Porta C, Eto M, Powles T, et al. Lenvatinib plus Pembrolizumab or Everolimus for Advanced Renal Cell Carcinoma. N Engl J Med. 2021 Apr 8;384(14):1289–300.

395. Truong LD, Shen SS. Immunohistochemical Diagnosis of Renal Neoplasms. Arch Pathol Lab Med. 2011 Jan 1;135(1):92–109.

396. Kim M, Joo JW, Lee SJ, Cho YA, Park CK, Cho NH. Comprehensive Immunoprofiles of Renal Cell Carcinoma Subtypes. Cancers 2020, Vol 12, Page 602. 2020 Mar 5;12(3):602.

397. Skinnider BF, Folpe AL, Hennigar RA, Lim SD, Cohen C, Tamboli P, et al. Distribution of cytokeratins and vimentin in adult renal neoplasms and normal renal tissue: Potential utility of a cytokeratin antibody panel in the differential diagnosis of renal tumors. Am J Surg Pathol. 2005 Jun;29(6):747–54.

398. Lugand L, Mestrallet G, Laboureur R, Dumont C, Bouhidel F, Djouadou M, et al. Methods for Establishing a Renal Cell Carcinoma Tumor Spheroid Model With Immune Infiltration for Immunotherapeutic Studies. Front Oncol. 2022 Jul 28;12:1.

399. Heinemann T, Kornauth C, Severin Y, Vladimer GI, Pemovska T, Hadzijusufovic E, et al. Deep Morphology Learning Enhances Ex Vivo Drug Profiling-Based Precision Medicine. Blood Cancer Discov. 2022 Nov 1;3(6):502–15.

400. Jiménez-Torres JA, Virumbrales-Muñoz M, Sung KE, Lee MH, Abel EJ, Beebe DJ. Patient-specific organotypic blood vessels as an in vitro model for anti-angiogenic drug response testing in renal cell carcinoma. EBioMedicine. 2019 Apr 1;42:408–19.

9. APPENDICES

9.1 APPENDIX 1: DATA MANAGEMENT PROTOCOL

Table 23: Summary of *ex-vivo* data management protocols
1. Description of the data
1.1 Type of study
Feasibility study using fresh tumour tissue to evaluate if *ex-vivo* high throughput drug screening can predict patient response to cancer therapies prior to treatment and identify potential novel treatments in bladder cancer.
1.2 Types of data
Qualitative: Phenotypic pharmacological profile of tumour, cell segmentation, genotyping, patient response to standard care treatment and clinical history recorded in case report forms. Quantitative, dose response to individual drugs, cell counts, and metabolic activity measurements. Pharmacological profiles will be calculated from the metabolic assays RAW images and will be processed and expressed as annotated images, graphs, tables, and heat maps.
1.3 Format and scale of the data
Formats and software used to analyse/process data generated in this study will all be common to the scientific community, enabling easy access and sharing and ensure long term validity of the data. 1) Clinical data will be stored in case report forms as physical hard copies and electronically in a XLXS format. 2) RAW metabolic data recorded from the *ex-vivo* screen will be stored in an .XML format created by the Moleculer Devices SpectralMax ID5. During processing, this will be converted to XLXS and analysed using R open-access software 3) RAW images recorded from the *ex-vivo* screen will be stored in CZI format using Zeiss software; these will be exported into JPEG/TIFF format for further analysis using Zeiss Zen software (186 samples, approx. 308000 merged images, 16Gb per sample) 4) Processed images including cell counts, reproducibility, cell segmentation, dose response curves, and drug response heatmaps will be stored in XLXS format 5) Genotypic RAW data will be generated in a BCL/FASTA. Processed aligned sequences will be stored as BAM files, viewable on an Integrative Genomics Viewer, Variants observed will be stored in a VCF/MAF format accessible using Excel/R
2. Data collection / generation
2.1 Methodologies for data collection / generation
The case support describes the methodologies and experiments used to generate data. Clinical data will be collected from medical records, electronic health records and administrative records using case report forms by trained individuals. Phenotypic drug profiles will be calculated from metabolic data. Genotype data will be generated by next generation sequencing (NGS) and processed using an established pipeline for sequence

alignment and variants annotated using a somatic variant caller. All bioinformatics software packages and versions will be recorded alongside variant calling parameters. Genotype data will be generated using a next generation sequencer. All processed data will be stored in LabCollector and on University of Sheffield (UoS) Servers. Samples and generated data will be identifiable through the sample unique pseudo-anonymised ID.

2.2 Data quality and standards

Investigator site file will be subject to audits checks from Sheffield Teaching Hospitals R&D department, where an annual progress report will have to be submitted to the REC/HRA. All processed data will be stored on the LIMS to ensure quality management and maintain a full audit trail. Data generated from the *ex-vivo* screen (both metabolic and imaging) will subject to negative and positive controls and samples run in triplicate on the main drug screen plate. NGS will include an internal control and various quality control (QC) checks during library preparation. All individuals involved we be appropriately trained in relevant techniques and procedures. Standard operating procedures (SOP) will ensure consistency in methods and analysis. Data will be checked to ensure quality in weekly meetings and in-house audits. Images will be reviewed by Dr Rantala (Lecturer, Department of Oncology and Metabolism, UoS) using his analytical pipeline in parallel to in-house analysis for comparison and QC.

3. Data management, documentation, and curation

3.1 Managing, storing and curating data.

Data collected in paper form will be stored at the UoS in secured areas. Pseudo-anonymised digital data will be stored on centrally provided university servers and research storage infrastructure. By default, two copies of data are kept across two physical plant rooms, with a 28-day snapshot made of data and backed up securely offsite at least daily. Processed data will also be stored on an electronic lab book within the LIMS (LabCollector) which will ensure an audit trail is generated. Methods will be stored on relevant SOPs. Samples and generated clinical data will be identifiable through the sample unique pseudo-anonymised ID.

3.2 Metadata standards and data documentation

SOPs for methodological protocols, instruments, and pipelines will be stored on the university servers and LabCollector. These SOPs will be reviewed and version controlled. Any deviation from the SOP will be documented within the electronic lab book (alongside recorded data from the experiment processes, under the relevant experiment page, identified by the pseud-anonymised ID). Project results published in journals will include relevant methods and suitable annotation where possible in open access journals. In the long term, if the *ex-vivo* project grows to include more cancer types we would like to develop a phenotypic screen, genetic, and clinical database for the cancer types which would be open access.

3.3 Data preservation strategy and standards

Patient identifiable data and the key to the pseudo-anonymised ID will be stored on a Sheffield Teaching Hospitals Foundation Trust (STH) network PC and only accessible by individuals associated with the study and with STH computer access. This personal data will be preserved for 1 year after the end of the study as stated in the protocol (STH20854). Pseudo-anonymised clinical data, RAW data, and processed research data will be retained for 20 years, as set out by MRC Guidance on data relating to clinical research (MRC Regulatory Support Centre: Retention Framework for research data and records, 2017).

Data will be archived in line with UoS Research Data Management Policy, a component of UoS Policy on Good R&I Practices ('GRIP' Policy).

4. Data security and confidentiality

4.1 Formal information/data security standards

Ethical review will be undertaken by the Research Ethics Committee (REC) to assess the study and check compliance with HRA and HCRW assessment criteria and standards. The application has been provisionally approved by South West - Frenchay Research Ethics Committee subject to minor amendments in the patient information sheet and this will be completed by 21/1/21 (STH20854, IRAS ID: 262315, REC reference: 20/SW/0193).

4.2 Main risks to data security

Personal data will be only stored on a password protected NHS STH trust computer in a password protected excel spreadsheet. This will only be accessible to STH staff and members involved in the *ex-vivo* research team (named on the project delegation log) who have completed relevant training and have appropriate access to the STH NHS trust network. No patient identifiable information will be transferred to the UoS, clinical sample and clinical data will only be identifiable by a unique pseudo-anonymised ID. All patient consent and further details are highlighted in the protocol (STH20854, IRAS ID: 262315, REC reference: 20/SW/0193). The study will be subject to STH audits for compliance.

5. Data sharing and access

5.1 Suitability for sharing

Data generated from this project will be of a high standard and documented accordingly. The data will be of interest to clinicians, scientists, and patients with oncological disease, to improve patient stratification in precision medicine, and in novel drug discovery/ development.

5.2 Discovery by potential users of the research data

Data will be made available for interested researchers via open access publication. All pseudo-anonymised clinical, processed and RAW data will be deposited in the UoS data repository [ORDA]. ORDA enables the research data to be preserved, discovered, and accessed. A digital object identifier (DOI) will be used for publications to link the publication to the data stored in ORDA.

5.3 Governance of access

The study investigators and collaborators will have to agree and decide when the data will be submitted to ORDA. All data deposited in ORDA, or any publications will only use a pseudo-anonymised ID to identify individual sample and corresponding data. No patient identifiable information will be stored in ORDA, presented, or published. This is clearly stated on the patient consent forms, which will be used for patient recruitment and informed consent.

5.4 The study team’s exclusive use of the data

At the time of publication data will be made available. Depending on the nature of the data itself, data may be made available earlier, on an individual basis either to interested researchers and/or potential new collaborators, or negative data publicly via deposition in ORDA.

5.5 Restrictions or delays to sharing, with planned actions to limit such restrictions

During the informed consent process, it is made clear to the patient that the data will be published and shared in an anonymised form. Delays in sharing data may arise through a delayed ability to analyse or publish the research findings. Delays in sharing data may arise

due to intellectual property rights; if this is a factor, advice will be sought from UoS Research & Innovation Services.
5.6 Regulation of responsibilities of users
If we develop industrial collaborations in the future, data sharing and transfer agreements will been put in place.
6. Responsibilities
Each member of the research team will be responsible for the management of data relevant to this study according to guidelines set by the EVIDENT study (STH20854, IRAS ID: 262315, REC reference: 20/SW/0193)
7. Relevant institutional, departmental or study policies on data sharing and data security
Data Management Policy & Procedures (University of Sheffield Data Management policy https://www.sheffield.ac.uk/polopoly_fs/1.891972!/file/GRIPPolicyExtractRDM.pdf)
Data Security Policy (http://www.shef.ac.uk/cics/policies/infosecpolicy)
Data Sharing Policy (MRC and RCUK principles http://www.mrc.ac.uk/research/policies-and-guidance-for-researchers/data-sharing/)
Institutional Information Policy (University of Sheffield Good Research and Innovation Practice (GRIP) Policy. University of Sheffield Data protection policy)

9.2 APPENDIX 2: GENERAL LABORATORY CONSUMABLES

Table 24: General Laboratory Consumables

Consumable	Supplier
Serological pipettes (5ml, 10ml, 25ml)	Sarstedt Inc
Sterile scalpels	Swann Morton®, UK
10, 20, 200 and 1000µl pipette tips	Sarstedt Inc
22x 22/32/50mm coverslips	Scientific Laboratory Supplies®, UK
Plastic disposable pipettes	Scientific Laboratory Supplies®, UK
Falcon tubes (15ml, 50ml)	Sarstedt Inc
Eppendorf Microfuge tubes (0.5, 1.5 and 2ml)	Scientific Laboratory Supplies®, UK
Latex examination gloves	Scientific Laboratory Supplies®, UK
Tissue Culture flasks (T25, T75, T175)	ThermoFisher Scientific
1.5ml cryovials	Sarstedt Inc
E1-ClipTip Electronic Multichannel Pipettes and Filter Tips (120uL)	ThermoFisher Scientific
25ml reagent reservoirs	ThermoFisher Scientific

9.3 APPENDIX 3: LIST OF R PACKAGES USED FOR DATA ANALYSIS

Table 25: List of R packages used for data analysis

Package name	Package on disk version	Package load version	Package date	Package source
AnnotationDbi	1.60.2	1.60.2	12/03/2023	Bioconductor
backports	1.4.1	1.4.1	13/12/2021	CRAN (R 4.2.0)
base64enc	0.1.3	0.1-3	28/07/2015	CRAN (R 4.2.0)
Biobase	2.58.0	2.58.0	07/11/2022	Bioconductor
BiocFileCache	2.6.1	2.6.1	19/02/2023	Bioconductor
BiocGenerics	0.44.0	0.44.0	07/11/2022	Bioconductor
BiocIO	1.8.0	1.8.0	07/11/2022	Bioconductor
BiocManager	1.30.22	1.30.22	08/08/2023	CRAN (R 4.2.0)
BiocParallel	1.32.6	1.32.6	19/03/2023	Bioconductor
biomaRt	2.54.1	2.54.1	22/03/2023	Bioconductor
Biostrings	2.66.0	2.66.0	07/11/2022	Bioconductor
bit	4.0.5	4.0.5	15/11/2022	CRAN (R 4.2.0)
bit64	4.0.5	4.0.5	30/08/2020	CRAN (R 4.2.0)
bitops	1.0.7	1.0-7	24/04/2021	CRAN (R 4.2.0)
blob	1.2.4	1.2.4	17/03/2023	CRAN (R 4.2.0)
boot	1.3.28.1	1.3-28.1	22/11/2022	CRAN (R 4.2.0)
BSgenome	1.66.3	1.66.3	19/02/2023	Bioconductor
BSgenome.Hsapiens.UCSC.hg19	1.4.3	1.4.3	31/07/2023	Bioconductor
cachem	1.0.8	1.0.8	01/05/2023	CRAN (R 4.2.0)
callr	3.7.3	3.7.3	02/11/2022	CRAN (R 4.2.0)
checkmate	2.2.0	2.2.0	27/04/2023	CRAN (R 4.2.0)
cli	3.6.1	3.6.1	23/03/2023	CRAN (R 4.2.0)
cluster	2.1.4	2.1.4	22/08/2022	CRAN (R 4.2.2)
codetools	0.2.19	0.2-19	01/02/2023	CRAN (R 4.2.0)
colorspace	2.1.0	2.1-0	23/01/2023	CRAN (R 4.2.0)
cowplot	1.1.1	1.1.1	30/12/2020	CRAN (R 4.2.0)
crayon	1.5.2	1.5.2	29/09/2022	CRAN (R 4.2.0)
curl	5.0.2	5.0.2	14/08/2023	CRAN (R 4.2.0)
data.table	1.14.8	1.14.8	17/02/2023	CRAN (R 4.2.0)
DBI	1.1.3	1.1.3	18/06/2022	CRAN (R 4.2.0)
dbplyr	2.3.3	2.3.3	07/07/2023	CRAN (R 4.2.0)
DelayedArray	0.24.0	0.24.0	07/11/2022	Bioconductor
desc	1.4.2	1.4.2	08/09/2022	CRAN (R 4.2.0)
devtools	2.4.5	2.4.5	11/10/2022	CRAN (R 4.2.0)
digest	0.6.33	0.6.33	07/07/2023	CRAN (R 4.2.0)
DNAcopy	1.72.3	1.72.3	22/01/2023	Bioconductor
doParallel	1.0.17	1.0.17	07/02/2022	CRAN (R 4.2.0)
dplyr	1.1.3	1.1.3	03/09/2023	CRAN (R 4.2.0)
ellipsis	0.3.2	0.3.2	29/04/2021	CRAN (R 4.2.0)
evaluate	0.21	0.21	05/05/2023	CRAN (R 4.2.0)
fansi	1.0.4	1.0.4	22/01/2023	CRAN (R 4.2.0)
fastmap	1.1.1	1.1.1	24/02/2023	CRAN (R 4.2.0)
filelock	1.0.2	1.0.2	05/10/2018	CRAN (R 4.2.0)
forcats	1.0.0	1.0.0	29/01/2023	CRAN (R 4.2.0)
foreach	1.5.2	1.5.2	02/02/2022	CRAN (R 4.2.0)
foreign	0.8.85	0.8-85	09/09/2023	CRAN (R 4.2.0)
Formula	1.2.5	1.2-5	24/02/2023	CRAN (R 4.2.0)
fs	1.6.3	1.6.3	20/07/2023	CRAN (R 4.2.0)
furrr	0.3.1	0.3.1	15/08/2022	CRAN (R 4.2.0)

future	1.33.0	1.33.0	01/07/2023	CRAN (R 4.2.0)
generics	0.1.3	0.1.3	05/07/2022	CRAN (R 4.2.0)
GenomeInfoDb	1.34.9	1.34.9	05/02/2023	Bioconductor
GenomeInfoDbData	1.2.9	1.2.9	31/07/2023	Bioconductor
GenomicAlignments	1.34.1	1.34.1	12/03/2023	Bioconductor
GenomicFeatures	1.50.4	1.50.4	25/01/2023	Bioconductor
GenomicRanges	1.50.2	1.50.2	18/12/2022	Bioconductor
GenVisR	1.30.0	1.30.0	07/11/2022	Bioconductor
ggplot2	3.4.3	3.4.3	14/08/2023	CRAN (R 4.2.0)
globals	0.16.2	0.16.2	21/11/2022	CRAN (R 4.2.0)
glue	1.6.2	1.6.2	24/02/2022	CRAN (R 4.2.0)
gridBase	0.4.7	0.4-7	24/02/2014	CRAN (R 4.2.0)
gridExtra	2.3	2.3	09/09/2017	CRAN (R 4.2.0)
GRmetrics	1.24.0	1.24.0	07/11/2022	Bioconductor
gtable	0.3.4	0.3.4	21/08/2023	CRAN (R 4.2.2)
gtools	3.9.4	3.9.4	27/11/2022	CRAN (R 4.2.0)
here	1.0.1	1.0.1	13/12/2020	CRAN (R 4.2.0)
Hmisc	5.1.1	5.1-1	12/09/2023	CRAN (R 4.2.0)
hms	1.1.3	1.1.3	21/03/2023	CRAN (R 4.2.0)
htmlTable	2.4.1	2.4.1	07/07/2022	CRAN (R 4.2.0)
htmltools	0.5.6	0.5.6	10/08/2023	CRAN (R 4.2.0)
htmlwidgets	1.6.2	1.6.2	17/03/2023	CRAN (R 4.2.0)
httpuv	1.6.11	1.6.11	11/05/2023	CRAN (R 4.2.0)
httr	1.4.7	1.4.7	15/08/2023	CRAN (R 4.2.0)
IRanges	2.32.0	2.32.0	07/11/2022	Bioconductor
iterators	1.0.14	1.0.14	05/02/2022	CRAN (R 4.2.0)
jsonlite	1.8.7	1.8.7	29/06/2023	CRAN (R 4.2.0)
KEGGREST	1.38.0	1.38.0	07/11/2022	Bioconductor
knitr	1.44	1.44	11/09/2023	CRAN (R 4.2.0)
later	1.3.1	1.3.1	02/05/2023	CRAN (R 4.2.0)
lattice	0.21.8	0.21-8	05/04/2023	CRAN (R 4.2.0)
lazyeval	0.2.2	0.2.2	15/03/2019	CRAN (R 4.2.0)
lifecycle	1.0.3	1.0.3	07/10/2022	CRAN (R 4.2.0)
listenv	0.9.0	0.9.0	16/12/2022	CRAN (R 4.2.0)
lubridate	1.9.2	1.9.2	10/02/2023	CRAN (R 4.2.0)
maftools	2.14.0	2.14.0	07/11/2022	Bioconductor
magrittr	2.0.3	2.0.3	30/03/2022	CRAN (R 4.2.0)
Matrix	1.5.4.1	1.5-4.1	18/05/2023	CRAN (R 4.2.0)
MatrixGenerics	1.10.0	1.10.0	07/11/2022	Bioconductor
matrixStats	1.0.0	1.0.0	02/06/2023	CRAN (R 4.2.0)
memoise	2.0.1	2.0.1	26/11/2021	CRAN (R 4.2.0)
mime	0.12	0.12	28/09/2021	CRAN (R 4.2.0)
miniUI	0.1.1.1	0.1.1.1	18/05/2018	CRAN (R 4.2.0)
munsell	0.5.0	0.5.0	12/06/2018	CRAN (R 4.2.0)
NMF	0.26	0.26	20/03/2023	CRAN (R 4.2.0)
nnet	7.3.19	7.3-19	03/05/2023	CRAN (R 4.2.0)
parallelly	1.36.0	1.36.0	26/05/2023	CRAN (R 4.2.0)
pheatmap	1.0.12	1.0.12	04/01/2019	CRAN (R 4.2.0)
pillar	1.9.0	1.9.0	22/03/2023	CRAN (R 4.2.0)
pkgbuild	1.4.2	1.4.2	26/06/2023	CRAN (R 4.2.0)
pkgconfig	2.0.3	2.0.3	22/09/2019	CRAN (R 4.2.0)
pkgload	1.3.2.1	1.3.2.1	08/07/2023	CRAN (R 4.2.0)
plotly	4.10.2	4.10.2	03/06/2023	CRAN (R 4.2.0)
plyr	1.8.8	1.8.8	11/11/2022	CRAN (R 4.2.0)
png	0.1.8	0.1-8	29/11/2022	CRAN (R 4.2.0)
prettyunits	1.1.1	1.1.1	24/01/2020	CRAN (R 4.2.0)
processx	3.8.2	3.8.2	30/06/2023	CRAN (R 4.2.0)
profvis	0.3.8	0.3.8	02/05/2023	CRAN (R 4.2.0)
progress	1.2.2	1.2.2	16/05/2019	CRAN (R 4.2.0)
promises	1.2.1	1.2.1	10/08/2023	CRAN (R 4.2.0)
ps	1.7.5	1.7.5	18/04/2023	CRAN (R 4.2.0)

purrr	1.0.2	1.0.2	10/08/2023	CRAN (R 4.2.0)
R.methodsS3	1.8.2	1.8.2	13/06/2022	CRAN (R 4.2.0)
R.oo	1.25.0	1.25.0	12/06/2022	CRAN (R 4.2.0)
R.utils	2.12.2	2.12.2	11/11/2022	CRAN (R 4.2.0)
R6	2.5.1	2.5.1	19/08/2021	CRAN (R 4.2.0)
rappdirs	0.3.3	0.3.3	31/01/2021	CRAN (R 4.2.0)
RColorBrewer	1.1.3	1.1-3	03/04/2022	CRAN (R 4.2.0)
Rcpp	1.0.11	1.0.11	06/07/2023	CRAN (R 4.2.0)
RCurl	1.98.1.12	1.98-1.12	27/03/2023	CRAN (R 4.2.0)
readr	2.1.4	2.1.4	10/02/2023	CRAN (R 4.2.0)
registry	0.5.1	0.5-1	05/03/2019	CRAN (R 4.2.0)
remotes	2.4.2.1	2.4.2.1	18/07/2023	CRAN (R 4.2.0)
reshape2	1.4.4	1.4.4	09/04/2020	CRAN (R 4.2.0)
restfulr	0.0.15	0.0.15	16/06/2022	CRAN (R 4.2.0)
rjson	0.2.21	0.2.21	09/01/2022	CRAN (R 4.2.0)
rlang	1.1.1	1.1.1	28/04/2023	CRAN (R 4.2.0)
rmarkdown	2.25	2.25	18/09/2023	CRAN (R 4.2.0)
rngtools	1.5.2	1.5.2	20/09/2021	CRAN (R 4.2.0)
rpart	4.1.19	4.1.19	21/10/2022	CRAN (R 4.2.2)
rprojroot	2.0.3	2.0.3	02/04/2022	CRAN (R 4.2.0)
Rsamtools	2.14.0	2.14.0	07/11/2022	Bioconductor
RSQLite	2.3.1	2.3.1	03/04/2023	CRAN (R 4.2.0)
rstudioapi	0.15.0	0.15.0	07/07/2023	CRAN (R 4.2.0)
rtracklayer	1.58.0	1.58.0	07/11/2022	Bioconductor
S4Vectors	0.36.2	0.36.2	01/03/2023	Bioconductor
scales	1.2.1	1.2.1	20/08/2022	CRAN (R 4.2.0)
sessioninfo	1.2.2	1.2.2	06/12/2021	CRAN (R 4.2.0)
shiny	1.7.5	1.7.5	12/08/2023	CRAN (R 4.2.0)
sigminer	2.2.2	2.2.2	21/08/2023	CRAN (R 4.2.0)
stringi	1.7.12	1.7.12	11/01/2023	CRAN (R 4.2.0)
stringr	1.5.0	1.5.0	02/12/2022	CRAN (R 4.2.0)
SummarizedExperiment	1.28.0	1.28.0	07/11/2022	Bioconductor
survival	3.5.7	3.5-7	14/08/2023	CRAN (R 4.2.0)
TCGAmutations	0.3.0	0.3.0	21/09/2023	Github (PoisonAlien/ TCGAmutations)
tibble	3.2.1	3.2.1	20/03/2023	CRAN (R 4.2.0)
tidyr	1.3.0	1.3.0	24/01/2023	CRAN (R 4.2.0)
tidyselect	1.2.0	1.2.0	10/10/2022	CRAN (R 4.2.0)
tidyverse	2.0.0	2.0.0	22/02/2023	CRAN (R 4.2.0)
timechange	0.2.0	0.2.0	11/01/2023	CRAN (R 4.2.0)
tzdb	0.4.0	0.4.0	12/05/2023	CRAN (R 4.2.0)
urlchecker	1.0.1	1.0.1	30/11/2021	CRAN (R 4.2.0)
usethis	2.2.2	2.2.2	06/07/2023	CRAN (R 4.2.0)
utf8	1.2.3	1.2.3	31/01/2023	CRAN (R 4.2.0)
VariantAnnotation	1.44.1	1.44.1	15/02/2023	Bioconductor
vctrs	0.6.3	0.6.3	14/06/2023	CRAN (R 4.2.0)
viridis	0.6.4	0.6.4	22/07/2023	CRAN (R 4.2.0)

9.4 APPENDIX 4: PSEUDO-RANDOMISED 384-WELL DRUG PLATE LAYOUT

	1	2	3	4	5	6	7	8	9	10	11	12	13	14	15	16	17	18	19	20	21	22	23	24
A	H2O	P2 H2O	H2O	P2 H2O	H2O	P2 H2O	H2O	P2 H2O	H2O	P2 H2O	H2O	P2 H2O	H2O	P2 H2O	H2O	P2 H2O	H2O	P2 H2O	H2O	P2 H2O	H2O	P2 H2O	H2O	P2 H2O
B	P3 H2O	MEDIA	**DMSO**	P4 DOCE	P3 GEMC	P4 CRBO	P3 CRBO	P4 8931	P3 2014	P4 4547	P3 ETOP	P4 PACL	**DMSO**	P4 GEMC	P3 8931	P4 1152	P3 8186	P4 6244	P3 1152	P4 MYTO	P3 GEMC	APHI	**DMSO**	P4 H2O
C	H2O	MEDIA	**DMSO**	P2 DOCE	GEMC	P2 CRBO	CRBO	P2 8931	2014	P2 4547	ETOP	P2 PACL	**DMSO**	P2 GEMC	8931	P2 1152	8186	P2 6244	1152	P2 MYTO	GEMC	P1 PEMB	**DMSO**	P2 H2O
D	P3 H2O	STAU	P3 VINB	P4 FULV	P3 1579	P4 ERDA	**DMSO**	P4 5363	P3 DOXO	STAU	P3 6244	P4 8186	P3 ERDA	P4 LENV	P3 NUTL	P4 1579	P3 LENV	P4 2014	**DMSO**	P4 CISP	P2 PEMB	P4 DOCE	P3 1579	P4 H2O
E	H2O	P1 PEMB	VINB	P2 FULV	1579	P2 ERDA	**DMSO**	P2 5363	DOXO	P3 PEMB	6244	P2 8186	ERDA	P2 LENV	NUTL	P2 1579	LENV	P2 2014	**DMSO**	P2 CISP	APHI	P2 DOCE	1579	P2 H2O
F	P3 H2O	P4 MYTO	P3 FULV	P4 VINB	P4 PEMB	P4 2014	P3 1152	P4 NUTL	P3 4547	P4 LENV	**DMSO**	P4 DOCE	P3 CISP	P4 VINB	**DMSO**	P4 5363	P3 MYTO	P4 8931	P3 4547	P4 ETOP	P3 DOXO	P4 CRBO	P3 CISP	P4 H2O
G	H2O	P2 MYTO	FULV	P2 VINB	STAU	P2 2014	1152	P2 NUTL	4547	P2 LENV	**DMSO**	P2 DOCE	CISP	P2 VINB	**DMSO**	P2 5363	MYTO	P2 8931	4547	P2 ETOP	DOXO	P2 CRBO	CISP	P2 H2O
H	P3 H2O	P4 ETOP	P3 DOXO	P4 PACL	P3 ERDA	P4 6244	P3 PACL	P4 5363	P4 PEMB	P4 FULV	P3 8186	P4 NUTL	P3 NUTL	P4 8186	P3 FULV	APHI	P3 5363	P4 PACL	P3 6244	P4 ERDA	P3 PACL	P4 DOXO	P3 ETOP	P4 H2O
I	H2O	P2 ETOP	DOXO	P2 PACL	ERDA	P2 6244	PACL	P2 5363	APHI	P2 FULV	8186	P2 NUTL	NUTL	P2 8186	FULV	P1 PEMB	5363	P2 PACL	6244	P2 ERDA	PACL	P2 DOXO	ETOP	P2 H2O
J	P3 H2O	P4 CISP	P3 CRBO	P4 DOXO	P3 ETOP	P4 4547	P3 8931	P4 MYTO	P3 5363	**DMSO**	P3 VINB	P4 CISP	P3 DOCE	**DMSO**	P3 LENV	P4 4547	P3 NUTL	P4 1152	P3 2014	STAU	P3 VINB	P4 FULV	P3 MYTO	P4 H2O
K	H2O	P2 CISP	CRBO	P2 DOXO	ETOP	P2 4547	8931	P2 MYTO	5363	**DMSO**	VINB	P2 CISP	DOCE	**DMSO**	LENV	P2 4547	NUTL	P2 1152	2014	P3 PEMB	VINB	P2 FULV	MYTO	P2 H2O
L	P3 H2O	P4 1579	P3 DOCE	APHI	P3 CISP	**DMSO**	P3 2014	P4 LENV	P3 1579	P4 NUTL	P3 LENV	P4 ERDA	P3 8186	P4 6244	P2 PEMB	P4 DOXO	P3 5363	**DMSO**	P3 ERDA	P4 1579	P3 FULV	P4 VINB	P4 PEMB	P4 H2O
M	H2O	P2 1579	DOCE	P3 PEMB	CISP	**DMSO**	2014	P2 LENV	1579	P2 NUTL	LENV	P2 ERDA	8186	P2 6244	STAU	P2 DOXO	5363	**DMSO**	ERDA	P2 1579	FULV	P2 VINB	STAU	P2 H2O
N	P3 H2O	**DMSO**	P2 PEMB	P4 GEMC	P3 MYTO	P4 1152	P3 6244	P4 8186	P3 1152	P4 8931	P3 GEMC	**DMSO**	P3 PACL	P4 ETOP	P3 4547	P4 2014	P3 8931	P4 CRBO	P3 CRBO	P4 GEMC	P3 DOCE	**DMSO**	MEDIA	P4 H2O
O	H2O	**DMSO**	APHI	P2 GEMC	MYTO	P2 1152	6244	P2 8186	1152	P2 8931	GEMC	**DMSO**	PACL	P2 ETOP	4547	P2 2014	8931	P2 CRBO	CRBO	P2 GEMC	DOCE	**DMSO**	MEDIA	P2 H2O
P	P3 H2O	P4 H2O	P3 H2O	P4 H2O	P3 H2O	P4 H2O	P3 H2O	P4 H2O	P3 H2O	P4 H2O	P3 H2O	P4 H2O	P3 H2O	P4 H2O	P3 H2O	P4 H2O	P3 H2O	P4 H2O	P3 H2O	P4 H2O	P3 H2O	P4 H2O	P3 H2O	P4 H2O

Figure 55: Image of the final 384-well drug plate layout. P1 - highest concentration of drug; P4 - lowest concentration of drug. DMSO vehicle controls are labelled in red.

9.5 APPENDIX 5: DESCRIPTION OF LONZA RPMI 1640

Table 26: Description of the Lonza RPMI 1640 without L-Glutamine formulation

Description	mg/L
Sodium Bicarbonate	2.000E+03
Sodium Chloride	6.000E+03
Ca (NO3)2.4H2O	100.000
Choline Chloride	3.000
D-Biotin (Vitamin H) (00129)	0.200
D-Calcium Pantothenate (Vitamin B5)	0.250
D-Glucose anhydrous	2.000E+03
Folic Acid	1.000
Glutathione Reduced	1.000
Glycine	10.000
Potassium Chloride	400.000
L-Arginine Hydrochloride (00095)	241.860
L-Asparagine Monohydrate	56.810
L-Aspartic Acid	20.000
L-Cystine Dihyrohydrochloride	65.190
L-Glutamic Acid	20.000
L-Histidine Monohydrochloride Monohydrate	20.270
L-Hydroxyproline	20.000
L-Isoleucine	50.000
L-Leucine	50.000
L-Lysine Monohydrochloride	40.000
L-Methionine	15.000
L-Phenylalanine	15.000
L-Proline	20.000
L-Serine	30.000
L-Threonine	20.000
L-Tryptophane	5.000
L-Tyrosine Disodium Salt, Dihydrate	28.830
L-Valine	20.000
Magnesium Sulfate Anhydrous	48.830
Myo-Inositol	35.000
Sodium Phosphate Dibasic, Anhydrous	800.490
Niacinamide (Nicotinamide)	1.000
P-Aminobenzoic Acid	1.000
Pyridoxine Monohydrochloride	1.000
Riboflavin (Vitamin B2)	0.200
Thiamine Monohydrochloride (Vitamin B1)	1.000
Cyanocobalamin (Vitamin B12)	5.000E-03
Phenol red sodium salt	5.100

9.6 APPENDIX 6: INITIAL WES SUMMARY DATA USING 1,000 GENOME FILTERING STRATEGY

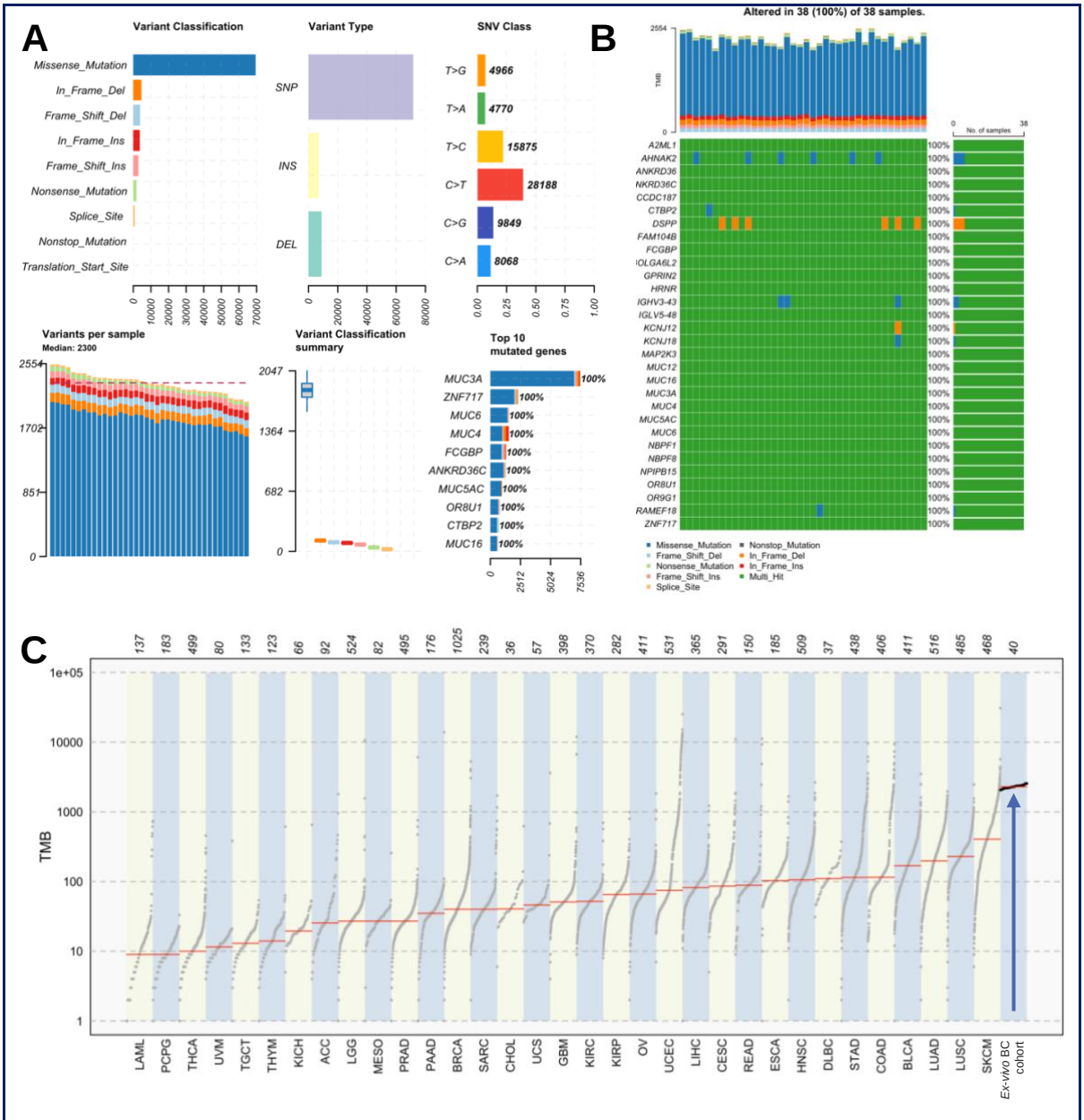

Figure 56: Whole exome sequencing summary results after filtering with 1,000 genome population data. A – summary figure for unfiltered WES data, showing a very high number of mutations per sample, most of which were mutated in every BC sample; B – oncoplot summary of top 30 mutations from the unfiltered results, all of which were mutated in all BC samples and were multi-hit mutations; C – comparison of unfiltered results versus other TGCA logged datasets, showing a higher TMB than any other TGCA sample type – even the BLCA (bladder cancer) subset.

9.7 APPENDIX 7: TARGETED GENE PANEL USED FOR WES FILTERING

ABL1	AXIN1	CDKN2C	DMD	FGFR2	IDH1	LATS2	MYC	PIK3CA	PTPN13	RQCD1	SRSF2	UNCX
ACVR1	AXIN2	CEBPA	DNMT3A	FGFR3	IDH2	LEMD2	MYCN	PIK3CB	PTPRC	RRAS2	STAG2	USP9X
ACVR1B	B2M	CHD2	EEF1A1	FLNA	IL6ST	LRP1B	MYD88	PIK3CG	PTPRD	RUNX1	STK11	VHL
ACVR2A	BAP1	CHD3	EEF2	FLT3	IL7R	LRRK2	MYH11	PIK3R1	PTPRT	RXRA	TAF1	WHSC1
AJUBA	BCL2	CHD4	EGFR	FOXA1	INPPL1	LZTR1	MYH9	PIK3R2	RAC1	SCAF4	TBL1XR1	WT1
AKT1	BCL2L11	CHD8	EGR3	FOXA2	IRF2	MACF1	NCOR1	PIM1	RAD21	SETBP1	TBX3	XPO1
ALB	BCOR	CHEK2	EIF1AX	FOXQ1	IRF6	MAP2K1	NF1	PLCB4	RAF1	SETD2	TCEB1	ZBTB20
ALK	BRAF	CIC	ELF3	FUBP1	JAK1	MAP2K4	NF2	PLCG1	RANBP2	SF1	TCF12	ZBTB7B
AMER1	BRCA1	CNBD1	ELL	GABRA6	JAK2	MAP3K1	NFE2L2	PLXNB2	RARA	SF3B1	TCF7L2	ZC3H12A
ANKRD11	BRCA2	COL5A1	EP300	GATA3	JAK3	MAP3K4	NIPBL	PMS1	RASA1	SIN3A	TERT	ZCCHC12
APC	BRD7	CREB3L3	EP400	GNA11	KANSL1	MAPK1	NOTCH1	PMS2	RB1	SMAD2	TET2	ZFHX3
APOB	BTG2	CREBBP	EPAS1	GNA13	KDM5C	MAX	NOTCH2	POLE	RBM10	SMAD4	TGFBR2	ZFP36L1
AR	CACNA1A	CSDE1	EPHA2	GNAQ	KDM6A	MDC1	NPM1	POLQ	RELN	SMARCA1	TGIF1	ZFP36L2
ARAF	CARD11	CTCF	EPHA3	GNAS	KEAP1	MECOM	NRAS	POLRMT	RET	SMARCA2	THRAP3	ZMYM2
ARHGAP35	CASP8	CTNNB1	ERBB2	GPS2	KEL	MED12	NSD1	PPM1D	REV3L	SMARCA4	TLR4	ZMYM3
ARID1A	CBFB	CTNND1	ERBB3	GRIN2D	KIF1A	MEN1	NUP133	PPP2R1A	RFC1	SMARCB1	TMSB4X	ZNF133
ARID1B	CBWD3	CUL1	ERBB4	GTF2I	KIT	MET	NUP93	PPP6C	RHEB	SMC1A	TNFAIP3	ZNF750
ARID2	CCND1	CUL3	ERCC2	H3F3A	KLF5	MGA	PAX5	PREX2	RHOA	SMC3	TP53	
ARID5B	CD70	CYLD	ESR1	H3F3C	KMT2A	MGMT	PBRM1	PRKAR1A	RHOB	SMG1	TPR	
ASXL1	CD79B	CYSLTR2	EZH2	HGF	KMT2B	MKI67	PCBP1	PRKDC	RIT1	SOS1	TRAF3	
ASXL2	CDH1	DACH1	FAM46D	HIST1H1C	KMT2C	MLH1	PCLO	PSIP1	RNF111	SOX17	TRRAP	
ATF7IP	CDK12	DAZAP1	FANCD2	HIST1H1E	KMT2D	MSH2	PDE4DIP	PTCH1	RNF213	SOX9	TSC1	
ATM	CDK4	DDX3X	FAT1	HLA-A	KNL1	MSH3	PDGFRA	PTEN	RNF43	SPEN	TSC2	
ATR	CDKN1A	DHX9	FAT4	HLA-B	KRAS	MSH6	PDS5B	PTMA	RPL22	SPOP	TXNIP	
ATRX	CDKN1B	DIAPH2	FBXW7	HRAS	KRT222	MTOR	PGR	PTPDC1	RPL5	SPTA1	U2AF1	
ATXN3	CDKN2A	DICER1	FGFR1	HUWE1	LATS1	MUC6	PHF6	PTPN11	RPS6KA3	SPTAN1	UBR5	

Figure 57: Targeted gene panel of 329 genes used for WES filtering

9.8 APPENDIX 8: KEY THERAPEUTIC TARGETS BASED ON WES DATA

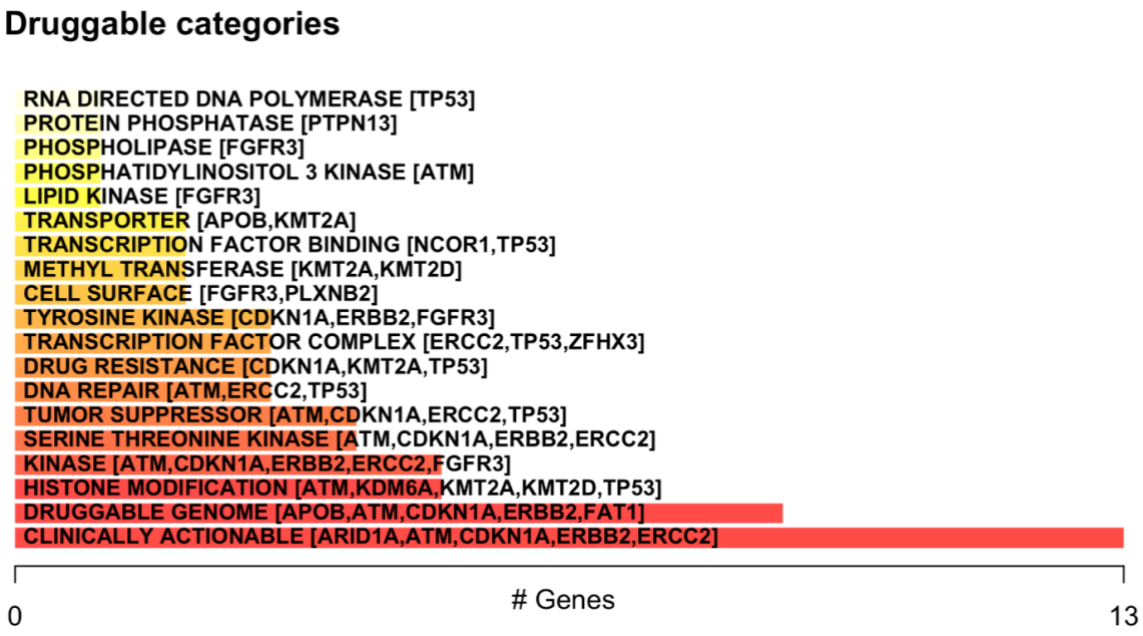

Figure 58: Therapeutic targets based on "drugInteractions" package of maftools, which uses genetic mutation data and cross references it against known or reported drug-gene interactions or druggable drug classes.